DOCTORAL THESIS

Computational Study of Adsorption and Diffusion in Zeolites with Cations

Almudena García Sánchez

Seville, November 2011

Almudena García Sánchez
PhD thesis, Universidad Pablo de Olavide (Seville, Spain), November 2011
ISBN
Cover Design: A. García-Sánchez

Computational Study of Adsorption and Diffusion in Zeolites with Cations

---

Estudio Computacional de los Procesos de Adsorción y difusión en Zeolitas con Cationes

Trabajo presentado para la obtención del título de Doctora con Mención Europea en el departamento de Sistemas Físicos, Químicos y Naturales, dentro del programa de Ciencia y Tecnología de Coloides e Interfases.

Almudena García Sánchez

Licenciada en Físicas

Directors/Directores

Prof. Dr. S. Calero Díaz	Universidad Pablo de Olavide
Prof. Dr. Ir. T. J. H. Vlugt	Delft University of Technology

Dissertation Committee/Miembros del Tribunal

Prof. Dr. S. Lago (Presidente)	Universidad Pablo de Olavide
Prof. Dr. Ir. S. Kjelstrup (Vocal)	Delft University of Technology
Prof. Dr. C. O. Ania (Vocal)	CSIC: Instituto Nacional del Carbón
Dr. T. van Erp (Vocal)	Katholieke Universiteit Leuven
Dr. J. M. Castillo (Secretario)	Universität Stuttgart

External Committee/Comité Externo Evaluador

Dr. Ir.D. Dubbeldam	Universiteit van Amsterdam
Dr. E. McGarrity	Delft University of Technology

The research described in this thesis was performed at the Department of Physical, Chemical and Natural System of the University Pablo de Olavide (Seville, Spain), at the Department of Chemical Engineering of the University of Amsterdam (Amsterdam, The Netherlands) and at the Process & Energy Department of the Delft University of Technology (Delft, The Netherlands), with support of the Dutch Organization for Scientific Research (NWO), the European Science Foundation and Delft University of Technology.

A mis padres

I've learned that people will forget what you said, people will forget what you did,
but people will never forget how you made them feel.

Maya Angelou

Acknowledgment

This thesis would have not been possible without the support and encouragement of my supervisors, colleagues, family and friends who in different ways encouraged me and shared this long way. To all of you, I express my grateful acknowledgement and sincere thanks for bringing this thesis to a successful end.

First of all, I would like to express my sincere gratitude to my supervisors: Prof. Sofía Calero and Prof. Thijs Vlugt. Thank you Sofia for your kind guidance, helpful advices and trust in my work. Also thank you for taking me as part of the Raspa group where you create a motivated environment, promoting collaboration and excellence. Thank you Thijs for your helpful attitude and for sharing with me your knowledge and enthusiasm about molecular simulation. Your patience and support allowed me to finish my PhD. Thank you for your inputs, English corrections and the proof reading of this thesis.

I had the pleasure to work with and learn of exceptional scientist, who directly contributed to the development of this work. First I want to mention Dr. David Dubbeldam, thank you for your support and valuable comments in this thesis, for your availability and for answering all my question-emails, doesn't matter which time I wrote them. I am thankful to Dr. Jasper van Baten for introducing me to the field of molecular simulation. I only have grateful words for Dr. Erin McGarrity, thank you for your encouragement, insightful comments and support. Thank you for always finding the time to answer all my questions. I was very lucky to receive contribution from Prof. J. B. Parra, Prof. C. O. Ania, thank you for providing me with experimental data and valuable comments. Thank you to Dr. Elena García-Pérez and Dr. Juan M. Castillo for making my day to day work a pleasure and for their kind help. Thank you to Emma Eggink for contributing to this thesis with her Master work. Thank you to Dr. J. van den Bergh and Dr. Kapetijn, for their contribution in chapter 5.
Thank you to Dr. Facundo Mattea for his help in picture 1.4 and TOC picture in chapter 6. Thanks to Kim McGarrity, Malole Díaz and Roberta Pacciani for helping me with the English. Many thanks to Mar García for hosting me in Granada during my PhD courses. Also thank you to Chantal Durant, Judith Blommart and María José Garrido for managing all the administrative issues related to this thesis. Although not directly involved, I wish to thank Prof. Antonio Hernando, Prof. Patricia Crespo and Dr. Alvaro Martinez for introducing me to the field of electromagnetism. Finally, I wish to

acknowledge Dr. Christof Krülle for hiring me as a Hi-wi and for giving the opportunity to collaborate with the Sand group.

"Success is not final, failure is not fatal; it is the courage to continue that counts." (Winston Churchil)
This quote is to thank to my family and friends for their support during the ups and downs over these years. Especially, I would like to thank Claudio for being an example and inspiration. Your smile and courage will be always with me. To Antonio García, Patro Sánchez, Paloma and Diego who cheered me up whenever I went through a difficult time. Their love and friendship have encouraged me to continue working hard. Thank you also to my whole family: Cande, Félix, MariCarmen, Félix Javier, Belinda, Javi, Choni, Maricarmen, Margit, Peter, Michael, David, Christiane and Oliver for giving me words of encouragement whenever I needed them. Gracias por estar siempre a mi lado, por animarme a seguir adelante y motivarme a conseguir nuevos retos.

I now wish to acknowledge my colleagues and friends although this list is by no means complete.
To my present and former colleagues in Amsterdam, Seville and Delft: Laura Pachón, Anil Gaidwak, Bei Liu, Jarek Juraszek, Maximiliano Corredor and Curro Huidobro: thanks for the meetings, barbeques and good moments we shared.
Gracias a mis compañeros del grupo Raspa: Elena García, Juanma Castillo, Juanjo Gutiérrez, Ana Martín, Said Hamad, Patrick Merkling, Rocío Bueno y Tom Caremans. Y al resto de compañeros del departamento, por los buenos momentos compartidos y hacer del trabajo un lugar divertido. Gracias a Elena Guillén, Paula Castillo, María Cortada, Tania Lopes, Alejandro Cuetos, Paula Zarenko, Tom Berger, Pablo González, Jose María Pedrosa, Bruno Martínez, Palma Mendoza, Javi Roales, Ana Rodríguez, Manolo Cano, Paola Hurtado, Paco Gámez and Juan Antonio Anta.
For the time during my thesis in Seville I want to thank my very good friends: Sofia, Fonchi, Mena, Malole, Claudia, Ana, Rosa, Natalia, Rosana, Bruno, Maribel, Emilio, Elisabeth, Caro, Sergio, Vicky, Alberto, Momi, Alfonso, Carmen, Paco y Fali y a todos los que me abrieron las puertas de sus casas en el barrio y en la Flora. Gracias a Luisa y a la gente del Centro Social "el Esqueleto" por compartir conmigo sus vivencias y dejarme aprender de ellas. Gracias a mis amigos yoguis por la buena energía que siempre me hacen llegar y por saber hacer las distancias tan cortas; gracias a María, Itziar, Jorge, Lourdes, Félix, Viviana y Fernando.
Thanks to my office mates in Delft: Mariëtte de Groen, Sondre Schnell and Xin Liu and my extra office mates: Erin McGarrity, Facundo Mattea, Stevia Sutanto, Bora Aydin, Mayte Mota, Sara Salvador, Somayeh Kazemi, Bernardo Oyarzun, Stephie Lefortier, Marcos Rodríguez and Sayee Prasaad. I really appreciate your friendship.

Thank you to Mónica, Xesc, Alondra, Henri, Rita, Christian, Anamaría, Cris, Ochi, Carsten, Michel, Dennis, Martina, Hélène, Georgiana, Mihai, Xiaohua, Wydia, Jessica, Somnath, Sergio, Marlous and Olivia. I enjoyed very much our time together! Special thanks to Agnese Boccalon for sharing her time with me in Delft from the beginning as well as to Verónica de Silva, Kim McGarrity, Alberto Martínez, Irene Oosting, Andra Mustata and Beatriz Zornoza for becoming great friends.

I also wish to thank many other friends who made my graduate studies memorable and contribute to the happy time there: Pampa Molina, Alina Santiago, Marta Balbás, Nacho Molina, Alvaro Tejero, Helio Cobaleda, Libertad Bullejos, Dani Paredes y al resto de la gente de Hypatia. Espero que sigamos con las reuniones anuales durante muchos años más. También a Álvaro Martínez, Miriam Andrés y Adela Sanvicente, Alessandra Cardinale, Michele di Nunno, Stefano Marcellini y Ricardo Sosa por su amistad. Y a Leticia Domínguez, Eva Migarri, Lola Madolell y Nieves Marín por su apoyo y ayuda.

Thanks to the people who made my time in Bayreuth so exceptional: Alberto de Lozar, Carmen Pérez, Alejandro Luque, Mar García, Alberto Rivera, Luismi Fernández, Damián Morán, Steffi Guhl, Beni Tränkle, Aurel Satlow, and all Kuwi's. ¡Siempre tengo ganas de que sea fin de año para veros!

Thanks to my very best friend: Sara Añino and Andrés Couceiro. For their love and support.

Special thanks to Dr. Lourdes Vega for giving me the opportunity to start a new stage in my life and career, and for being so generous and supportive.

Finally, I want to thank Dominik for teaching me that a smile is the shortest distance between two people.

Contents

Summary

Zeolites are nanoporous materials that are of great importance in many technological fields and environmental applications[1]. Zeolites consist of aluminosilicates with diverse structures: channels, windows or cages of molecular dimensions. The presence of aluminium atoms in the framework induces an electrical imbalance leading to a negatively charged framework that is compensated by additional non-framework cations, such as sodium or calcium. Due to their molecular structure, zeolites can selectively adsorb the components of gaseous and/or liquid mixtures according to their molecular size; the adsorption properties often strongly depend on the presence of non-framework cations[2].

Zeolites are used in gas separation processes of industrial interest such as CO_2 removal from natural gas[3]. Remarkable separations effects can be achieved by the interplay of mixture adsorption and diffusion. Zeolites play a major role in petrochemical industry where they are used as catalysts in cracking and hydro-cracking of hydrocarbons[2].

For the practical application of zeolites, molecular simulation techniques provide an efficient tool to understand their thermodynamic properties. A well-designed computer simulation can predict thermodynamic properties and can be a substitute for experiments. Molecular simulation can also provide measurements that are difficult or inaccessible through experimental methods or when the experiment has components that are too dangerous or too expensive.

This research focused on the understanding, from a theoretical point of view, of the mechanism of adsorption and diffusion of gases in zeolites with or without non-framework cations by applying molecular simulations. We used molecular

simulations techniques to study the adsorption and the diffusion processes of gases in zeolites. In particular, we calculated adsorption isotherms by Monte Carlo simulations in the grand-canonical ensemble. Diffusion coefficients have been calculated by molecular dynamics simulations.

The thesis is organized as follows:
In chapter 1, we first presented a state of the art on molecular simulations and on the description of zeolites in order to provide a general overview on these fields and introduce the scientific work done in this thesis.

We related the importance in technological fields and environmental applications with the simulation of the zeolite structures, as they allow to selectively adsorb the gases according to their molecular size. In chapter 2 we studied the adsorption and diffusion of small hydrocarbons in Linde Type A (LTA) zeolites as a function of their calcium/sodium ratio[4]. The diffusion studies focused on methane whereas the adsorption simulations were performed from methane up to pentane. Our simulation results are consistent with previous experimental studies. They provide a molecular picture of the influence of the zeolite type, the amount of cations contained and their location in the structure on the adsorption and diffusion of small hydrocarbons.

In chapter 3, we studied the effect of flexibility on the adsorption and diffusion of methane in four types of zeolite A: two pure silica structure (ITQ-29 and LTA_{Si}), the sodium form (LTA-4A), and the sodium/calcium form (LTA-5A)[5]. Simulations were performed at different temperatures and for different methane loadings. Both processes, adsorption and diffusion, are strongly determined by the cations. In this chapter, we described how the framework flexibility affects differently to the adsorption and diffusion of methane, and we discuss about when the zeolite framework should be considered rigid or flexible.

Several force fields are available to describe thermodynamic properties of light gases in zeolites but most of them are only valid to all-silica structures (zeolites without non-frameworks cations)[6,7]. Unfortunately, many force fields are not transferable to other systems rather than those for which they were developed[8-10].

In chapter 4, an accurate and transferable force field was developed to reproduce the thermodynamic properties of CO_2 in all-silica structures and aluminosilicates bearing sodium non-framework cations[11]. This force field allows calculating the adsorption isotherms in excellent agreement with experimental data, thereby providing a more accurate and reliable tool for screening zeolites with a wide range of Al/Si ratios as well as all-silica zeolites.

Regarding the diffusion process of CO_2 in zeolites, in chapter 5 we investigated their diffusion in three LTA-type zeolites: ITQ-29, LTA_{Si} and LTA-4A. In order to understand the diffusion behaviour of CO_2 in LTA-type zeolites and the influence of the guest-host interactions, we have compared the results for two available force fields in the literature[12]. The observed concentration dependencies of the self- and transport diffusions are strongly affected by the choice of the force field. To understand the physical origin of the different diffusion behaviour of CO_2 in LTA-type zeolites, we have used the Relevant Site Model (RSM). This model describes the concentration dependency of CO_2 in these zeolites. In addition, we investigated the influence of non-framework cations in this process.

The selection or design of a zeolite for a particular use requires knowledge of the interaction between the zeolite and the adsorbate. Developing force fields is still a major task, as it requires a very large number of molecular simulations. Therefore, there is a significant interest in reducing this number. We aimed at developing a method to fit the force field parameters for describing adsorption in zeolites in a computationally easier and less time consuming way. In chapter 6 we developed a method to describe the result of a molecular simulation without performing the simulation itself[13]. This model represents the zeolite channel as an annular pore, where oxygen atoms are uniformly distributed over the inside of the annulus.

References

1 M. E. Davis. *Nature* **417**, 813-821 (2002).

2 S. B. Wang and Y. L. Peng. *Chemical Engineering Journal* **156**, 11-24 (2010).

3 S. U. Rege, R. T. Yang and M. A. Buzanowski. *Chemical Engineering Science* **55**, 4827-4838 (2000).

4 A. García-Sánchez, E. García-Pérez, D. Dubbeldam, R. Krishna and S. Calero. *Adsorption Science & Technology* **25**, 417-427 (2007).

5 A. García-Sánchez, D. Dubbeldam and S. Calero. *Journal of Physical Chemistry C* **114**, 15068-15074 (2010).

6 Li P. and F. H. Tezel. *Journal of Chemical and Engineering Data* **53**, 2479-2487 (2008).

7 R. J. H. Vlugt, R. Krishna and B. Smit. *Journal of Physical Chemistry B* **103**, 1102-1118 (1999).

8 E. D. Akten, R. Siriwardane and D. S. Sholl. *Energy & Fuels* **17**, 977-983 (2003).

9 E. Jaramillo and M. Chandross. *Journal of Physical Chemistry B* **108**, 20155-20159 (2004).

10 L. P. Maurin G, Bell RG. *Journal of Physical Chemistry B* **109**, 16084-16091 (2005).

11 A. García-Sánchez, C. O. Ania, J. B. Parra, D. Dubbeldam, T. J. H. Vlugt, R. Krishna and S. Calero. *Journal of Physical Chemistry C* **113**, 8814-8820 (2009).

12 A. García-Sánchez, J. v. d. Bergh, J. M. Castillo, S. Calero, F. Kapteijn and T. J. H. Vlugt. *submitted*.

13 A. García-Sánchez, E. Eggink, E. S. McGarrity, S. Calero and T. J. H. Vlugt. *Journal of Physical Chemistry C* **115**, 10187-10195 (2011).

Resumen

Las zeolitas son materiales cristalinos de gran importancia en procesos ambientales y tecnológicos[1]. Su estructura consiste en átomos de silicio, aluminio y oxígeno que se unen formando una red tridimensional con canales y cavidades bien definidos. Para mantener la estructura con carga neutra se añaden cationes, principalmente sodio y calcio. Las formas peculiares que adoptan las zeolitas, dotan a estos materiales de propiedades tales como la capacidad de intercambio iónico, la adsorción selectiva de gases o sus cualidades catalíticas. Estas propiedades junto a una gran estabilidad térmica hacen de las zeolitas materiales interesantes para su aplicación industrial, por ejemplo como catalizadores en el craqueo de hidrocarburos[2]. Las zeolitas también están consideradas como uno de los mejores materiales para la adsorción y la separación selectiva de CO_2 en procesos de flujo y la eliminación de agua y CO_2 del gas natural[3].

Las aplicaciones de las zeolitas vienen determinadas por el conocimiento de los procesos termodinámicos que llevan a cabo los gases en su interior. Los métodos de simulación molecular juegan un papel importante, ya que permiten la descripción exacta de las interacciones entre los gases adsorbidos, la de éstos con la zeolita y con los cationes. Una de las ventajas adicionales de la simulación es que permite obtener resultados en sistemas de difícil acceso experimental, o cuando el sistema contiene componentes peligrosos o excesivamente caros, lo que puede complicar su estudio mediante técnicas experimentales.

Este trabajo de tesis tiene como objetivo estudiar, desde un punto de vista teórico, los mecanismos de adsorción y difusión de los gases en el interior de zeolitas con y sin cationes. Para ello se han utilizado diversas técnicas de simulación molecular. En concreto, se han calculado las isotermas de adsorción

mediante el método de Monte Carlo en el colectivo gran canónico. Los coeficientes de difusión se han obtenido mediante dinámica molecular.

En el primer capítulo, presentamos el marco teórico de la simulación molecular y la descripción de las zeolitas para generar una visión global e introducir el trabajo científico llevado a cabo.

La importancia de las zeolitas en las aplicaciones tecnológicas y ambientales se refleja en el capítulo 2, donde se detalla la investigación realizada en los procesos de adsorción y difusión de hidrocarburos pequeños en zeolitas tipo Linde Type A (LTA) en función del ratio de carbono/sodio. La difusión se ha estudiado principalmente en el metano, mientras que los estudios en adsorción se realizaron con cinco hidrocarburos: metano, etano, propano, butano y pentano[4]. Los resultados, obtenidos mediante simulación molecular, son consistentes con estudios experimentales anteriores, proporcionando información a nivel molecular de la influencia de los cationes en la zeolita en relación a su número y a su localización en la estructura.

La estructura de la zeolita puede reproducirse mediante un modelo rígido o uno flexible. En el capítulo 3 se han estudiado las diferencias en las estructuras de las siguientes zeolitas tipo A: dos estructuras pura sílica (ITQ-29 and LTA_{Si}), la estructura con sodio y aluminio (LTA-4A), y la estructura con calcio, sodio y aluminio (LTA-5A)[5]. El estudio se realizó a diversas temperaturas demostrando que la adsorción y específicamente la difusión del metano están influenciadas por el tipo de estructura considerado.

En la literatura podemos encontrar diversos campos de fuerzas capaces de describir los procesos termodinámicos de gases de pequeño tamaño[6,7]. La mayoría de estos campos de fuerzas sólo pueden utilizarse para zeolitas sin cationes. Para zeolitas con cationes, los campos de fuerzas que encontramos han sido desarrollados para un único tipo de estructura (FAU o LTA)[8-10] y fallan cuando los aplicamos a otras estructuras (FAU, LTA, MOR o MFI)[11]. En el capítulo 4 se presenta un campo de fuerzas capaz de reproducir las propiedades termodinámicas del CO_2 tanto en pura sílica como en zeolitas con cationes de

sodio. Este campo de fuerzas permite reproducir con precisión las isotermas de adsorción experimentales, proporcionando una excelente herramienta para investigar zeolitas con una amplia distribución de silicio y aluminio, además de las estructuras sin cationes.

Los procesos de difusión del dióxido de carbono también ha sido objeto de estudio. En el capítulo 5 se muestran los resultados de los coeficientes de difusión del CO_2 en tres tipos de zeolitas LTA: ITQ-29, LTA_{Si} y LTA-4A[12]. El estudio se realizó empleando distintos campos de fuerzas, mostrando entre ellos una gran diferencia en la difusión de CO_2. Para comprender el significado físico de los distintos resultados de la difusión y a su vez, la influencia de los parámetros de los campos de fuerzas en la difusión del CO_2, se aplicó el "Relevant Site Model" (RSM) a nuestros resultados. Este modelo describe la dependencia de la concentración de CO_2 en diversas zeolitas. En este estudio también se analizó la influencia de los cationes de la estructura en el proceso de difusión.

La selección y el diseño de zeolitas para usos concretos requieren la comprensión de las interacciones entre la zeolita y el adsorbato. Para ello es necesario utilizar campos de fuerzas que reproduzcan las propiedades termodinámicas de los gases, pero el desarrollo de un nuevo campo de fuerzas tiene un elevado coste computacional. En el capítulo 6 se introduce un método para ajustar los parámetros de los campos de fuerzas que describen los procesos de adsorción en zeolitas de manera rápida y sin apenas coste computacional[13]. Este método permite obtener buenos resultados sin necesidad de realizar la simulación en sí. El modelo propuesto representa los canales de las zeolitas mediante un cilindro coaxial donde los átomos de oxígeno están uniformemente distribuidos en el cilindro interior.

Referencias

1 M. E. Davis. *Nature* **417**, 813-821 (2002).

2 S. B. Wang and Y. L. Peng. *Chemical Engineering Journal* **156**, 11-24 (2010).

3 S. U. Rege, R. T. Yang and M. A. Buzanowski. *Chemical Engineering Science* **55**, 4827-4838 (2000).

4 A. García-Sánchez, E. García-Pérez, D. Dubbeldam, R. Krishna and S. Calero. *Adsorption Science & Technology* **25**, 417-427 (2007).

5 A. García-Sánchez, D. Dubbeldam and S. Calero. *Journal of Physical Chemistry C* **114**, 15068-15074 (2010).

6 Li P. and F. H. Tezel. *Journal of Chemical and Engineering Data* **53**, 2479-2487 (2008).

7 R. J. H. Vlugt, R. Krishna and B. Smit. *Journal of Physical Chemistry B* **103**, 1102-1118 (1999).

8 E. D. Akten, R. Siriwardane and D. S. Sholl. *Energy & Fuels* **17**, 977-983 (2003).

9 E. Jaramillo and M. Chandross. *Journal of Physical Chemistry B* **108**, 20155-20159 (2004).

10 L. P. Maurin G, Bell RG. *Journal of Physical Chemistry B* **109**, 16084-16091 (2005).

11 A. García-Sánchez, C. O. Ania, J. B. Parra, D. Dubbeldam, T. J. H. Vlugt, R. Krishna and S. Calero. *Journal of Physical Chemistry C* **113**, 8814-8820 (2009).

12 A. García-Sánchez, J. v. d. Bergh, J. M. Castillo, S. Calero, F. Kapteijn and T. J. H. Vlugt. *submitted*.

13 A. García-Sánchez, E. Eggink, E. S. McGarrity, S. Calero and T. J. H. Vlugt. *Journal of Physical Chemistry C* **115**, 10187-10195 (2011).

Chapter 1

Introduction

The main aim of this chapter is to summarice the present state of the art in the computational study of adsorption and diffusion in zeolites with cations. After a historical perspective, a description of the zeolites structure is presented. Then, we focus on the properties of zeolites and that leads us to the application possibilities. This background on the subject is required to discuss adequately the computational methods employed in this thesis.

1.1 Preamble

When we are looking at reality, we are confronting ourselves with the "whole". If we wish to approach reality in order to manage, treat or study it, we have no other option but to narrow our focus. This is because our minds as well as our bodies have a limited capacity. On the other hand, it is necessary to establish a veneer that can reflect such a "whole". The ability for reflection enables us to model upon the reality and further, it seems everything we are aware of is possible to model. It is within this context that the sense of what it means to model the "whole" can be achieved.

Whatever can be imagined could, in principle, also be modelled. The outcome of such an action is a reproduction of reality to varying degrees of precision and satisfaction that depends on the details and the portion of reality that are within reach of the scope of the model. Although the current scientific models were already present from Thales[I] and the Ionian thought, their concept is still discussed nowadays, especially in the discourse of scientific philosophy.

The comprehension of the concept of Nature and its ways of observance reached the actual understanding as science (Newton for example, understood himself as a natural philosopher). The technological development enabled the observer to a very different representation of Nature as the Greeks once did. In fact, the conditions of the Nature are still the same but human research and usage of natural materials are completely different and nowadays multi-functional. Therefore, the model becomes the manifestation of the complexity between the supposed ideas (theory) and the observed occurrences (experiment). In this context, Hacking[1] argues that the experiment has the central position within the scope of science. On the other hand, Woolgar[2] critically refers to the model with the same argument exposited by dualists: as much as the essence and perception

---

I Thales of Miletus (an Ionian city in the coast of Asia Minor, now Turkey) is considered one of the Seven Greek Sages and the founder of Milesian school. He was a great astronomer, mathematician engineer and philosopher. He has famous theorems as mathematician: "A circle is bisected by its diameter" or "The angles at base of isosceles triangle are equal" between others. Anaximander and Aristotle were some of his disciple.

of the object leads us to diverging conclusions about its own scientific activity. Woolgar proposes that representation is not the only option for the starting point of scientific work.

Besides experimental or theoretical features, another scientific approach is a computer-aided program based on both theoretical reflection and practical proof. Such an approach provides a means of going beyond the status quo, combining the ideal conditions created in the model and the accessible conditions created in the experiment. In fact, the scientist goes beyond the limitation of the capabilities of the experimental equipment.

In combination with statistical mechanics, the techniques of molecular simulations create a connection between what can be studied in the microscopic world by molecular simulations and what is observed in the macroscopic world by experiments. That is to say, the representation of the models allows us to contemplate the process of studying, the research itself. The essence of creating a theory or model is to explain what occurs in nature and to give a justification for it in accordance with a scientific approach. In addition, models should be able to predict what will happen when the conditions change. The experiments can be considered as points of departure from the theory and modelling, since a good model can provide the tools necessary to predict any experimental result. The experimental observation needs theory and vice versa.

We do not want to go too deeply into this single subject, since our work is not the study of the way in which the model represents reality, but instead, if we accept digital tools, we come closer to the interpretation of Hacking, where we understand that the representation approaches closest to an isomorphic reality.

Thanks to technical software, we can combine the three main frameworks through which models are interpreted: structural, dynamic and functional frameworks. The structural framework considers not only how many components are necessary to precisely represent the object, it is also necessary to precisely resemble the object. The atomic model put forward by Niels Bohr (1885-1965) is an example. This model provides a picture of something familiar, electrons

tracing an orbit around the nucleus, but this is not an actual representation of what is really happening. This model provides for us, first, the possibility to reaffirm the imagination about what is nature, and second, it allows us to think further or explore beyond the observable limits of the experiments. The dynamic framework of the model allows us to study the complex variables of a structural system, which is part of an open system that arises from the various interactions within that system. This aspect bears similarity to the mathematical formalism, in the ability to order, group or arrange the elements according to the results of the investigation. The model should be also functional, since this representation can evolve and the scientific experiences accumulate.

The current work explores only a very small part of the "whole". Theory requires experimental confirmation to provide any true sense of meaning to the results. For the theory to be justified, it must reproduce the results that have been observed experimentally. Therefore, our proposal is to bring together experimental measurements and the models currently used to represent them in a manner that adequately explains reality and that can encompass all of the dynamic conditions.

Molecular simulations provide an alternative method for determining equilibrium and the dynamic properties compared with the theory or experiments. We show how this method can be used to predict the properties of the molecules in confined systems. In particular, we concentrate on the adsorption and diffusion of small gases and quadrupoles in crystalline materials called zeolites and its interaction with diffusing gas. Using the developed model it will be possible to predict how a gas might behave under determined and desirable conditions in this crystalline material that has both micro- and meso-porosity. It will also consider the behaviour of the gas: how it diffuses if it is adsorbed by the material. This model employs classical, non-quantum mechanical methods.

1.2 Zeolite Description

1.2.1 From "Boiling Stones" to Zeotypes

The material we are exploring is referred as "zeolite". Zeolites are molecular sieve materials that are of great importance in many technological fields and environmental applications[3-10]. Zeolites are a system of channels, windows or cages of molecular dimensions. Basically, zeolite frameworks consist of silicon and aluminium atoms, so-called T-atoms, and oxygen in the crystal lattice. The presence of aluminium atoms in the framework induces an electrical imbalance leading to a negatively charged framework that is compensated by additional non-framework cations, such as calcium, sodium or potassium. The T-atoms are surrounded by four oxygen atoms forming an approximate tetrahedron. A zeolite framework consist of a crystalline structure of a three-dimensional network with cavities and channels in the different directions that allow for some properties like ion-exchange and reversible dehydration.

The chemical formula of aluminosilicates, zeolites with cations, is:

$$M_{x/n}\,[(AlO_2)_x\,(SiO_2)_y]\,wH_2O.$$

The formula within parentheses represents the framework composition. M is the non-framework cation of valence n. *w* is the number of water molecules present in a unit cell and x the number of Al atoms per unit cell, usually $1 \leq y/x \leq 5$. These values of the variables x and y depend upon the structure. The total number of tetrahedra in a unit cell is the sum (x+y). The exact Si/Al ratio depends on the crystallite size and the porosity.

1.2.1.1 Natural Zeolites

The geologist Alex Fredick **Cronstedt** (1722-1765) discovered a tectosilicate, called Stibilite, from the copper mine in Tornea, Sweden. In 1756 he published the article "Observation and description of an unknown species of rock, called ZEOLITES", in a Swedish magazine where he explained that this mineral visibly lost water when heated by a flame. By cooling the structure it could be rehydrated[11]. Cronstedt gave these minerals an aptly descriptive name: "zeolite",

a term that etymologically comes from classic Greek ζεω (zeo), which means to boil, and λιθοζ (lithos) which means stone. Therefore, these materials are literarily called "boiling stones." At that time, it was impossible to imagine all the ways in which zeolites could be exploited.

Figure 1.1: Four natural zeolite exhibit in Museo Geominero (IGME) at Madrid (Spain). Stilbite (up left), the type of zeolite discovered by Cronstedt. Chabacite (up right), Sodalite (down left) and Laumonite (down right).

Zeolites can be found in a variety of geological environments containing siliceous materials (volcanic rocks, clays, feldspar, biogenic silica and other silica rocks). These natural zeolites have a volcanic origin and are formed when flowing water of high pH and salt content interacts with volcanic ash, causing rapid crystal formation[12]. Many years ago, they were considered to only be museum pieces admired for their beauty and used exclusively in jewellery. Figure 1.1 shows a variety of natural zeolites that are often appreciated for their differences and beauty.

Since the first zeolite was discovered by Cronstedt, around forty natural types have been found[13]. The most abundant structures are: mordenite, cliptilolita, erionite, chabazite, phillipsite, stibilite and analcime.

1.2.1.2 Synthetic Zeolites

Synthetic zeolites are created in the laboratory to mimic the behaviour and properties similar to natural conditions. The first time it was demonstrated that a zeolite could be reversibly hydrated several times without any change or loss in morphology and appearance, similar to the observation by Cronstedt, was in 1840 by Damour[14]. Afterwards, science began in-depth studies into these minerals where a synthetical processing of zeolites became constantly frequent. Von Schafhäutl performed the first trial of hydrothermal synthesis of a porous material with quartz[15] in 1845. Some years later, in 1862, de St. Claire-Deville[16] described the first hydrothermal synthesis of a zeolite: Levynita. At this time techniques were not available to observe zeolites and there was not even information regarding atomic characterization. Thus, these initial works were unable to provide information about the structure and suffered from low reproducibility. However, in 1930 the development of new experimental techniques like X-ray diffraction motivated Pauling[17,18] to lead experiments which made him able to describe the first structure of a zeolite.

The adsorption was not limited to water. In 1909, Grandjean observed that zeolites could adsorb other molecules, like hydrogen, ammonia or air[12]. It was in 1948 when Barrer reported the first precise confirmation of hydrothermal

synthesis of an analogue mordenite[19]. As well, Barrer demonstrated that some zeolites could be synthesized in a form identical to their natural counterparts[20]. Further, Milton developed zeolite synthetization experiments to find new approaches for the separation and purification of mixture gases. Later on, together with Breck, their research produced a shift for industrial applications[12]. That lead to one of the most commercially succesfully zeolite that has no natural counterpart, Linde type A (LTA). In 1954, Union Carbide, was the first company that commercialized zeolite for separation, purification of air and for drying refrigerant gas and natural gas.

1.2.1.3 Zeotypes

Since the introduction of the term zeolite by Cronstedt, it was discussed and used in different ways[12,21]. The present understanding of what a zeolite is, is defined by Coombs et al[22]. This replaced a previous definition, which restricted the term to only alumosilicates with water content. Now also water-free and frameworks with other elements than Si and Al, such as Be, B, Mg, P, Ti, V, Cr, Mn, Fe, Cu, Zn, Ga and Ge were considered being part of the zeolite family. However, these materials are usually called zeotypes in general[23].

Particularly, the family of zeotypes with P atoms in the framework are called ALPO for aluminophosphate[24] and SAPO for silicoaluminophosphate[25]. Many minerals formerly (in 19th Century) attributed to the class of zeolites – like Apophyllite – actually do not have a zeolite framework and therefore are neither zeolites nor zeotypes.

Until now, 197 zeolite framework types are classified by the Structure Commission of the International Zeolite Association[13]. This commission assigns three letter codes to each framework topology. The codes are normally derived from the name of the natural zeolite, for example MOR to designate “mordenite” or FAU for “faujasite”. The codes also include the name for synthesized zeolites like LTA for Linde Type A. More than one zeolite could have the same topology. For example, for MFI-type zeolite there are 21 different zeolites with different

pore size, symmetry and chemical composition[26]. As a consequence, the number of different zeolites classified today is larger than 250.

In the early 1990's a lot of attention was given to the development of “mesoporous zeolites” which provide larger pores by a conversion of large molecules. Some of these “mesoporous zeolites” that have attracted much research interest are FSM-16 (Folde Sheet Mesoporous material), ITQ-21 (Instituto de Tecnología Química de Valencia) and MCM-41 (Mobil Composition of Matter). These zeolites were synthesized by research groups in Japan[27-30], Spain[31-33] and at the company Mobil Co.[34,35] respectively. After these groups, many researchers have investigated the synthetic methods and the formation mechanism of mesoporous silica. The synthesis of mesoporous materials is important in the field of study of gas adsorption and catalysis.

Recently, there has been tremendous activity to synthesize new nanoporous materials[4] with specific functional properties[36] according to specific uses, such as selective separation. Optimization of separation selectivity requires proper understanding of the adsorption behaviour of zeolites.

In the middle of the 90’s, new mesoporous materials called Metal Organic Frameworks (MOFs) were developed. The majority of such new materials were synthesized by investigators located in Japan[37-40], France[41-45] and United States[46-51]. MOFs were expected to replace zeolites due to their potential storage capacity, but they proved to be thermally unstable. In sharp contrast, zeolites have been shown to be thermally stable; however, many of their properties are still unclear.

1.2.2 Structure

All zeolites are considered to be molecular sieves because of their ordered structures when dried, and their high internal surface area. The term "molecular sieve" for a zeolite is due to McBain[52]. It refers to a solid with pores between 0.3 and 2 nm in diameter that could be used as sieve for molecules. In 1932, he

studied the ion-exchange capacity and the selective adsorption of gases in the natural zeolite Chabazite**.** McBain classified these porous materials in two groups: **sieves with a disordered structure**, such as activated carbon, inorganic gels, etc.; and **sieves with an ordered structure**, as is the case of zeolites and zeotypes.

Molecules of kinetic diameter larger than the diameter of the pores cannot pass through the windows and enter the canal system, which is why zeolites are also known as molecular sieves[53]. The molecular sieve property may be affected by dehydration and heat. Heating can produce distortions in the lattice and increase the void volume of the channels, while dehydration causes a cation interchange and subsequent changes in charge distribution within the structure. At room temperature, the zeolite framework is somewhat flexible. The pore diameter depends on the spatial arrangement of the tetrahedral structure caused by constant molecular vibration. This molecular vibration increases with temperature and leads to flexibility of pores in both shape and size.

1.2.2.1 Primary Building Units

The zeolite base compounds are silicon and oxygen connected together in a form of a tetrahedron: SiO_4, calling Primary Building Units (PBUs). Each tetrahedron has a siliceous atom in the centre and four oxygen atoms at the four apexes. Each oxygen is shared between two tetrahedra. Fig 1.2 shows a schematic representation of the tetrahedral PBUs which are the building blocks of the framework structure.

The non-framework cations are always coordinated by the lattice oxygen atoms. They are useful for ion-exchange reactions and introduce electrical fields over the framework, effectively polarizing it. The layout of tetrahedral units in a zeolite determines its properties. These units are called Member Rings (MR) and the tetrahedral metals in the centre are called T-atoms for short. The quantity of siliceous and aluminium atoms in a zeolite is determinate by Löwenstein rule[54] where the relation Si/Al could be between 1 and infinity. In favour of a neutral

charge, there is not a second adjacent of aluminium bonds, if we follow Löwenstein rule. This rule does not allow two adjacent aluminium bonds.

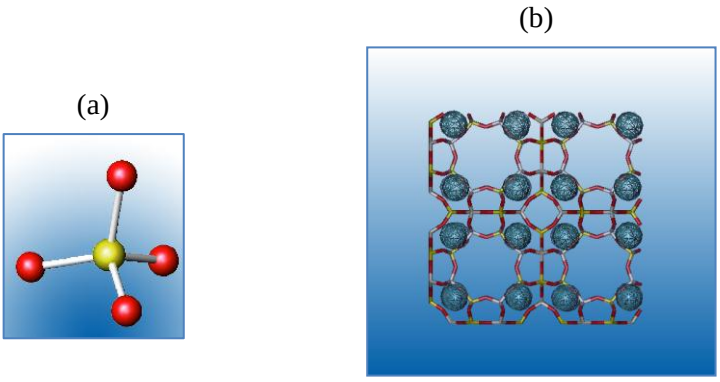

Figure 1.2: The majority of zeolites are aluminosilicates formed by tetrahedral units that contain an aluminium or silicon atom (shown in yellow) surrounded by 4 oxygen atoms (red spheres), as is showed in figure (a). The tetraedra join up forming the framework structure, with non-framework cations to compensate the aluminium charge. Figure (b) shows a snapshot of the structure with cations.

However, some tetravalent siliceous atoms could be replaced by trivalent atoms, like aluminium, resulting in a negatively charged structure. This net charge is compensated, in principle, with alkaline and alkaline-earth metal ions, but other metals, or even non-metals and organic cations could also be added. These so-called non-framework ions are usually allowed to move freely inside the zeolite.

1.2.2.2 Secondary Building Units

In order to simplify the zeolite structure description and systematically classify them, Meier[55] proposed a set of Secondary Building Units (SBU) from simple 4 or 6 MRs to sodalite cages. The large majority of zeolite structures are constructed by repeating the SBUs. There are presently 19 SBUs[56]. The way that SBUs are assembled determines the physical and chemical properties of the zeolite they form[56].

Breck proposed a structural zeolite classification system based on SBU's[56]. There are seven groups of Breck's family characterized by one kind of SBU that makes

up a zeolite. The seven SBUs groups proposed by Breck are shown schematically in Fig. 1.3. This classification simplifies comparisons in terms of adsorptive, molecular sieving and catalytic properties.

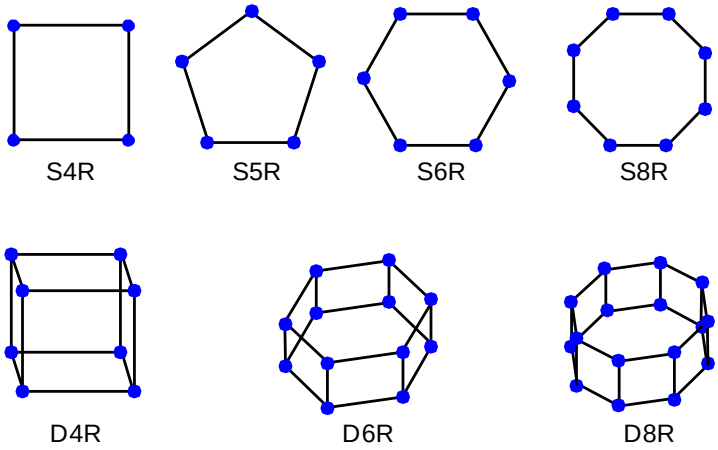

Figure 1.3: The seven Secondary Structure Units (SBU) groups proposed by Breck. Each line represents a bond T-O-T (S4R= Single 4 Member Ring; D4R= Double 4 MR, etc.) [53].

The entry to the channels and cavities inside a zeolite is through a $[T\text{-}O]_n$ ring, known as a window, where n is the number of tetrahedra in the window. The ring dimensions depend of the number of tetrahedra that constitute it. It limits the particle size that can access the channels and cavities refer to sieving effect.

Each structure is described by its own system of channels, cavities and their connectivity. Some zeolites have only one large cavity or cage, openings to cylindrical channels, which are interconnected in one, two or three dimensions[57].

Fig. 1.4 shows an example on how a zeolite is built up. First, the basic tetraedral units are joined between them. A small group of this tetrahedra form the SBU. The way to ensemble the SBU unit will build up the different zeolite network. For example, by joining the D4R, S6R and S8R will model the results in LTA-type zeolite.

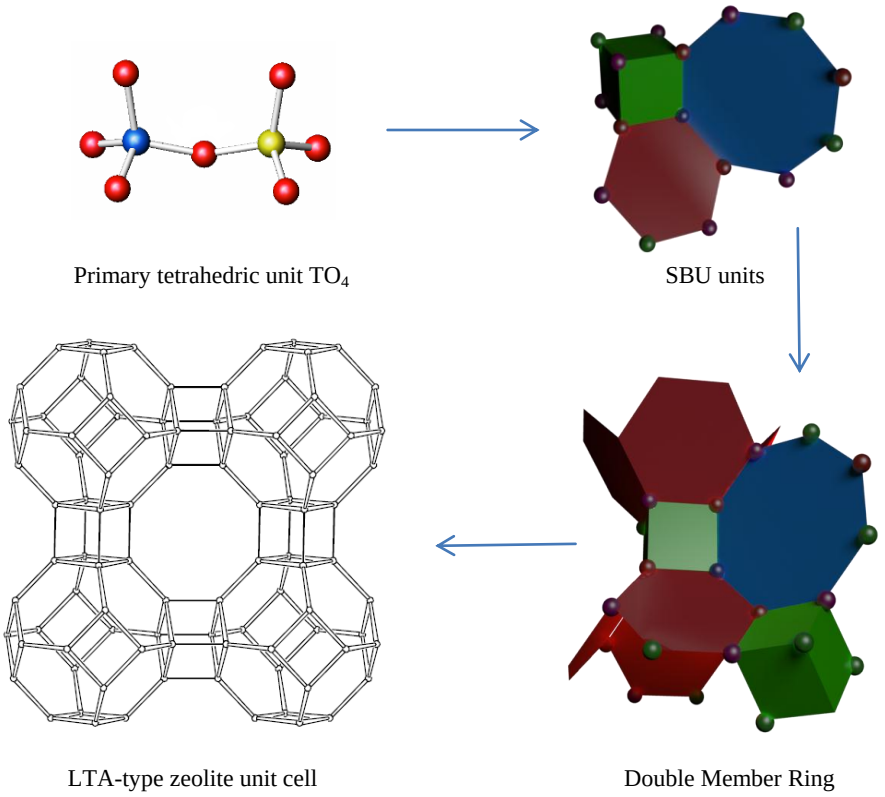

Figure 1.4: Building zeolite framework process from primary tetrahedric units TO_4 to unit cell.

Another way to classify zeolites takes into account their pore openings and the dimensionality of their channels. One distinguishes **small pore** zeolites, with 8 MR pores and diameter between 3 and 5 Å, such as CHA and LTA-type zeolite; **medium pore** zeolites with 10 MR and pore diameter between 5 and 6 Å such as ZSM-5; and **large pore** zeolites formed with 12 MR pore which diameter between 6 and 9 Å such as OFF and FAU-type zeolite. Recently, an **extra-large pore** zeolite category has been added with 14 MR pores and diameter higher that 9 Å, such as Cloverite or VPI-5 with 18MR[58-61].

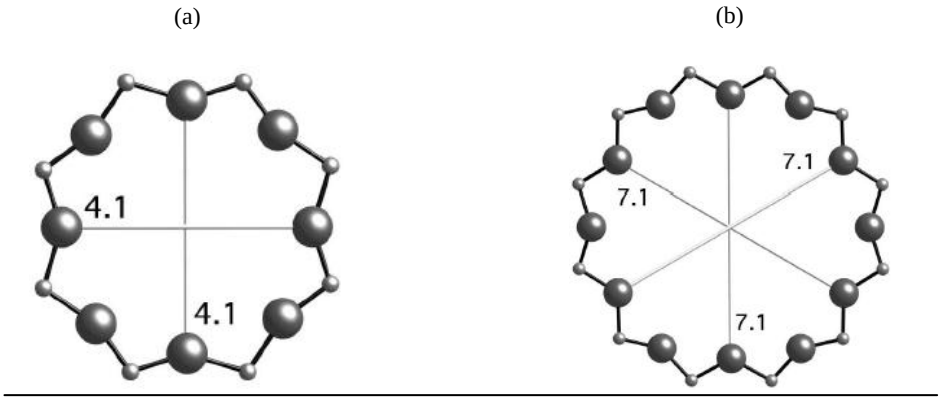

Figure 1.5: (a) LTA-4A zeolite pore, formed by 8MR. LTA-4A is a tridimensional structure has a small pore of 4.1 Å in the direction <100> of the plane. (b) Ring from Offretite (OFF) zeolite. OFF is a one-dimensional structure with the cavity in the direction (001) and a big pore of 7.1 Å, formed by 12 MR.

1.2.3 Properties

1.2.3.1 Adsorption

Zeolites are unique adsorbent materials, characterized by 20% to 50% void volumes and internal surface areas of several hundred thousand square meters per kilogram. The adsorption of guest molecules can occur on the outer surface of crystallites or on the inner surface of the micropores, depending on the geometry and dimensions of the molecules, and on the diameter of the pores of the zeolite in question. Molecules of kinetic diameter larger than the diameter of the pores cannot pass through the windows and enter the canal system, which is why zeolites are also known as molecular sieves. The molecular sieve property may be affected by dehydration and heat. Heating can produce distortions in the lattice and increase the void volume of the channels, while dehydration causes a cation interchange and subsequent changes in charge distribution inside the structure.

The size and shape of the channels in zeolites have extraordinary effects on the properties of these materials for adsorption processes. One of the most interesting

properties of zeolites, from the point of view of their possible applications, is their ability to adsorb certain molecules inside their structure. The adsorption of guest molecules can occur on the outer surface or on the inner surface of the micropores, depending on the geometry and dimensions of the molecules, and on the diameter of the pores of the zeolite in question.

Adsorption Selectivity depends largely on polarity of both adsorbent and adsorbate. In the case of zeolites, the parameter that governs the polarity is the Si/Al ratio. The polarity determines the molecules that can be adsorbed in the zeolite. For a low Si/Al ratio, the polarity increases and the zeolite is hydrophilic. Then, more polar molecules occupy the sites with high charge density within the lattice. Zeolites are used for the adsorption of a variety of materials. This includes applications in drying, purification and separation. They can remove water to very low partial pressures and are a very effective desiccant, capable of containing more than 25wt% water. They can also remove volatile organic chemicals from air streams, separate isomers and mixed gases. In particular zeolite LTA is used for separation of N_2 and CO_2 from air, taking advantage of the different polarities of the two types of molecules[53].

1.2.3.2 Catalyst

Further zeolites are studied as catalysts in chemical reactions. The main reason is for improvement in the activity and the selectivity. These are given by the confinement effect that occurs within the cavities and acid-base properties of the molecular sieve. The presence of acid sites on the network and the possibility to introduce new acid sites make zeolites excellent catalysts. Zeolites can also promote the emergence of catalytic reactions such as acid-base and metal-induced reactions. In addition, zeolites can be used as support for active metals or reagents, or as catalysts for selective catalytic acid both for the transition state selectivity and for the exclusion of competing reactants depending on the diameter of the molecule. They also have been used as oxidation catalysts. The reactions occur within the pores of the zeolite, which allow greater control of the product.

1.2.3.3 Ion exchange

Another interesting property of zeolites is their ability to exchange cations[53]. This property, known as ion exchange, allows them to be used as water softeners, detergents and soaps. Hydrated cations within the pores of the zeolite are weakly attached and ready to exchange with other cations when in an aqueous medium. The reason for that are the trivalent aluminium ions that cause an imbalance in the structure characterized by an excess of negative charges. To compensate this excess, zeolites incorporate cations such Na^+, K^+ and Ca^{2+} into structures[53]. These cations are easily interchangeable with others, which gives the zeolite a high ion exchange capacity. Through this exchange other metal cations can be introduced into the zeolite and thus modify their catalytic properties or molecular sieve properties. In general, by increasing the ratio of Al/Si, the exchange capacity of zeolites increases. Organic cations can also be introduced, for example in dye manufacturing[62].

1.2.4 Applications

The widespread use of zeolites is due to their unique adsorption, diffusion, and catalytic properties which, together with their pore size, allows perfect shape selectivity[63,64]. For several decades, natural zeolites have been used for the treatment of various diseases in animals and humans. One of the most important is the use of Clinoptilolite as adjuvant in cancer therapy[65,66].

The biggest advantage of zeolites is that their properties are easy modified for specific needs in many technological fields and environmental applications[67]. Due to their molecular sieve structure, zeolites can selectively adsorb components of gaseous or liquid mixtures according to their molecular size and the presence of non-framework cations[5,67,]. Most often, zeolites are used to make detergents, replacing the use of phosphates as water softening agents, since phosphates have irreversible adverse effects on lakes and rivers. The ion exchange property is currently exploited in detergents in aluminium-rich zeolites, such as LTA- and FAU-type. They are used primarily to reduce the severity of domestic and industrial water as tensoactives. This is one of the primary purposes

of LTA-type zeolites. For example, in detergents, ion exchange is performed by replacing the sodium ions of the zeolite LTA-4A by calcium and magnesium atoms in the water. It can also remove reactive ions even in contaminated water. Zeolite LTA-5A is usually used for the molten salt ion exchange[68]. The ion exchange property has also been used as fertilizer because it helps support mineral nutrition and moisture retention[52]. These zeolites have also been used for the separation and purification of radioisotopes of Cs and Sr[69].

From the point of view of industry, zeolites are the perfect material to be used for catalysis in green chemistry[9] due his high chemical and thermal stability. The vast majority of zeolites could be dehydrated and heated up to 1200 K without any alteration in their framework, which is an advantage for many industrial applications[5,70-72]. Zeolites offer a good control in the reaction selectivity that saves feed cost. They can be used at mild temperatures and pressures, reducing the operating cost. The use of zeolites also reduces waste stream, saving treatment cost.

Therefore, zeolites are considered as effective structures for the adsorption and selective separation of carbon dioxide[73], for the removal of carbon dioxide, water and sulphur compounds from natural gas streams[74] and hydrogen purification[75]. Zeolites are optimal ion-exchange beds for purification of drinking water[3,76] and environmental decontamination of heavy and radioactive metals[77-79]. Zeolites are also used in fertilizers to control pH and humidity [12] and they are an essential component of detergents[80,81] and construction materials such as asphalt and concrete[82,83]. They are also used to remove animal odors in animal sands[84], as thermal collectors and for adsorption refrigeration[85]. Zeolites play a major role in the petrochemical industry where they are used as catalysts in cracking and hydro-cracking of hydrocarbons[86-92]. As well, zeolites are used in gas separation processes of industrial interest [93] and remarkable separation effects can also be achieved by the interplay of mixture adsorption and mixture diffusion. Some examples of separation and purification processes where zeolites may be used are: separation of CO_2/CH_4 [94-103], H_2/CO_2 [94,97,104-106], N_2/CO_2 [94,97,100,107-109], H_2/N_2 [110,111], H_2/CH_4 [108,112], N_2/CH_4 [97,113] and water/alcohols[114-116].

To reduce time-consuming adsorption experiments, there is a clear need for molecular simulation techniques being able to model the adsorption and diffusion behaviour in these materials. Molecular simulations are currently a powerful tool to accurately predict adsorption[9,63] and diffusion[93,117] processes in zeolites.

1.3 Molecular Simulations

Molecular simulation methods play an important role in the study of the behaviour of microscopic and macroscopic processes. A well-designed computer simulation can predict thermodynamic properties and can be a substitute for experiments. Molecular simulation can also provide data that is inaccessible through experimental methods or when the experiment has components that are too dangerous or too expensive. At the same time, they offer the possibility to create hypothetical scenarios and to test theories. Computer simulations can also help to provide a molecular understanding of why the observed events occur.

The term "**molecular simulation**" refers to computational methods in which the molecular properties are explicitly taken into account. Molecular simulations provide a unified theoretical framework based on statistical mechanics to model the thermodynamic properties of a substance. For example, with molecular simulations we can compute the number of molecules that are absorbed into a surface pore at a given pressure, detect phase transitions or calculate solubilities.

A key ingredient for simulations is a **force field**. A force field is the set of equations with corresponding parameters that defines specific interactions between molecules in a system, *i.e.*, a description of how the molecules interact as a function of their positions. This determines the behaviour of the system as a whole. A force field is typically described in terms of parameters that are developed for a specific system, and different force fields should be used for different systems. Ideally, we would like to have a unique and transferable force field that can be used to obtein the properties of any system, regardless of the composition or conditions of the system.

1.3.1 Statistical Mechanics

Statistical mechanics is the study of the macroscopic behaviour of a system using the microscopic properties of its constituents. This theory allows us to study a compound with a large number of molecules (around 10^{24}), by examining the statistical properties of a much smaller system (ca. 10^4 particles). It provides a molecular level interpretation of thermodynamic quantities like free energy, entropy, heat or work. Using statistical mechanics we are able to understand and interpret the measurable macroscopic properties of materials in terms of the properties of their constituent particles and the interactions that they have with each other.

There are two fundamental postulates in statistical mechanics. The first one says that given an isolated system in equilibrium, each accessible microstate corresponding to the same total energy can be found with equal probability, *i.e.* a system in equilibrium does not have any preference for any of its microstates. The other postulate is so-called the Ergodic Hypothesis. This hypothesis, fundamental in statistical mechanics, postulates that if a system is in equilibrium, at any point in time the average thermodynamic properties remain constant. This hypothesis, supported by experimental evidence, enables the use of the statistical thermodynamics and, therefore, molecular simulation methods.

The workhorse of statistical mechanics is the **partition function** or in other words “the sum over all microstates”. This refers to a mathematical formula which expresses the statistical weight of all the phase space configurations of the system. If the partition function is known exactly, then all thermodynamic properties, such as the energy of the system, the chemical potential, the pressure, or the entropy, etc., can be determined from it. Usually, the partition function cannot be computed. Instead we can compute averages corresponding to a certain statistical ensemble.

1.4 Techniques

To address the calculation of thermophysical properties, two molecular simulation techniques are the most common: Monte Carlo and Molecular Dynamics. Bellow is presented a short overview of the simulation techniques. For a detailed description of these techniques we refer the reader to the text books by Allen and Tildesley[118], and Frenkel and Smit[119].

1.4.1 Monte Carlo

The Monte Carlo (MC) method is a technique for computing ensemble averages of macroscopic system properties, such as pressure, volume, temperature, etc. In the MC method, system configurations are generated with a probability proportional to their statistical weight. The weight of a configuration is proportional to Boltzmann factor ($P \propto \exp[-E / k_B T]$) in turns. This means that low energy configurations have a larger statistical weight on the average.

The algorithm introduced by Metropolis, Rosenbluth and Teller[120] in 1953 allows to generate the set of configurations according to a Markovian stochastic process. Starting from a certain configuration, a so-called trial move that changes the system state is performed. Depending on the energy difference and a random number, the new state is either rejected or accepted. The acceptance rule is constructed such as the probability that the system is in a certain configuration is proportional to its statistical weight.

The strength of the Monte Carlo method lies in its capability to calculate statistical averages without explicitly sampling the entire partition function. The capability to deal with complex variation in spatial and energetic variables is what makes Monte Carlo such an attractive method. It is used for simulating the behaviour of physical and mathematical systems in multiple scenarios such as: medical application like PET (Position Emission Tomography), SPECT (Single Photon Emission Computed Tomography), dosage calculations in radiotherapy,

X-ray characterization of sources and detectors[121,122], traffic flow[123], simulation of galactic formation[124], and financial and economic systems[125].

One of the shortcomings of the conventional Metropolis Monte Carlo method is that it is does not use any information about the energy landscape around the current configuration when generating trial moves. Often times, the trial move brings the system to regions of configuration space with high energy and the trial move is rejected. Therefore, MC techniques are usually applied with a bias to improve the sampling. Biased Monte Carlo methods have been used to improve sampling in many cases. The basic idea is to probe the configurations around the current one and to propose moves that are more likely to be accepted.

The Monte Carlo simulations described above are performed as follows:
Each configuration is generated from the previous type using randomly selected trial moves (translation, rotation, ...). The choice of trial moves is crucial for an adequate sampling of phase space. These trial moves can be sometimes quite unnatural, *e.g.*, switching the identity of two random molecules. The trial moves of rotation and traslation are used in all statistical ensembles. The trial move of insertion/deletion is used in the grand-canonical ensemble, as well as a "swap" trial move for exchange and replacement of molecules. There are other trial moves for flexible molecules such as regrowth. For more details on the use of the MC technique, we refer the reader to Ref 119.

1.4.2 Molecular Dynamics

The second important technique in molecular simulation is Molecular Dynamics (MD). The idea behind MD is to generate a representative trajectory of the system over time. To do so, one calculates the forces between the atoms explicitly and calculates how the system evolves in time using Newton's equations of motion. At each time step, the forces on the atoms are calculated and combined with their current positions and velocities to create new positions and velocities. The atoms are moved to their new positions, the forces updated and a new cycle begins. These dynamically generated states are averaged in time to

determine the system properties. A simulation must be carried out for a large number of time-steps to obtain reliable averages.

The starting conditions are the positions and the velocities of the constituent atoms. The velocities can be generated from a previous run or by using random numbers and later scaled to the desired temperature. The Maxwell-Boltzmann distribution is rapidly reached by molecular collisions typically within a few hundred time steps.

1.5 Simulation Applications

Often in simulations the purpose is to simulate the bulk behaviour of gases and liquids. Simply placing a number of molecules in a vacuum would produce a cluster that will have properties different from bulk finite size. It is therefore customary both in MC and MD to perform calculations with periodic boundary conditions. The cell containing the ensemble is then surrounded by replicas of itself.

The calculations of the thermodynamic properties studied in this thesis were performed using the Monte Carlo and Molecular Dynamic methods in the different ensembles described bellow. For a detailed description of the simulation algorithms used in the different ensembles, we refer the reader to Frenkel and Smit[119].

1.5.1 Canonical ensemble

In the canonical ensemble (*N*, *V*, *T*) the number of particles, *N*, the volume, *V* and the temperature, *T*, are held constant. In this ensemble the system is not thermally isolated, so the total energy will fluctuate. However, this variation is proportional to $N^{1/2}$.

The canonical ensemble (*N*, *V*, *T*) can be used for both MC and MD simulations. In this work, it has been used to study the diffusion properties in zeolites. The canonical ensemble is the most convenient ensemble for MC method, for using in MD we have to add an algorithm to keep the energy in the system constant. The algorithm is the so-called "thermostat" and there are several of these available in the literature. In this work we used the Nosé-Hoover thermostat implemented by Martyna *et al.*[126].

1.5.2 Grand-Canonical ensemble

The grand-canonical ensemble is used for open systems and denoted by (μ, *V*, *T*) ensemble. Here the number of particles, *N*, can fluctuate but the chemical potential μ, remains constant as well as the volume, *V*, and the temperature, *T*. To study the adsorption properties the grand-canonical ensemble is a natural choice. To compute this property we need to use non-physical trial moves, such as the insertion and deletion of particles, in order to change the number of particles in the system.

1.5.3 Microcanonical ensemble

In the microcanonical ensemble the energy, *E*, the volume, *V*, and the number of particles, *N*, are held constant in an isolated system, *i.e.* in a system which does not exchange particles or energy. Usually it is denoted by the (*N*, *V*, *E*) ensemble. Under these conditions, the only possible distribution is the one that places each system at the energy level *E*. This level will generally have degeneracy, so the system can be found in any of the states of identical energy. The microcanonical ensemble is the simplest ensemble for Molecular Dynamics. We used this ensemble in addition to canonical ensemble to calculate diffusion properties.

1.5.4 Gibbs ensemble

The Gibbs ensemble represents a system in thermal, chemical and mechanical equilibrium, where the temperature, *T*, the chemical potential, μ, and the

pressure, *P*, remain constants. Those are the thermodynamic requirements for phase coexistence. Therefore this ensemble is used to calculate the phase equilibrium behaviour directly. The application of Gibbs ensemble by simulation techniques was proposed at first time by Panagiotopoulos[127] to simulate the vapour-liquid equilibrium phase without presence of an interface.

We used this ensemble to represent two coexisting phases by two simulation boxes where *T*, μ, and *P* are the same for each box. One box represents the gas phase and the other one the liquid phase.

1.6 Models

The molecular models used to describe the interactions in a system could be established on two scales: quantum mechanics and classical mechanics.

1.6.1 Quantum mechanical models

The quantum mechanical models are based on solving Schrödinger´s equation ($H\Psi = E\Psi$) and allow the study of properties associated with the electron density of the system as this equation contains all the information of the system. There are several methods to solve Schrödinger equation. The simplest, but least accurate, is the Hartree-Fock model. The post Hartree-Fock methods, also called ab-initio methods, like Density Functional Theory (DFT), multi-configurationally self-consistent field theory (MCSCF) or Møller-Plesset perturbation theory (MP). These methods are very accurate but also very computationally expensive. Ab-initio methods do not depend on any empirical input, they rely only on the elementary quantum mechanical postulates.

In general, the quantum mechanical methods can be used only in small systems. They are limited to about 100 atoms on a supercomputer. Since the number of electron wave functions for a large system is too expensive to compute over an ensemble with quantum mechanical methods, we will only use classical

molecular mechanical methods to measure the thermodynamic properties of our system.

The quantum mechanical methods are often used to calculate parameters for classical force fields. They can calculate accurately the infrared spectra and then related with the bond stretching; bond bending and dispersion interactions; torsion and partial charges.

1.6.2 Molecular mechanics methods

The molecular mechanical methods are based on classical mechanics. These methods allow the study of materials at atomic level and determine the bulk properties through force fields, which are a set of potential functions and parameters. The potential functions define the interactions in a molecular system. These functions can be parameterised in a while variety of analytical forms to give the correct energies and forces. The parameters encompass optimal values of balance, such as distances, bond angles and force constants.

In the force field based approach the molecules are represented as a set of spheres of different sizes and masses, connected by springs of different lengths and spring continuously. The atoms interact through a series of forces like bond stretching, bond bend and dihedral torsion, and through interactions between non-bonded atoms such as van der Waals and electrostatic interactions. Those forces can be written in term of potential energy functions. Sometimes, more sophisticated functions such as improper torsions, hydrogen bonds, polarizability and cross terms are used.

The sum of the different contributions to the potential energy is the potential function:

$$U^{total} = U^{bond} + U^{bend} + U^{torsion} + U^{cross\ terms} + U^{non\text{-}bonded} \qquad (1.1)$$

A brief description of the potential energy terms is given below.

1.6.2.1 Bond Stretching

The bond stretching interaction describes the change of energy when a bond between atoms is enlarged or reduced in length. For molecules that do not deviate too much from their equilibrium positions Hooke law's is a reasonable choice for this potential. If this is not the case, other more accurate and computationally expensive potentials like the Morse potential, cubic potential or quadratic potential should be used. In this thesis the bond interaction is described using a harmonic potential:

$$U^{bond}(r_{AB}) = \frac{k_{AB}}{2}\left(r_{AB} - r_{AB}^{0}\right)^2, \tag{1.2}$$

where k_{AB} is the bond constant, r_{AB} is the vector position of interatomic distances and r_{AB}^{0} is the equilibrium position.

1.6.2.2 Bond Bending

The angular or bending interactions are described in a similar manner to the bond stretching terms, using a harmonic potential to describe this energy:

$$U^{bend}(\theta_{ABC}) = \frac{k_{ABC}}{2}\left(\theta_{ABC} - \theta_{ABC}^{0}\right)^2, \tag{1.3}$$

where k_{ABC} is the bend constant for the atoms ABC that form the angle θ_{ABC} and θ_{ABC}^{0} is the equilibrium angle.

1.6.2.3 Torsion interactions

Most of the intramolecular structure variations are due to the torsion interactions terms. However, these interactions are weaker than the bond stretching and bend bond interactions.

In a chain of atoms A-B-C-D the angle of twist or dihedral angle is defined as the angle between the plane containing the first three atoms (A, B and C) and the plane containing the last three atoms (B, C and D) of the chain. The value of this angle can vary between 0 and 180 degrees. The equation that describes torque is a harmonic cosine potential and it depends on the type of atoms B and C:

$$U^{torsion}(\phi_{ABCD}) = \omega_{ABCD}\left[1+\cos\left(n\phi_{ABCD}-\gamma\right)\right]. \qquad (1.4)$$

In this equation, ω_{ABCD} is the torsion barrier, n is the number of minimums presents (periodicity), ϕ_{ABCD} is the torsion angle formed by the atoms ABCD and γ is a phase factor.

1.6.2.4 Cross Terms

In addition to the classical interactions described above, sometimes it is necessary to include terms that reflect the coupling between the coordinates of different atoms in the framework. For example, when an angle consists of three atoms is reduced, the terminal atoms of this angle tend to move away from the central atom to reduce steric interactions between them, so the bond length will be larger and the angle value (angle bend) smaller.

The inclusion of interactions due to cross terms in force fields is important to reproduce the vibrational spectra and to properly compute the diffusion of molecules in zeolites, as detailed in chapter 3 and appendix A.

1.6.2.5 Non-bonded interactions

The non-bonded interaction term described how the molecules and atoms interrelate with each other through forces that are not due to chemical bonds. These interactions play an important role in determining the structure of adsorbed molecules and evaluation of their energies. Non-bonded interactions do not depend on whether the atoms are bonded with each other. We considered two

different sets of non-bonding interactions: van der Waals and electrostatic interactions.

i) van der Waals interactions

van der Waals interactions are due to the fluctuating densities of electrons surrounding atoms. When two atoms approach each other, the fluctuations become correlated. This correlation causes them to be attracted. This interaction is referred to *London dispersion* or *van der Waals dispersion*. Since this attraction is due to induced dipoles, it is dependent on the inverse sixth power of the distance.

If the two atoms approach closer than the sum of their two van der Waals radii, and the atoms are not capable of forming a new covalent bond, then they repel each other. This is due to electron cloud overlap. This repulsion is the so-called *Pauli repulsion* and it increases very rapidly as the distance between the atoms decreases. One of the most used expressions for this term is the Lennard-Jones (LJ) potential due to its computational advantage, but other potentials like Buckingham are used too.

The Lennard-Jones potential represents the behaviour of neutral molecules and atoms and only depends on particles coordinates. If we include the induce dipole term and the empirical repulsion term we obtain the Lennard-Jones 12-6 potential:

$$U_{vdW} = U_{LJ}(r_{ij}) = 4\varepsilon_{ij}\left[\left(\frac{\sigma_{ij}}{r_{ij}}\right)^{12} - \left(\frac{\sigma_{ij}}{r_{ij}}\right)^{6}\right]. \qquad (1.5)$$

The first term in the brackets represents an approximation to Pauli repulsion. The second one is the induced dipole term. That means that the force field is repulsive at short distances and attractive at long distances.

The parameters ε and σ are specific for every kind of atom and they must be known to carry out a molecular mechanic calculation. The parameter σ represents the distance between atoms at which attraction and repulsion is balanced to the total interaction energy equals zero. The parameter ε corresponds to the depth of the minimum energy and r_{ij} is the distance between particles *i* and *j*.

In zeolites, the interactions between same atoms species (framework-framework for flexible structures, adsorbate-adsorbate or cations-cations interactions), will be defined by reproducing the critical values and adsorption isotherm. The interactions between different atoms (adsorbent-adsorbate) are computed using the Lorentz-Berthelot mixing rules:

$$\varepsilon_{ij} = \sqrt{\varepsilon_{ii}\varepsilon_{jj}} \quad \text{and} \quad \sigma_{ij} = \frac{\sigma_{ii} + \sigma_{jj}}{2}. \tag{1.6}$$

ii) Electrostatics

The electrostatic interactions are written using the classical Coulomb potential:

$$U_{elec}(r_{ij}) = \frac{1}{4\pi\varepsilon_r\varepsilon_0}\frac{q_i q_j}{r_{ij}} \tag{1.7}$$

where ε_r is the electric constant of the medium where the charges are placed, ε_0 is the permittivity in the vacuum, q_i and q_j are the charges of the interacting atoms and r_{ij} the distance between the atoms *i* and *j*.

The van der Waals term and the electrostatic terms must be calculated carefully. Note that these interactions terms are zero only when the distance between atoms is infinite. As a consequence, all atoms in a finite system interact with each other, which has a large computational cost. The easiest way to solve this problem in the van der Waals interactions is to shift and integrate them beyond a certain distance between a pair of atoms. As the long range term rapidly decays, a cutoff ratio r_c is introduced to ignore the interaction at distances longer than r_c and

perform simulations computationally less expensive. Usually this value depends on the Lennard-Jones size parameter as $r_c \geq 2.5\sigma$. In our simulation the Lennard-Jones potential will be truncated and shifted at r_c =12 Å. The cutoff distance is chosen to be the half of our unit cell, this allow us to be consistent with *periodic boundary conditions*, to avoid "wall effects", and the *nearest image convection*[119] when the unit cell of the zeolite is replicated. In the nearest image convention when an atom leaves one simulation unit cell, one of its images comes into simulation unit cell in opposite side.

Electrostatic interactions are more difficult to calculate than the van der Waals interaction because the integral of the interaction potential over volume is diverging. The coulombic interactions are usually calculated using the Ewald sum method[118,119]. This methodology was introduced in 1921 as a technique to add long-range interactions between particles and their infinite periodic images[128].

1.7 Framework Models

1.7.1 Rigid Structure Model

To define the zeolite structure by molecular mechanics, most simulation studies are performed using the method proposed by Kiselev *et al.*[10]. In a Kiselev-type potential the atoms from the zeolite framework are fixed at their crystallographic position. In this model the potential energy is described just by the non-bonded term to define the interactions between the guest-host molecules:

$$U^{non-bonded} = U_{vdW} + U_{elec} = 4\varepsilon_{ij}\left[\left(\frac{\sigma_{ij}}{r_{ij}}\right)^{12} - \left(\frac{\sigma_{ij}}{r_{ij}}\right)^{6}\right] + \frac{1}{4\pi\varepsilon_0}\frac{q_i q_j}{r_{ij}}. \qquad (1.8)$$

1.7.2 Flexible Structure Model

Some thermodynamic properties could only be studied taking into account the flexibility of the framework, especially when the molecules of the adsorbate have diameters close to the size of the largest framework pore. The potential interaction that control the framework atoms movement are described by the sum of all the potential interactions, described in Appendix A. The influence of the framework flexibility and the values used for the energy constants, distances and angles are described in detail in chapter 3.

1.8 Molecular Models

Normally, in classical methods the non-host molecules are considered to be rigid molecules modelled as atoms or pseudo-atoms. The pseudo-atoms are a set of atoms considered to be the interaction centre of dispersive forces, with or without partial charge and with their own effective potentials.

1.8.1 Cations

The non-framework cations are moved freely through the zeolite structure. Due to the strong electrostatic interactions with the atoms of the framework, the cations are distributed around the oxygen atoms bonded with aluminium atoms. A detailed description of the non-framework calcium and sodium cations in LTA-type zeolite can be found in chapter 2. The cation localization will strongly depend on the host atom interactions, but also on the interactions with other cations and guest molecules.

These interactions are:

i) Interactions between cations

The non-bonded potential defines the interactions between cations. The van der Waals interaction is neglected due to the strong electrostatic interactions. The

cation charges, used to describe the Coulombic interactions (potentials), could be determined by experimental measurements or by fitting simulation to experimental data.

ii) Interactions between cation and host atoms

The non-bonded cation-host interactions are dominated by the oxygen host atoms with the cations through a Lennard-Jones potential. The electrostatic interactions between the host atoms and the cations are described by a Coulombic potential.

1.8.2 Adsorbate

There are two types of molecules that could be adsorbed in a zeolite: non-polar and polar molecules. In this thesis the **non-polar guest molecules** studied are lineal hydrocarbons, built up by covalently bonding carbon and hydrogen without functional groups.

Hydrocarbons are one of the molecules most studied both computationally and experimentally. This is due to the importance of this adsorbate in industry for energy sources, such as petroleum and its derivatives or natural gas. In the literature, we can find several flexible models to describe hydrocarbons[129-131]. In this work, the hydrocarbons are described following the Unit Atom (UA) approach proposed by Ryckaert and Ballemans[132]. In this model, the CH_x groups are considered as single pseudo-atoms. These pseudo-atoms are modelled with a single interaction centre, without charge and with their own effective potentials.

The interactions for hydrocarbons are modelled as follow:

i) Interactions between alkanes

The potential energy terms considered to described the alkane-alkane interactions, $U^{C\text{-}C}$, are:

$$U^{C\text{-}C} = U^{bond} + U^{bend} + U^{torsion} + U_{vdW}. \qquad (1.9)$$

Bond stretching and bond bending in the chain are described by Eq. (1.2) and (1.3) respectively, where the atoms A, B and C correspond to the pseudo-atoms CH_x.

For alkanes with free rotation as butane and pentane, the torsion energy equation described above, in Eq. (4), can be rewritten as:

$$U^{torsion}(\phi_{ABCD}) = \sum_{n=0}^{5} C_n \cos^n(\phi_{ABCD}) \qquad (1.10)$$

where C_n is the torsion constant for lineal hydrocarbons and ϕ_{ABCD} is the dihedral angle. For a detailed description of the constant values used, we refer the reader to chapter 2.

The non-bonded interactions between alkanes are described by Lennard-Jones potential following Eq. (1.5).

ii) Interaction between alkanes and framework atoms

To described the interaction between non-bonded atoms from the zeolite structure and the alkane pseudo-atoms, we take into account only the van der Waals interactions by a Lennard-Jones potential, as we consider the pseudo-atoms without charge.

The **polar guest molecules** studied in this thesis are modelled as rigid molecules, following the models proposed for CO_2[133,134], N_2[134,135] and O_2[136].

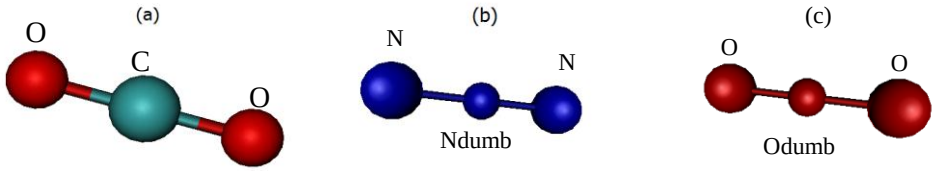

Figure 1.6: Schematic representation of the guest polar molecules. Carbon dioxide at left, nitrogen in the middle, and oxygen molecules at the right.

CO_2 molecules are modelled as three atoms with charge at the centre at each atom. The O_2 and N_2 molecules are modelled as two atoms with a dumbbell charge at the centre of mass of the molecules. A snapshot of these polar guest molecules is shown in Fig. 1.6.

The charges for these three polar molecules have been assigned to reproduce their molecular quadrupole. Therefore, the CO_2 molecule has a positive point charge of +0.6512 *e* for the carbon centre and a negative charge of -0.3256 *e* for each oxygen centre. The charges assigned for O_2 molecules are -0.112 *e* for the oxygen atoms and 0.224 *e* for the dumbbell point charge. The N_2 molecules have a negative point charge of -0.405 *e* for the nitrogen atoms and a positive point charge of 0.810 *e* at their centre of mass.

The interactions for polar molecules are modelled as follow:

i) Interactions between polar guest molecules

The energy of those interactions are described by the following potentials: Lennard-Jones and Coulombic. Their expression are given in Eq. (1.5), and (1.7), respectively.

The bond lenght for carbon-oxygen[137] (1.149 Å) is taken from experiments, while the interactions for the nitrogen-dumbbell[138] (1.1 Å) and oxygen-dumbbell[136] (1.2 Å) are taken from quantum mechanical calculations.

ii) Interactions between polar adsorbate and framework atoms or non-framework cations

The dispersion term in the non-bond interactions for adsorbed molecules are usually obtained by computer simulations of a Gibbs ensemble using Monte Carlo techniques. In this thesis, we fitted the Lennard-Jones parameters and reproduce the experimental vapour-liquid equilibrium (VLE) curve. For a MC simulation in a Gibbs ensemble, one define two boxes, one in the liquid phase and the other in the vapour phase. The number of particles, the volume, and the temperature in the total system are held constant while executing three MC trial

moves: particle displacement, volume exchange and particle exchange through the two boxes.

The Lennard-Jones parameters to reproduce the polar molecule interactions with the framework and non-framework atoms were fitted simultaneously. For a detailed explanation about the fitting procedure, we refer the reader to chapter 4.

1.9 Transferable Force Field

As previously stated, the force fields are the set of potential functions that define the properties in a system. For example, with molecular simulations we can know the number of molecules that are absorbed in a zeolite, detect transition or inflection points, and find the heat of adsorption or Henry coefficients.

Usually the parameters that define a force field are designed for a specific system and for each energetic term. In the vast majority of cases, the transfer of parameters and functions between different force fields is not possible because the parameters values are specific for a certain system, instead of being suitable for many different systems. In this work, we develop only transferable force fields. A force field is transferable if it can be extended to different systems, phases or configurations.

The development of force fields capable of reproducing adsorption and diffusion experiments [139-145] are vital to understanding adsorption and diffusion at the molecular scale. Molecular simulations critically rely on the availability of accurate force fields to describe the interactions between the guest molecules themselves and the zeolite hosts.

Several force fields are available to describe thermodynamic properties of light gases in all silica structures (zeolites without non-frameworks cations) [146-148] but most of them are only applicable to all-silica structures,[108,134,149-154] and thus, not transferable to other systems beyond those for which they were developed[155-157].

So far, less attention has been paid to interactions between polar guest molecules and the zeolite host. We will fill this gap by developing a new force field to reproduce thermodynamic properties of polar molecules such as quadrupolar gases.

Constructing a transferable force field for describing the adsorption of small molecules in zeolites is a very complex task that requires the simultaneous fitting of *all* force field parameters to an initial set of experimental data. The first difficulty is to choose an appropriate experimental data set because experimental measurements under the same conditions by different groups often provide different results[145,155,156,158]. To avoid the danger that the force field is only applicable for the conditions set by the experimental data to which it was fitted, it is crucial to have a set of control experiments that were not used in fitting the force field. These can be used to verify the quality and transferability of the obtained force field. The second difficulty is to apply a method to fit the force field parameters. It is important to note that all force field parameters have to be fitted simultaneously and that the number of parameters can be quite large. For example, for CO_2 adsorption in aluminosilicates with sodium non-framework cations we must fit nine parameters at the same time. Several methods have been proposed for fitting force field parameters[159-162]. All of them require a large number of iterations, and therefore, a large number of time-consuming molecular simulations. For example, constructing a force field for CO_2 adsorption in zeolites with sodium non-framework cations using the Simplex algorithm[159] required a total of 264 molecular simulations, each typically using 90 hours on a modern PC, resulting in almost 3 years of CPU time.

The development of accurate and transferable force fields is essential for the proper study of thermodynamic properties, for example, adsorption isotherms, where the zeolite structure is very sensitive to small differences in the parameters of the force field[141].

1.10 Properties Studied in Zeolite with Computer Methods

Computational methods, based on both classical and quantum approaches, have been widely used in the study of zeolite materials providing knowledge which has not been obtained by experimental studies.

Experimental studies of the position and the displacement of the molecules within the zeolite frameworks have required a periodic monocrystal (especially if they have long chains) inside the structure. Both conditions make them extremely difficult to perform because periodic monocrystal rarely occur in nature and are difficult to synthesize. Computational methods based on molecular mechanics model constitute an essential and complementary tool to study such problems. Having that in mind and with the models and techniques described above, we can study several properties of a system. We will focus on two of them: adsorption and diffusion.

1.10.1 Adsorption

Adsorption of a gas on a solid is the enrichment of molecules in an interfacial layer adjacent to a solid wall[163]. In the context of this thesis the solid wall refers to the inner surface of the zeolite pore accessible to gas molecules. The substance that is adsorbed is called adsorbate and the material taking on the adsorbate is the adsorbent. There are two kind of adsorption: *physisorption* or physical adsorption and *chemisorption* or chemical adsorption. The physical adsorption is a weak binding caused by van der Waals forces without a charge redistribution in the molecule and on the pore surface. There is no change in the chemical nature of the adsorbate in the physisorption. Chemical adsorption implies the creation of bonds and a change in the electron density between the adsorbent and the adsorbate. The nature of the link could be between ionic and covalent.

The adsorption phenomena are characterized experimentally by measuring adsorption isotherms which represent the amount of adsorbed molecules in the adsorbate as a function of gas pressure or liquid outside.

Monte Carlo techniques can be applied to understand the adsorption behaviour of molecules. In this work, we obtain the adsorption isotherms by performing simulations with the Monte Carlo method in the grand-canonical ensemble (GCMC). The number of adsorbed particles, N, varies during the simulation. The equilibrium conditions are obtained by setting the temperature, T, and chemical potential, μ, inside and outside of the gas to the same values.

In this work, the chemical potential is related to fugacity, f, through the Peng-Robinson equation of state:

$$\mu = \mu_0 + \mathrm{R}T \ln \frac{f}{f_0}, \tag{1.11}$$

where μ_0 is the reference chemical potential, R is the ideal gas constant and f_0 is a constant usually set at $f_0 = 1$. The fugacity and pressure of the system are related by the equation:

$$f = \varphi \cdot p. \tag{1.12}$$

The value of the fugacity coefficient φ follows from the equation of state of the gas phase, in which φ is the fugacity coefficient. For ideal gases, $\varphi = 1$. Non-ideal gases at pressures lower than 1 bar usually can be considered as ideal gases.

The results obtained in our simulations are represented by adsorption isotherms, which express the number of adsorbed molecules in the pore of the zeolite as a function of pressure.

The zeolite structure is modelled by a Kiselev-type potential[10,164], where the framework atoms are held rigid at the crystallographic position. The number of

atoms that make up the framework and the number of non-framework cations, which also remain constant, determines the density of the zeolite. For our simulations, we use the method of configurational-bias Monte Carlo (CBMC) for molecules constitute by several bonding atoms, like alkanes.

The simulations are generated by cycles, where the trial move for our study molecule is chosen randomly, ensuring the microscopic reversibility of the system. The possible trial moves are: translation, rotation around the centre of mass of the molecule, the addition or removal of a molecule and the growth of part or entire of the molecule, which is made by moving the newly formed molecule into a randomly chosen position.

The transactional maximum displacement and maximum rotation angle were adjusted such that on average with the acceptance probability of 50% were accepted.

1.10.2 Diffusion

Diffusion in liquids, gases and solids has been studied for decades. The discovery of Brownian motion helped to understand the atomic behaviour in solids and the kinetic theory of liquids and gases. Diffusion is an irreversible physical process that describes mass transport, which is due to thermal variations that cause collisions between molecules. Diffusion processes are encountered in various fields of physics and they are related to the collective movement of a large number of particles through a permeable medium. The phenomenon is stochastic at the microscopic level, as each particle undergoes an individual random walk process while colliding with its surroundings. A typical example is the mixing of gases or liquids initially separated from each other. The common feature to all diffusion processes is that the motion takes place, without a net external force, from a higher to a lower concentration.

In zeolites, the molecules diffuse through the channels and pores, where there exists a constant interaction between the diffusing molecules and the structure

components of the zeolite. Depending on the relation between the pore size of the lattice and the ratio of the guest molecules, different interactions between the adsorbate molecules and the wall lattice occur. Moreover, the movement is more affected by the size and the shape of the zeolite than by the concentration of the gas or the temperature. Therefore, several types of diffusion are used to describe those effects. All of them are equal at infinite dilution. In literature we can find a vast number of studies for the different types of diffusion in zeolites. [8,165-172].

In this thesis we will study two types of diffusion: The self-diffusion and the Maxwell-Stefan diffusion.

The ***self-diffusion*** takes place in a system in equilibrium and it is related to the motion of individual particles. The self-diffusion is usually studied in terms of self-diffusion constant *Ds* and could be caused by vacancies or by interstices, depending on whether the atoms take empty or interstitial positions in the lattice. Studying the self-diffusion by molecular dynamics simulations, we can observe the evolution of the system.

The self-diffusion coefficient is described by the Einstein relation:

$$D_s^{\alpha} = \lim_{t\to\infty} \frac{1}{2Nt} \left\langle \sum_{i=1}^{N} \left(r_{i\alpha}(t) - r_{i\alpha}(0) \right)^2 \right\rangle \tag{1.13}$$

where α = x, y, z is the direction which produces the mean square displacement (MSD), N is the number of molecules, t the time and $r_{i\alpha}$ the α-component of the centre of mass of molecule i.

Using molecular dynamic techniques in the microcanonical ensemble we calculate the self-diffusivity in every direction of the zeolite pore. The directional self-diffusion coefficient average is:

$$D_s = \frac{D_s^x + D_s^y + D_s^z}{3}. \tag{1.14}$$

Maxwell-Stefan (MS) diffusion or transport diffusion arises from velocity correlations between different particles. The mass transport is due to a gradient in the atomic concentration of components in the zeolite.

For a single component system adsorbed in a zeolite, the MS diffusivity directly follows from the trajectory of the molecules at equilibrium:

$$D_c^{\alpha} = \lim_{t\to\infty} \frac{1}{2Nt} \left\langle \left(\sum_{i=1}^{N} r_{i\alpha}(t) - r_{i\alpha}(0) \right)^2 \right\rangle . \qquad (1.15)$$

The directional Maxwell-Stefan diffusion coefficient is the average in any direction, as is described in Eq. 1.14.

The temperature is kept constant by adding the Nosé-Hoover algorithm, which extends the Lagrangian formulation of positions and velocities of the system at constant temperature in the canonical ensemble. The implementation of this algorithm was made according to the work of Martyna et al.[126] in which the dynamics remain reversible.

1.11 Outline and Scope of this Thesis

The main objective in this thesis is to use accurately and transferable force fields to reproduce experimental values of adsorption and diffusion of alkanes and quadrupolar gases in zeolites with cations. Those force fields have to take into account the nature and properties of the molecules involved in the adsorption and diffusion processes. This difficult task requires detailed knowledge on computational methods and simulation techniques. In order to acquire this knowledge to develop our force field, we will first use the available force fields to fill in some missing studies with hydrocarbons in zeolites with sodium and calcium non-framework cations.

The outline of this thesis is as follows:

In chapter 2, the relation between the light alkanes (methane, ethane, propane, butane and pentane) with different non-framework cation ratios is studied. We also investigate the influence of the structure in the adsorption and diffusion processes for zeolites with sodium and calcium non-framework cations.

Chapter 3 shows adsorption and diffusion results to study the flexibility of the framework structure. We based on force fields developed by Nicholas *et al.*[146] and Hill and Sauer[148]. We study the influence on diffusion in LTA-type zeolite, both with and without cations in methane.

The current knowledge we have about the adsorption of apolar molecules can be applied and extended to polar molecules. For this purpose we develop a transferable force field that accurately predicts the adsorption properties of CO_2 in zeolites with and without non-framework cations.

In chapter 4 we will show how to develop a force field that allow us to screen the carbon dioxide adsorption process for a wide range of zeolites.

We will study the main differences between various force fields on the diffusion processes of CO_2 in LTA-type zeolite in chapter 5. In this study, we will examine how the cation influences ton the diffusion process and provide an accurate model to describe the diffusion coefficient obtained with different force fields.

Finally, due to the computational cost of developing new force fields, we developed a method for fitting the force field parameters that requires less computational time. This is explained in chapter 6.

A final conclusion chapter will summarize the previous chapters on molecular simulation of adsorption and diffusion in zeolites with and without cations.

1.12 Bibliography

1 I. Hacking. *Representar e intervenir*. (Consejo Nacional de Ciencia y Tecnología, 1992).

2 S. Woolgar. *Ciencia: abriendo la caja negra*. (Anthropos, 1991).

3 S. B. Wang and Y. L. Peng. *Chemical Engineering Journal* **156**, 11-24 (2010).

4 J. Caro and M. Noack. *Microporous and Mesoporous Materials* **115**, 215-233 (2008).

5 J. Caro, M. Noack, P. Kolsch and R. Schafer. *Microporous and Mesoporous Materials* **38**, 3-24 (2000).

6 A. Corma. *Chemical Reviews* **97**, 2373-2419 (1997).

7 B. Smit and T. L. M. Maesen. *Nature* **451**, 671-678 (2008).

8 B. Smit and T. L. M. Maesen. *Chemical Reviews* **108**, 4125-4184 (2008).

9 M. Guisnet and J.-P. Gilson. *Zeolites for cleaner technologies*. Vol. 3 (Imperial College Press, 2002).

10 A. G. Bezus, A. V. Kiselev, A. A. Lopatkin and P. Q. Du. *Journal of the Chemical Society-Faraday Transactions II* **74**, 367-379 (1978).

11 A. F. Cronstedt. Svenska Vetenskaps Akademiens Handlingen Stockholm **18** (1756).

12 A. Dyer. *An Introduction to Zeolite Molecular Sieves*. (John Wiley & Sons Ltd., 1988).

13 C. Baerlocher and L. B. McCusker. *Database of Zeolite Structures: www.iza-structure.org/databases* (April 2011).

14 A. Damour. *Annales des Mines* **17**, 191-202 (1840).

15 G. W. Morey and F. E. Ingerson. *Economic Geology* **32**, 607-761 (1937).

16 M. H. de St. Claire-Deville. *Compt. Rend.* **54** (1862).

17 L. Pauling. Proceedings of the National Academy of Sciences of the United States of America **16**, 453-459 (1930).

18 L. Pauling and H. J.L. *Zeitschrift fuer Kristallographie* **74**, 546-551 (1930).

19 R. M. Barrer. Journal of the Chemical Society (Resumed), 2158-2163 (1948).

20 R. M. Barrer and D. W. Riley. *Journal of the Chemical Society (Resumed)*, 133-143 (1948).

21 H. van Bekkum, E. M. Flanigen, , P. A. Jacobs and J. J. C. *Studies in Surface Science and Catalysis*. Vol. 137 (Elsevier Science B. V, 20011).

22 D. S. Coombs *et al. European Journal of Mineralogy* **10**, 1037-1081 (1998).

23 D. S. Wragg, G. M. Fullerton, P. J. Byrne, A. M. Z. Slawin, J. E. Warren, S. J. Teat and R. E. Morris. *Dalton Transactions* **40**, 4926-4932 (2011).

24 S. T. Wilson, B. M. Lok, C. A. Messina, T. R. Cannan and E. M. Flanigen. *Journal of the American Chemical Society* **104**, 1146-1147 (1982).

25 B. M. Lok, C. A. Messina, R. L. Patton, R. T. Gajek, T. R. Cannan and E. M. Flanigen. *Journal of the American Chemical Society* **106**, 6092-6093 (1984).

26 M. E. Davis and R. F. Lobo. *Chemistry of Materials* **4**, 756-768 (1992).

27 J. Y. Ying, C. P. Mehnert and M. S. Wong. *Angewandte Chemie-International Edition* **38**, 56-77 (1999).

28 D. Y. Zhao, J. L. Feng, Q. S. Huo, N. Melosh, G. H. Fredrickson, B. F. Chmelka and G. D. Stucky. *Science* **279**, 548-552 (1998).

29 H. P. Lin and C. Y. Mou. *Science* **273**, 765-768 (1996).

30 C. G. Wu and T. Bein. *Science* **266**, 1013-1015 (1994).

31 A. Corma, M. Diaz-Cabanas, J. Martinez-Triguero, F. Rey and J. Rius. *Nature* **418**, 514-517 (2002).

32 A. Corma, M. J. Diaz-Cabanas and F. Rey. *Chemical Communications*, 1050-1051 (2003).

33 T. Blasco, A. Corma, M. J. Diaz-Cabanas, F. Rey, J. Rius, G. Sastre and J. A. Vidal-Moya. *Journal of the American Chemical Society* **126**, 13414-13423 (2004).

34 J. S. Beck et al. Journal of the American Chemical Society **114**, 10834-10843 (1992).

35 J. S. Beck, J. C. Vartuli, G. J. Kennedy, C. T. Kresge, W. J. Roth and S. E. Schramm. *Chemistry of Materials* **6**, 1816-1821 (1994).

36 S. S. Y. Chui, S. M. F. Lo, J. P. H. Charmant, A. G. Orpen and I. D. Williams. *Science* **283**, 1148-1150 (1999).

37 M. Fujita, J. Yazaki and K. Ogura. *Journal of the American Chemical Society* **112**, 5645-5647 (1990).

38 S. Kitagawa, R. Kitaura and S. Noro. *Angewandte Chemie-International Edition* **43**, 2334-2375 (2004).

39 S. Noro, R. Kitaura, M. Kondo, S. Kitagawa, T. Ishii, H. Matsuzaka and M. Yamashita. *Journal of the American Chemical Society* **124**, 2568-2583 (2002).

40 T. Kokubo, H. M. Kim and M. Kawashita. *Biomaterials* **24**, 2161-2175 (2003).

41 A. K. Cheetham, G. Ferey and T. Loiseau. *Angewandte Chemie-International Edition* **38**, 3268-3292 (1999).

42 T. Devic, C. Serre, N. Audebrand, J. Marrot and G. Ferey. *Journal of the American Chemical Society* **127**, 12788-12789 (2005).

43 T. Loiseau, C. Serre, C. Huguenard, G. Fink, F. Taulelle, M. Henry, T. Bataille and G. Ferey. *Chemistry-a European Journal* **10**, 1373-1382 (2004).

44 C. Serre *et al*. *Advanced Materials* **19**, 2246-+ (2007).

45 F. Salles, H. Jobic, A. Ghoufi, P. L. Llewellyn, C. Serre, S. Bourrelly, G. Ferey and G. Maurin. *Angewandte Chemie-International Edition* **48**, 8335-8339 (2009).

46 M. Eddaoudi, J. Kim, N. Rosi, D. Vodak, J. Wachter, M. O'Keeffe and O. M. Yaghi. *Science* **295**, 469-472 (2002).

47 N. L. Rosi, J. Eckert, M. Eddaoudi, D. T. Vodak, J. Kim, M. O'Keeffe and O. M. Yaghi. *Science* **300**, 1127-1129 (2003).

48 C. D. Wu, A. Hu, L. Zhang and W. B. Lin. *Journal of the American Chemical Society* **127**, 8940-8941 (2005).

49 O. M. Yaghi, C. E. Davis, G. M. Li and H. L. Li. *Journal of the American Chemical Society* **119**, 2861-2868 (1997).

50 O. M. Yaghi, G. M. Li and H. L. Li. *Nature* **378**, 703-706 (1995).

51 B. L. Chen, N. W. Ockwig, A. R. Millward, D. S. Contreras and O. M. Yaghi. *Angewandte Chemie-International Edition* **44**, 4745-4749 (2005).

52 J. W. McBain. *The Sorption of Gases and Vapors by Solids*. (Routleger and Sons, 1932).

53 D. W. Breck. *Zeolite Molecular Sieves*. (Wiley, 1974).

54 W. Loewenstein. *American Mineralogist* **39**, 92-96 (1954).

55 W. M. Meier. Zeitschrift fuer Kristallographie, Kristallgeometrie, Kristallphysik, Kristallchemie **115**, 439 (1961).

56 C. Baerlocher, W. M. Meier and D. H. Olson. *Atlas of Zeolite Structure Types*. Fifth edn, (Elsevier, 2001).

57 M. D. Allendorf, C. A. Bauer, R. K. Bhakta and R. J. T. Houk. *Chemical Society Reviews* **38**, 1330-1352 (2009).

58 C. C. Freyhardt, M. Tsapatsis, R. F. Lobo, J. K. Balkus Jr. and M. E. Davis. *Nature* **381**, 295-298 (1996).

59 M. A. Zwijnenburg, S. T. Bromley, J. C. Jansen and T. Maschmeyer. *Chemistry of Materials* **16**, 12-20 (2003).

60 M. Yoshikawa et al. The Journal of Physical Chemistry B **102**, 7139-7147 (1998).

61 E. G. Derouane. *Applied Catalysis* **51**, L13-L20 (1989).

62 G. Calzaferri. *Dye loaded zeolite material*. Universitaet Bern (Bern, CH), US 2008/0272338-A1 (2008).

63 J. Caro, M. Noack and P. Kolsch. Adsorption-Journal of the International Adsorption Society **11**, 215-227 (2005).

64 Y. Watanabe, H. Yamada, J. Tanaka, Y. Komatsu and Y. Moriyoshi. *Separation Science and Technology* **39**, 2091-2104 (2004).

65 K. Pavelic et al. Journal of Molecular Medicine **78**, 708-720 (2001).

66 N. Zarkovic, K. Zarkovic, M. Kralj, S. Borovic, S. Sabolovic, M. P. Blazi, A. Cipak and K. Pavelic. *Anticancer Research* **23**, 1589-1595 (2003).

67 T. Frising and P. Leflaive. *Microporous and Mesoporous Materials* **114**, 27-63 (2008).

68 M. Liquornik and Y. Marcus. *The Journal of Physical Chemistry* **75**, 2523-2525 (1971).

69 P. B. Weisz. *Chemtech*, 498-505 (1973).

70 T. Maesen, B. Marcus, E. M. F. P. A. J. H. van Bekkum and J. C. Jansen. in *Studies in Surface Science and Catalysis* Vol. Volume 137 1-9 (Elsevier, 2001).

71 M. A. Banares. *Catalysis Today* **51**, 319-348 (1999).

72 E. E. McLeary, J. C. Jansen and F. Kapteijn. *Microporous and Mesoporous Materials* **90**, 198-220 (2006).

73 K. M. Bonenfant D, Niquette P, et al. *Science and Technology of Advanced Materials* **9** (2008).

74 S. Reut and A. Prakash. *Fuel Processing Technology* **87**, 217-222 (2006).

75 J. Dong, Y. S. Lin, M. Kanezashi and Z. Tang. *Journal of Applied Physics* **104** (2008).

76 S. E. Bailey, T. J. Olin, R. M. Bricka and D. D. Adrian. *Water Research* **33**, 2469-2479 (1999).

77 S. Kesraouiouki, C. R. Cheeseman and R. Perry. *Journal of Chemical Technology and Biotechnology* **59**, 121-126 (1994).

78 S. K. Ouki and M. Kavannagh. *Waste Management & Research* **15**, 383-394 (1997).

79 V. Ramamurthy, J. V. Caspar, D. F. Eaton, E. W. Kuo and D. R. Corbin. *Journal of the American Chemical Society* **114**, 3882-3892 (1992).

80 H. Bauer, G. Schimmel and P. Jurges. *Tenside Surfactants Detergents* **36**, 225-229 (1999).

81 H. Koch, R. Beck and H. Roper. *Starch-Starke* **45**, 2-7 (1993).

82 B. Ahmadi and M. Shekarchi. *Cement & Concrete Composites* **32**, 134-141 (2010).

83 D. Fragoulis, E. Chaniotakis and M. G. Stamatakis. *Cement and Concrete Research* **27**, 889-905 (1997).

84 S. Tsengas. Animal litter, e.g. cat litter, comprises combination of filler and modified starch, Yucca schidigera to inhibit urease enzyme from converting urine to ammonia, and zeolite. US 7089882-B1 (2006).

85 B. Dawoud, E. H. Amer and D. M. Gross. *International Journal of Energy Research* **31**, 135-147 (2007).

86 A. Corma. *Chemical Reviews* **95**, 559-614 (1995).

87 T. L. M. Maesen, R. Krishna, J. M. van Baten, B. Smit, S. Calero and J. M. C. Sanchez. *Journal of Catalysis* **256**, 95-107 (2008).

88 M. Schenk, B. Smit, T. J. H. Vlugt and T. L. M. Maesen. *Angewandte Chemie-International Edition* **40**, 736-739 (2001).

89 M. Arruebo, J. L. Falconer and R. D. Noble. *Journal of Membrane Science* **269**, 171-176 (2006).

90 D. H. Park, S. S. Kim, H. Wang, T. J. Pinnavaia, M. C. Papapetrou, A. A. Lappas and K. S. Triantafyllidis. *Angewandte Chemie-International Edition* **48**, 7645-7648 (2009).

91 T. Koyama et al. Physical Chemistry Chemical Physics **12**, 2541-2554 (2010).

92 Z. W. Wang, G. Y. Jiang, Z. Zhao, X. Feng, A. J. Duan, J. Liu, C. M. Xu and J. S. Gao. *Energy & Fuels* **24**, 758-763 (2010).

93 F. Rezaei and P. Webley. *Separation and Purification Technology* **70**, 243-256 (2010).

94 R. Babarao and J. W. Jiang. *Journal of the American Chemical Society* **131**, 11417-11425 (2009).

95 R. Babarao and J. W. Jiang. *Langmuir* **24**, 5474-5484 (2008).

96 M. A. Carreon, S. G. Li, J. L. Falconer and R. D. Noble. *Journal of the American Chemical Society* **130**, 5412-+ (2008).

97 R. Krishna and J. M. van Baten. *Separation and Purification Technology* **61**, 414-423 (2008).

98 D. Saha, Z. B. Bao, F. Jia and S. G. Deng. *Environmental Science & Technology* **44**, 1820-1826 (2010).

99 Y. Y. Tian, L. L. Fan, Z. Y. Wang, S. L. Qiu and G. S. Zhu. *Journal of Materials Chemistry* **19**, 7698-7703 (2009).

100 S. G. Li, J. L. Falconer and R. D. Noble. *Microporous and Mesoporous Materials* **110**, 310-317 (2008).

101 M. Hong, S. Li, H. F. Funke, J. L. Falconer and R. D. Noble. *Microporous and Mesoporous Materials* **106**, 140-146 (2007).

102 S. Himeno, T. Tomita, K. Suzuki and S. Yoshida. *Microporous and Mesoporous Materials* **98**, 62-69 (2007).

103 P. G. Leyssale JM, Theodorou DN. *Journal of Physical Chemistry B* **110**, 22742-22753 (2006).

104 R. Krishna and J. M. van Baten. *Separation and Purification Technology* **60**, 315-320 (2008).

105 X. H. Gu, Z. Tang and J. H. Dong. *Microporous and Mesoporous Materials* **111**, 441-448 (2008).

106 S. K. Wirawan and D. Creaser. *Separation and Purification Technology* **52**, 224-231 (2006).

107 S. Himeno, M. Takenaka and S. Shimura. *Molecular Simulation* **34**, 1329-1336 (2008).

108 Li P. and F. H. Tezel. *Journal of Chemical and Engineering Data* **53**, 2479-2487 (2008).

109 R. Krishna, S. Li, J. M. van Baten, J. L. Falconer and R. D. Noble. *Separation and Purification Technology* **60**, 230-236 (2008).

110 O. Shekhah et al. Journal of the American Chemical Society **129**, 15118 (2007).

111 S. B. Liu, J. F. Wu, L. J. Ma, M. W. Lin and T. L. Chen. *Acs Symposium Series* **517**, 272-288 (1993).

112 M. Hong, S. G. Li, J. L. Falconer and R. D. Noble. *Journal of Membrane Science* **307**, 277-283 (2008).

113 R. Krishna and J. M. van Baten. *Chemical Physics Letters* **446**, 344-349 (2007).

114 J. Kuhn, J. M. Castillo-Sanchez, J. Gascon, S. Calero, D. Dubbeldam, T. J. H. Vlugt, F. Kapteijn and J. Gross. *Journal of Physical Chemistry C* **113**, 14290-14301 (2009).

115 J. Y. Wu, Q. L. Liu, Y. Xiong, A. M. Zhu and Y. Chen. *Journal of Physical Chemistry B* **113**, 4267-4274 (2009).

116 G. Rutkai, E. Csanyi and T. Kristof. *Microporous and Mesoporous Materials* **114**, 455-464 (2008).

117 L. P. Frising T. *Microporous and Mesoporous Materials* **114**, 27-63 (2008).

118 M. P. Allen and D. J. Tildesley. *Computer simulation of liquids*. (Clarendon, 1989).

119 D. Frenkel and B. Smit. Understanding Molecular Simulations: From Algorithms to Applications. Second edn, (Academic Press, 2002).

120 A. W. Rosenbluth, N. Metropolis and A. H. Teller. *Journal of Chemical Physics* **21**, 1087–1092 (1953).

121 L. Jonsson, M. Ljungberg and S. E. Strand. *Journal of Nuclear Medicine* **46**, 1679-1686 (2005).

122 H. Paganetti, H. Y. Jiang, K. Parodi, R. Slopsema and M. Engelsman. *Physics in Medicine and Biology* **53**, 4825-4853 (2008).

123 K.-H. Hoffmann and M. E. Schreiber. *Computational statistical physics: from billards to Monte Carlo*. Vol. XV (Springer, 2002).

124 P. Williams, & Nelson, A. *Astronomy & Astrophysics* **374**, 839-860 (2001).

125 P. Jäckel. *Monte Carlo Methods in Finance* (John Wiley, 2002).

126 G. J. Martyna, M. E. Tuckerman, D. J. Tobias and M. L. Klein. *Molecular Physics* **87**, 1117-1157 (1996).

127 A. Z. Panagiotopoulos. *Molecular Physics* **61(4)**, 813-826 (1987).

128 P. P. Ewald. *Annalen Der Physik* **64**, 253-287 (1921).

129 R. J. H. Vlugt, W. Zhu, J. Moulijn, B. Smit and R. Krishna. *Journal of the American Chemical Society* **120**, 5599-5600 (1998).

130 Z. M. Du, G. Manos, T. J. H. Vlugt and B. Smit. *AIChE Journal* **44**, 1756-1764 (1998).

131 M. D. Macedonia, D. D. Moore and E. J. Maginn. *Langmuir* **16**, 3823-3834 (2000).

132 J. P. Ryckaert and A. Bellemans. *Faraday Discussions*, 95-106 (1978).

133 J. G. Harris and K. H. Yung. *Journal of Physical Chemistry* **99(31)**, 12021-12024 (1995).

134 K. Makrodimitris, G. K. Papadopoulos and D. N. Theodorou. *Journal of Physical Chemistry B* **105**, 777-788 (2001).

135 C. S. Murthy, K. Singer, M. L. Klein and I. R. McDonald. *Molecular Physics* **41**, 1387-1399 (1980).

136 C. Mellot and J. Lignieres. *Molecular Simulation* **18**, 349-365 (1996).

137 R. D. Etters and B. Kuchta. *Journal of Chemical Physics* **90**, 4537-4541 (1989).

138 C. Murthy, , K. Singer, and I. McDonald. *Molecular Physics* **44**, 135-143 (1981).

139 D. Dubbeldam, S. Calero, T. L. M. Maesen and B. Smit. *Physical Review Letters* **90**, 245901 (2003).

140 D. Dubbeldam, S. Calero, T. J. H. Vlugt, R. Krishna, T. L. M. Maesen, E. Beerdsen and B. Smit. *Physical Review Letters* **93**, 088302 (2004).

141 D. Dubbeldam, S. Calero, T. J. H. Vlugt, R. Krishna, T. L. M. Maesen and B. Smit. *Journal of Physical Chemistry B* **108**, 12301-12313 (2004).

142 D. Dubbeldam, E. Beerdsen, S. Calero and B. Smit. *Proceedings of the National Academy of Sciences of the United States of America* **102**, 12317-12320 (2005).

143 S. Calero, D. Dubbeldam, R. Krishna, B. Smit, T. J. H. Vlugt, J. F. M. Denayer, J. A. Martens and T. L. M. Maesen. *Journal of the American Chemical Society* **126**, 11377-11386 (2004).

144 E. García-Pérez, D. Dubbeldam, T. L. M. Maesen and S. Calero. *Journal of Physical Chemistry B* **110**, 23968-23976 (2006).

145 A. García-Sánchez, C. O. Ania, J. B. Parra, D. Dubbeldam, T. J. H. Vlugt, R. Krishna and S. Calero. *Journal of Physical Chemistry C* **113**, 8814-8820 (2009).

146 J. B. Nicholas, A. J. Hopfinger, F. R. Trouw and L. E. Iton. *Journal of the American Chemical Society* **113**, 4792-4800 (1991).

147 J. R. Hill and J. Sauer. *Journal of Physical Chemistry* **98**, 1238-1244 (1994).

148 J. R. Hill and J. Sauer. *Journal of Physical Chemistry* **99**, 9536-9550 (1995).

149 A. Goj, D. S. Sholl, E. D. Akten and D. Kohen. *Journal of Physical Chemistry B* **106**, 8367-8375 (2002).

150 A. Hirotani *et al*. *Applied Surface Science* **120**, 81-84 (1997).

151 P. Demontis, G. B. Suffritti, S. Quartieri, E. S. Fois and A. Gamba. *Journal of Physical Chemistry* **92**, 867-871 (1988).

152 R. J. H. Vlugt, R. Krishna and B. Smit. *Journal of Physical Chemistry B* **103**, 1102-1118 (1999).

153 R. L. June, A. T. Bell and D. N. Theodorou. *Journal of Physical Chemistry* **96**, 1051-1060 (1992).

154 M. D. Macedonia and E. J. Maginn. *Fluid Phase Equilibria* **160**, 19-27 (1999).

155 E. D. Akten, R. Siriwardane and D. S. Sholl. *Energy & Fuels* **17**, 977-983 (2003).

156 E. Jaramillo and M. Chandross. *Journal of Physical Chemistry B* **108**, 20155-20159 (2004).

157 L. P. Maurin G, Bell RG. *Journal of Physical Chemistry B* **109**, 16084-16091 (2005).

158 H. Ahn, J. H. Moon, S. H. Hyun and C. H. Lee. *Adsorption-Journal of the International Adsorption Society* **10**, 111-128 (2004).

159 W. H. Press, Teukolsky, S. A., Vetterling, W. T., Flannery, B. P. *Numerical recipes in Fortran 77 : the art of scientific computing*. (Cambridge University Press, 2001).

160 M. Hulsmann, T. Koddermann, J. Vrabec and D. Reith. *Computer Physics Communications* **181**, 499-513 (2010).

161 P. Ungerer, C. Beauvais, J. Delhommelle, A. Boutin, B. Rousseau and A. H. Fuchs. *Journal of Chemical Physics* **112**, 5499-5510 (2000).

162 E. Bourasseau, M. Haboudou, A. Boutin, A. H. Fuchs and P. Ungerer. *Journal of Chemical Physics* **118**, 3020-3034 (2003).

163 K. S. W. Sing, D. H. Everett, R. A. W. Haul, L. Moscou, R. A. Pierotti, J. Rouquerol and T. Siemieniewska. *Pure and Applied Chemistry* **57**, 603-619 (1985).

164 A. H. Fuchs and A. K. Cheetham. *Journal of Physical Chemistry B* **105**, 7375-7383 (2001).

165 D. Dubbeldam and R. Q. Snurr. *Molecular Simulation* **33**, 305-325 (2007).

166 J. Karger, J. Caro and M. Bulow. Bulletin of the Academy of Sciences of the Ussr Division of Chemical Science **26**, 2464-2468 (1977).

167 J. Karger and H. Pfeifer. *Zeolites* **7**, 90-107 (1987).

168 J. Karger and D. M. Ruthven. in Progress in Zeolite and Microporous Materials, Pts a-C Vol. 105 Studies in Surface Science and Catalysis 1843-1850 (1997).

169 R. Krishna and J. A. Wesselingh. *Chemical Engineering Science* **52**, 861-911 (1997).

170 R. Krishna and J. M. van Baten. *Journal of Physical Chemistry B* **109**, 6386-6396 (2005).

171 E. Beerdsen, B. Smit and D. Dubbeldam. *Physical Review Letters* **93**, 248301 (2004).

172 A. Schuring, S. M. Auerbach, S. Fritzsche and R. Haberlandt. *Journal of Chemical Physics* **116**, 10890-10894 (2002).

Chapter 2

A Simulation Study of Alkanes in LTA-type Zeolites*

* This chapter is based on: A. García-Sánchez, E. García-Pérez, D. Dubbeldam, R. Krishna, and S. Calero: "A Simulation Study of Alkanes in Linde Type A Zeolites" *Adsorption Science & Technology*, **25**, 417-427 (2007).

ABSTRACT: Monte Carlo simulations were performed to study the adsorption and diffusion of small hydrocarbons in Linde Type A zeolites as a function of their calcium/sodium ratio. The diffusion studies were focused on methane whereas the adsorption simulations were performed from methane up to pentane. The results obtained showed that an increase in the number of cations in the structure (exchange of univalent sodium ions by divalent calcium ions) led to an increase in the adsorption of linear alkanes at low and medium pressure, but caused a decrease in adsorption at the highest pressures. An increase in the amount of cations favours molecular attraction and hence results in lower mobility. At higher cation loading the ions block the windows interconnecting the LTA cages, leading to a further decrease in diffusion. Methane self-diffusion coefficients obtained from our simulations were twice as high for the Linde Type 5A zeolite as for the Linde Type 4A zeolite. These results are consistent with previous experimental studies and provide a molecular picture of the influence of the zeolite type, the amount of cations contained and their location in the structure.

2.1 Introduction

Zeolites are crystalline aluminosilicates based on frameworks with well-defined channels and cavities. The structure consists of TO_4 (T = Si, Al) primary building units linked together by corner-sharing, forming bent oxygen bridges[1] The presence of Al atoms induces an electrical imbalance leading to a negatively charged framework that is compensated by additional cations. The inner surface of the zeolite can act as a catalyst and they are also widespread used as water softeners (by exchanging non-framework cations with those of a nearby solution), as drying agents (anhydrous activated zeolites with a high affinity for water), for environmental clean-up, and as molecular sieves in industrial separation processes[2].

Zeolites A (LTA, Linde Type A) are well-known representatives. They can crack chain paraffins to singly straight-chain products being the first zeolites used in shape selective catalysis in 1960[3]. They are also used as water softener in detergents and in horticulture, as drying agents and as adsorbents for air and hydrocarbon separations. Zeolite A was first prepared by Breck *et al*. in 1956[4,5] and the high silica LTA (ITQ-29) has only recently synthesised[6]. LTA-type zeolites are often synthesized in their sodium form and according to the rule of Löwenstein[7]. The sodium form shows a chemical composition of $Na_{96}Al_{96}Si_{96}O_{384}$ with a unit cell parameter of 24.555 Å, and space group *Fm* 3*c*[8].

The structure of LTA-type zeolite consists of a cubic array of α-cages (diameter $\approx$ 11.2 Å), interconnected through 8-membered oxygen windows of free effective diameter about 4.1 Å (although this may be reduced by the presence of an exchangeable cation). The LTA unit cell is formed by 8 α-cages, and each cage has 12 negative charges to be compensated by exchangeable cations. The effective size of the windows in Zeolite A can be modified by the correct choice of cations which partially block the pore windows. In such a way pore cross sections of 3 Å (K^+ exchanged form), 4 Å (Na^+ exchanged form), or 5 Å (Ca^{2+}/Na^+ form) can be produced. The Ca^{2+}/Na^+ form (Zeolite LTA-5A) is obtained by replacing the sodium with calcium cations in a post synthesis

exchange. The names LTA-3A, 4A and 5A do not originate, but fortuitously coincides with windows sizes of 3, 4, and 5 Å respectively.

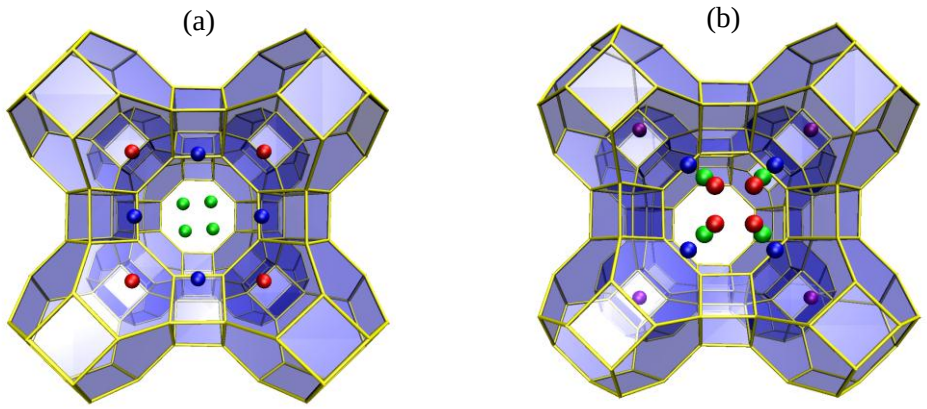

Figure 2.1: The Linde Type A zeolite framework contains three types of aluminosilicate rings that coordinate the cations. (a) Linde 4A has 12 sodiums per α-cage distributed among three crystallographic sites: eight in the centre of the six rings (positions in red), three in the eight ring window (positions in green), and one opposite to a four ring (positions in blue). (b) Linde 5A has four crystallographic sites for cations: the eight ring window (positions in red), the six ring window (positions in blue) and two more sites displaced into either the α-cage (positions in green) or the sodalite unit (positions in purple) from the centre of the six rings.

The Linde Type A framework contains three types of aluminosilicate rings that coordinate the cations as shown in Fig. 2.1. LTA-4A has 12 sodiums per α-cage distributed among three crystallographic sites [see Fig.2.1(a)]: eight in the centre of the six ring, three in the eight ring window, and one opposite to a four ring[8]. In Linde 5A four crystallographic sites are considered [see Fig. 2.1(b)]: the eight ring window, the six ring window, and two more sites displaced into either the α-cage or the sodalite unit from the centre of the six rings. In the calcium form all six doubly charged cations are coordinated to 6-rings and not to 8-rings[9]. The preference of the cations to coordinate 6-rings is also observed in the mixed Ca^{2+}/Na^{+} form[10].

The distribution of the cations influences has a significant influence on the adsorption and diffusion properties of zeolite A. Simulation studies on these systems can provide a better understanding of the effect of the Ca^{2+}/Na^{+} ratio,

thereby leading to the control of molecular adsorption and diffusion in LTA-type zeolites through tuning the Ca^{2+}/Na^{+} ratio. A variety of simulation studies have undertaken for the *pure silica* structure on adsorption and diffusion[11-24], but only a few papers have reported simulations of adsorption in LTA-4A and LTA-5A with sodium and calcium cations[25-27] and we are not aware of simulations studies of diffusion in these systems.

In the present chapter we provide new insights on the effect that the Ca^{2+}/Na^{+} ratio exerts on the adsorption and diffusion of hydrocarbons in LTA-4A and LTA-5A. The remainder of the paper is organized as follows: in Section 2.2 we present our simulation methods, including descriptions of the force fields used in this work. We continue in Section 2.3 with the simulations results and finally in section 2.4 we give some concluding remarks.

2.2 Methods

2.2.1 Zeolite Model

The Linde Type A framework was constructed from silicon, aluminium, and oxygen using the crystallographic positions of Pluth and Smith[8]. The Si/Al-ratio is exactly one, leading to an alternating arrangement of Si and Al atoms (the Löwenstein rule forbids Al–O–Al linkages). Simulations were performed for 10 structures by varying the cation ratio: $96Na^{+}/0Ca^{2+}$, $80Na^{+}/8Ca^{2+}$, $72Na^{+}/12Ca^{2+}$, $56Na^{+}/20Ca^{2+}$, $48Na^{+}/24Ca^{2+}$, $38Na^{+}/29Ca^{2+}$, $32Na^{+}/32Ca^{2+}$, $24Na^{+}/36Ca^{2+}$, $4Na^{+}/46Ca^{2+}$, together with the pure silica structure with $0Na^{+}/0Ca^{2+}$. The Na-O and Ca-O interactions were calibrated to reproduce the experimentally known positions in LTA-4A and LTA-5A (Fig. 1.1), employing the charges $q_{Na} = +1$, and $q_{Ca} = +2$. In addition, the crystallographic locations of the sites obtained through molecular simulations are within 0.2 Å from those obtained through X-ray diffraction[26,28]. The charge distribution on the oxygen framework was considered static; i.e., polarization of oxygen by nearby cations was neglected. We use a model that explicitly distinguishes silicon from aluminium with a

difference of 0.3 e^- between q_{Si} and q_{Al}[29], considering different charges for oxygen atoms bridging two silicon atoms, q_{OSi}, and oxygen atoms bridging one silicon and one aluminium atom, q_{OAl}. All partial charges are listed in Table 2.1. The exchangeable cation density is adjusted to match the framework aluminium density, and the density of the zeolite is determined by the framework atoms (aluminium, silicon, and oxygen) and the cations (sodium and calcium). In our model, the cations could move freely and adjust their position depending on their interactions with the framework atoms, other cations, and alkane molecules. The simulations were performed using one unit cell with eight α-cages. Test-simulations using eight unit cells gave identical results but were deemed too computational expensive to use with the Ewald summation for all the simulations.

	O_{Si}	O_{Al}	Si	Al	Na^+	Ca^{2+}	CH_4	CH_3	CH_2
CH_4	115 3.47	115 3.47	-	-	582 2.72	590 2.56	158.5 3.72	130.84 3.74	94.21 3.84
CH_3	93.2 3.48	93.2 3.48	-	-	443 2.65	400 2.6	130.84 3.74	108 3.76	77.7 3.86
CH_2	60.5 3.58	60.5 3.58	-	-	310 2.95	440 2.8	94.21 3.84	77.7 3.86	56.0 3.96
Na^+	23.0 3.4	23.0 3.4	-	-	-	-	582 2.72	443 2.65	310 2.95
Ca^{2+}	18.0 3.45	18.0 3.45	-	-	-	-	590 2.56	400 2.6	440 2.8
Charge [e^-]	q=-1.025	q=-1.2	q=+2.05		q=+1.75	q=+1.0	q=+2.0	--	-

Table 2.1: Lennard-Jones parameters used in this study: ε/k_B (K) in the top-left corner, σ (Å) in the bottom-right corner of each field, partial charges (e^-) of the framework, sodium, and calcium are also included. All values have been taken from our previous works[24,26,28,30].

2.2.2 Interatomic potentials

A realistic description of the interaction between the sodium and calcium cations, the zeolite framework, and the alkanes is employed. The interactions between guest molecules (alkanes and cations) with the zeolite host framework were modelled by Lennard-Jones and Coulombic potentials[26,28,30,31]. All the used parameters are listed in Table 1. The Coulombic interactions in the system were calculated using Ewald summations[32]. In our simulations, the convergence parameter was chosen as 0.3 with k = 9 wave vectors for high accuracy. The alkanes were described with a united atom model, in which CH_x groups were considered as a single interaction centres with their own effective potentials[33]. The beads in the chain were connected by harmonic bonding potentials. The bond-bending between three neighbouring beads was modelled by a harmonic cosine bending potential, and changes in the torsional angle were controlled by a Ryckaert-Bellemans potential. The beads in a chain separated by more than three bonds interacted with each other through a Lennard-Jones potential. The silicon van der Waals interactions were taken into account through an effective potential with only the oxygen atoms of the zeolite[34-36] and an "average" polarization was included implicitly in the parameterization by means of the polarization induced by the cation on the zeolite and by the cation on the alkanes[28]. It should be noted that effective Lennard-Jones potentials implicitly includes, in an average sense, many-body interactions (polarization), the contributions arising from instantaneous dipole-quadrupole and quadrupole-quadrupole interactions, flexibility of the framework, etc. The flexibility of the framework has a minor effect for small alkanes[37].

2.2.3 Simulation Techniques

The adsorption isotherms of alkanes were computed using Configurational Bias Monte Carlo (CBMC) simulations in the grand-canonical ensemble[32]. In CBMC simulations, molecules are grown segment by segment, avoiding overlap. For each segment, a set of trial orientations is generated. One of the trial positions is selected according to the Boltzmann weight of the zeolite energy, and this

selected trial orientation is added to the chain. The procedure is repeated until the entire molecule has been grown. The rules for acceptance or rejection of a grown molecule are chosen in a way that they exactly remove the bias caused by this growing scheme. A simulation are performed in cycles and in each cycle one move is chosen at random with a fixed probability of performing a molecule displacement (0.15), rotation around the centre of mass (0.15), exchange with the reservoir (0.55), and partial regrowth of a molecule (0.15). The maximum translational and rotational displacements are adjusted to achieve an acceptance probability of 50%. The number of cycles for methane and ethane was $2 \cdot 10^7$ and at least $3 \cdot 10^7$ for propane, butane and pentane. The total number of cations remains constant during simulations. To sample cation motions, we used displacements and insertions at new randomly selected positions that bypass energy barriers.

Self-diffusion coefficients were computed using MD simulations. In MD simulations successive configurations of the system are generated by integrating Newton's laws of motion, which then yields a trajectory that describes the positions, velocities and accelerations of the particles as they vary with time. The Verlet integration scheme with a time-step of 0.5 fs was used providing a relative energy drift smaller than 10^{-4}. Simulations were performed using the NVT ensemble. Simulations using the NVE ensemble gave equivalent results. More details can be found in reference[38]. The self-diffusion coefficients are computed by taking the slope of the mean-squared displacement at long times[12,39].

2.3 Results and Discussion

The effect of exchanged cations on the adsorption and diffusion behaviour of alkanes in Linde Type A zeolites has also been studied. This behaviour is strongly dependent on the amount and distribution of the sodium and calcium cations in the structure. Adsorption isotherms were computed for methane [Fig. 2.2(a)], ethane [Fig. 2.2(b)], propane [Fig. 2.2(c)], butane [Fig. 2.3(a)], and pentane [Fig. 2.3(b)] at 273 K in LTA-type structures where the amounts of

calcium and sodium cations were varied. Available experimental data at that temperature are included for comparison.

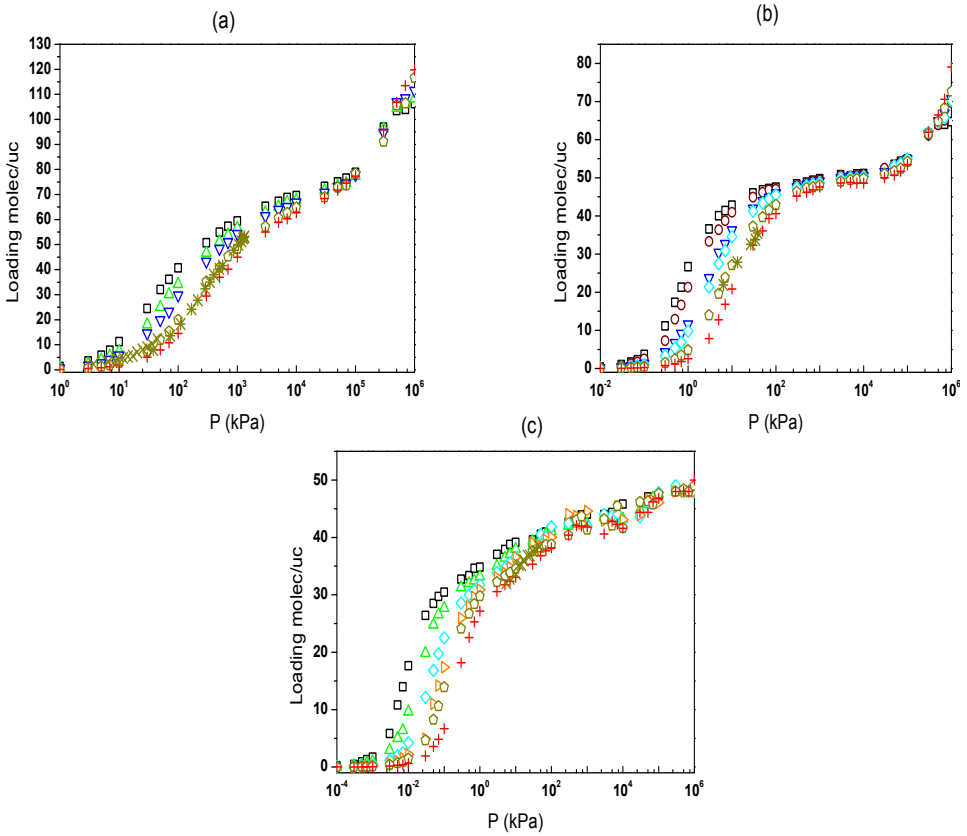

Figure 2.2: Adsorption isotherms of (a) methane, (b) ethane, and (c) propane at 273 K in Linde Type A zeolites. (□) $96Na^{+}/0Ca^{2+}$; (○) $80Na^{+}/8Ca^{2+}$; (△) $72Na^{+}/12Ca^{2+}$; (⬠) $56Na^{+}/20Ca^{2+}$; (◇) $48Na^{+}/24Ca^{2+}$; (▷) $32Na^{+}/32Ca^{2+}$; (▽) $24\ Na^{+}/36Ca^{2+}$, and (+) $4\ Na^{+}/46Ca^{2+}$. Experimental data for the structure $24Na^{+}/36Ca^{2+}$ are included for comparison[40,41]. (×) Ruthven at 273 K; (∗) Loughlin at 273-275 K.

The effect of exchanged cations on the adsorption and diffusion behaviour of alkanes in Linde Type A zeolites has also been studied. This behaviour is strongly dependent on the amount and distribution of the sodium and calcium cations in the structure. Adsorption isotherms were computed for methane [Fig. 2.2(a)], ethane [Fig. 2.2(b)], propane [Fig. 2.2(c)], butane [Fig. 2.3(a)], and pentane [Fig. 2.3(b)] at 273 K in LTA-type structures where the amounts of

calcium and sodium cations were varied. Available experimental data at that temperature are included for comparison.

Although much scatter exists between the experimental data of various authors, the experimental data are in overall very good agreement with our previous simulations for methane up to octadecane[40,41]. Our simulations show that the lowest adsorption corresponds to the lowest density of cations ($46Na^{+}/4Ca^{2+}$), and the highest adsorption corresponds to the highest density of cations ($96Na^{+}/0Ca^{2+}$). Adsorption follows the opposite behaviour at high pressures; with the saturation capacities are roughly independent of the amount of exchanged cations. The adsorption isotherm for the pure silica structure were also computed showing that (1) the pressure necessary to attain a particular loading in the structure in the absence of cations was up to three orders of magnitude higher than that necessary for the structure containing cations and (2) the saturation loading in the pure silica structure was similar to those obtained with structures containing cations.

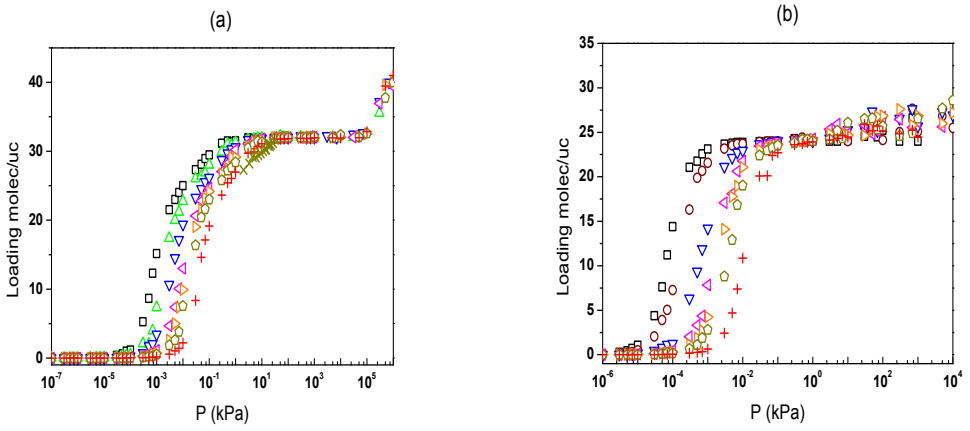

Figure 2.3: Adsorption isotherms of **(a)** butane and **(b)** pentane at 273 K in Linde Type A zeolites. (□) $96Na^{+}/0Ca^{2+}$; (○) $80Na^{+}/8Ca^{2+}$; (△) $72Na^{+}/12Ca^{2+}$; (◁) $38Na^{+}/20Ca^{2+}$; (▷) $32Na^{+}/32Ca^{2+}$; (⬠) $24Na^{+}/36Ca^{2+}$, and (+) $4\ Na^{+}/46Ca^{2+}$. Experimental data for the structure $36Ca^{2+}/24Na^{+}$ are included for comparative purpose[40]: **(×)** Ruthven at 273 K..

The explanation for this behaviour is that the cations create additional adsorption sites and also occupy free volume. The first effect dominates at low and

intermediate loadings in zeolite A. We also computed the void fraction of a structure with and without cations ($32Na^{+}/32Ca^{2+}$) probed with a helium atom and found that the excluded volume effect is small. Thus, the void fractions were 0.39 and 0.38 for the structure devoid of cations and the cation loaded structure, respectively. Note that the sodalite cages were blocked for helium, but not for cations. The cations are not randomly located in the cages, but are well-ordered and "buried" inside the six-membered rings for the $32Na^{+}/32Ca^{2+}$ structure. We would like to highlight that both, the cation density and the cation location are vital factors during the adsorption and the diffusion of alkanes in the structure. Differences up to three orders of magnitude in adsorption were also observed in our previous studies in all silica and sodium faujasites[28] (another type of cage-like zeolites), where we also demonstrated that the mobility of cations is indispensable to allowing a correct reproduction of the adsorption of alkanes in aluminosilicates. The use of frozen cations leads to an over-estimation of the adsorption at low pressures and an under-estimate the adsorption at high pressures.

The explanation for this behaviour is that the cations create additional adsorption sites and also occupy free volume. The first effect dominates at low and intermediate loadings in zeolite A. We also computed the void fraction of a structure with and without cations ($32Na^{+}/32Ca^{2+}$) probed with a helium atom and found that the excluded volume effect is small. Thus, the void fractions were 0.39 and 0.38 for the structure devoid of cations and the cation loaded structure, respectively. Note that the sodalite cages were blocked for helium, but not for cations. The cations are not randomly located in the cages, but are well-ordered and "buried" inside the six-membered rings for the $32Na^{+}/32Ca^{2+}$ structure. We would like to highlight that both, the cation density and the cation location are vital factors during the adsorption and the diffusion of alkanes in the structure. Differences up to three orders of magnitude in adsorption were also observed in our previous studies in all silica and sodium faujasites[28] (another type of cage-like zeolites), where we also demonstrated that the mobility of cations is indispensable to allowing a correct reproduction of the adsorption of alkanes in aluminosilicates. The use of frozen cations leads to an over-estimation of the

adsorption at low pressures and an under-estimate the adsorption at high pressures.

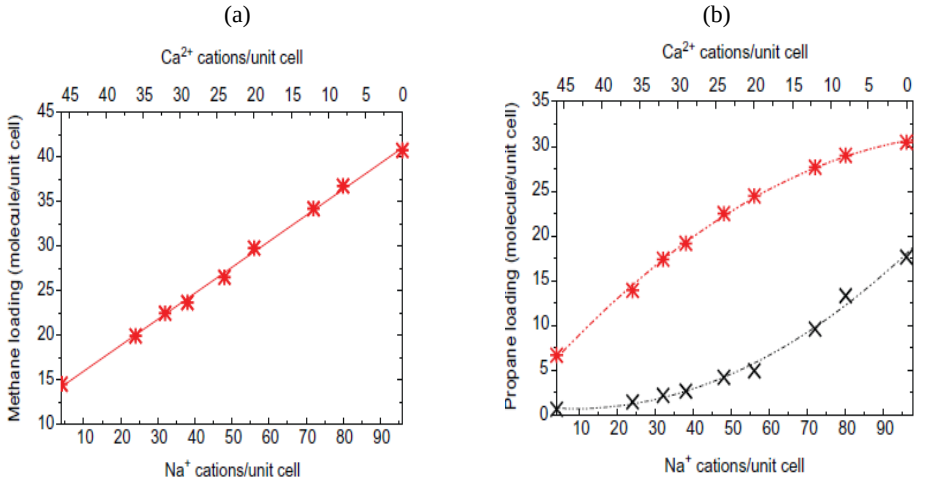

Figure 2.4: Amount of alkane adsorbed as a function of the sodium and calcium density (a) methane at 10^{2} kPa, (b) propane at 10^{-2} kPa (×), and 10^{-1} kPa (*).

Fig. 2.4 plots adsorption of methane and propane as a function of the sodium and calcium density at a given pressure. Fig. 2.4(a) shows that at 100 kPa the adsorption of methane and the density of sodium or calcium cations in the structure are linearly dependent. However, this linearity is not conserved at lower pressures where the trend becomes polynomial. The adsorption of propane as a function of cation density also proves polynomial behaviour at several pressures as shown in Fig. 2.4(b) for 0.01 and 0.1 kPa. We have observed similar trends for ethane, butane, and pentane.

The adsorption of alkanes in the zeolite is found to influence the location of the non-framework cations even at low loadings. Fig. 2.1(b) depicts the four crystallographic sites for the cations in empty zeolite LTA-5A (without molecules adsorbed on it). Site 1 in the six ring window, sites 2 and 3 displaced into either the α-cage or the sodalite unit from the centre of the six rings, and site 4 in the eight ring window. Crystallographic studies indicate that cations in LTA-5A are only near to the six rings (sites 1, 2, and 3) and not near to the 8 rings[9].

This is in agreement with our simulations that yield occupations of 87.7% (site 1), 3.3% (site 2) and 9% (site 3).

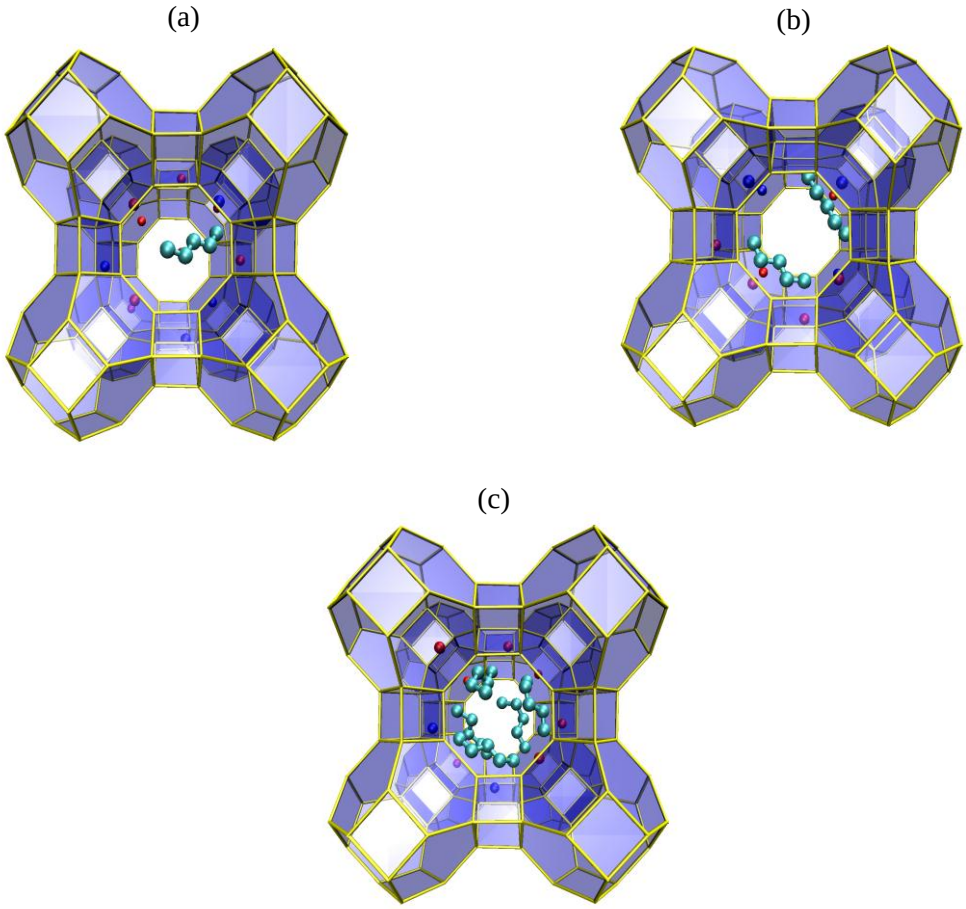

Figure 2.5: Snapshots of the adsorption of pentane in $48Na^{+}/24Ca^{2+}$ LTA-5A zeolite at 273 K and **(a)** 1 kPa, **(b)** 10^3 kPa, and **(c)** 10^6 kPa.

The adsorption isotherms of methane, ethane, propane, butane, and pentane have also been compared, and the resulting simulation data for $48Na^{+}/24Ca^{2+}$ LTA-5A are shown in Fig. 2.6. Adsorption of 2 molecules per α-cage (16 molecules/uc) requires a pressure of 0.002 kPa for pentane, 0.01 kPa for butane, 0.05 kPa for

propane, 2 kPa for ethane and 50 kPa for methane and at around 10^3 kPa every α-cage adsorbs in average 3, 4, 5, 6 and 7 molecules of C_5, C_4, C_3, C_2, and C_1, respectively.

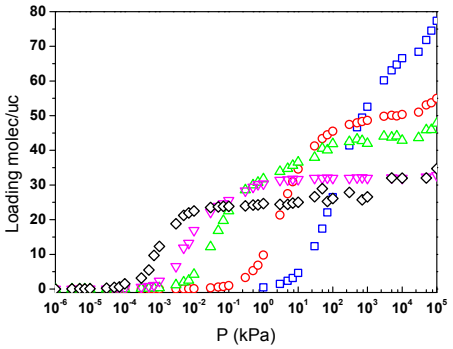

Figure 2.6: Adsorption isotherms of (□) methane; (○) ethane; (△) propane; (▽), butane and (◇) pentane in $24Na^+/36Ca^{2+}$ LTA-5A zeolite at 273 K.

The diffusion coefficients of methane have been computed from the slope of the mean-squared displacement at long times in silica, LTA-5A ($32Na^+/32Ca^{2+}$) and LTA-4A ($96Na^+/0Ca^{2+}$). The 96 molecules of methane per unit cell at 500 K and the cations in LTA-5A and LTA-4A were considered as being initially located in the crystallographic positions[8,9]. The computed values for the diffusion coefficients were $2.9 \cdot 10^{-11}$ m^2/s for the *pure silica* structure $2.4 \cdot 10^{-11}$ m^2/s for $32Na^+/32Ca^{2+}$ LTA-5A, and ca. $3 \cdot 10^{-14}$ m^2/s for $96Na^+/0Ca^{2+}$ zeolite LTA-4A.

Diffusion coefficients are much lower in zeolite LTA-4A than in LTA-5A due to the distribution of the cations. Diffusive hopping processes take place through the 8-rings windows. In zeolite LTA-5A none of the windows are blocked by a cation, with a free diameter of the window of 5 Å. Zeolite LTA-4A contains 12 sodium cations per α-cage and all the windows are occupied with a cation, reducing the effective size to 4 Å. To show the influence of the cations, we performed additional simulations by placing the sodium and calcium cations at random starting positions in the $32Na^+/32Ca^{2+}$ LTA-5A. These simulations provided a diffusion coefficient of $1.1 \cdot 10^{-11}$ m^2/s, which is clear indication that part of the windows were blocked by the randomly located cations.

2.4 Conclusions

We have performed a computational study of the effect of exchanged sodium and calcium cations on the adsorption and diffusion of alkanes in Linde Type A zeolites. We have demonstrated that the density and the location of cations induce marked variations in the alkane properties, and also that the adsorption of alkanes in the zeolite induces relocations of the cations in the structure even at low loadings. During adsorption, the increase of the number of exchanged cations leads to higher loadings at low pressures and to lower loadings at high pressures. Diffusion is mostly influenced by the spatial distribution of the cation. It is slower in LTA-4A than in LTA-5A zeolite, since the eight-ring windows are partially blocked in the former and completely unoccupied in the later.

2.5 Bibliography

1 W. M. Meier, D. H. Olson and C. Baerlocher. Zeolites 17, 1-229 (1996).

2 M. Guisnet and J.-P. Gilson. Zeolites for cleaner technologies. Vol. 3 (Imperial College Press, 2002).

3 N. Y. Chen, W. E. Garwood and F. G. Dwyer. Shape Selective Catalysis in industrial applications. 2nd edn, (Marcel Dekker Inc., 1996).

4 D. W. Breck, W. G. Eversole, R. M. Milton, T. B. Reed and T. L. Thomas. Journal of the American Chemical Society 78, 5963-5971 (1956).

5 T. B. Reed and D. W. Breck. Journal of the American Chemical Society 78, 5972-5977 (1956).

6 A. Corma, F. Rey, J. Rius, M. J. Sabater and S. Valencia. Nature 431, 287-290 (2004).

7 W. Loewenstein. American Mineralogist 39, 92-96 (1954).

8 J. J. Pluth and J. V. Smith. Journal of the American Chemical Society 102, 4704-4708 (1980).

9 J. J. Pluth and J. V. Smith. Journal of the American Chemical Society 105, 1192-1195 (1983).

10 R. L. Firor and K. Seff. Journal of the American Chemical Society 100, 3091-3096 (1978).

11 S. P. Bates, W. J. M. van Well, R. A. van Santen and B. Smit. Journal of the American Chemical Society 118, 6753-6759 (1996).

12 D. Dubbeldam, E. Beerdsen, S. Calero and B. Smit. Journal of Physical Chemistry B 110, 3164-3172 (2006).

13 D. Dubbeldam and B. Smit. Journal of Physical Chemistry B 107, 12138-12152 (2003).

14 S. Fritzsche, M. Gaub, R. Haberlandt and G. Hofmann. Journal of Molecular Modeling 2, 286-292 (1996).

15 S. Fritzsche, R. Haberlandt, J. Karger, H. Pfeifer and M. Waldherrteschner. in Zeolites and Related Microporous Materials: State of the Art 1994 Vol. 84 Studies in Surface Science and Catalysis 2139-2146 (1994).

16 S. Fritzsche, R. Haberlandt and M. Wolfsberg. Chemical Physics 253, 283-294 (2000).

17 S. Fritzsche, M. Wolfsberg, R. Haberlandt, P. Demontis, G. B. Suffritti and A. Tilocca. Chemical Physics Letters 296, 253-258 (1998).

18 T. L. M. Maesen, E. Beerdsen, S. Calero, D. Dubbeldam and B. Smit. Journal of Catalysis 237, 278-290 (2006).

19 C. Tunca and D. M. Ford. Chemical Engineering Science 58, 3373-3383 (2003).

20 A. Schuring, S. M. Auerbach, S. Fritzsche and R. Haberlandt. in Recent Advances in the Science and Technology of Zeolites and Related Materials, Pts a - C Vol. 154 Studies in Surface Science and Catalysis 2110-2117 (2004).

21 A. Schuring, S. M. Auerbach, S. Fritzsche and R. Haberlandt. Journal of Chemical Physics 116, 10890-10894 (2002).

22 E. Beerdsen, D. Dubbeldam and B. Smit. Journal of Physical Chemistry B 110, 22754-22772 (2006).

23 E. Beerdsen, D. Dubbeldam and B. Smit. Physical Review Letters 96, 44501 (2006).

24 E. Beerdsen, B. Smit and D. Dubbeldam. Physical Review Letters 93, 248301 (2004).

25 E. Jaramillo and M. Chandross. Journal of Physical Chemistry B 108, 20155-20159 (2004).

26 E. García-Pérez, D. Dubbeldam, T. L. M. Maesen and S. Calero. Journal of Physical Chemistry B 110, 23968-23976 (2006).

27 I. Daems, G. V. Baron, S. Punnathanam, R. Q. Snurr and J. F. M. Denayer. Journal of Physical Chemistry C 111, 2191-2197 (2007).

28 S. Calero, D. Dubbeldam, R. Krishna, B. Smit, T. J. H. Vlugt, J. F. M. Denayer, J. A. Martens and T. L. M. Maesen. Journal of the American Chemical Society 126, 11377-11386 (2004).

29 E. Jaramillo and S. M. Auerbach. Journal of Physical Chemistry B 103, 9589-9594 (1999).

30 D. Dubbeldam, S. Calero, T. J. H. Vlugt, R. Krishna, T. L. M. Maesen and B. Smit. Journal of Physical Chemistry B 108, 12301-12313 (2004).

31 D. Dubbeldam, S. Calero, T. J. H. Vlugt, R. Krishna, T. L. M. Maesen, E. Beerdsen and B. Smit. Physical Review Letters 93, 088302 (2004).

32 D. Frenkel and B. Smit. Understanding Molecular Simulations: From Algorithms to Applications. Second edn, (Academic Press, 2002).

33 J. P. Ryckaert and A. Bellemans. Faraday Discussions, 95-106 (1978).

34 A. G. Bezus, A. V. Kiselev, A. A. Lopatkin and P. Q. Du. Journal of the Chemical Society-Faraday Transactions II 74, 367-379 (1978).

35 A. V. Kiselev, A. A. Lopatkin and A. A. Shulga. Zeolites 5, 261-267 (1985).

36 R. J. H. Vlugt, R. Krishna and B. Smit. Journal of Physical Chemistry B 103, 1102-1118 (1999).

37 T. J. H. Vlugt and M. Schenk. Journal of Physical Chemistry B 106, 12757-12763 (2002).

38 D. Dubbeldam, E. Beerdsen, S. Calero and B. Smit. Proceedings of the National Academy of Sciences of the United States of America 102, 12317-12320 (2005).

39 D. Dubbeldam, E. Beerdsen, T. J. H. Vlugt and B. Smit. Journal of Chemical Physics 122, 224712 (2005).

40 D. M. Ruthven and K. F. Loughlin. J. Chem. Soc., Faraday Trans. I 68, 696 (1972).

41 K. F. Loughlin, M. A. Hasanain and H. B. Abdulrehman. Industrial & Engineering Chemistry Research 29, 1535-1546 (1990).

Chapter 3

Modelling Adsorption and Self-Diffusion of Methane in LTA-type Zeolites: Influence of Framework Flexibility*

* This chapter is based on: A. García-Sánchez, D. Dubbeldam, and S. Calero: "Modeling Adsorption and Self-Diffusion of Methane in LTA Zeolites: The Influence of Framework Flexibility". *Journal of Physical Chemistry C* **114**, 15068-15074 (2010).

ABSTRACT: The influence of framework flexibility on the adsorption and diffusion of methane in LTA zeolites was investigated by Monte Carlo and molecular dynamics simulations. In particular, we analysed the framework flexibility of the pure silica structure (ITQ-29), the sodium form (LTA-4A), and the sodium/calcium form (LTA-5A). Simulations were performed at different temperatures and for different methane loadings. We found that the framework flexibility affects differently adsorption and diffusion of methane. The effect that flexibility exerts on adsorption is quite small. However, the influence on diffusion seems to be much larger and strongly dependent on three factors: the density and type of the non-framework cations located in the LTA zeolite, the loading of methane in the structure, and, most importantly, the force field parameters used to model the framework.

3.1. Introduction

Zeolites are widely used as adsorbents, molecular sieves, ion exchangers or catalysts in a number of significant industrial processes. The performance of these processes is highly determined by the diffusion rates of the hydrocarbon molecules in the zeolite pores. Molecular simulation of diffusion has become a powerful tool to study the details of the diffusive processes of simple molecules adsorbed in the micropores of zeolites and is essential to understand the role of the framework structure and dynamics of these complex systems. From a simulation point of view, computing diffusion coefficients is challenging, and several reviews on this topic have been published recently[1-3]. The first simulation studies for diffusion in confined systems focused on self-diffusivities calculations for a single component using equilibrium Molecular Dynamics (MD) simulations[4]. Most recently, the increase of computer power made it possible to extend those calculations for obtaining diffusivities over loading providing insights into the mechanisms that control the molecular traffic along the zeolite pores[5-7]. Earlier diffusion studies in zeolites date back to the 1970s[8], and they have been increasing in complexity over the years. In the 1990s, simulation methods were applied to compute molecular diffusion at infinite dilution in MFI[9-11] and FAU[12-14]. These studies were later extended to other complex topologies such as LTA, LTL, ERI, and CHA not only for infinite dilution, but also for low, medium, and high loadings[15-20].

Most molecular simulation studies in zeolites are performed using the Kiselev-type potentials, where the zeolite atoms are held rigid at the crystallographic positions[21]. However, some authors have also investigated the effect of flexibility, using a variety of potentials for the framework atoms[22-25] and testing the accuracy and viability by comparison of the computed adsorption[26,27], diffusion[28,29], IR spectra[22,23,27], or structural parameters[24,25] with experimental data.

Rigid-framework simulations provide predictions of equilibrium adsorption which are in good agreement with experimental data or show low differences from results obtained with flexible-framework models[30-36]. However, diffusion coefficients are found to be strongly dependent on the flexibility of the framework[37-40], though, in some special cases, this influence seems to be cancelled out by opposite effects induced by model[38]. Rigid-framework simulations have proved to be accurate for molecules smaller than the smallest pore aperture, though the assumption of a rigid framework can introduce significant errors when applied to molecules with diameters close to the size of the largest framework pore[19,22,41-43]. In most of these studies the flexible lattices can enhance the diffusion coefficients, but still most simulations of diffusion are carried out using rigid frameworks.

Previous simulation studies on the influence of lattice flexibility in diffusion of hydrocarbons and other non-polar molecules were performed in pure silica zeolites. Most of these studies used the model proposed by Demontis et al[22,26,29], though several works suggested that, for diffusion of methane in MFI and cation-free LTA, there are substantial discrepancies depending on the flexibility model chosen[41].

In this chapter, we study adsorption and self-diffusion of methane in Linde-type A zeolites. We have taken into account the flexibility of the framework structure to study the effect on diffusion in LTA both with and without cations. In order to understand the flexible lattice influence we have chosen the models of Nicholas *et al.*[23] and Hill and Sauer[25]. We performed simulations using these flexible models as well as rigid frameworks for all zeolites studied. The structures chosen were LTA-4A, LTA-5A, ITQ-29 and hypothetical pure silica LTA (e.g., LTA-4A without ions and all aluminium replaced by silicon). We compare our simulations results with available experimental and simulation data from the literature. Experimental diffusivities of methane in LTA-5A at several temperatures were measure using the neutron spin echo (NSE) technique by Jobic *et al.*[44]. Heink *et al.* measured self-diffusion of methane for LTA-5A with different calcium contents[45,46] by pulse field gradient nuclear magnetic resonance spectroscopy. Most recently, Reyes *et al.*[47] and Corma *et al.*[48] used the same

technique to obtain self-diffusivity of methane in cation-free LTA[47]. With the aid of molecular dynamics, Fritzsche *et al*. computed self-diffusion of methane in a cation-free LTA and also taking into account the polarization interaction on exchangeable cations in the structure[49-51]. To our knowledge the only values of self-diffusivity of methane in flexible LTA were reported by Demontis *et al*.[52] for the cation-free structure. In this chapter, we compare these values with the results obtained using more complex flexible models, and we extend the study to structures with sodium and calcium cations. In addition, we performed molecular simulations of adsorption to prove the consistency of the results obtained with the flexible models chosen, comparing them to those obtained using a rigid framework structure.

3.2. Models and Simulation Details

Adsorption isotherms and self-diffusivity of methane were computed in rigid and flexible LTA-type zeolites containing 96 sodium cations per unit cell (LTA-4A), 32 sodium and 32 cations per unit cell (LTA-5A) and all silica structures (ITQ-29 and LTA_{si}). The adsorption isotherms were obtained from Monte Carlo (MC) simulations in the Grand Canonical ensemble (GCMC) where volume, temperature, and chemical potential were kept constant. The number of adsorbed molecules was changed during the simulation and the total number of cations remains constant. To sample cation motions, we used displacements and insertions at new randomly selected positions that bypass energy barriers[30].

Self-diffusion coefficients were calculated using Molecular Dynamics (MD) simulations. In MD simulations, successive configurations of the system are generated by integrating Newton's laws of motion, which then yields a trajectory that describes the positions, velocities and accelerations of the particles as they vary with time. The equations of motion were integrated using the velocity-Verlet algorithm. For methane diffusion in rigid zeolite, we used an integration time step of 0.01 fs and 0.005 fs when we consider the flexible structures, to

ensure satisfactory energy conservation during nanoseconds runs. Calculations were performed using NVT ensemble for rigid and flexible structures at 500 K. The self-diffusion coefficients are computed by taking the slope of the mean-squared displacement at extended times[16,19].

Zeolite LTA-4A, was synthesized at first time by Breck et al[53]. This zeolite present a cubic crystal structure, space group *Fm*3*c*, and $a = b = c = 24.555$ Å. The unit cell composition is $Na_{96}Si_{96}Al_{96}O_{384}$. The structure consists of an arrangement of sodalite units placed at the vertices of a simple cubic lattice and linked to each other by oxygen bridges. The central cavity formed by eight sodalite cages is called an α-cage. This cage is inaccessible to, for example, alkanes. Each α-cage is connected to six other α-cages in an octahedral way, forming what is called a β-cage, and the interconnection is via the eight-member ring by windows of about 4.2 Å diameter. One unit cell of this zeolite consists of eight α-cages and its diameter is about 11.4 Å. The unit cell of LTA-4A zeolite has three types of oxygen rings; eight-, six-, and four-membered rings. The charge compensating non-framework sodium cations are distributed over the surface of the α-cage. The cations occupy three distinct positions detected by X-ray diffraction[54]. Eight of them are Na I type cations and are located at the centre of 6-member ring corresponding to the window between the sodalite cage and the β-cage. Three sodium cations are near the centre of the 8-member ring that constitutes the window between two β-cages; those cations are called Na type II; and one Na III type cation is inside the cage in front of the 4-membered connecting two sodalite cages. Cations on site Na II will partially block the aperture of the β-cage's window and the adsorbed molecules cannot diffuse into the interior of this zeolite.

Zeolite LTA-5A is obtained by replacing 64 sodium monovalent cations from the LTA-4A by 32 bivalent calcium ions in an exchange after synthesis. These cations are preferentially located in four crystallographic positions: in the window formed by 8-membered ring; in the window of the 6-membered ring; displaced inside α-cage; or in the sodalites displaced into the centre of 6-membered ring. In this structure there are no cations blocking the windows of the 8-member ring[55]. A snapshot of LTA-5A structure is shown in Fig. 3.1.

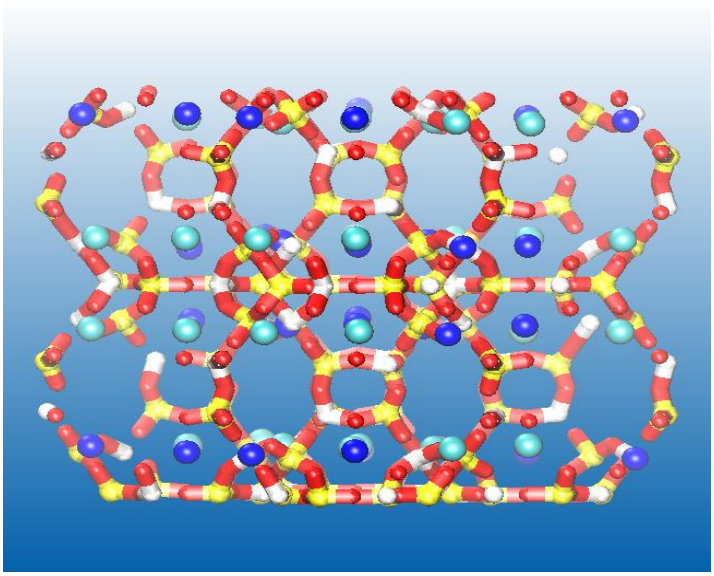

Figure 3.1: Snapshot of LTA-5A zeolite. The oxygen framework atoms are represented in red, silicon in yellow and aluminium in white. The sodium non-framework cations are shown in light blue and calcium in dark blue.

We also performed simulations in two all silica LTA-type structures; the hypothetical model obtained from the LTA-5A structure dealuminized, labelled as LTA_{si} in this work, and the silica stable form ITQ-29 obtained by Corma *et al.*[56]. The ITQ-29 topology is a simple cubic cell with space group *Fm*3*c*, and $a = b = c = 11.867$ Å. The crystallographic unit cell is 8 times smaller than LTA-5A, but with the same type of channels and cages. LTA-4A consists of a three-dimensional interconnected channel system. This structure has the 8 large spherical α-cages of approximately 11.4 Å interconnected via windows of about 4.2 Å in diameter and β-cages with an average diameter of 6.6 Å alternating with the α-cages and separated by 2.2 Å openings. We use a single unit cell for the simulations in LTA_{Si}, LTA-4A, and LTA-5A, and 8 unit cells (2x2x2) for ITQ-29. Note that the unit cell of ITQ-29 is a single cage. LTA-4A and LTA-5A have an alternating silicon and aluminium arrangement that can only be periodically described in terms of $2 \times 2 \times 2$ β-cages. Without aluminium, the unit cell can be described as a single α-cage.

The interactions between guest molecules (methane and cations) with the zeolite host framework were modelled by Lennard-Jones and Coulombic potentials[30-34]. The Coulombic interactions in the system were calculated using Ewald summations. An "average" polarization was included implicitly in the parameterization by means of the polarization induced by the cation on the zeolite and by the cation on the methane[30]. The Na–O and Ca–O interactions were calibrated to reproduce the experimentally known positions in LTA-4A and LTA-5A[30,33]. The charge distribution on the oxygen framework was considered to be static; that is, polarization of oxygen by nearby cations was neglected. The model used for the rigid frameworks explicitly distinguishes silicon from aluminium with a difference of 0.3e between q_{Si} and q_{Al}[57]. We consider different charges for oxygen atoms bridging two silicon atoms, q_{OSi}, and oxygen atoms bridging one silicon and one aluminium atom, q_{OAl}[30].

There are several force fields in the literature that describe the flexibility of the zeolite framework[4]. Among them, we have focused on these reported by Nicholas *et al*.[23] and Hill and Sauer[25]. The reasons for choosing these two force fields are that they can be applied to pure silica structures and, using straightforward modifications, they can be easily extended to aluminosilicates with sodium and calcium cations. Following a previous work reported by Vlugt and Schenk[26], we additionally improved these models in such a way that the equilibrium distances are no longer constant[26]. The flexible model of Nicholas *et al*. was developed for all-silicate sodalite and contains terms that represent the valence and non-bonded interactions of the structure. This model is able to reproduce the structure and dynamics of all-silica sodalite and is also transferable enough to reproduce the infrared spectrum of MFI. The Si-O-Si bond was modelled using a fourth-order polynomial; all other bends were harmonic in functional form. We extended this model with similar functions to describe the interaction with the aluminium, and we took into account contributions of dihedral-angle-dependent potential functions, Lennard-Jones interactions between non-bonded atoms, and Coulombic potentials. Detailed information of this model and all additional implementations can be found in the original work of Nicholas *et al*.[23] as well as in Table 1 in the Appendix A.

To check the consistency of flexible models we also have used the model reported by Hill and Sauer[25]. They developed a method to derive the parameters of a consistent force field type (CFF) from *ab initio* calculations that was firstly applied to aluminium free zeolites[24] and afterwards to protonated aluminosilicates[25]. The force field[58] is defined by bonds, angles, torsions, out-of-plane, bond-bond, angle-angle, bond-angle, angle-torsion-angle, and non-bond energy expressions. Detailed information about this force field can be found in the original works of Hill and Sauer[24,25] and in Table 2 of the Appendix A.

3.3. Results and Discussion

Fig. 3.2 shows the computed absolute adsorption of methane in rigid ITQ-29, LTA-4A, and LTA-5A at 273 K (Fig. 3.2a) and 500 K (Fig. 3.2b). The adsorption isotherms were obtained for a range of pressure that spans from 1 to 10^{11} kPa. The force field used provides very good agreement available experimental data, as shown in previous works[33,34,59].

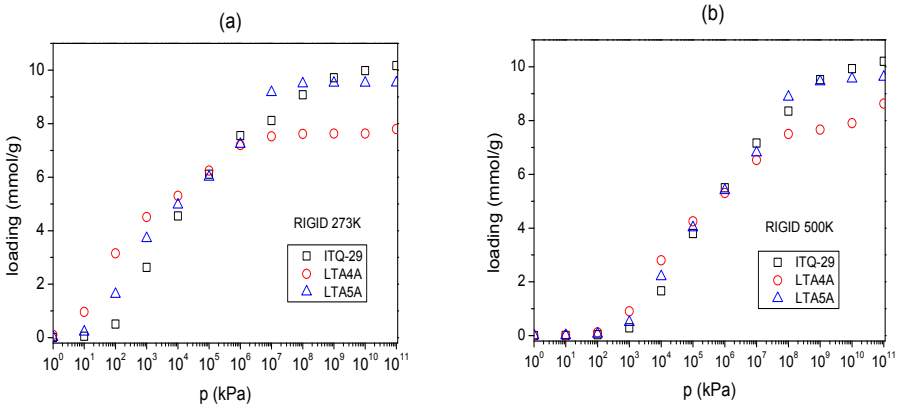

Figure 3.2: Computed adsorption isotherms of methane in rigid ITQ-29 (squares), LTA-4A (circles), and LTA-5A (triangles) at a) 273 K and b) 500 K.

The adsorption of methane in LTA-type structures is determined by the number and distribution of cations in the structure. In particular, the effect of the number

of cations in LTA structures is similar to that observed for FAU-type structures[30,60], where cations act as additional adsorption sites at low pressures while competing for the available free volume with methane at the highest pressures. However, an essential difference with FAU structures is that, in LTA zeolites, the computed adsorption for methane is insensitive to the initial set of positions of the cations. We can explain this finding based on the Si/Al ratios of both structures. The composition of a single unit cell in FAU is $Na_xAl_xSi_{192-x}O_{384}$, where $96 \geq x \geq 0$, with two types of oxygen atoms in the framework: oxygen atoms bridging two silicon atoms and oxygen atoms bridging one silicon and one aluminium atom. Since the cation interaction is stronger with the latter than with the former, the aluminium positions determine the cation distribution in FAU. LTA-type zeolites show Si/Al =1 with alternation silicon and aluminium atoms in order to follow the Lowenstein rule[61]. In these structures, all oxygen atoms are bridging one silicon and one aluminium atom, providing a symmetrical ion distribution that is independent of the positions of the cations selected as starting configuration.

Even though simulations for methane adsorption in LTA-type structures are not sensitive to the initial distribution of cations[34], the positions of these cations are of critical importance for adsorption kinetics in these structures. If the cations are located in the eight-ring windows, they obstruct diffusion. LTA-4A with 96 sodium cations would show very high adsorption capacity, but experimentally, it has all the eight-ring windows blocked. The Ca/Na form LTA-5A contains approximately 32 sodium and 32 calcium per unit cell and none of the windows are blocked by the cations. This leads to diffusion values of methane similar to the ones obtained for the pure silica structure ITQ-29.

Fig. 3.3 shows self-diffusivity for methane in ITQ-29 and LTA-5A as a function of loading at 500 K. Diffusivities are very similar for both structures up to 9 molecules per cage (72 molecules of methane per unit cell) and decrease at a loading for the structure with sodium and calcium cations at a loading of 10 molecules and higher. Direct comparison between self-diffusivity values obtained for LTA_{si} and LTA-5A shows that the interaction methane-cation dominates over the interaction methane-zeolite for methane loading up to 12

molecules per cage. However, at higher loadings, the effect of the cation is diluted by the increase of the molecule-molecule interactions as indicated by similar values obtained for methane diffusivity in both, the structure with sodium and calcium cations and the hypothetical pure silica structure. To analyse the influence of host-guest, host-cation and cation-guest interactions, we have additionally computed self-diffusivity of methane as a function of loading in a hypothetical pure silica and cation free structure labelled as LTA_{si}. As mentioned in the previous section, this structure was obtained from the substitution of all aluminium atoms of LTA-5A by silicon. The obtained results are in qualitatively good agreement with the simulation data reported by Fritzsche *et al.*[49,50], but quantitatively they obtained higher values for self-diffusion (Fig. 3.3) and consequently lower values for adsorption (Fig. 3.4). These results support the finding that the diffusion coefficient depends sensitively on the choice of the Lennard-Jones parameters[50].

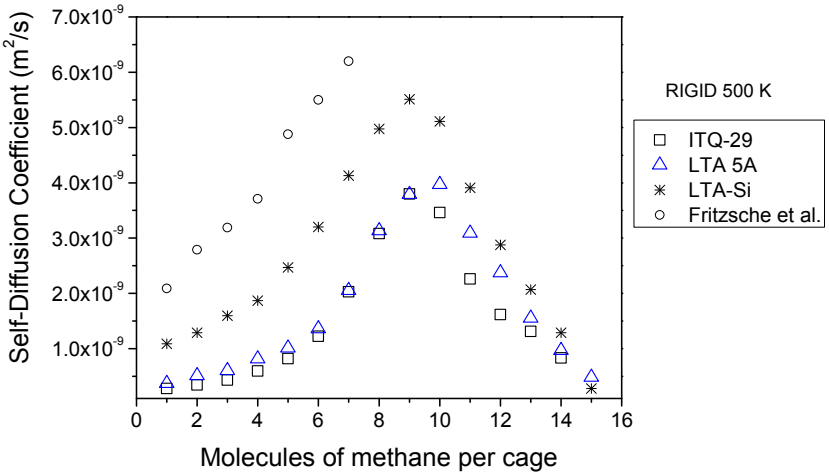

Figure 3.3: Computed self-diffusion of methane as a function of loading in rigid ITQ-29 (squares), LTA-5A (triangles), LTA_{Si} (asterisks) at 500 K. Simulation data of Fritzsche *et al.*[49] in LTA_{Si} at 500 K are included for comparison (circles).

Despite the fact that both LTA_{si} and ITQ-29 have the same morphology, the computed self-diffusion is much higher for the hypothetical structure than for ITQ-29, independently of methane loading. However, differences in adsorption are less remarkable as shown in Fig. 3.4. The different behaviours in adsorption

and diffusion can be explained from the window size and from the pore size distributions (PSDs) calculated with the method reported by Gelb and Gubbins[62]. Fig. 3.5 shows distributions of $V(r)$ and the PSD. The function $V(r)$ is the fraction of space "coverable" by spheres of radius r or smaller; at $r = 0$, it corresponds to the void-fraction. $V(r)$ is a monotonically decreasing function.

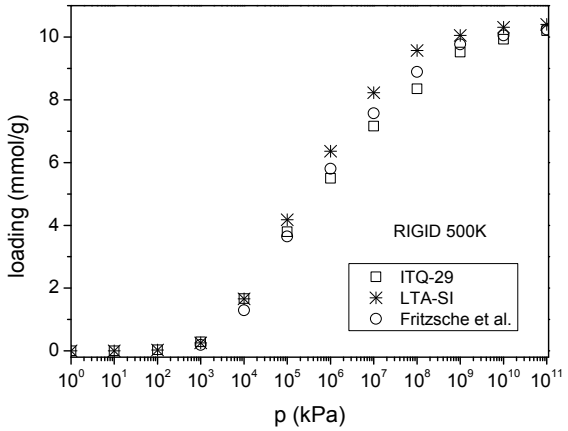

Figure 3.4: Computed adsorption isotherms of methane at 500 K in rigid ITQ-29 (squares), LTA_{Si} (asterisks). Simulation data of Fritzsche *et al.*[49] in LTA_{Si} at 500 K are included for comparison (circles).

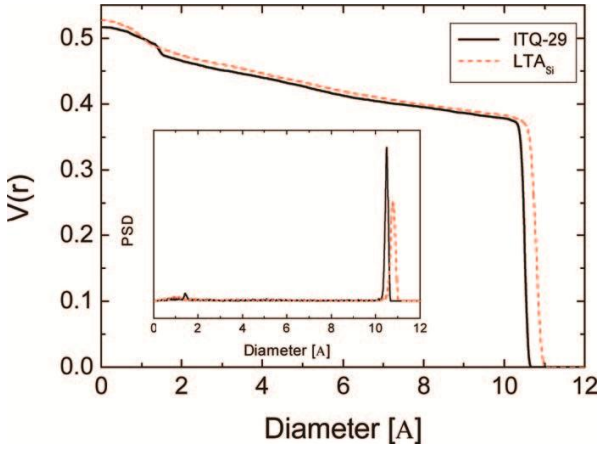

Figure 3.5: $V(r)$ functions as the fraction of space "coverable" by spheres of radius r or smaller for ITQ-29 (dashed line) and LTA_{si} (solid line). The inset provides pore size distributions calculated for ITQ-29 (solid line) and LTA_{si} (dashed line).

The derivative of this function is the PSD with peaks at around 10-11 Å for the size of the β-cage. The windows of ITQ-29 are slightly smaller than for LTA_{si}, and the PSD distributions are narrower and have pore diameters slightly smaller for ITQ-29 than for LTA_{si}.

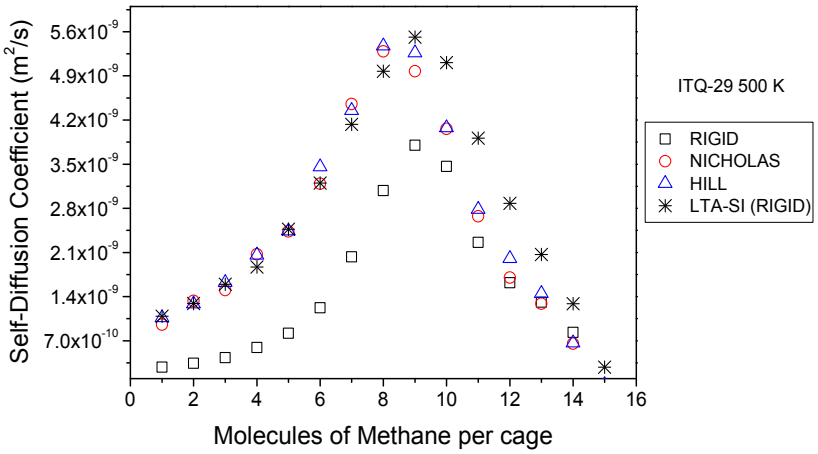

Figure 3.6: Computed self-diffusion for methane as a function of loading in ITQ-29 at 500 K using a rigid structure (squares), flexibility with the model of Nicholas *et al*. (circles), and flexibility with the model of Hill and Sauer (triangles). Computed self-diffusion for methane in rigid LTAsi at 500 K is also included for comparison (asterisks).

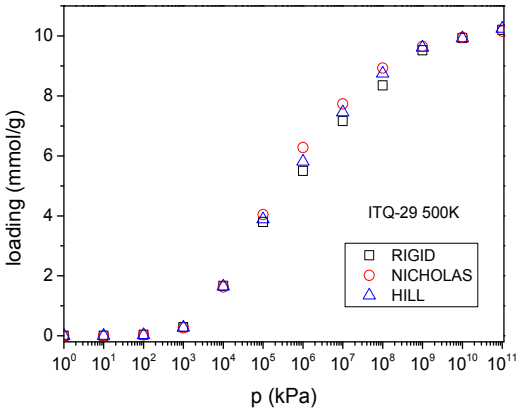

Figure 3.7: Computed adsorption isotherms for methane in ITQ-29 at 500 K using a rigid structure (squares) and flexible models of Nicholas et al (circles) and Hill and Sauer (triangles).

This suggests that the adsorption and self-diffusion values obtained for methane in LTA_{si} could be probably analogous to those obtained for a flexible model of ITQ-29. To investigate the effect of framework flexibility in ITQ-29, we have computed self-diffusivity of methane as a function of loading at 500 K (Fig. 3.6) as well as the adsorption isotherm of methane at 500 K using both, Nicholas *et al*.[23] and Hill and Sauer[25] model (Fig. 3.7). Differences between the self-diffusion values obtained for the rigid and the two flexible models are striking, but again, there seems to be hardly any influence of the framework flexibility on the adsorption isotherm.

It is interesting to speculate about the reasons that make the use of flexibility essential to compute methane self-diffusion but needless for adsorption. These reasons are probably very much related with the LTA topology that consists on cubically arranged cages of about 10 Å in size. The cages are connected by narrow windows in such a way that the windows form entropic barriers[20]. In these structures, the diffusion is an activated process where the molecules of methane hop from one cage to the next and the crossing time is negligible compared to the time a particle spends inside the cage[16]. These hops can easily be disturbed by small variations of the bond length between the silicon and oxygen atoms of the framework. The silicon-oxygen bond lengths for ITQ-29, and LTA-5A are around 1.57-1.61 Å and 1.59-1.60 Å, respectively. However, the aluminium-oxygen bond lengths for LTA-5A are around of 1.72-1.74 Å.

Since the hypothetical LTA_{si} was built from direct substitution of the 96 aluminium atoms of the structure by silicon, without any posterior minimization of the bond lengths, 50% of its silicon-oxygen bond lengths are around 0.13-0.14 Å larger than the average silicon-oxygen bond lengths. This results in slightly wider pores for the rigid structure and, additionally, an abnormal deformation in its flexible models, as can be deduced from the extremely high values on self-diffusion of methane that we show in Fig. 3.8. This anomalous deformation –also reported by Demontis and Suffritti using a more simplistic flexible model[52]– does not affect methane adsorption in LTA_{si} as this molecule has most of its distinct adsorption sites in the cage and only one in the windows regions. The adsorption behaviour is shown in Fig. 3.9, that compares the computed adsorption isotherms

obtained using the rigid structure, the flexible model of Nicholas *et al*.[23], and the flexible model of Hill and Sauer[24].

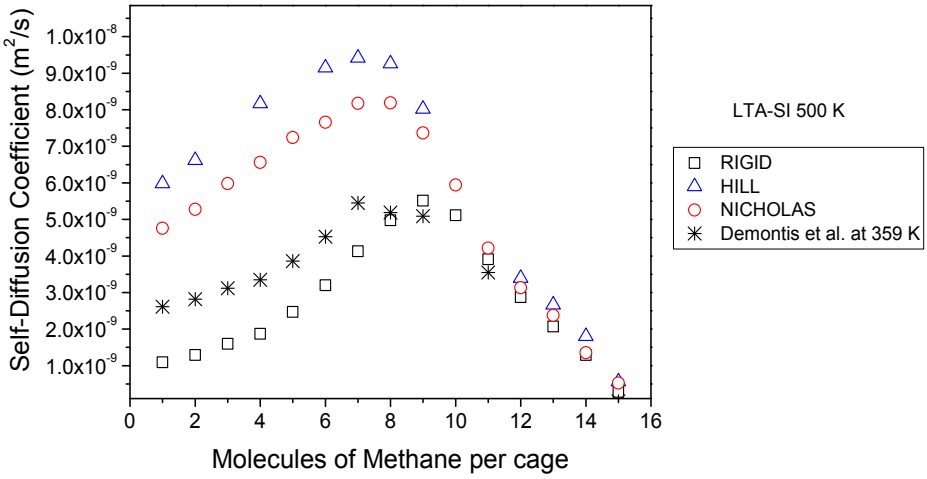

Figure 3.8: Computed self-diffusion for methane as a function of loading in LTAsi at 500 K using a rigid structure (squares), flexibility with the model of Nicholas et al. (circles), and flexibility with the model of Hill and Sauer (triangles). Simulations from Demontis et al[52]. using a simplistic flexible model for LTA_{Si} at 359 K are also included. (asterisks).

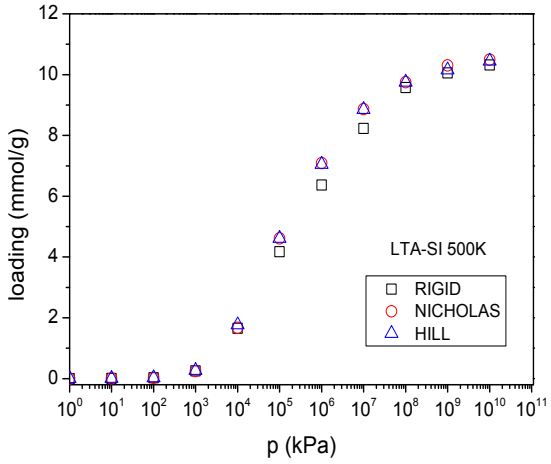

Figure 3.9: Computed adsorption isotherms for methane in LTAsi at 500 K using a rigid structure (squares) and flexible models of Nicholas *et al* (circles) and Hill and Sauer (triangles).

For LTA-4A and LTA-5A structures, we found the same effect; the influence of framework flexibility is large for diffusion and almost negligible for adsorption. In Fig. 3.10 we show that the adsorption isotherms almost overlap using rigid and flexible models, with only slight differences at the highest pressures.

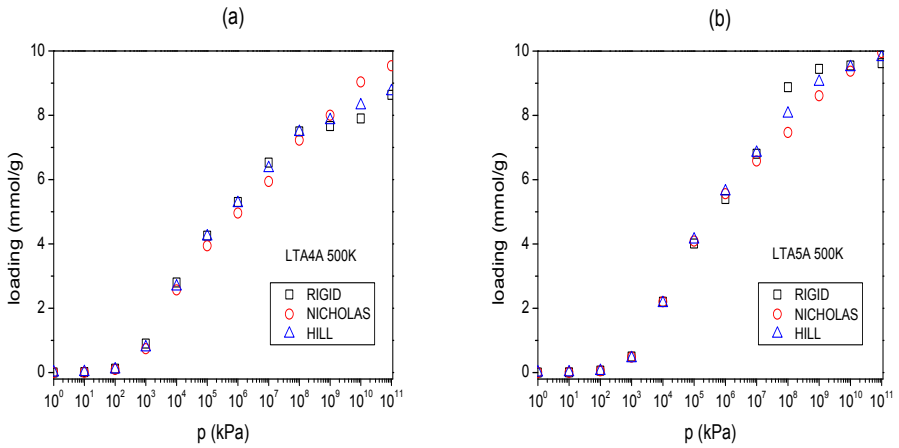

Figure 3.10: Computed adsorption isotherms for methane at 500 K using a rigid structure (squares) and flexible models of Nicholas et al (circles) and Hill and Sauer (triangles) in (a) LTA-4A and (b) LTA-5A.

However, the computed data for self-diffusivity of methane prove to be different for different models. According to the computed values depicted in Fig. 3.11, up to five molecules per cage we obtain analogous diffusion using both, the rigid structure and the flexible model of Hill and Sauer. However, more than five molecules of methane per cage enhance the flexibility effect at the windows as inferred from the higher self-diffusion obtained with the flexible model. It is interesting to note that the flexible model of Nicholas et al. provides reverse behaviour than the model of Hill and Sauer. Here, self-diffusion is higher than for the rigid structure up to nine molecules of methane per cage, becoming similar and even lower for the highest loadings. The fact that the two flexible models only show differences in diffusion for the LTA-5A structure leads us to conclude that the reverse behaviour is essentially attributed to the interactions between the zeolite framework and the sodium and calcium cations.

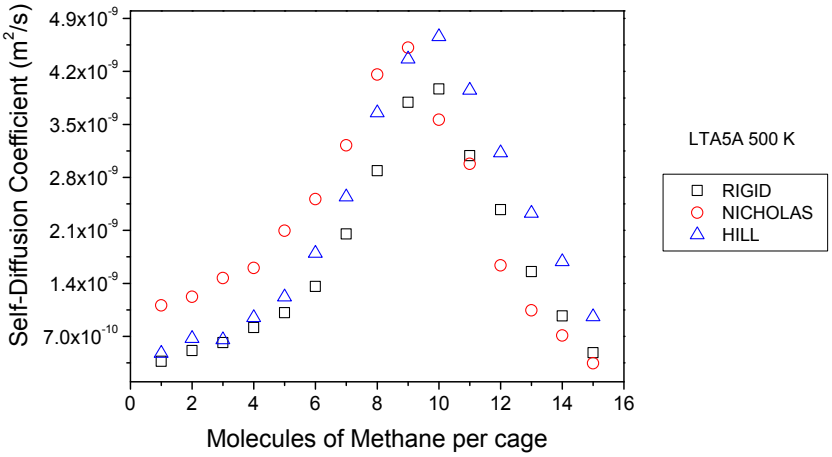

Figure 3.11: Computed self-diffusion for methane as a function of loading in LTA-5A at 500 K using a rigid structure (squares), flexibility with the model of Nicholas *et al.* (circles), and flexibility with the model of Hill and Sauer (triangles).

These interactions are probably overrated for model of Hill and Sauer, leading to self-diffusivity value $3.7 \cdot 10^{10}$ m^2/s at 500 K when one single methane is located in the cage. At the same conditions, the self-diffusivity value obtained for the model of Nicholas *et al.* is $1.1 \cdot 10^{9}$ m^2/s, in reasonable agreement with the experimental data provided by Jobic *et al.*[44] ($1.0 \cdot 10^{9}$ m^2/s at 475 K) and Corma *et al.*[48] ($3 \cdot 10^{9}$ m^2/s at 500 K).

We conclude this section by addressing the question whether flexible models provide better predictions of the self-diffusion than rigid models. One could argue that flexible models are -in principle- more realistic descriptions of the LTA zeolite. There is a wide agreement in the literature that flexibility has a negligible effect on adsorption. The results presented in this work provides evidence that small variation in the bond lengths between the zeolite atoms lead to large differences in diffusion and, depending on the system, the obtained results can be worse than those obtained using a rigid model. The reason is that none of the current force fields are able to capture the average structure exactly, specifically, the 8-ring window separating the cages. A small deviation of the window from the crystal structure leads to very different diffusivities. A

"perfect" flexible model should, *on average*, have the same structure as the crystal structure from experiment (at the same temperature). Only then can one assess the true influence of flexibility on diffusion. Currently, we are stuck with two options (using flexibility or a rigid model) of which both have a proven error. However, we note that the rigid model *does* contain flexibility effects, albeit only the average effect (namely, via the parameterization procedure to fit to experimental data). Until somebody comes up with the perfect flexible model (there is a need to provide criteria on which model gives the most realistic predictions[63,64]), the rigid model might still be reliably used for a lot of purposes, especially when one wants to compare theoretical effects and want to avoid flexibility. In fact, there are only a few known cases where flexibility would be really essential, among them, the famous MIL-53[65] (that changes structure as a function of temperature and loading) and MFI zeolite[27,66] (that has structural orthorhombic/monoclinic phase transitions).

3.4. Conclusions

We have analysed the effect of the framework flexibility on the adsorption and self-diffusion of methane in LTA-type structures. We focused on four structures: pure silica LTA_{si}, the pure silica ITQ-29, LTA-4A with 96 sodium cations per unit cell, and LTA-5A with 32 sodium cations and 32 calcium cations per unit cell. In LTA-4A and LTA-5A, the adsorption and diffusion of methane is strongly determined by the cations. In these structures, the effect of cations is multifold: (1) they create additional adsorption sites at low pressures, (2) they occupy free volume, modifying the adsorption and diffusion properties, especially at high methane loading, and (3) they control diffusion by blocking or allowing methane entrance to the windows. The influence of the framework flexibility on methane adsorption seems to be rather small in the LTA-type zeolites analysed, but it is large for self-diffusion. We found that the models of Hill and Sauer and Nicholas *et al*. equally influence self-diffusion in the pure silica structure, but they lead to contradictory results for the Na/Ca structure. Hence, the main conclusion of this work is that the diffusion results when

flexibility is included depend very much on the model used. If there are no structural changes of the framework, then the rigid models would also allow reliable computations of both adsorption *and* diffusion.

3.5 Bibliography

1 R. Krishna. *Journal of Physical Chemistry C* **113**, 19756-19781 (2009).

2 D. S. Sholl. *Accounts of Chemical Research* **39**, 403-411 (2006).

3 D. Dubbeldam and R. Q. Snurr. *Molecular Simulation* **33**, 305-325 (2007).

4 P. Demontis and G. B. Suffritti. *Chemical Reviews* **97**, 2845-2878 (1997).

5 D. Dubbeldam, S. Calero, T. L. M. Maesen and B. Smit. *Angewandte Chemie-International Edition* **42**, 3624-3626 (2003).

6 D. Dubbeldam, S. Calero, T. L. M. Maesen and B. Smit. *Physical Review Letters* **90**, 245901 (2003).

7 R. Krishna, J. M. van Baten and D. Dubbeldam. *Journal of Physical Chemistry B* **108**, 14820-14822 (2004).

8 D. M. Ruthven and I. H. Doetsch. *AIChE Journal* **22**, 882-886 (1976).

9 R. L. June, A. T. Bell and D. N. Theodorou. *Journal of Physical Chemistry* **95**, 8866-8878 (1991).

10 T. R. Forester and W. Smith. *Journal of the Chemical Society-Faraday Transactions* **93**, 3249-3257 (1997).

11 E. J. Maginn, A. T. Bell and D. N. Theodorou. *Journal of Physical Chemistry* **100**, 7155-7173 (1996).

12 F. Jousse and S. M. Auerbach. *Journal of Chemical Physics* **107**, 9629-9639 (1997).

13 T. Mosell, G. Schrimpf and J. Brickmann. *Journal of Physical Chemistry B* **101**, 9476-9484 (1997).

14 T. Mosell, G. Schrimpf and J. Brickmann. *Journal of Physical Chemistry B* **101**, 9485-9494 (1997).

15 D. Dubbeldam, E. Beerdsen, S. Calero and B. Smit. *Proceedings of the National Academy of Sciences of the United States of America* **102**, 12317-12320 (2005).

16 D. Dubbeldam, E. Beerdsen, S. Calero and B. Smit. *Journal of Physical Chemistry B* **110**, 3164-3172 (2006).

17 P. K. R. Ghorai, S. Yashonath and R. M. Lynden-Bell. *Molecular Physics* **100**, 641-647 (2002).

18 A. Schuring, S. M. Auerbach, S. Fritzsche and R. Haberlandt. *Journal of Chemical Physics* **116**, 10890-10894 (2002).

19 D. Dubbeldam, E. Beerdsen, T. J. H. Vlugt and B. Smit. *Journal of Chemical Physics* **122**, 224712 (2005).

20 E. Beerdsen, B. Smit and D. Dubbeldam. *Physical Review Letters* **93**, 248301 (2004).

21 A. G. Bezus, A. V. Kiselev, A. A. Lopatkin and P. Q. Du. *Journal of the Chemical Society-Faraday Transactions II* **74**, 367-379 (1978).

22 P. Demontis, G. B. Suffritti, S. Quartieri, E. S. Fois and A. Gamba. *Journal of Physical Chemistry* **92**, 867-871 (1988).

23 J. B. Nicholas, A. J. Hopfinger, F. R. Trouw and L. E. Iton. *Journal of the American Chemical Society* **113**, 4792-4800 (1991).

24 J. R. Hill and J. Sauer. *Journal of Physical Chemistry* **98**, 1238-1244 (1994).

25 J. R. Hill and J. Sauer. *Journal of Physical Chemistry* **99**, 9536-9550 (1995).

26 T. J. H. Vlugt and M. Schenk. *Journal of Physical Chemistry B* **106**, 12757-12763 (2002).

27 E. Garcia-Perez, J. B. Parra, C. O. Ania, D. Dubbeldam, T. J. H. Vlugt, J. M. Castillo, P. J. Merkling and S. Calero. *Journal of Physical Chemistry C* **112**, 9976-9979 (2008).

28 F. Leroy and H. Jobic. *Chemical Physics Letters* **406**, 375-380 (2005).

29 N. E. R. Zimmermann, S. Jakobtorweihen, E. Beerdsen, B. Smit and F. J. Keil. *Journal of Physical Chemistry C* **111**, 17370-17381 (2007).

30 S. Calero, D. Dubbeldam, R. Krishna, B. Smit, T. J. H. Vlugt, J. F. M. Denayer, J. A. Martens and T. L. M. Maesen. *Journal of the American Chemical Society* **126**, 11377-11386 (2004).

31 D. Dubbeldam, S. Calero, T. J. H. Vlugt, R. Krishna, T. L. M. Maesen, E. Beerdsen and B. Smit. *Physical Review Letters* **93**, 088302 (2004).

32 D. Dubbeldam, S. Calero, T. J. H. Vlugt, R. Krishna, T. L. M. Maesen and B. Smit. *Journal of Physical Chemistry B* **108**, 12301-12313 (2004).

33 E. García-Pérez, D. Dubbeldam, T. L. M. Maesen and S. Calero. *Journal of Physical Chemistry B* **110**, 23968-23976 (2006).

34 A. García-Sánchez, E. García-Pérez, D. Dubbeldam, R. Krishna and S. Calero. *Adsorption Science & Technology* **25**, 417-427 (2007).

35 E. Garcia-Perez, J. B. Parra, C. O. Ania, A. Garcia-Sanchez, J. M. Van Baten, R. Krishna, D. Dubbeldam and S. Calero. *Adsorption-Journal of the International Adsorption Society* **13**, 469-476 (2007).

36 D. M. Ford, D. Dubbeldam and R. Q. Snurr. in *In Diffusion Fundamentals III* (eds C. Chmelik *et al.*) 459 (2009).

37 P. Demontis and G. B. Suffritti. *Chemical Physics Letters* **223**, 355-362 (1994).

38 S. Fritzsche, M. Wolfsberg, R. Haberlandt, P. Demontis, G. B. Suffritti and A. Tilocca. *Chemical Physics Letters* **296**, 253-258 (1998).

39 A. W. C. van den Berg, S. T. Bromley, N. Ramsahye and T. Maschmeyer. *Journal of Physical Chemistry B* **108**, 5088-5094 (2004).

40 D. I. Kopelevich and H. C. Chang. *Journal of Chemical Physics* **115**, 9519-9527 (2001).

41 F. Leroy, B. Rousseau and A. H. Fuchs. *Physical Chemistry Chemical Physics* **6**, 775-783 (2004).

42 P. Santikary and S. Yashonath. *Journal of Physical Chemistry* **98**, 9252-9259 (1994).

43 A. Bouyermaouen and A. Bellemans. *Journal of Chemical Physics* **108**, 2170-2172 (1998).

44 H. Jobic, A. Methivier, G. Ehlers, B. Farago and W. Haeussler. *Angewandte Chemie-International Edition* **43**, 364-366 (2004).

45 W. Heink, J. Karger, H. Pfeifer and F. Stallmach. *Journal of the American Chemical Society* **112**, 2175-2178 (1990).

46 W. Heink, J. Karger, S. Ernst and J. Weitkamp. *Zeolites* **14**, 320-325 (1994).

47 N. Hedin, G. J. DeMartin, W. J. Roth, K. G. Strohmaier and S. C. Reyes. *Microporous and Mesoporous Materials* **109**, 327-334 (2008).

48 A. Corma, J. Kärger and C. Krause. in *Diffusion Fundamentals* Vol. 2 (ed J. Kärger) 87.81 - 87.82 (2005).

49 S. Fritzsche, M. Gaub, R. Haberlandt and G. Hofmann. *Journal of Molecular Modeling* **2**, 286-292 (1996).

50 S. Fritzsche, R. Haberlandt, G. Hofmann, J. Karger, K. Heinzinger and M. Wolfsberg. *Chemical Physics Letters* **265**, 253-258 (1997).

51 S. Fritzsche, R. Haberlandt, J. Karger, H. Pfeifer, K. Heinzinger and M. Wolfsberg. *Chemical Physics Letters* **242**, 361-366 (1995).

52 P. Demontis and G. B. Suffritti. *Journal of Physical Chemistry B* **101**, 5789-5793 (1997).

53 D. W. Breck, W. G. Eversole, R. M. Milton, T. B. Reed and T. L. Thomas. *Journal of the American Chemical Society* **78**, 5963-5971 (1956).

54 J. J. Pluth and J. V. Smith. *Journal of the American Chemical Society* **102**, 4704-4708 (1980).

55 R. L. Firor and K. Seff. *Journal of the American Chemical Society* **100**, 3091-3096 (1978).

56 A. Corma, F. Rey, J. Rius, M. J. Sabater and S. Valencia. *Nature* **431**, 287-290 (2004).

57 E. Jaramillo and S. M. Auerbach. *Journal of Physical Chemistry B* **103**, 9589-9594 (1999).

58 J. R. Maple, M. J. Hwang, T. P. Stockfisch, U. Dinur, M. Waldman, C. S. Ewig and A. T. Hagler. *Journal of Computational Chemistry* **15**, 162-182 (1994).

59 A. García-Sánchez, C. O. Ania, J. B. Parra, D. Dubbeldam, T. J. H. Vlugt, R. Krishna and S. Calero. *Journal of Physical Chemistry C* **113**, 8814-8820 (2009).

60 E. Garcia-Perez *et al. Applied Surface Science* **252**, 716-722 (2005).

61 W. Loewenstein. *American Mineralogist* **39**, 92-96 (1954).

62 L. D. Gelb and K. E. Gubbins. *Langmuir* **15**, 305-308 (1999).

63 A. Sartbaeva, S. A. Wells, M. M. J. Treacy and M. F. Thorpe. *Nature Materials* **5**, 962-965 (2006).

64 P. Demontis and G. B. Suffritti. *Microporous and Mesoporous Materials* **125**, 160-168 (2009).

65 C. Serre, F. Millange, C. Thouvenot, M. Nogues, G. Marsolier, D. Louer and G. Ferey. *Journal of the American Chemical Society* **124**, 13519-13526 (2002).

66 C. J. Guo, O. Talu and D. T. Hayhurst. *AIChE Journal* **35**, 573-578 (1989).

Chapter 4

Transferable Force Field for Carbon Dioxide Adsorption in Zeolites*

* This chapter is based on: A. García-Sánchez, C.O. Ania, J.B. Parra, D. Dubbeldam, T.J.H. Vlugt, R. Krishna, and S. Calero: "Transferable Force field for Carbon Dioxide Adsorption in Zeolites" *Journal of Physical Chemistry C* **113**, 8814-8820 (2009).

ABSTRACT: We have developed a complete force field that accurately reproduces the adsorption properties of carbon dioxide in a variety of zeolites with different topologies and compositions. The force field parameters were obtained by fitting to our own experimental data and validated with available data taken from the literature. The novelty of this force field is that it is fully transferable between different zeolite framework types, and therefore it is applicable to all possible Si/Al ratios –with sodium as extra-framework cation– and for the first time affording the prediction of topology-specific and chemical composition-specific adsorption properties.

4.1 Introduction

The prediction of carbon dioxide adsorption on porous materials is of crucial importance today for several reasons: from the need to develop cost-efficient CO_2 capture technologies that allow us to slow down the consequences of climate change, to the improvement of gas separation processes of industrial interest (*i.e.*, natural gas cleaning, CO_2 storage, separation from other gases generated in coal combustion, etc.). Carbon dioxide adsorption and separation over a range of porous solids has received much attention in the last decades, the most common adsorbents being activated carbons and zeolites.

Among the porous materials, zeolites are effective structures for the adsorption and selective separation of carbon dioxide, due to their regular porous structure along with their large internal surface areas[1-8]. In addition to traditional adsorbents, recent novel porous adsorbents such as metal-organic frameworks (MOFs) are emerging as promising materials for carbon dioxide capture[9-16].

From an experimental point of view, the pressure, temperature, and moisture content seem to be the most important operating conditions that influence the adsorption of carbon dioxide[2]. As in most gas-solid systems, high gas phase pressures and low temperatures favour carbon dioxide adsorption on porous solids. However the adsorption efficiency strongly depends on the zeolite type and composition[17-23]. For instance, at low pressure the amount of CO_2 adsorbed appears to be highly influenced by the nature and density of the cations inside the zeolite pores[5,24,25], whereas the pore shape and volume appear to control the adsorption capacity at high pressures[2,26]. Zeolites are molecular sieves with a three-dimensional framework structure of alumina or silica tetrahedra whose negative charge is neutralized by cations such as sodium. The nature, number and distribution of the extra-framework cations, affects the basicity and electric field in the cavities of zeolites. These parameters tend to vary inversely with the Si/Al ratio of the framework. The charge imbalance due to the presence of aluminium in the framework determines the ion exchange properties of zeolites and induces potential acidic sites. As the Si/Al ratio increases, the cation content decreases,

the thermal stability increases, the nature of the surface changes from hydrophilic to hydrophobic and the zeolite loses its ion exchange or catalytic properties.

Molecular simulations are currently a powerful tool to accurately predict adsorption[27-29] and diffusion[30] processes in zeolites, but efficient methods[31-33] and good force fields capable of reproducing ideal experimental conditions for all zeolites[5,26,34-36] are vital for this purpose. A variety of works reporting force fields for carbon dioxide in zeolites can be found in literature, most of them only applicable to all-silica structures[37-40], *i.e.* with Si/Al = ∞. In contrast, there are only three sets of force field parameters available for CO_2 adsorption in zeolites containing aluminium atoms and sodium non- framework cations. Two of these sets were developed for the LTA-4A zeolite[41,42], and the third set for faujasites[43]. Unfortunately, none of these force fields is transferable between different zeolite framework types and Si/Al ratios.

We have developed a new force field that (1) accurately reproduces carbon dioxide adsorption in zeolites, (2) is transferable to all zeolite structures, and (3) is applicable to Si/Al ratio that spans from unity (*i.e.* maximum aluminium substitution) to infinity (*i.e.* all-silica structure), using sodium atoms as extra-framework cation. In this paper we firstly discuss the methodology for the development of the force field and secondly compare the results obtained using the new set of parameters with those obtained using previous sets reported in the literature.

4.2 Methodology

The development of our force field requires (1) models for adsorbents and adsorbates and interatomic potentials, (2) experimental isotherms for the fitting and *a posteriori* validation, and (3) an optimization of parameters using Monte Carlo Simulations in combination with the Downhill Simplex Method.

4.2.1 Models and Simulation Techniques

Zeolites were built from silicon, aluminium, and oxygen atoms using their crystallographic positions. LTA-4A ($Na_{96}Al_{96}Si_{96}O_{384}$) and FAU ($Na_xAl_xSi_{192-x}O_{384}$, $96 \geq x \geq 0$) have a cubic unit cell dimension of 24.555 Å, and 25.028 Å, respectively[44,45]. FAU-type zeolites have been labelled either X or Y, depending on their framework aluminium density. Zeolite X has a framework aluminium density between 96 and 77 aluminium atoms per unit cell, whereas zeolite Y contains fewer than 77 framework aluminium atoms per unit cell. The precise crystallographic location of some sodium cations remains uncertain for NaX and NaY[46].

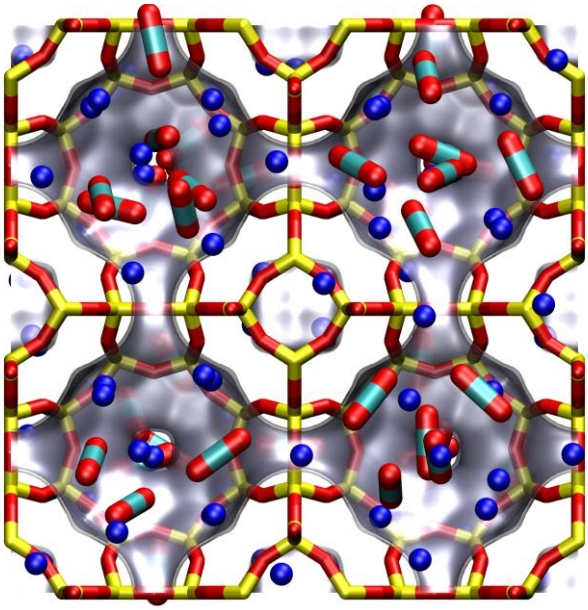

Figure 4.1: Typical snapshot showing the adsorption of carbon dioxide in LTA-4A with 96 sodium cations per unit cell at 10^4 Pa and 298 K.

In contrast, there appears to be general agreement for LTA-4A in which the sodium cations in the bare zeolite are distributed among three crystallographic sites: in the centre of the six ring (97.2% occupation), in the eight ring windows (24.2% occupation), and opposite to the four rings (6.6% occupation)[44,47].

The cation positions are modified with carbon dioxide adsorption as we show in Fig. 4.1 for a pressure of 10^4 Pa and 298 K. MOR ($Na_xAl_xSi_{48-x}O_{96}$, $8 \geq x \geq 0$) and MFI ($Na_xAl_xSi_{96-x}O_{192}$, $0 \geq Si/Al \geq 8$) are structures consisting of interconnected channels. MOR is formed by channels parallel to [001] that are connected with small side channels parallel to [010], with cross sections called side-pockets[48] On the other hand, MFI is formed by straight, parallel channels intersected by zigzag channels[49]. Four (MOR) and twelve (MFI) distinct crystallographic T sites (T=Si, Al) can be found on these structures influencing the sodium cation distribution.

The zeolite structure is considered rigid, as previous studies demonstrated that flexibility of the framework has a minor effect on the adsorption of small molecules for the range of temperatures considered in this thesis[50,51]. The structures with Si/Al ratio other than unity or infinity were obtained by randomly substituting aluminium by silicon, satisfying the Löwenstein rule. In this way it is possible to reproduce a reasonable approximation of the framework aluminium distribution obtained by experimental methods[28,52-54]. Our model explicitly distinguish silicon from aluminium, using different charges for oxygen atoms bridging two silicon atoms q_{OSi}, and oxygen atoms bridging one silicon and one aluminium atom q_{OAl}. The non-framework sodium cation density was adjusted to match the framework aluminium density. Non-framework sodium cations can move freely adjusting their position depending on their interactions with the framework atoms, other sodium cations and the carbon dioxide molecules[35].

Our model for CO_2 has three Lennard-Jones sites with charges centred at each atom. The charge on the carbon and on the oxygen centres are +0.6512 and -0.3256 e^-, respectively. The carbon-oxygen bonds are rigid and 1.149Å long. The bond length and the assigned values for the point charges are taken from the model of Harris and Yung[55], and the Lennard-Jones parameters were fitted using Gibbs ensemble Monte Carlo simulations to reproduce the vapour-liquid coexistence curves, using a Lennard-Jones 12-6 potential that is truncated at 12 Å and shifted so that the potential is zero at the cutoff. The Lennard-Jones interactions between CO_2 and the zeolite was modelled taking into account the interactions between carbon dioxide and the zeolite O atoms and Na cations,

because they contribute most to the repulsive and dispersion forces; Lennard-Jones interactions between Si-CO_2 and Al-CO_2 were not taken into account. The Coulombic interactions in the system were calculated using the Ewald summation[56].

4.2.2 Experiments

Experimental carbon dioxide adsorption isotherms were performed in FAU and MFI zeolites at several temperatures ranging from 253 up to 298 K. All silica MFI (Si/Al = ∞) was kindly supplied by ITQ (CSIC) and corresponds to a pure porous crystalline silicon dioxide. FAU with a Si/Al ratio 2.5 (54 Na^+ per unit cell) was purchased from Zeolyst International SA. Prior to the adsorption measurements, the samples were in-situ outgassed under primary vacuum (~ $1.33 \cdot 10^{-3}$ kPa) at 673 K overnight to remove any adsorbed impurities. The CO_2 adsorption isotherms were carried out in a TriStar 3000 volumetric equipment from Micromeritics, in the pressure range from 10^{-1} kPa up to 120 kPa. The instrument was equipped with a pressure transducer (0 to 133 kPa, uncertainty within 0.5 % of reading) that guarantees an excellent sensitivity for carbon dioxide adsorption in the low pressure range, which is especially useful in adsorption studies on highly microporous materials. The temperature of the isotherms was controlled using a circulating thermostatic bath. Carbon dioxide was purchased with an ultra-high purity (*i.e.*, 99.995 %).

	This Work	Akten et al.[42]	Jaramillo and Chandross[41]	Maurin et al.[43]
	a. Lennard-Jones Force Field ε / k_B [K] Parameter Used.			
O_{co2}-O_{co2}	85.671	79.000	110.236	76.474
C_{co2}-C_{co2}	29.93	27.000	29.195	46.650
O_{co2}-C_{co2}	50.640	46.184	56.880	18.335
O_{co2}-O_{zeo}	78.980	41.69	118.793	69.743
C_{co2}-O_{zeo}	37.595	24.372	61.410	42.125
O_{co2}-Na	200.831	25.140	47.316	31.332
C_{co2}-Na	362.292	14.697	24.161	88.079
O_{zeo}-Na	23.000	13.266	--	--
	b. Lennard-Jones Force Field σ [Å] Parameter Used.			
O_{co2}-O_{co2}	3.017	3.050	3.470	3.360
C_{co2}-C_{co2}	2.742	2.800	2.753	3.830
O_{co2}-C_{co2}	2.880	2.925	3.112	3.310
$O_{co2}O_{zeo}$	3.237	3.025	3.255	3.480
C_{co2}-O_{zeo}	3.511	2.900	2.897	3.900
O_{co2}-Na	2.758	2.950	3.335	2.95
C_{co2}-Na	3.320	2.825	2.977	3.35
O_{zeo}-Na	3.400	2.925	--	--
	c. Charges [e^-] and Carbon-Oxygen Bond Distance [Å].			
q (O_{co2})	-0.3256	-0.35	-0.40	-0.36
q (C_{co2})	0.6512	0.70	0.80	0.72
q (Si)	0.7860	0.80	3.70	2.40
q (Al)	0.4860	1.42	2.775	1.70
q (O_{Si})	-0.3930	-0.4	-1.85	-1.20
q (O_{Al})	-0.4138	-0.74	-1.86875	-1.20
q (Na)	0.3834	0.74	1.00	0.70
d (C-O)	1.149	1.16	1.143	1.143

Table 4.1: Lennard-Jones force field parameters and the values of the partial charges used in this work and in the published literature.

The experimental isotherms obtained in this way were used to fit, optimize, and validate our force field parameters. Consequently to guarantee the accuracy of the experiments, all the isotherms were generated in triplicate and the data is reproducible with an error below 0.1 %.

4.3 Results and Discussion

Here we present a force field obtained using Monte Carlo simulations of carbon dioxide in zeolites. In what follows we describe the parameter optimization and the force field validation using faujasite with Si/Al ratio 2.5, the extension to other Si/Al ratio and other topologies and the improvement of this work compared to preceding models and force fields already available from the literature. Details on the partial charges and the other force field parameters used in this work are listed in Table 4.1.

4.3.1 Parameter Optimization and Force Field Validation

To construct a transferable force field for all frameworks, pressures, temperatures, and Si/Al ratios is a very complex task that requires the fitting of all force field parameters simultaneously. The zeolite framework partial charges and the adsorbate-adsorbent Lennard-Jones interaction parameters were fitted using the Downhill Simplex Method[57] and grand-canonical Monte Carlo simulations. We adjusted the force field parameters to obtain the excess adsorption that accurately reproduces our experimental isotherms at 273 K for FAU with Si/Al ratio 2.5 that corresponds to 54 aluminium atoms and 54 sodium cations per unit cell. We fit to the entire isotherm following the methodology reported by Dubbeldam et al.[33]

The main reasons to select Na-Y type zeolite for the fitting were that (1) it is a well-tested material with very low degree of defects; (2) it has been previously shown that the adsorption properties of small molecules on this material are insensitive to the aluminium distribution, whereas for other classes of structures,

the distribution matters[28]; (3) in contrast to LTA-4A, the Si/Al ratio can be easily varied; and (4) most experimental data on carbon dioxide adsorption are available for faujasites, providing a valuable number of isotherms from independent groups to the force field validation. Additional experimental isotherms at 253, 263, 283, 298 and 303 K were measured and subsequently used for the validation of the force field.

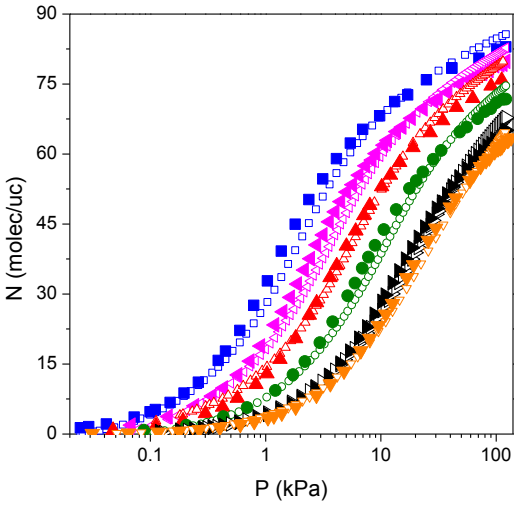

Figure 4.2: Comparison of computed (open symbols) and experimental (solid symbols) carbon dioxide adsorption isotherms in FAU with Si/Al ratio 2.5 (54 Na+ / unit cell). The isotherms are obtained at 253 K (□, ■), 263 K (◁, ◀), 273 K (△, ▲), 283 K (○, ●), 298 K (▷, ▶), and 303 K (▽, ▼).

Fig. 4.2 shows an excellent agreement in all ranges of pressures and temperatures between our experimental and simulation data. These results are also in agreement with previous experimental isotherms as shown in Fig. 4.3, where our data (54 Na^+/uc at 298 K) are compared with those from Pires *et al.*[58] (56 Na^+/uc at 298 K), Walton *et al.*[59] (58 Na^+/uc at 298 K), and Maurin *et al.*[43](56 Na^+/uc at 300 K). Our computed excess adsorption isotherms in faujasites with Si/Al ratio other than 2.5 are also in very good agreement with experimental data taken from the literature. Fig. 4.4 compares our computed isotherms with those of Pires *et al.*[58] for a Si/Al ratio 4.8 (33 Na^+/uc) at 298 K and with those of Dunne *et al.*[19] for Si/Al ratio 1.2 (87 Na^+/uc) at 305 K.

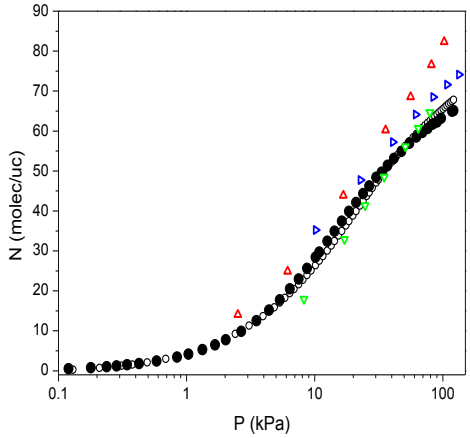

Figure 4.3: Carbon dioxide adsorption isotherms in faujasites with Si/Al ratio around 2.5 (54-58 aluminium atoms and sodium cations per unit cell) at 298-300 K. Comparison of the experimental (○) and simulation (●) data obtained in this work with previous experimental results from Maurin *et al.*[43] at 300 K (▷), Pires *et al.*[58] at 298 K (△) and Walton *et al.*[59] at 298 K (▽).

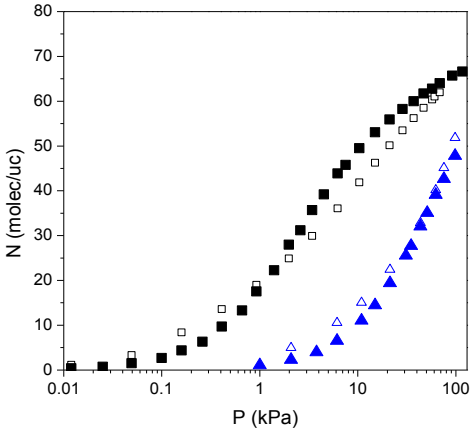

Figure 4.4: Comparison of computed (solid symbols) and previous experimental (open symbols) carbon dioxide adsorption isotherms in faujasites with Si/Al ratio 4.8 at 298 K (triangles) and Si/Al ratio 1.2 at 305 K (squares). Previous experimental data have been taken from Dunne *et al.*[19] and Pires *et al.*[58].

For our simulations shown in Fig. 4.4, we have adjusted both the temperature and the Si/Al ratio to that of the corresponding experiment available in the literature. In all cases, there is a good agreement between our simulations and the experiments in the whole pressures range analysed. We have verified that the

error in the computed loadings is smaller than the symbol size for all the figures shown in this chapter.

4.3.2 Extension to Other Topologies (MFI, MOR and LTA)

To confirm that the new force field parameters are transferable to other structures (in addition to FAU), we have selected MFI, MOR, and LTA-type zeolites. Our simulated isotherms for pure silica MFI are compared with our experimental isotherms in Fig. 4.5 (a), and with other previous available experimental data in Fig. 4.5 (b). Both figures show an excellent agreement between simulation and experiments.

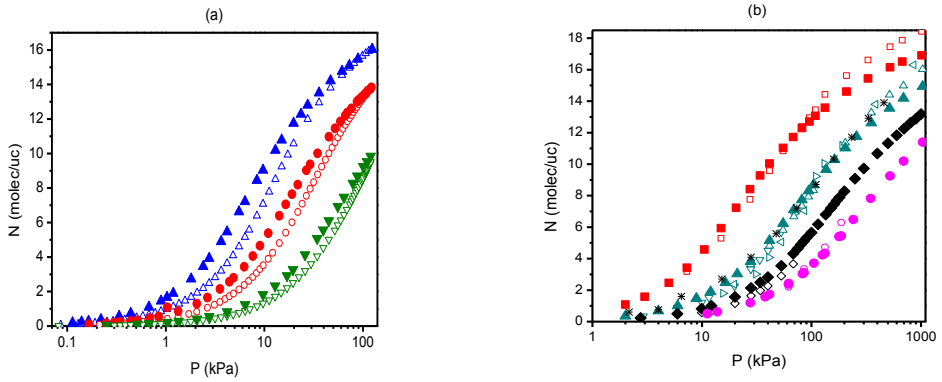

Figure 4.5: Comparison of computed (solid symbols) and experimental (open symbols) carbon dioxide adsorption isotherms in pure silica MFI zeolite; **(a)** Comparison with our own experimental data at 253 K (△, ▲), 273 K (○, ●), and 303 K (▽, ▼); (b) Comparison with previous experimental data taken from Sun *et al.*[23] at 277 K (□, ■) and 308 K (△, ▲), Hirotani *et al.*[39] at 303 K (▽), 305 K (◁),and 330 K (◇, ◆), and Choudhary *et al.*[17] at 303 K (▷) and 353 K (○, ●); and Li *et al.*[40] at 313 K (*).

Fig. 4.6 compares our simulation results for MFI and MOR type structures with several Si/Al ratios. The isotherms for MFI were computed at 297 K and for Si/Al ratio 95 (1Na^+/uc) and 31 (3 Na^+/uc), and compared with previous experimental data of Dunne *et al.*[19].

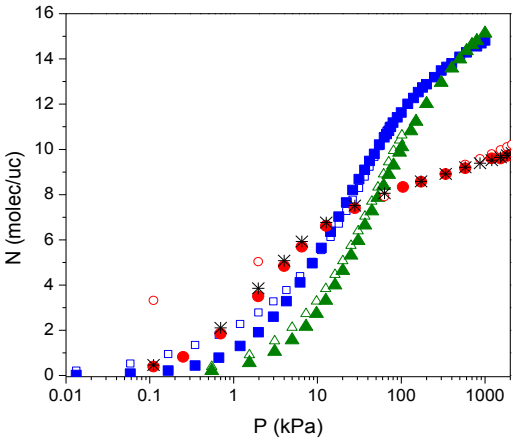

Figure 4.6: Comparison of computed (solid symbols) and experimental (open symbols) carbon dioxide adsorption isotherms in MFI- and MOR- type zeolites for several Si/Al ratios. The computed isotherms in MFI were compared with the experimental values of Dunne et al.[19] at 297 K for the structures with Si/Al ratio 95 and 1Na^+/uc (△, ▲) and Si/Al ratio 31 and 3 Na^+/uc (□, ■). The isotherms in MOR was obtained at 279 K for the structure with Si/Al ratio 5.8, 7 Na^+/uc and a random distribution for the aluminium atoms, but keeping the preferential sites and the fraction of aluminium atoms at the four T-sites in MOR as reported by Meier[48] (structure 1, ●) and by Alberti[60] (structure 2, *). The computed isotherms (●, *) were compared with the experimental data of Delgado *et al.*[61] (○).

The isotherm for MOR was computed at 293 K for a Si/Al ratio 5.8 (7 Na^+/uc) for direct comparison with the experimental values reported by Delgado *et al.*[61]. The agreement is excellent for MFI in the entire pressures range and at both Si/Al ratios, whereas for MOR there is only a good agreement at high pressures. At low pressures our simulations under predict the CO_2 adsorption behaviour in MOR. For small, nonpolar hydrocarbons, these discrepancies have been attributed to differences in the aluminium distribution between the experimental and simulated structure[28,53].

However, molecular simulations for carbon dioxide in MOR using structures in which the aluminium atoms are randomly distributed but keeping the preferential sites and the fraction of aluminium atoms at the four T-sites of MOR as reported by Meier[48] (structure 1) and by Alberti[60] (structure 2) show that this explanation is not applicable to carbon dioxide adsorption (Fig. 4.6).

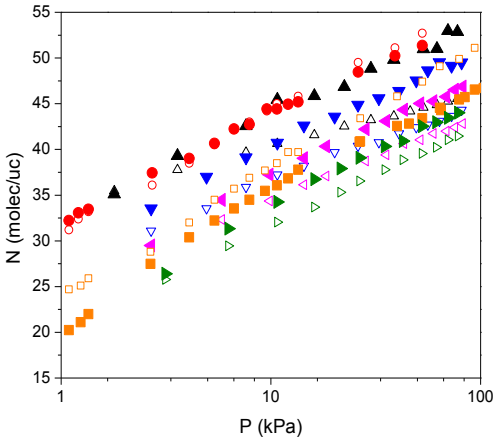

Figure 4.7: Comparison of computed (solid symbols) and experimental (open symbols) carbon dioxide adsorption isotherms in LTA-4A. The computed isotherms were compared to the experimental isotherms of Ahn *et al.*[51] at 273 K (△, ▲), 283 K (▽, ▼), 293 K (◁, ◀) and 303 K (▷, ▶), and with the experimental values taken from ref. 13 of Jaramillo and Chandross[32] at 273 K (○,●) and 298 K (□, ■).

As shown in Fig. 4.7, simulation obtained with our force field is also in good agreement with available experimental data for CO_2 adsorption in LTA-4A (LTA–type zeolite with Si/Al ratio 1 and 96 sodium cations per unit cell) in the range of 273 - 303 K[41,62].

4.3.3 Comparing this Work and Preceding Models

To show the improvement of this work compared to previous force fields, we have performed simulations in LTA, FAU, MOR, and MFI zeolites using the new set of parameters and those from previous approaches. Previous force fields were developed to calculate adsorption of carbon dioxide in LTA-4A (Jaramillo and Chandross[41] and Atken et al.[42]) and in faujasites (Maurin et al.[43]). All atomic partial charges and force field parameters for our and other force fields can be found in Table 4.1.

Jaramillo and Chandross[41] and Atken et al.[42] considered the same zeolite model and potential that was used by Faux and co-workers[63], but they differ in the CO_2

model; the former uses the model of Makrodimitris et al[30] and the latter the TraPPE force field of Potoff and Siepmann[64]. The force field parameters of Jaramillo and Chandross[41] were fitted to experimental isotherms at 298 K, and they completely disregard the mobility of the sodium cations. However, it is well known that ignoring the mobility of the cations results in artefacts[35]. Atken et al.[42] fitted the force field parameters to match their own experimental data at 298 K. They constrained the sodium cations associated with the six-membered oxygen rings, whereas cations associated with the eight and four membered rings were allowed to move. Maurin et al.[43] fitted the force field parameters to reproduce their experiments for faujasites with Si/Al ratio 1 and 2.4 that corresponds to 92 and 56 sodium cations, respectively. Similarly to the force field of Jaramillo and Chandross[41], the sodium cations were considered as an immobile part of the zeolitic framework and therefore they are restricted to their crystallographic positions during the simulations.

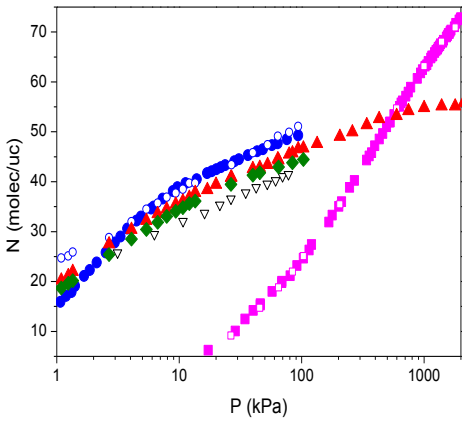

Figure 4.8: Comparison of computed (solid symbols) and experimental (open symbols) carbon dioxide adsorption isotherms in LTA-4A at 298 K. The computed isotherms were obtained using the force fields from Jaramillo and Chandross[41] (●), Akten *et al.*[42] (■), Maurin *et al.*[43] (◆) and our new force field (▲). Experimental data for comparison were taken from Jaramillo and Chandross[41] at 298 K (○), Ahn *et al.*[62] at 303 K (▽) and Akten *et al.*[42] at 298 K (□).

Fig. 4.8 shows the computed carbon dioxide adsorption isotherms in LTA-4A at 298 K using the three previous force fields, the experimental data that Jaramillo and Chandross[41] and Akten *et al.*[42] used for their fitting, and the adsorption isotherm at the 298 K using our new force field. It should be stressed out that

although all isotherms were obtained at the same temperature and, in theory, for the same structure; discrepancies between the experimental sets used by the authors are large, leading to complete different carbon dioxide adsorption curves.

Our results are in agreement with those of Jaramillo and Chandross[41], as well as with the computed isotherms obtained using the force field of Maurin *et al*.[43] and the experimental data of Ahn *et al*. at 303 K[62] also included in Fig. 4.8 for comparison. It is striking that experimental isotherms reported by Akten *et al*.[42] do not match those reported by Jaramillo *et al*.[41] and Ahn *et al*.[41]. On the basis of the experimental procedure described in the literature,[65,66] this disagreement might be due to the low outgassing temperature (*i.e.*, 25 °C) used in the preparation of the samples prior to running the isotherms. Coping with IUPAC recommendations, such experimental conditions do not guarantee the corrected evacuation of the zeolite,[65,66] and therefore, those data from Akten *et al*. may be seriously affected by experimental errors. Thus, it appears that their force field parameters have been fitted using an incorrect experimental data set.

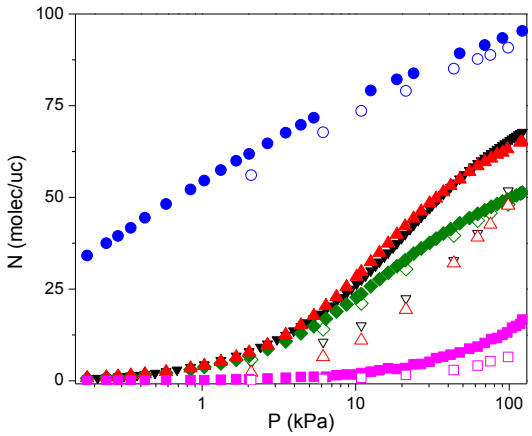

Figure 4.9: Comparison of computed and experimental carbon dioxide adsorption isotherms in faujasites with Si/Al ratio 2.5 (solid symbols) and 4.8 (open symbols) at 298 K. The computed isotherms were obtained using the force fields from Jaramillo and Chandross[41] (●, ○), Akten *et al*.[42] (■, □), Maurin *et al*.[43] (◆, ◇) and our new force field (▲, △). Experimental data for comparison were taken from this work for Si/Al ratio 2.5 at 298 K (▼) and Pires *et al*.[58] for Si/Al ratio 4.8 at 298 K (▽).

Fig. 4.9 shows the computed and experimental adsorption isotherms of carbon dioxide in faujasites with Si/Al ratio 126 (33 Na^+/uc) and 2.5 (54 Na^+/uc) at 298 K. The computed isotherms were obtained using the four set of force fields and compared with available experimental data for various Si/Al ratios: this work (Si/Al ratio 2.5) and Pires *et al*. (Si/Al ratio 4.8)[58]. The isotherms obtained from our force field parameters reproduce the experimental data, regardless the Si/Al ratio, as opposed to the simulations obtained using the force field parameters by Akten *et al*.[42] as well as those by Jaramillo and Chandross[41]. The experimental values are underestimated using the parameters of Jaramillo and Chandross[41], and overestimated with those reported by Akten *et al*.[42].

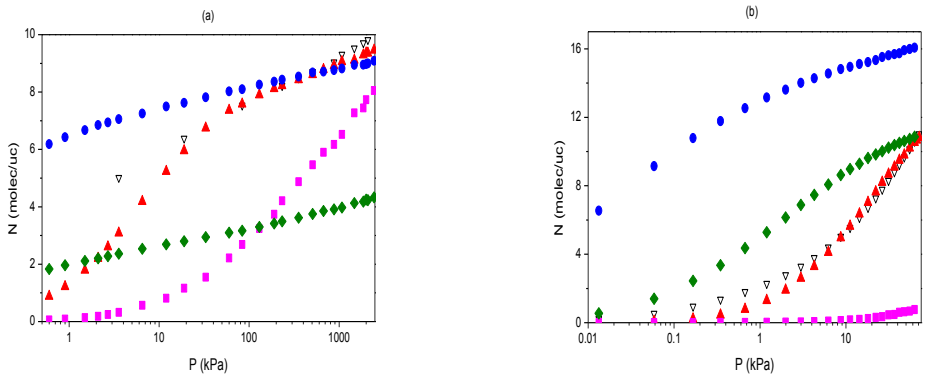

Figure 4.10: Comparison of computed (solid symbols) and experimental (open symbols) carbon dioxide adsorption isotherms in (a) MOR with Si/Al ratio 5.8 at 293 K and (b) MFI with Si/Al ratio 31 at 297 K. The computed isotherms were obtained using the force fields from Jaramillo and Chandross[41] (●), Akten *et al*.[42] (■), Maurin *et al*.[43] (◆) and our new force field (▲). Experimental data for comparison (▽) were taken from Delgado *et al*.[61] in MOR and from Dunne *et al*.[19] in MFI.

The isotherms obtained with the force field of Maurin *et al*.[43] show a reasonable agreement with the experimental data, though they are almost insensitive to the aluminium density. The fact that our force field reproduces experimental adsorption isotherms for different aluminium framework densities in sharp contrast to previous force fields can be attributed to both, the restrictions on cation mobility and the underestimations of the Na-CO_2 Lennard-Jones interactions in the latter. Taking into account the excellent agreement with experimental data using our force field parameters, it appears that this mobility becomes vital to accurately reproduce carbon dioxide adsorption in faujasites; the

outstanding role of cation mobility has also been found an essential factor on the adsorption of alkanes in this type of structures[35].

Our force field clearly outperforms previous available approaches not only for LTA-4A and faujasites, but also for MOR and MFI type structures containing aluminium atoms, as shown in Fig. 4.10 (a) and Fig. 4.10 (b).

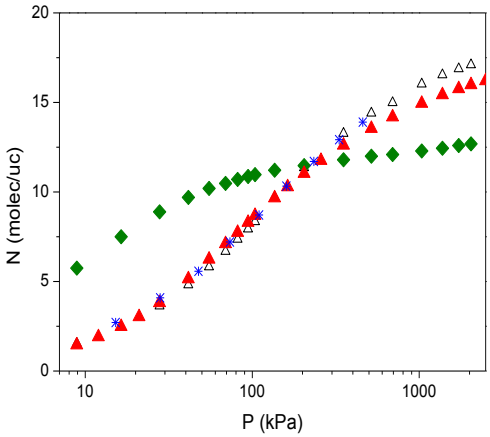

Figure 4.11: Comparison of computed (solid symbols) and experimental (open symbols) carbon dioxide adsorption isotherms in pure silica MFI at 308 K. The computed isotherms were obtained using the force fields from Maurin et al.[43] (◆) and our new force field (▲). Experimental data for comparison were taken from Sun *et al.*[23] at 308 K (△) and Li *et al.*[40] at 313 K (*).

In addition, our force field accurately reproduces pure silica MFI (Fig. 4.11), whereas those from Jaramillo and Chandross[41] and Atken *et al.*[42] cannot be applied to all-silica structures (the electro-neutrality of the framework is not preserved) and the force field from Maurin *et al.*[43] clearly over predicts carbon dioxide adsorption at low pressures whereas the adsorption at high pressures is under predicted.

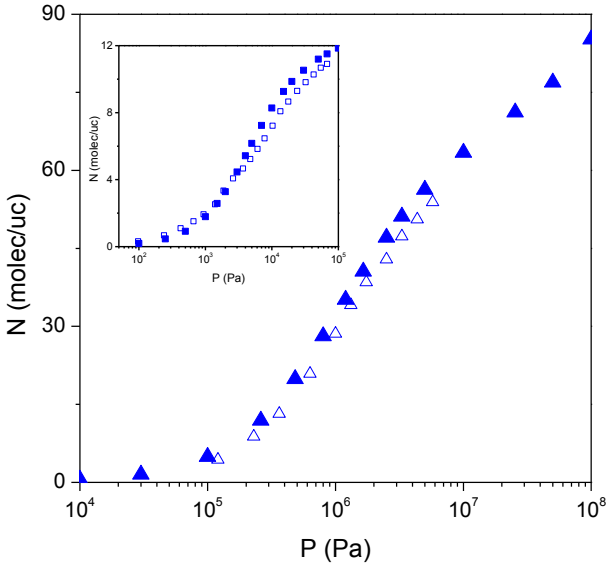

Figure 4.12: Comparison of computed (solid symbols) and previous experimental[19,67] adsorption isotherms (open symbols) of methane in faujasite with Si/Al ratio 3 at 323 K (▲, △) and ethane (inset) in MFI with Si/Al ratio 31 at 296 K (■, □).

The applicability of the new set of charges developed for the zeolite framework and the sodium cations is by no means limited to carbon dioxide adsorption, for it also successfully reproduces the adsorption of alkanes in zeolitic structures.

Fig. 4.12 shows the computed adsorption isotherms for methane in a faujasite structure with 48 aluminium atoms per unit cell at 323 K and for ethane in a MFI structure with 3 aluminium atoms per unit cell at 296 K. The isotherms were obtained using a combination of our previously reported models and Lennard-Jones parameters for alkanes[34,35], and the new set of charges presented in this work, showing a very good agreement with available experimental data[19,67]. This additional feature of the force field set of charges is of particular interest to study processes of industrial interest, such as those related to natural gas separation and purification.

4.4 Conclusions

We have developed a general force field for the adsorption of carbon dioxide in zeolites using Monte Carlo simulations and fitting to our own experimental data. Validation was carried out using both our experiments and available experimental data from the literature. The force field clearly outperforms previous force field as it is more accurate, transferable between zeolite structures, and applicable to all Si/Al ratios. The work reported here can be expected to help the development of CO_2 separation and sequestration technologies by providing vastly improved molecular simulation data inputs.

4.5 Bibliography

1 T. Baimpos, I. G. Giannakopoulos, V. Nikolakis and D. Kouzoudis. *Chemistry of Materials* **20**, 1470-1475 (2008).

2 K. M. Bonenfant D, Niquette P, et al. *Science and Technology of Advanced Materials* **9** (2008).

3 W. H. Gao, D. Butler and D. L. Tomasko. *Langmuir* **20**, 8083-8089 (2004).

4 S. Himeno, T. Tomita, K. Suzuki and S. Yoshida. *Microporous and Mesoporous Materials* **98**, 62-69 (2007).

5 R. Krishna, J. M. van Baten, E. Garcia-Perez and S. Calero. *Chemical Physics Letters* **429**, 219-224 (2006).

6 R. Krishna, J. M. van Baten, E. Garcia-Perez and S. Calero. *Industrial & Engineering Chemistry Research* **46**, 2974-2986 (2007).

7 V. E. Zorine, P. C. M. Magusin and R. A. van Santen. *Journal of Physical Chemistry B* **108**, 5600-5608 (2004).

8 E. Garcia-Perez, J. B. Parra, C. O. Ania, A. Garcia-Sanchez, J. M. Van Baten, R. Krishna, D. Dubbeldam and S. Calero. *Adsorption-Journal of the International Adsorption Society* **13**, 469-476 (2007).

9 E. Garcia-Perez, J. Gascon, V. Morales-Florez, J. M. Castillo, F. Kapteijn and S. Calero. *Langmuir* **25**, 1725-1731 (2009).

10 S. Keskin. *Journal of Physical Chemistry C* **115**, 800-807 (2011).

11 P. L. Llewellyn *et al. Langmuir* **24**, 7245-7250 (2008).

12 A. Martin-Calvo, E. Garcia-Perez, J. M. Castillo and S. Calero. *Physical Chemistry Chemical Physics* **10**, 7085-7091 (2008).

13 Q. Y. Yang, C. L. Zhong and J. F. Chen. *Journal of Physical Chemistry C* **112**, 1562-1569 (2008).

14 R. Babarao, Z. Q. Hu, J. W. Jiang, S. Chempath and S. I. Sandler. *Langmuir* **23**, 659-666 (2007).

15 K. S. Walton, A. R. Millward, D. Dubbeldam, H. Frost, J. J. Low, O. M. Yaghi and R. Q. Snurr. *Journal of the American Chemical Society* **130**, 406 (2008).

16 A. R. Millward and O. M. Yaghi. *Journal of the American Chemical Society* **127**, 17998-17999 (2005).

17 V. R. Choudhary and S. Mayadevi. *Zeolites* **17**, 501-507 (1996).

18 V. R. Choudhary, S. Mayadevi and A. P. Singh. *Journal of the Chemical Society-Faraday Transactions* **91**, 2935-2944 (1995).

19 J. A. Dunne, M. Rao, S. Sircar, R. J. Gorte and A. L. Myers. *Langmuir* **12**, 5896-5904 (1996).

20 J. Lee, J. Kim, J. Kim and e. al. *Journal of Chemical and Engineering Data* **47**, 1237-1242 (2002).

21 S. Pakseresht, M. Kazemeini and M. M. Akbarnejad. *Separation and Purification Technology* **28**, 53-60 (2002).

22 R. Siriwardane, Shen, M.S., Fisher, P., Losch, J. *Energy & Fuels* **19**, 1153-1159 (2005).

23 M. S. Sun, D. B. Shah, H. H. Xu and O. Talu. *Journal of Physical Chemistry B* **102**, 1466-1473 (1998).

24 D. F. Plant, G. Maurin, I. Deroche, L. Gaberova and P. L. Llewellyn. *Chemical Physics Letters* **426**, 387-392 (2006).

25 D. F. Plant, G. Maurin, H. Jobic and P. L. Llewellyn. *Journal of Physical Chemistry B* **110**, 14372-14378 (2006).

26 E. García-Pérez, D. Dubbeldam, T. L. M. Maesen and S. Calero. *Journal of Physical Chemistry B* **110**, 23968-23976 (2006).

27 A. H. Fuchs and A. K. Cheetham. *Journal of Physical Chemistry B* **105**, 7375-7383 (2001).

28 E. Garcia-Perez, D. Dubbeldam, B. Liu, B. Smit and S. Calero. *Angewandte Chemie-International Edition* **46**, 276-278 (2007).

29 E. Garcia-Perez, J. B. Parra, C. O. Ania, D. Dubbeldam, T. J. H. Vlugt, J. M. Castillo, P. J. Merkling and S. Calero. *Journal of Physical Chemistry C* **112**, 9976-9979 (2008).

30 D. Dubbeldam, E. Beerdsen, S. Calero and B. Smit. *Proceedings of the National Academy of Sciences of the United States of America* **102**, 12317-12320 (2005).

31 D. Dubbeldam, S. Calero, T. L. M. Maesen and B. Smit. *Physical Review Letters* **90**, 245901 (2003).

32 T. J. H. Vlugt, E. Garcia-Perez, D. Dubbeldam, S. Ban and S. Calero. *Journal of Chemical Theory and Computation* **4**, 1107-1118 (2008).

33 D. Dubbeldam, S. Calero, T. J. H. Vlugt, R. Krishna, T. L. M. Maesen, E. Beerdsen and B. Smit. *Physical Review Letters* **93**, 088302 (2004).

34 D. Dubbeldam, S. Calero, T. J. H. Vlugt, R. Krishna, T. L. M. Maesen and B. Smit. *Journal of Physical Chemistry B* **108**, 12301-12313 (2004).

35 S. Calero, D. Dubbeldam, R. Krishna, B. Smit, T. J. H. Vlugt, J. F. M. Denayer, J. A. Martens and T. L. M. Maesen. *Journal of the American Chemical Society* **126**, 11377-11386 (2004).

36 S. Calero *et al. Journal of Physical Chemistry B* **110**, 5838-5841 (2006).

37 A. Goj, D. S. Sholl, E. D. Akten and D. Kohen. *Journal of Physical Chemistry B* **106**, 8367-8375 (2002).

38 K. Makrodimitris, G. K. Papadopoulos and D. N. Theodorou. *Journal of Physical Chemistry B* **105**, 777-788 (2001).

39 A. Hirotani *et al. Applied Surface Science* **120**, 81-84 (1997).

40 Li P. and F. H. Tezel. *Journal of Chemical and Engineering Data* **53**, 2479-2487 (2008).

41 E. Jaramillo and M. Chandross. *Journal of Physical Chemistry B* **108**, 20155-20159 (2004).

42 E. D. Akten, R. Siriwardane and D. S. Sholl. *Energy & Fuels* **17**, 977-983 (2003).

43 L. P. Maurin G, Bell RG. *Journal of Physical Chemistry B* **109**, 16084-16091 (2005).

44 J. J. Pluth and J. V. Smith. *Journal of the American Chemical Society* **102**, 4704-4708 (1980).

45 D. H. Olson. *Zeolites* **15**, 439-443 (1995).

46 A. N. Fitch, H. Jobic and A. Renouprez. *Journal of Physical Chemistry* **90**, 1311-1318 (1986).

47 W. J. Mortier, E. Vandenbossche and J. B. Uytterhoeven. *Zeolites* **4**, 41-44 (1984).

48 W. M. Meier. *Zeitschrift fuer Kristallographie, Kristallgeometrie, Kristallphysik, Kristallchemie* **115**, 439 (1961).

49 C. Baerlocher, W. M. Meier and D. H. Olson. *Atlas of Zeolite Structure Types*. Fifth edn, (Elsevier, 2001).

50 T. J. H. Vlugt and M. Schenk. *Journal of Physical Chemistry B* **106**, 12757-12763 (2002).

51 A. García-Sánchez, D. Dubbeldam and S. Calero. *Journal of Physical Chemistry C* **114**, 15068-15074 (2010).

52 M. T. Melchior, D. E. W. Vaughan and A. J. Jacobson. *Journal of the American Chemical Society* **104**, 4859-4864 (1982).

53 E. Beerdsen, B. Smit and S. Calero. *Journal of Physical Chemistry B* **106**, 10659-10667 (2002).

54 B. K. Peterson. *Journal of Physical Chemistry B* **103**, 3145-3150 (1999).

55 J. G. Harris and K. H. Yung. *Journal of Physical Chemistry* **99(31)**, 12021-12024 (1995).

56 D. Frenkel and B. Smit. *Understanding Molecular Simulations: From Algorithms to Applications*. Second edn, (Academic Press, 2002).

57 W. H. Press, Teukolsky, S. A., Vetterling, W. T., Flannery, B. P. *Numerical recipes in Fortran 77 : the art of scientific computing*. (Cambridge University Press, 2001).

58 J. Pires, M. B. Decarvalho, F. R. Ribeiro and E. G. Derouane. *Journal of Molecular Catalysis* **85**, 295-303 (1993).

59 K. S. Walton, M. B. Abney and M. D. LeVan. *Microporous and Mesoporous Materials* **91**, 78-84 (2006).

60 A. Alberti. *Zeolites* **19**, 411-415 (1997).

61 J. A. Delgado, M. A. Uguina, J. M. Gomez and L. Ortega. *Separation and Purification Technology* **48**, 223-228 (2006).

62 H. Ahn, J. H. Moon, S. H. Hyun and C. H. Lee. *Adsorption-Journal of the International Adsorption Society* **10**, 111-128 (2004).

63 D. A. Faux, W. Smith and T. R. Forester. *Journal of Physical Chemistry B* **101**, 1762-1768 (1997).

64 S. J. Potoff JJ. *AIChE Journal* **47**, 1676-1682 (2001).

65 K. S. W. Sing. *Pure and Applied Chemistry* **54**, 2201-2218 (1982).

66 J. Rouquerol *et al. Pure and Applied Chemistry* **66**, 1739-1758 (1994).

67 O. Talu, S. Y. Zhang and D. T. Hayhurst. *Journal of Physical Chemistry* **97**, 12894-12898 (1993).

Chapter 5

Influence of Force Field Parameters on Computed Diffusion Coefficients of CO_2 in LTA-type Zeolites*

* This chapter is based on: A. García-Sánchez, J. van den Bergh, J.M. Castillo, S. Calero, F. Kapteijn and T.J.H. Vlugt: "Influence of Force Field Parameters on Computed Diffusion Coefficients of CO_2 LTA-type Zeolites". *In preparation.*

ABSTRACT: Molecular Dynamics simulations were used to study the diffusion behaviour of carbon dioxide in Linde Type A (LTA) zeolites. The observed concentration dependencies of the self- and transport diffusions are strongly affected by the choice of the force field. The Relevant Site Model (RSM) is used to describe the loading dependency of diffusion coefficients. In addition, we investigated the influence of non-framework cations on diffusion. For zeolites without non-framework cations, the RSM accurately describes the concentration dependency of CO_2 diffusivities in LTA-type zeolite calculated using different force fields. The preferential siting of the adsorbate molecules is discussed to elucidate the origin of the differences in the concentration dependence of computed diffusivities using different force fields.

5.1 Introduction

It is well known that the increasing atmospheric carbon dioxide concentration affects global warming. Thus, efforts to find an energy-efficient CO_2 capture method[1] are highly relevant for effectively separating CO_2 from natural gas[2]. Zeolites are suitable microporous materials for the selective capture of CO_2[1]. One of the required key factors for separating CO_2 from gas streams using microporous materials is knowledge on adsorption and diffusion behaviour. The study of CO_2 adsorption and diffusion in zeolites and other porous materials is an important topic as was shown in several recent studies[3-7].

Zeolites are microporous molecular sieves containing channels and cages of molecular dimensions. Their frameworks consist of TO_4 tetrahedral units that share vertices[8]. In all-silica zeolites, the T-atom is a silicon atom, and the structure does not have any net charge[9]. In some zeolites, silicon atoms are replaced by aluminium. This results in a negative charge in the framework which is compensated with non-framework cations such as sodium or calcium. The synthetic aluminosilicalite LTA-type zeolite is one of the most studied zeolites, together with FAU-type zeolite, due to the ability of cation exchange[10,11]. LTA-type zeolite has a well-known three-dimensional network that consists of cages connected to each other by narrow windows. The crystallographic positions of all the atoms in the zeolite structure are known exactly[12].

The adsorption and diffusion of light alkanes has been extensively studied in LTA-type zeolites using both experimental[13-20] and computational[21-26] techniques. There are several force fields in the literature aiming to predict the adsorption behaviour of carbon dioxide in all-silica zeolites[27,28]. The adsorption behaviour of hydrocarbons in all-silica zeolites is well reproduced using the force field described by Dubbeldam *et al.*[15], but often large differences are found between experimental and computed diffusivities[29]. These differences are mainly due to differences in microscopic and macroscopic measurement methods[30]. This can also explain differences in diffusion studies in other cage-type zeolites such as DDR- and CHA-type zeolites. As an example, Hedin *et al.*[31] performed experimental studies in different cage-type zeolites for short n-alkanes at low

loading. Their results differ from previous simulation studies from Krishna *et al.*[32,33] but are in agreement with simulations results provided by Jee and Sholl[34]. Furthermore, the results published by Krishna *et al.*[33] for single-components diffusion in DDR-type zeolites at 300 K show that methane diffuses more rapidly than carbon dioxide. For the same zeolite type, and for almost the same temperature, 298 K, Jee and Sholl[34] predicted a much larger diffusivity for carbon dioxide than for methane. Recently, we developed a transferable force field to accurately reproduce the CO_2 adsorption behaviour in different zeolite structures that include sodium non-framework cations[19]. This force field accurately describes CO_2 adsorption in FAU-, MOR-, LTA- and MFI-type zeolites with different Si/Al ratios. Therefore, it offers the possibility to screen many zeolites with different framework structure for CO_2 adsorption. If a force field accurately describes the interactions between the adsorbate and the framework structure, then, in principle, any thermodynamic property can be predicted. Ideally, a force field should accurately describe not only thermodynamic properties, but also transport properties.

Experimental diffusion measurements for guest molecules adsorbed in zeolites are a challenging task. Research groups often provide diffusivities for the apparently same system that differ up to three orders of magnitude[3,35-37]. These differences are mainly due to imperfections in the zeolite crystals[38], and in the difficulty to reach equilibrium in the system[39,40]. Therefore, molecular simulation is an important tool to provide a detailed understanding of the diffusion processes. Until now, the only experimental data available in literature for CO_2 diffusion in various zeolite structures are at very low loading[3,41-44], and the differences in reported diffusivities between different studies are larger than two orders of magnitude. For example, Kärger *et al*. reported intracristalline self-diffusion coefficients for CO_2 in LTA-5A type zeolite and provided two different values for the diffusion coefficient at the same temperature and pressure[43,44], $(1.5 \pm 0.8)\ 10^{-8}$ m^2/s and $(2 \pm 1)\ 10^{-10}$ m^2/s, respectively. Both measurements were obtained by Pulsed Field Gradient (PFG) NMR in the same zeolite structure, LTA-5A type zeolite with 32 sodium and 32 calcium cations per unit cell. To the best of our knowledge, these are the only experimental measurements in the literature of CO_2 diffusion in LTA-type zeolite with non-framework cations.

Molecular simulation studies on diffusion in zeolites are usually focused on zeolites without non-framework cations[6,45,46]. Simulations thus often do not cover a wide range of zeolite structures that include non-framework cations. Therefore, the influence of cations on the diffusion of guest molecules is not yet fully understood.

The reported diffusivities in literature for cage- and channel-type zeolites can be classified into two main groups. The observed concentration dependence of diffusivities for these two groups can be classified following Kärger and Pfeifer[47]: self-diffusion of type I and self-diffusion of type IV. Type I shows an almost linear decreasing self-diffusivity for increasing loading. Kärger and Pfeifer observed this behaviour for diffusion of light alkanes in silicalite and FAU-type zeolite at 300 K[47]. Other experimental measurements show the same trend for methane and CO_2 in all silica MFI–[47,48], and LTA-type zeolites[31], as well as numerous computational studies for FAU-[48-53], MFI-[45,49,51,53-55], LTL-[49,51], CHA-[49], MWW-[56], DDR-[34,49] and LTA-type[57] zeolites. Self-diffusion of type IV presents a completely different behaviour; the diffusivity increases to maximum and then decreases as a function of loading. This was experimentally observed in FAU-type zeolites for water and acetonitrile[47], and for methane at 200 K[3], as well as by simulation studies in different all-silica zeolite structures, such as LTA-[7,49,51,53,58] , CHA-[7,51,53] and DDR- type[7,34,53] zeolites. Other light gases such as Ar, Xe and N_2 also show type IV self-diffusion in MFI-[7,46,49,54,58-60], CHA-[53], DDR-[53,59] and LTA-type[52] zeolites. Dubbeldam *et al.*[58] showed that for all-silica LTA-type zeolites the diffusion coefficient of methane as a function of loading shows a clear maximum.

The diffusivity of guest molecules adsorbed in zeolites with narrow windows often strongly depends on loading, e.g. in zeolites with cages separated by large windows, such as FAU-type zeolite, or channels, such as LTL- or MFI-type zeolites[51]. The Reed-Ehrlich model for surface diffusion[53,61] was successfully developed and applied to zeolites by Krishna *et al.*[53]. Unfortunately, the Reed-Ehrlich model is not applicable to all zeolites and, in particular, to LTA-type zeolites[62]. For this reason, other models are needed to explain the loading dependence in these zeolites. The Relevant Site Model (RSM)[62-64] was

successfully developed and applied to describe the loading dependency of diffusion of different small molecules such as CO_2, CH_4, Ar and Ne in several zeolites such as DDR-, CHA-, MFI- and FAU-type zeolites[62-64]. In this work, we apply the RSM model to study the diffusion of CO_2 in LTA-type. We study the influence of the guest-host interactions on the loading dependence of CO_2 diffusivities in a zeolite with non-framework sodium cations, LTA-4A, and in all-silica LTA-type zeolites, such as ITQ-29 and LTA_{Si}. The latter is the hypothetical all silica version of LTA-4A. Both self- and Maxwell-Stefan diffusivities are computed.

To understand the diffusion behaviour of CO_2 in LTA-type zeolites and the influence of the guest-host interactions, we have used two force fields available in the literature. The first was developed by Calero *et al.*[17], and has been applied to study adsorption[20,65-67] and diffusion[32,58,68] of hydrocarbons and CO_2 in various all-silica zeolites. From this force field, we adopted the Lennard-Jones interactions and the partial charges to describe the interactions between the framework atoms and the non-framework cations. Lennard-Jones interactions between the framework and the adsorbate were taken from Ref. 65. The second force field was recently published by our group and provides an accurate interaction model to screen the adsorption of CO_2 in both all-silica zeolites and zeolites with sodium non-framework cations[19]. The Lennard-Jones interactions and partial charges were taken from Ref. 19. To identify these force fields, we denote them by FF1 and FF2, respectively. Note that the Lennard-Jones parameters for guest-guest and guest-host interactions and the partial charges for host atoms are different. To understand the origin of the differences between those two force fields, we also consider the adsorption and diffusion of CO_2 in an hybrid force field, denoted by FF3, where the partial charges of atoms of the guest molecules as well as the zeolite framework were taken from FF1[17,65] and the Lennard-Jones parameters for guest-guest and guest-host interaction were taken from FF2[19].

The remainder of this chapter is organized as follows. In section 5.2 we explain the simulation methods and the models used in this work, including a brief description of the Relevant Site Model (RSM). In section 5.3, we present the

results for (i) CO_2 adsorption in LTA-type zeolites; (ii) CO_2 self-diffusion in LTA-type zeolites; (iii) Maxwell-Stefan diffusion coefficients of CO_2; (iv) the application of the RSM to describe the concentration dependence of Maxwell-Stefan diffusivities in LTA-type zeolites; and (v) analysis of CO_2 adsorbate sites and non-framework cations in LTA-type zeolites. Our findings are summarized in section IV.

5.2 Simulation Methods and Models

LTA-type zeolites are constructed from truncated octahedra, so-called sodalite or β-cages. The diameter of these cages is about 10 Å. The crystal structure has the space group Fm3c[69]. The LTA-type unit cell is formed by eight sodalite cages arranged on a cubic lattice. The sodalite cages form an eight membered ring (MR) and creates a channel parallel to the <100> plane. The intersecting channels are called α-cages and join each other sharing the 8 MR, which has a 4.1 Å pore size[69]. LTA-4A was modelled as a simple cubic lattice with $a = b = c = 24.555$ Å[12]. The aluminium and sodium atoms were placed at the experimental crystallographic positions[12]. By substituting the Al atoms in the LTA-4A structure by Si atoms, we obtain the hypothetical LTA_{Si} structure used in some of our simulations. The experimental all-silica LTA-type structure is called ITQ-29[70] and its unit cell is approximately two times smaller in each direction than LTA-4A. The ITQ-29 structure consists of the same type of channel and cages as LTA-4A but with different unit cell dimensions: $a = b = c = 11.867$ Å. Therefore, LTA_{Si} has 8 cages per unit cell while ITQ-29 has 1 cage per unit cell.

In LTA-4A, there are 12 sodium non-framework cations per α-cage distributed among three crystallographic sites: Na I, Na II and Na III. In Fig. 5.1, the sodium non-framework cation positions are shown as coloured spheres. The site Na I is located in the centre of the six membered oxygen rings (positions coloured red) and include eight positions for the cations. The Na II site can accommodate sodium cations in three different positions in the eight MR window (positions coloured green), and finally the twelfth cation is located opposite to the four MR

(positions coloured blue). For obtaining a better understanding of the CO_2 diffusion in LTA-type zeolites we also study the CO_2 positioning. In Fig. 5.1, the CO_2 adsorption sites in LTA-type are denoted by circles with different colours. In this study, we consider four different sites for the carbon dioxide locations as follows: the CO_2 I site (so-called *Window*) is denoted by a red circle in the eight MR connecting the α-cage; the CO_2 II or *Cube* site is in the four MR (brown circle); the *Centre* or CO_2 III site (green circle) is in the centre of the eight MR in the window and the CO_2 IV or *Sodalite* site (orange circle) is in the sodalite cages.

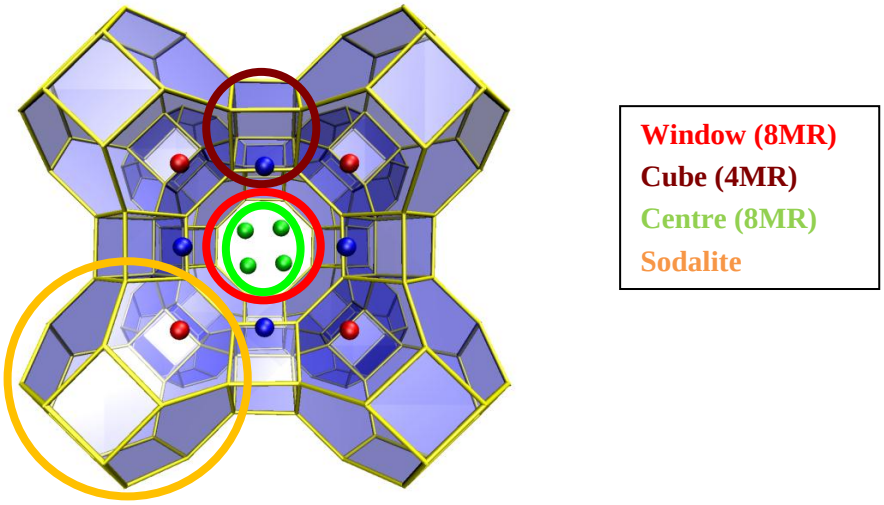

Figure 5.1: Description of the crystallographic Na positions and the CO_2 adsorption sites. The non-framework cations, represented by spheres, can be located at the three following crystallographic sites: Na I (positions in red) in the centre of the 6 membered ring (MR); Na II in the 8 MR (positions in green); and Na III in the 4 MR (positions in blue). The potential CO_2 adsorption sites are indicated by circles. We considered four different sites located as follows: CO_2 I or *Window* in the 8 MR (red circle); CO_2 II or *Cube* in the 4 MR (brown circle); CO_2 III or *Centre* in the centre of the 8 MR (green circle); and CO_2 IV or *Sodalite* in the truncated octahedra (orange circle).

5.2.1 Models

Molecular simulations are used to study the adsorption and diffusion of CO_2 for three different force fields. The force field parameters for FF1 and FF2 are taken directly from literature. To understand the influence of the Lennard-Jones and Coulombic interactions for CO_2 adsorption and diffusion in LTA-type zeolites, we introduce a new hybrid force field, here denoted by FF3. This force field is defined with the Coulombic interactions from FF1 and the Lennard-Jones interactions from FF2. The parameters of all force fields are listed in Table 5.1. The main differences between these force fields are: 1) the Lennard-Jones parameters for guest-guest interactions; 2) the Lennard-Jones parameters for guest-host interactions; 3) the charges of the framework atoms; and 4) the charges of non-framework atoms.

We study the CO_2 adsorption and diffusion in the three mentioned LTA-type zeolites. All framework structures were considered rigid[71]. Non-framework cations in LTA-4A zeolite were able to move freely. The central α-cages were blocked to avoid the adsorption of CO_2 in this inaccessible region[72]. Carbon dioxide was modelled as a triatomic linear and rigid molecule[19]. The partial charges and bond lengths are taken from Harris and Yung[73]. Adsorption isotherms were computed using grand-canonical Monte Carlo (GCMC) simulations where the volume, the chemical potential and the temperature were held constant and the number of adsorbed guest molecules was fluctuating. Chemical potentials of CO_2 can be transformed into pressures using the Peng-Robinson equation of state[15,74]. Self- and Maxwell-Stefan diffusivities were both calculated by Molecular Dynamics (MD) calculations in the NVT ensemble with a time of 0.001 ps. The simulations were at least 180 ns which is long enough to extract self- and transport diffusivities[75]. For simulation details, and details on how to extract self- and Maxwell-Stefan diffusivities from MD simulations, we refer the reader to Refs[29,32,58,76,77].

	FF1	FF2	FF3
		CO_2-CO_2	
$\varepsilon/k_{B\ O\text{-}O}$ /[K]	80.507	85.671	85.671
$\sigma_{O\text{-}O}$ /[Å]	3.033	3.017	3.017
$\varepsilon/k_{B\ C\text{-}C}$ /[K]	28.129	29.933	29.933
$\sigma_{C\text{-}C}$ /[Å]	2.76	2.745	2.745
$\varepsilon/k_{B\ C\text{-}O}$ /[K]	47.59	50.640	50.640
$\sigma_{C\text{-}O}$ /[Å]	2.89	2.880	2.880
		CO_2-zeolite	
$\varepsilon/k_{B\ C\text{-}Oz}$ /[K]	50.2	37.595	37.595
$\sigma_{C\text{-}Oz}$ /[Å]	2.7815	3.511	3.511
$\varepsilon/k_{B\ O\text{-}Oz}$ /[K]	84.93	78.980	78.980
$\sigma_{O\text{-}Oz}$ /[Å]	2.9195	3.237	3.237
$\varepsilon/k_{B\ Na\text{-}C}$ /[K]	362.292	362.292	362.292
$\sigma_{Na\text{-}C}$ /[Å]	3.320	3.320	3.320
$\varepsilon/k_{B\ Na\text{-}O}$ /[K]	200.831	200.831	200.831
$\sigma_{Na\text{-}O}$ /[Å]	2.758	2.758	2.758
$\varepsilon/k_{B\ Na\text{-}Oz}$ /[K]	23.000	23.000	23.000
$\sigma_{Na\text{-}Oz}$ /[Å]	3.400	3.400	3.400
		Partial charges and C=O bond length (CO_2)	
q_C /[e^-]	0.6512	0.6512	0.6512
q_O /[e^-]	-0.3256	-0.3256	-0.3256
l_{CO} /[Å]	1.161	1.149	1.149
		Partial charges (zeolite)	
q_{Si} /[e^-]	2.05	0.78598	2.05
q_{Al} /[e^-]	1.75	0.48598	1.75
q_{OSi} /[e^-]	-1.025	-0.39299	-1.025
q_{OAl} /[e^-]	-1.2	-0.41384	-1.2
q_{Na} /[e^-]	1	0.38340	1

Table 5.1: Lennard-Jones force field parameters and partial charges for the three force fields used in this work. The CO_2 molecule is modelled following Harris and Yung[73] in all cases. For FF1, the values of the partial charges for the framework atoms and non-framework cations are taken from Calero *et al.*[17] and the LJ parameters for the interactions between the framework and the adsorbate from García-Pérez *et al.*[65] The values of the partial charges and the LJ parameters for FF2 are taken from García-Sánchez *et al.*[19]. The values of the partial charges for the zeolite in FF3 were taken from Calero *et al.*[17] and the LJ parameters from García-Sánchez *et al.*[19]. The values of the LJ parameters for the non-framework cations interactions with the framework are taken from Calero *et al.*[17] in all cases. The values of the LJ parameters for the non-framework cations and the adsorbate are taken from García-Sánchez *et al.*[19] in all cases. The subscripts C and O denote the CO_2 atoms. The subscript Oz denotes the oxygen atoms of the zeolite.

5.2.2 Relevant Site Model

To explain the concentration dependence of diffusivities, the Reed–Ehrlich model[53,61] is often applied. This model assumes that the intermolecular repulsions are the origin of the observed loading dependency of diffusion. However, the Reed–Ehrlich model fails to describe concentration dependence of diffusivities in zeolites with narrow windows such as LTA-, CHA- or DDR-type zeolites[51]. An important improvement was provided by the Relevant Site Model (RSM)[62-64]. This model distinguishes between the total loading, denoted by *q*, and the loading of molecules in the so-called relevant site, denoted by *q**. It is assumed that only molecules adsorbed at the relevant site have a contribution to diffusion. As mentioned earlier, LTA-type zeolite consists of cages connected by windows. In this type of zeolite, the loading dependency of diffusivity is strong since the molecules are strongly confined in the zeolite[52,64,78]. It is natural to assume that the relevant site will be located in the window of LTA-type zeolite. For methane, this was confirmed numerically in Ref. 64.

In the RSM, the free space relevant for adsorption of guest molecules is denoted by (*1-θ*) where the occupancy $\theta = \frac{q}{q^{sat}}$ is defined as the ratio of the loading, *q*, and the saturation loading, q^{sat}. The fraction of molecules located at the relevant site (*Window*) is described by a single-site Langmuir isotherm related to the fugacity *f:*

$$q^{*} = \frac{q^{sat*} k^{*} f}{1 + k^{*} f} \tag{5.1}$$

The constants q^{sat*} and *k** represent the saturation loading at the relevant site, and the relevant site adsorption equilibrium constant, respectively. The occupancy of guest molecules in the relevant site is described as $\theta^{*} = \frac{q^{*}}{q^{sat*}}$. Following van den Bergh *et al.*[62], we also consider the loading associated with the space relevant for mass transport. We distinguish between the adsorption sites relevant for transport diffusion and those sites that represent the free space irrelevant for

transport diffusion, denoted by the superscript #. The free space relevant for mass transport is given by[62]:

$$\left(1-\theta^{\#}\right)=1-\frac{q-q^{\#}}{q^{sat}-q^{sat\#}} \tag{5.2}$$

In this equation, q^{sat} is the saturation loading of the zeolite, $q^{\#}$ is the loading at the space irrelevant for transport diffusion and $q^{sat\#}$ is the saturation loading at the space irrelevant for diffusion. The loading at the space irrelevant for diffusion is also described by a single-site Langmuir isotherm:

$$q^{\#}=q^{sat\#}\frac{k^{\#}f}{1+k^{\#}f} \tag{5.3}$$

When the free space relevant for the transport diffusion and the total loading are known, the RSM can be used to compute the collective or transport diffusivity[62]:

$$Đ=Đ^{*}(0)\left(1-\theta^{\#}\right)\frac{q^{*}}{q} \tag{5.4}$$

in which $Đ^{*}(0)$ is a constant. Combining Eqs (5.1)-(5.4), we can rewrite Eq. (5.4) as follows:

$$Đ=q^{sat*}Đ^{*}(0)\left(1-\theta^{\#}\right)\frac{\theta^{*}}{q}=q^{sat*}Đ^{*}(0)\left[1-\frac{q-\dfrac{q^{sat\#}k^{\#}f}{1+k^{\#}f}}{q^{sat}-q^{sat\#}}\right]\frac{1}{q}\frac{k^{*}f}{1+k^{*}f} \tag{5.5}$$

in which the following constants have to be fitted: the lumped diffusivity parameter $\left(q^{sat*}Đ^{*}(0)\right)$; the Langmuir constant of the relevant site, k^{*}; the Langmuir constant of the site irrelevant for diffusion, $k^{\#}$; the saturation loading for the space irrelevant for diffusion, $q^{sat\#}$; and the total saturation loading, q^{sat}. As the latter is sometimes difficult to obtain from GCMC simulations, we decided to fit this value rather than obtaining it from the adsorption isotherm.

5.3 Results and Discussion

We report computed carbon dioxide diffusivities and adsorption isotherms in LTA-type zeolites with the different force fields, see Table 1. Below, we discuss the obtained results, which are divided into the following sections: (i) adsorption of CO_2 in LTA-type zeolites at different temperatures, (ii) self-diffusion of CO_2 in LTA-type zeolites, (iii) transport diffusion of CO_2 in LTA-type zeolites, (iv) application of the Relevant Site Model (RSM) for Maxwell-Stefan diffusion, and (v) analysis of adsorbate CO_2 positions and sodium non-framework cations positions.

5.3.1 Adsorption of carbon dioxide in LTA type zeolites

We compute CO_2 adsorption isotherms for the three mentioned LTA-type zeolites: LTA_{Si}, ITQ-29 and LTA-4A, using the GCMC simulation technique.

As is shown in Fig. 5.2, all force fields provide nearly the same adsorption isotherm for ITQ-29 at 300 K and 600 K at low pressures. For pressures larger than 10^3 kPa and 10^6 kPa for 300 K and 600 K respectively, FF1 shows a slightly larger adsorption.

As expected for ITQ-29, the differences in the partial charges of the zeolite framework atoms for FF2 and FF3 do not strongly influence the computed adsorption isotherms. The origin of the differences observed at high pressure for CO_2 adsorption in ITQ-29 type zeolites are due to the differences in the Lennard-Jones parameters. In particular, the larger values for guest-host size interactions, σ, for FF2 and FF3, results in a lower maximum loading compared to that of FF1. If the value of σ for guest-host interactions is larger, the effective pore size will be smaller and the maximum loading will decrease.

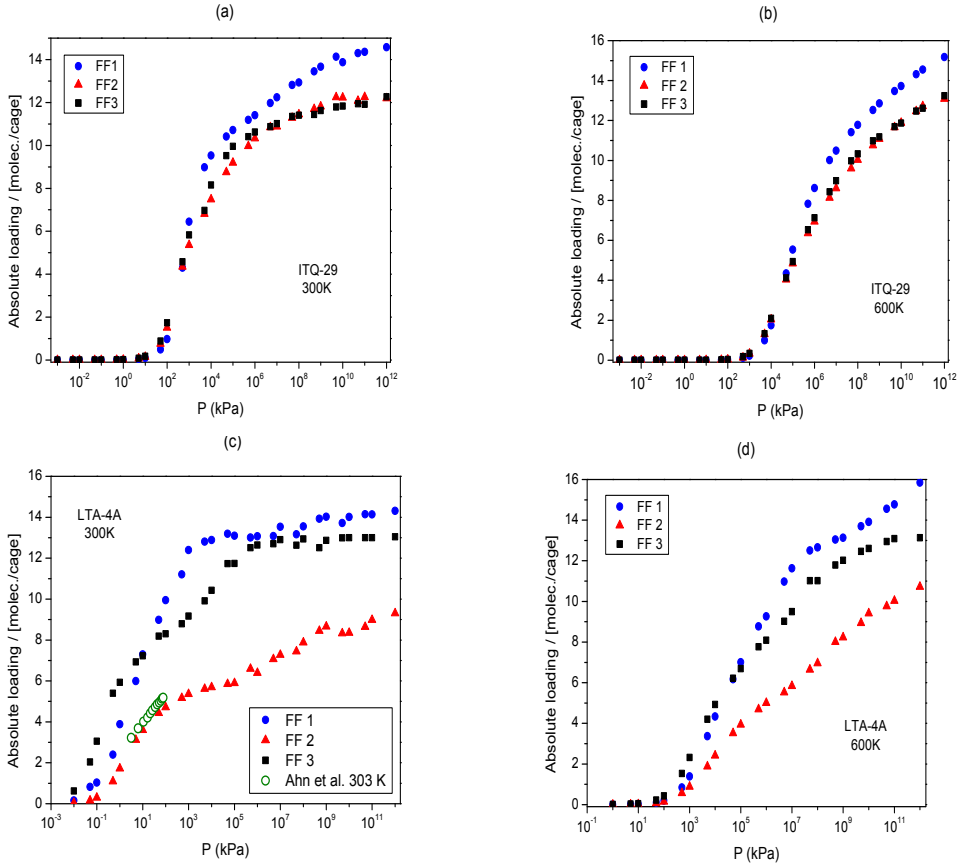

Figure 5.2: Computed CO_2 adsorption isotherms for (a) ITQ-29 at 300 K, (b) ITQ-29 at 600 K, (c) LTA-4A at 300 K and (d) LTA-4A at 600 K using the three force fields considered in this study. Experimental adsorption data in LTA-4A at 303 K are taken from Ahn *et al.*[79]

The differences in the CO_2 adsorption using the various force fields are much larger for LTA-4A, as is shown in Figs. 5.2 (c) and (d). Force field FF1, which has larger partial atomic charges of the framework and non-framework atoms, results in a larger CO_2 adsorption at both 300 K and 600 K. The experimental results for CO_2 adsorption in LTA-4A at 303 K are taken from Ahn *et al.*[79] To the best of our knowledge, for this system there is no experimental adsorption data available at 600 K. The experimental results shown in Fig. 5.2 (c) are in agreement with the data obtained from FF2 and are overstimated by FF1. As expected, the CO_2 adsorption in ITQ-29 at both 300 K and 600 K calculated

using FF3 leads to similar results as for FF2. However, for LTA-4A at 300 K and 600K, the adsorption data obtained for FF3 are similar to that obtained using FF1. Only the isotherm obtained with FF2 is in agreement with the experimental results shown at 300 K.

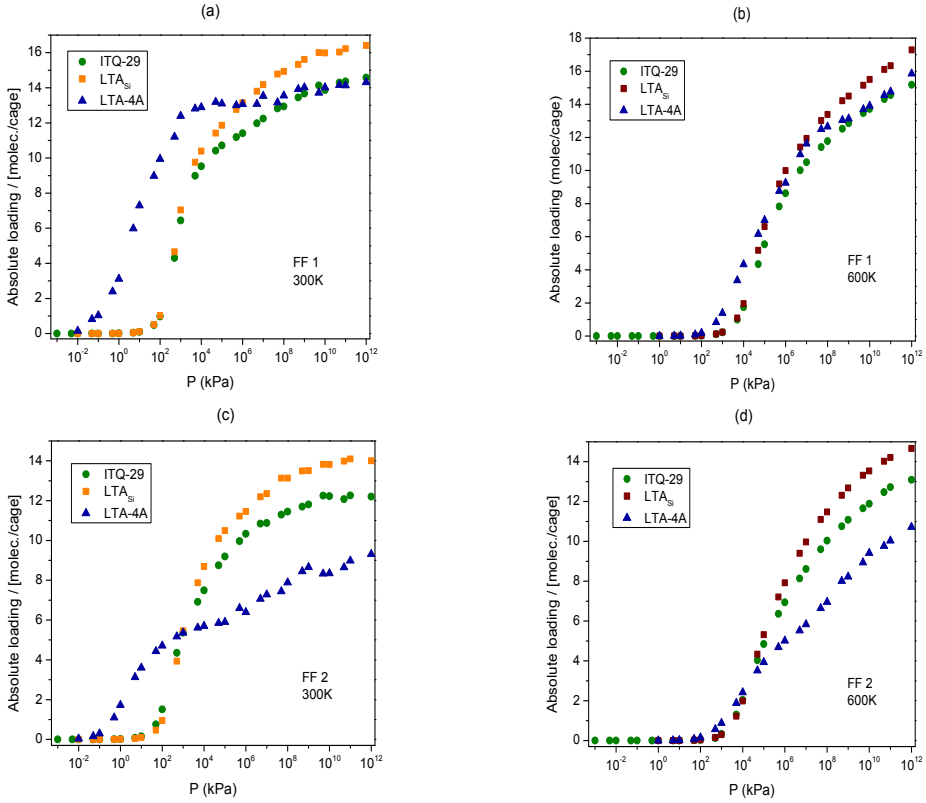

Figure 5.3: Computed CO_2 adsorption isotherms in LTA-type zeolites using FF1 at 300 K (a) and 600 K (b) and FF2 at 300 K (c) and 600 K (d). The force field parameters and partial charge for FF1 and FF2 are listed in Table 5.1.

A comparison between the different LTA-type zeolites for the force fields FF1 and FF2 is shown in Fig. 5.3. At low temperatures, the LTA-4A structure leads to a larger adsorption of CO_2 than the all-silica structures. It is well known that the presence of non-framework cations increases the adsorption at low pressures and decreases the loading at high pressures[18,20]. At low temperature and pressures

larger than 10^4 kPa, the CO_2 adsorption for the structures with sodium non-framework cations is significantly lower than for the all-silica structures, especially for those where FF2 force field was used. At 600 K [Fig 5.3 (b) and 5.3 (d)] there are no differences at low pressures between the different LTA-type structures. However, using FF2 [Fig 5.3 (d)], at pressures exceeding 10^5 kPa the amount of adsorbed CO_2 is lower. The number of CO_2 molecules adsorbed at saturation is around 13 molecules per cage for all-silica structures, and 10 molecules per cage for the structure with cations.

5.3.2 Self-diffusivities

Self-diffusion is related to the motion of individual particles[75]. The values of self-diffusion coefficients were computed by analysing the mean square displacements[58,80]. Fig. 5.4 shows the CO_2 self-diffusivities in LTA-type zeolites (LTA_{Si}, ITQ-29 and LTA-4A) at 300 K and 600 K, using the three different force fields. The self-diffusivities for LTA_{Si} at 300 K reported by Krishna *et al.*[33] are in exact agreement with our result shown in Fig. 5.4 (a), as we used exactly the same force field. The computed diffusivities using FF1 show a high diffusivity at low loading that decreases as the loading increases. Low values for the self-diffusivity are obtained with FF2 and FF3 at low loading, which increase with loading to a maximum and then decrease at higher loading. These observations are in line with earlier simulations by Krishna and co-worker for Ar diffusion in CHA-type zeolite: decreasing the Lennard-Jones size parameter for guest-host interactions results in (1) larger diffusivities and (2) the disappearance of the maximum in the loading dependence of the diffusivity[53].

The CO_2 self-diffusivity in LTA-4A is lower than in all silica LTA-type zeolites because the Na non-framework cations partially block the window regions. This was verified by analysing simulation snapshots. The computed diffusivities for FF2 are shown in Fig. 5.4 (d). As the Lennard-Jones size parameter for guest-host interactions is smaller, the CO_2 molecules can pass the window and cross the energy barrier. The diffusivities for FF1 were too low to be calculated by MD simulations (diffusivity smaller than $1 \cdot 10^{-12}$ m^2/s).

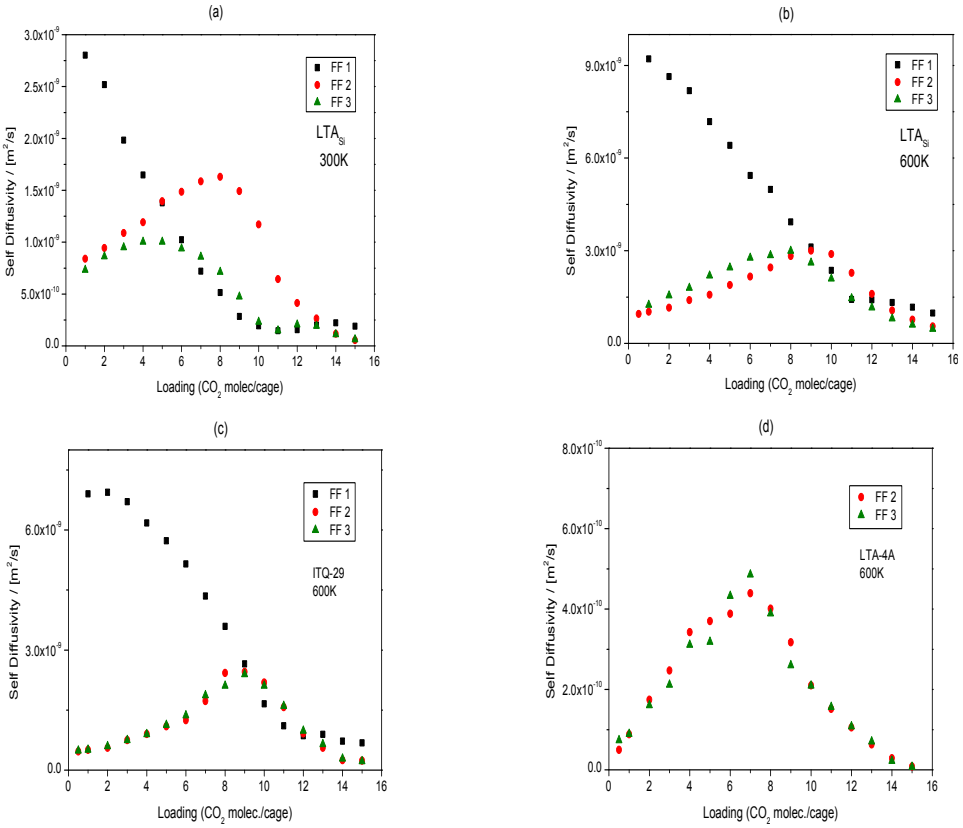

Figure 5.4: Computed CO_2 self-diffusivities diffusivities in LTA_{Si} at 300 K (a) and 600 K (b) for the studied force fields; ITQ-29 at 600 K (c); and LTA-4A at 600 K (d).

5.3.3 Maxwell-Stefan Diffusivities

Maxwell-Stefan diffusion coefficients are also known as collective diffusion or transport diffusion coefficients[75], and they are related to the collective motion of adsorbed guest molecules in the system. Transport diffusion coefficients are usually larger than the self-diffusion coefficient[75]. At zero loading, both diffusivities are identical.

Figs. 5.4 and 5.5 show that the differences in the framework charges between FF2 and FF3 do not result in very large differences between computed diffusion coefficients results. Note that for LTA_{Si} at low temperatures, FF2 results in a

more pronounced maximum in the MS diffusivity (Fig. 5(a)). For LTA-4A, there are large differences in adsorption for FF2 and FF3, while these differences are absent in the loading dependence of the MS diffusivity. Fig. 5.5 shows Maxwell-Stefan diffusivities for the three frameworks, LTA_{Si}, ITQ-29 and LTA-4A for the three force fields. At 300 K, the diffusion of CO_2 in LTA-4A is blocked by sodium cations. At this temperature the sodium cations remain at the *window* sites, partially blocking CO_2 molecules. At 600 K, the sodium cations are displaced from their crystallographic position and CO_2 molecules can diffuse inside the zeolite as shown in Fig. 5.5 (d).

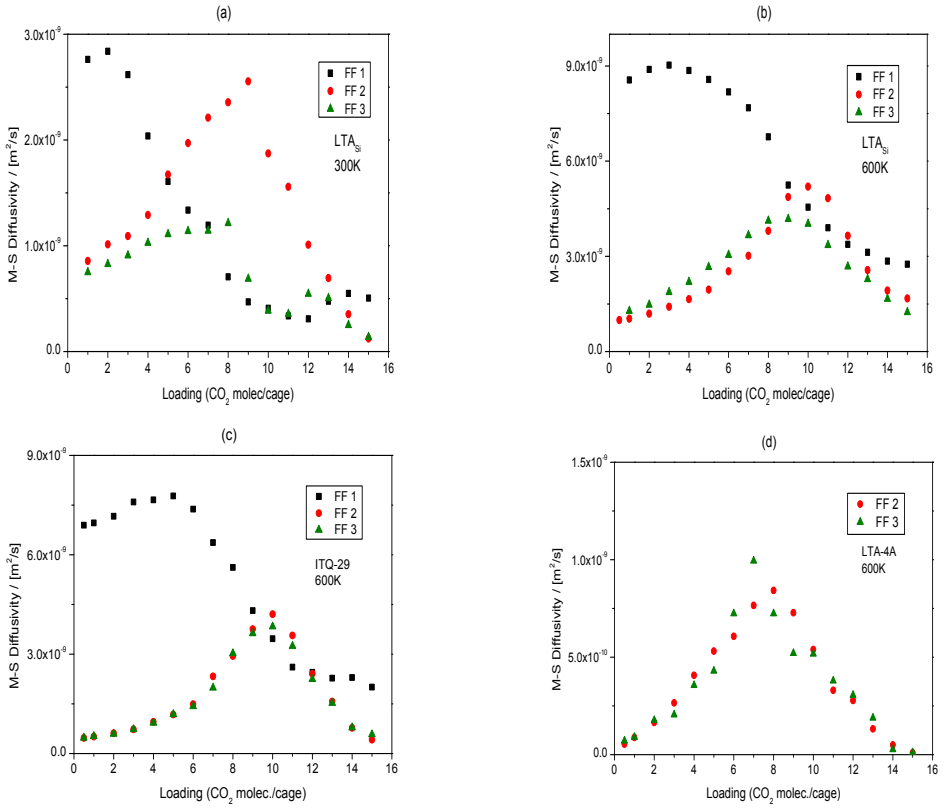

Figure 5.5: Computed CO_2 Maxwell-Stefan diffusivities in LTA_{Si} at 300 K (a) and 600 K (b) for the different studied force fields; ITQ-29 at 600 K (c); and LTA-4A at 600 K (d).

The concentration dependence of self- and Maxwell-Stefan diffusivities for CO_2 in LTA-4A, LTA_{Si} and ITQ-29 are compared in Fig. 5.6.

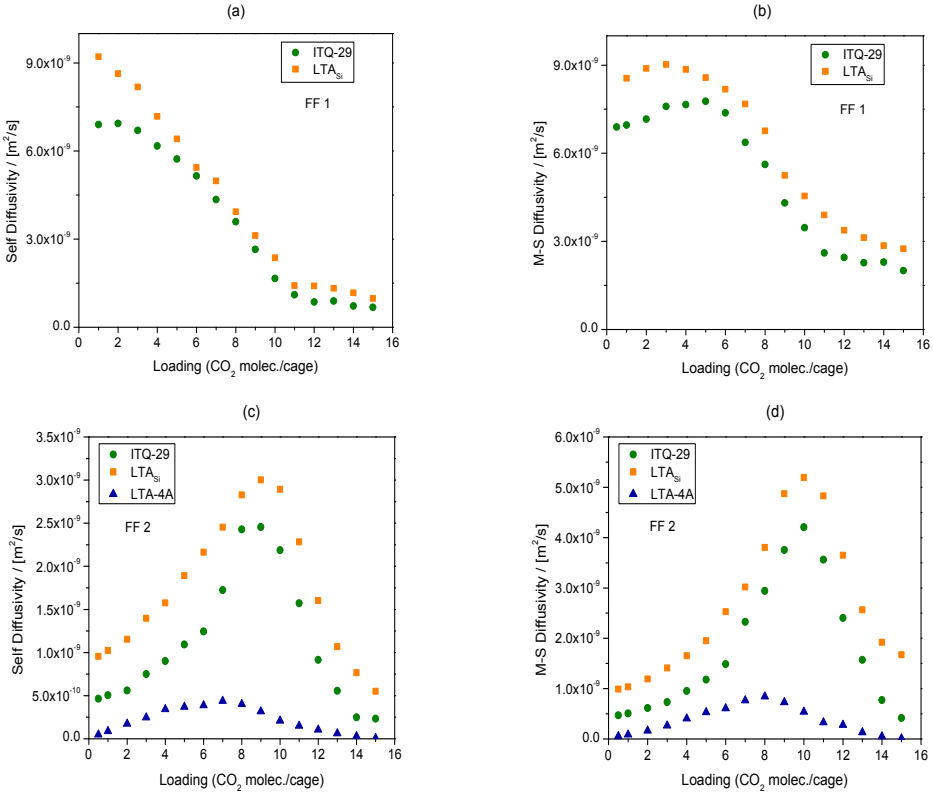

Figure 5.6: Computed diffusion coefficients in LTA-type zeolite at 600 K using the FF1 force field for self-, (a), and Maxwell-Stefan, (b), diffusion coefficients. The corresponding data for FF2 is shown in (c) and (d).

The results for FF1, shown in Fig 5.6 (a) and (b), show similar self- and transport diffusion coefficients. The CO_2 diffusivities in LTA_{Si} are slightly larger than in ITQ-29. At low loading, up to 4 molecules per cage, the differences in the self- and Maxwell-Stefan diffusivities are slightly larger than at higher loading. The self- and transport diffusion of CO_2 in LTA-4A are not shown because diffusion is too slow (diffusivities smaller than $1 \cdot 10^{-12}$ m^2/s) to be computed by MD. The diffusivities of CO_2 as a function of the loading for LTA-type zeolites using FF2 are shown in Fig 5.6 (c) and (d). The largest values for both self- and transport diffusivity occur for LTA_{Si} due to its bigger window size compared to ITQ-29[71].

Diffusion coefficients for ITQ-29 are close to those of LTA_{Si}. The diffusion coefficients for CO_2 in LTA-4A are lower than for all-silica structures due to the partial blocking of the windows by the cations.

5.3.4 Relevant Site Model

To understand the loading dependence of Maxwell-Stefan diffusivities, our computed diffusivities were fitted to the Relevant Site Model. There is an excellent fit of the computed Maxwell-Stefan diffusivities from MD simulations for the FF1 and FF2 force fields for LTA_{Si} zeolite, as is shown in Figs. 5.7 (a) and (c). Table 5.2 provides a list of the fitted parameters.

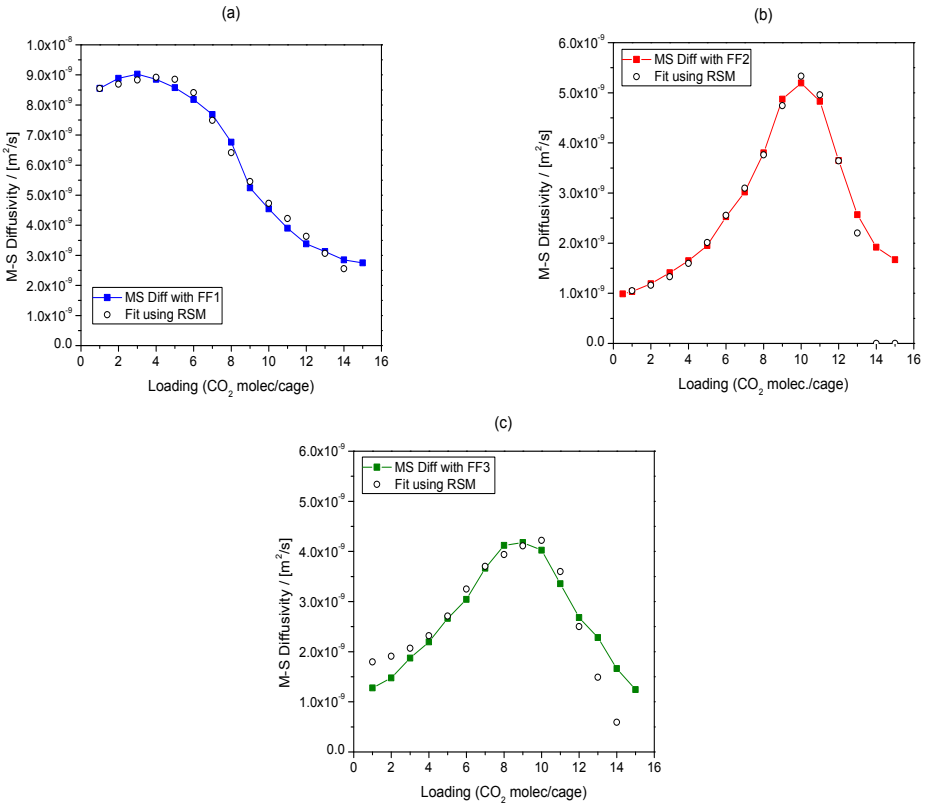

Figure 5.7: Computed Maxwell Stefan-diffusivities $Đ_{MS}$ from MD simulations for CO_2 in all-silica LTA_{Si}-type zeolite at 600 K. The data is fitted using the Relevant Site Model. (a) FF1; (b) FF2; (c) FF3.

		FF1	FF2	FF3
LTA_{Si}	q^{sat*} $Đ(0)$ [molec·cage^{-1}·m^2·s^{-1}]	$8.63\cdot10^{-8}$	$1.54\cdot10^{-7}$	$1.04\cdot10^{-7}$
	$q^{sat\#}$ [molec·cage^{-1}]	1.830	5.338	5.392
	k^{*} [kPa^{-1}]	$1.24\cdot10^{-8}$	$3.58\cdot10^{-8}$	$1.20\cdot10^{-7}$
	$k^{\#}$ [kPa^{-1}]	$3.89\cdot10^{-6}$	$2.46\cdot10^{-7}$	$6.61\cdot10^{-7}$
	q^{sat} [molec·cage^{-1}]	22.600	14.750	14.750

		FF1	FF2	FF3
ITQ-29	q^{sat*} $Đ(0)$ [molec·cage^{-1}·m^2·s^{-1}]	$1.09\cdot10^{-7}$	$1.10\cdot10^{-7}$	$7.13\cdot10^{-8}$
	$q^{sat\#}$ [molec·cage^{-1}]	3.894	5.213	6.723
	k^{*} [kPa^{-1}]	$1.42\cdot10^{-9}$	$7.28\cdot10^{-8}$	$2.78\cdot10^{-7}$
	$k^{\#}$ [kPa^{-1}]	$1.52\cdot10^{-5}$	$1.15\cdot10^{-6}$	$2.32\cdot10^{-6}$
	q^{sat} [molec·cage^{-1}]	18.669	14.226	14.853

		FF1	FF2	FF3
LTA-4A	q^{sat*} $Đ(0)$ [molec·cage^{-1}·m^2·s^{-1}]	-	$6.42\cdot10^{-9}$	-
	$q^{sat\#}$ [molec·cage^{-1}]	-	6.250	-
	k^{*} [kPa^{-1}]	-	$1.08\cdot10^{-8}$	-
	$k^{\#}$ [kPa^{-1}]	-	$6.96\cdot10^{-8}$	-
	q^{sat} [molec·cage^{-1}]	-	12.250	-

Table 2: Fitted parameters of the Relevant Site Model for the computed Maxwell-Stefan diffusivities of CO_2 in LTA_{Si}, ITQ-29 and LTA-4A type zeolite calculated with the three different force fields used in this study (see table 1).

The fitted values for the saturation loadings q^{sat} are in agreement with those obtained from the adsorption isotherms presented earlier. However, the behaviour of the diffusion coefficient as a function of loading is completely different for these two force fields. The RSM reproduces the computed Maxwell-Stefan diffusivity data for the FF3 model, as shown in Fig. 7 (c), but at very low and very high loading the fitted diffusivities slightly deviates from the computed values.

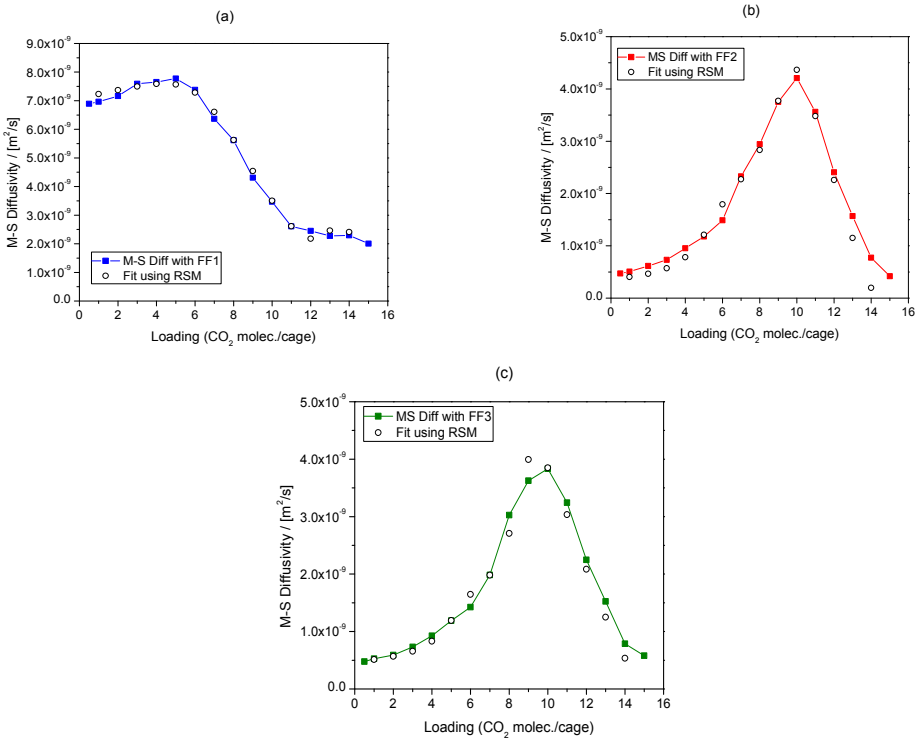

Figure 5.8: Computed CO_2 Maxwell-Stefan diffusivities from MD simulations in all-silica ITQ-29-type zeolite at 600 K. The data is fitted using the Relevant Site Model. (a) FF1; (b) FF2; (c) FF3.

In Fig. 5.8, the computed Maxwell-Stefan diffusivity is fitted using the Relevant Site Model (RMS) for ITQ-29 type zeolite. Similar to the LTA_{Si} structure, the RSM provides an excellent fit to the simulation results, regardless of the force field. As is shown in Fig. 5.9, the RSM qualitatively reproduces the shape of the computed Maxwell-Stefan diffusivity for LTA-4A using the FF2 model, but

there are large differences between the simulations and the RSM. The differences result from the partial blocking of the window by the sodium cations which decrease diffusion. It is important to note that this effect is not captured by the RSM.

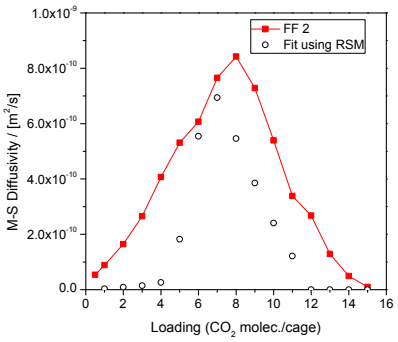

Figure 5.9: Computed Maxwell Stefan-diffusivities from MD simulations in LTA-4A-type zeolite at 600 K. The data is fitted using the Relevant Site Model.

5.3.5 Analysis of adsorbate positions and non-framework cations positions

We analyse the occupancy of CO_2 molecules at the different sites of LTA-type structures and relate it to the computed diffusivities. For the three force fields studied, the CO_2 molecules adsorbed in the different LTA-type zeolites are located either in the *Window* sites or in the *Centre* sites but never in the *Sodalite* sites or in the *Cube* sites, as these sites were selectively blocked during the simulation. We carefully checked that our analysis is not very sensitive to the definition of the various adsorption sites.

Fig. 5.10 shows the concentration dependency of the occupancy of the *Window* sites for the three different force fields. The concentration dependency for LTA_{Si} at 300 K is shown in Fig. 5.10 (a). For FF1 at low loading, the occupancy of CO_2 molecules in the *Window* sites is more than half (65%) and decreases as the number of molecules increases. For FF2, at low loading the *Window* sites occupancy is only 20% and slowly increases as the loading increases until 8

molec./cage. From this loading, the *Window* occupancy is almost constant until 12 molec./cage and it slowly increases again with the loading to occupy almost 40% of the sites. For FF3 the occupancy in the *Window* sites remains almost constant around 30%.

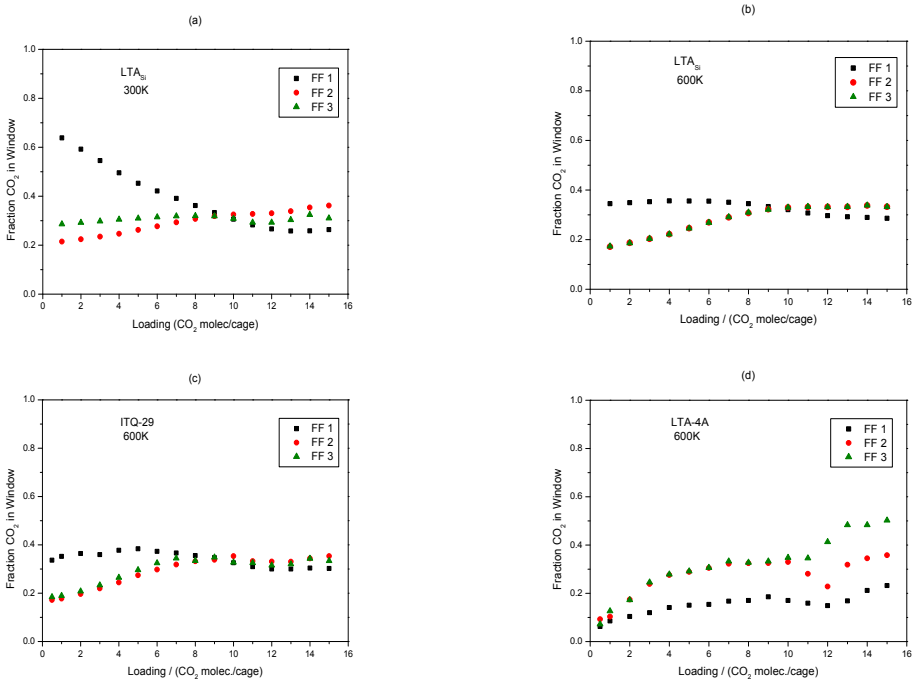

Figure 5.10: Fraction of CO_2 molecules in the *window* sites in LTA_{Si} at 300 K (a) and 600 K (b) for the studied force fields. Data is shown for ITQ-29 at 600 K (c) and LTA-4A at 600 K (d).

It is interesting to compare the occupancy of the *Window* sites with the self-diffusivity shown in Fig. 5.4 (a). The decreasing occupancy behaviour for FF1 is similar to the behaviour of the self-diffusion coefficient. The increase of the occupancy in the *Window* sites for FF2 with loading correspond to the increase of the self-diffusion coefficient until the diffusion maximum at 8 molec./cage is reached. From this loading, the self-diffusion coefficient decreases with loading but the occupancy in the *Window* sites remains constant and slowly increases at high loadings.

The CO_2 occupancy in the *Window* sites in LTA_{Si} at 600 K is shown in Fig. 5.10 (b). At this temperature, the occupancy for FF1 does not show a strongly decrease behaviour with loading as was observed at 300 K. At low loading, the occupancy in the *Window* sites remains almost constant until 9 molec./cage and then, slowly decrease with the loading. For FF2 and FF3, the fraction of CO_2 in the *Window* sites is almost the same. The occupancy increases with loading until 9 molec./cage and remains practically constant at higher loadings. This maximum for CO_2 occupancy in the *Window* sites is directly related to the maximum loading of the self-diffusivity. Fig 5.10 (c) shows the CO_2 occupancy in the *Window* sites in ITQ-29 type zeolite at 600 K. The occupancy behaviour for FF1, FF2 and FF3 is very similar as observed in Fig 5.10 (b) for LTA_{Si} at 600 K with these force fields. Fig. 5.10 (d) shows the CO_2 site occupancy for LTA-4A type zeolite at 600 K. It is interesting to note that for LTA-4A, the fraction of CO_2 molecules at the relevant *Window* sites for FF1 increases with loading, contrary to the dependency observed for LTA_{Si} and ITQ-29. The occupancy in the *Window* sites monotonically increases until 10 molecules per cage, and then decreases until a minimum at 12 molecules per cage and increases again at higher loading. At low loading, FF2 and FF3 also show a very low occupancy of CO_2 in the *Window* sites that slowly increases until 10 molecules per cage. At this loading, the occupancy of the *Window* sites for FF2 decreases until a minimum at 12 molecules per cage and increase again with the loading. This decrease for 12 molecules per cage is also observed for FF1 but not for FF3. This means that the number of molecules that contributes to diffusion increases proportionally to the number of molecules present in the cage. This dependency is not shown in Fig. 5.10 (a), (b) and (c) for ITQ-29 and LTA_{Si} respectively, where the fraction of CO_2 has a different dependency with the loading for each force field used.

As is shown in Fig. 5.10 (a), (b) and (c) for ITQ-29 and LTA_{Si} respectively, for FF1 at low loading, the probability to have the CO_2 molecules in the *Window* sites is very large. The probability to find the molecules in the *Window* sites decreases when the loading increases. This clearly shows that there is a correlation between the diffusion coefficient and the number of molecules at the relevant site. This correlation is reflected in the good agreement obtained

between the diffusion coefficients fitted using RSM as is shown in Fig. 5.8 and 5.9 respectively.

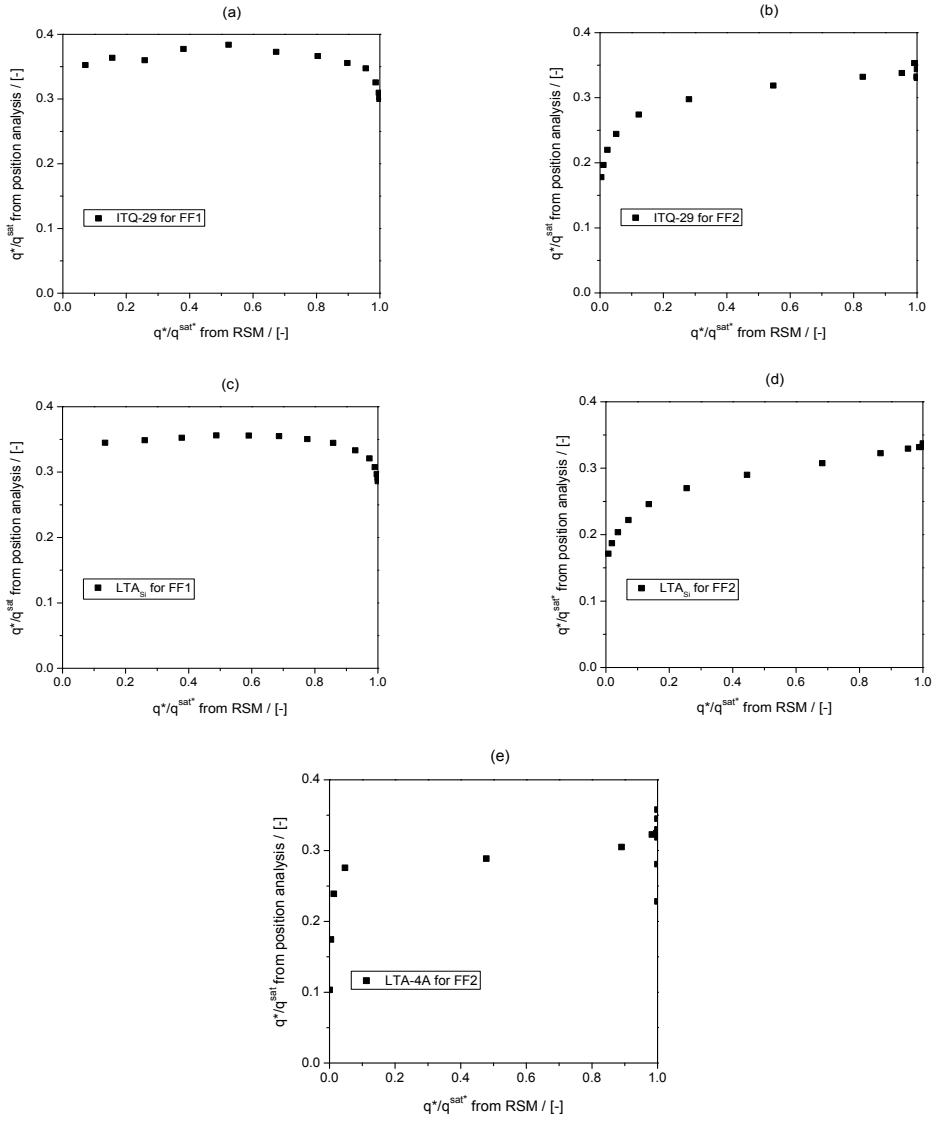

Figure 5.11: Relation between the computed fraction of CO_2 molecules at relevant *Window* sites and the fraction of molecules in the *Window* sites calculated with the RSM at 600 K for (a) ITQ-29 for FF1, (b) ITQ-29 for FF2, (c) LTA_{Si} for FF1, (d) LTA_{Si} for FF2, and (e) LTA-4A for FF2.

Fig. 5.11 shows the relation between the fraction of CO_2 molecules located at the *Window* sites calculated by Molecular Dynamics, $\frac{q^*}{q^{sat}}(MD)$, and the fraction of CO_2 molecules located at the relevant *Window* sites obtained with the RSM, $\frac{q^*}{q^{sat*}}(RSM)$. Fig. 5.11 (a) and (c) show the relation between $\frac{q^*}{q^{sat}}(MD)$ and $\frac{q^*}{q^{sat*}}(RSM)$ at 600 K using FF1 for ITQ-29 and LTA_{Si}. At low loading for both ITQ-29 and LTA_{Si} using FF2, the number of molecules in the relevant site slowly increases until saturation, as is shown in Fig 11 (b) and (c) respectively. Fig. 5.11 (e) shows the relation between $\frac{q^*}{q^{sat}}(MD)$ and $\frac{q^*}{q^{sat*}}(RSM)$ for LTA-4A using FF2. Here, the fraction of molecules at the window is nearly identical to that of the all-silica structures. In all cases, $\frac{q^*}{q^{sat}}(MD)$ and $\frac{q^*}{q^{sat*}}(RSM)$ for both FF1 and FF2 force fields, are not proportional. This is in sharp contrast to the diffusion of methane in LTA-type zeolite, for which the fraction of guest molecules at transition state (as obtained from molecular simulation) is directly proportional to the fraction of guest molecules at the relevant site (as obtained by a fit of the loading dependence of the diffusivity using the RSM)[64]. This may suggest that the diffusion mechanisms of methane and CO_2 in LTA-type zeolites are different.

5.4 Conclusions

The adsorption- and diffusion behaviour of carbon dioxide in LTA-type zeolites was investigated using molecular dynamics simulations. It is clear that small differences in the Lennard-Jones size parameter for guest-host interactions have a large influence on the loading dependence of the self- and Maxwell-Stefan diffusivities. Differences in adsorption isotherms are quite small in this respect. To understand the physical origin of the different diffusion behaviour of CO_2 in LTA-type zeolites, we have used the Relevant Site Model (RSM). This model results in an excellent fit of the loading dependence of the computed CO_2 diffusivities for the studied force fields, and qualitatively describes the shape of the loading dependence of the transport diffusivity. The latter already becomes clear by multiplying the relative loadings in Fig.10 with the accessible space for diffusion, $(1-\theta)$, as this already reveals the trends observed in Figs. 4-9. Unlike for methane in LTA-type zeolite, the fitted fraction of molecules at the relevant site is not identical to the fraction of molecules in the 8 membered ring that follows from the analysis of MD trajectories. This suggests that for CO_2, a more careful investigation is needed to precisely locate the relevant site for diffusion..

5.5 Bibliography

1 D. M. D'Alessandro, B. Smit and J. R. Long. *Angewandte Chemie International Edition* **49**, 6058-6082 (2010).

2 S. Choi, J. H. Drese and C. W. Jones. *Chemistry & Sustainability, Energy & Materials* **2**, 796-854 (2009).

3 I. Deroche, G. Maurin, B. J. Borah, S. Yashonath and H. Jobic. *Journal of Physical Chemistry C* **114**, 5027-5034 (2010).

4 Q. L. Liu, N. C. O. Cheung, A. E. Garcia-Bennett and N. Hedin. *Chemistry & Sustainability, Energy & Materials* **4**, 91-97 (2011).

5 E. Atci, I. Erucar and S. Keskin. *Journal of Physical Chemistry C* **115**, 6833-6840 (2011).

6 L. Madison, H. Heitzer, C. Russell and D. Kohen. *Langmuir* **27**, 1954-1963 (2011).

7 R. Krishna and J. M. van Baten. *Microporous and Mesoporous Materials* **137**, 83-91 (2011).

8 W. M. Meier, D. H. Olson and C. Baerlocher. *Zeolites* **17**, 1-229 (1996).

9 E. M. Flanigen, J. M. Bennett, R. W. Grose, J. P. Cohen, R. L. Patton, R. M. Kirchner and J. V. Smith. *Nature* **271**, 512-516 (1978).

10 L. Y. Hu, S. J. Xie, Q. X. Wang, S. L. Liu and L. Y. Xu. *Science and Technology of Advanced Materials* **10** (2009).

11 S. Kulprathipanja. *Zeolites In Industrial Separation And Catalysis*. (Wiley, 2010).

12 J. J. Pluth and J. V. Smith. *Journal of the American Chemical Society* **102**, 4704-4708 (1980).

13 D. Dubbeldam, S. Calero, T. L. M. Maesen and B. Smit. *Physical Review Letters* **90**, 245901 (2003).

14 D. Dubbeldam, S. Calero, T. J. H. Vlugt, R. Krishna, T. L. M. Maesen, E. Beerdsen and B. Smit. *Physical Review Letters* **93**, 088302 (2004).

15 D. Dubbeldam, S. Calero, T. J. H. Vlugt, R. Krishna, T. L. M. Maesen and B. Smit. *Journal of Physical Chemistry B* **108**, 12301-12313 (2004).

16 D. Dubbeldam, E. Beerdsen, S. Calero and B. Smit. *Proceedings of the National Academy of Sciences of the United States of America* **102**, 12317-12320 (2005).

17 S. Calero, D. Dubbeldam, R. Krishna, B. Smit, T. J. H. Vlugt, J. F. M. Denayer, J. A. Martens and T. L. M. Maesen. *Journal of the American Chemical Society* **126**, 11377-11386 (2004).

18 E. García-Pérez, D. Dubbeldam, T. L. M. Maesen and S. Calero. *Journal of Physical Chemistry B* **110**, 23968-23976 (2006).

19 A. García-Sánchez, C. O. Ania, J. B. Parra, D. Dubbeldam, T. J. H. Vlugt, R. Krishna and S. Calero. *Journal of Physical Chemistry C* **113**, 8814-8820 (2009).

20 A. García-Sánchez, E. García-Pérez, D. Dubbeldam, R. Krishna and S. Calero. *Adsorption Science & Technology* **25**, 417-427 (2007).

21 J. B. Nicholas, A. J. Hopfinger, F. R. Trouw and L. E. Iton. *Journal of the American Chemical Society* **113**, 4792-4800 (1991).

22 P. Demontis, G. B. Suffritti, S. Quartieri, E. S. Fois and A. Gamba. *Journal of Physical Chemistry* **92**, 867-871 (1988).

23 J. R. Hill and J. Sauer. *Journal of Physical Chemistry* **98**, 1238-1244 (1994).

24 J. R. Hill and J. Sauer. *Journal of Physical Chemistry* **99**, 9536-9550 (1995).

25 S. M. Auerbach, L. M. Bull, N. J. Henson, H. I. Metiu and A. K. Cheetham. *Journal of Physical Chemistry* **100**, 5923-5930 (1996).

26 E. Jaramillo and S. M. Auerbach. *Journal of Physical Chemistry B* **103**, 9589-9594 (1999).

27 K. Makrodimitris, G. K. Papadopoulos and D. N. Theodorou. *Journal of Physical Chemistry B* **105**, 777-788 (2001).

28 A. Goj, D. S. Sholl, E. D. Akten and D. Kohen. *Journal of Physical Chemistry B* **106**, 8367-8375 (2002).

29 D. Dubbeldam and B. Smit. *Journal of Physical Chemistry B* **107**, 12138-12152 (2003).

30 R. Krishna, D. Paschek and R. Baur. *Microporous and Mesoporous Materials* **76**, 233-246 (2004).

31 N. Hedin, G. J. DeMartin, W. J. Roth, K. G. Strohmaier and S. C. Reyes. *Microporous and Mesoporous Materials* **109**, 327-334 (2008).

32 R. Krishna, J. M. van Baten, E. Garcia-Perez and S. Calero. *Chemical Physics Letters* **429**, 219-224 (2006).

33 R. Krishna and J. M. van Baten. *Separation and Purification Technology* **61**, 414-423 (2008).

34 S. E. Jee and D. S. Sholl. *Journal of the American Chemical Society* **131**, 7896-7904 (2009).

35 S. M. Auerbach. *International Reviews in Physical Chemistry* **19**, 155-198 (2000).

36 Li P. and F. H. Tezel. *Journal of Chemical and Engineering Data* **53**, 2479-2487 (2008).

37 M. A. Granato, M. Jorge, T. J. H. Vlugt and A. E. Rodrigues. *Chemical Engineering Science* **65**, 2656-2663 (2010).

38 S. Brandani. *Diffusion Fundamentals* **6** (2007).

39 R. Valiullin, S. Naumov, P. Galvosas, J. Karger, H. J. Woo, F. Porcheron and P. A. Monson. *Nature* **443**, 965-968 (2006).

40 S. Naumov, R. Valiullin, P. A. Monson and J. Karger. *Langmuir* **24**, 6429-6432 (2008).

41 H. Jobic and D. N. Theodorou. *Microporous and Mesoporous Materials* **102**, 21-50 (2007).

42 G. K. Papadopoulos, H. Jobic and D. N. Theodorou. *Journal of Physical Chemistry B* **108**, 12748-12756 (2004).

43 F. Stallmach, J. Karger and H. Pfeifer. *Journal of Magnetic Resonance Series A* **102**, 270-273 (1993).

44 J. Karger, H. Pfeifer, F. Stallmach, N. N. Feoktistova and S. P. Zhdanov. *Zeolites* **13**, 50-55 (1993).

45 R. Babarao and J. W. Jiang. *Langmuir* **24**, 5474-5484 (2008).

46 R. Krishna and J. M. van Baten. *Journal of Membrane Science* **360**, 323-333 (2010).

47 J. Karger and H. Pfeifer. *Zeolites* **7**, 90-107 (1987).

48 J. Caro, M. Bulow, W. Schirmer, J. Karger, W. Heink, H. Pfeifer and S. P. Zdanov. *Journal of the Chemical Society-Faraday Transactions I* **81**, 2541-2550 (1985).

49 R. Krishna and J. M. van Baten. *Chemical Engineering & Technology* **29**, 1429-1437 (2006).

50 R. Krishna and J. M. van Baten. *Chemical Engineering & Technology* **30**, 1235-1241 (2007).

51 E. Beerdsen, D. Dubbeldam and B. Smit. *Journal of Physical Chemistry B* **110**, 22754-22772 (2006).

52 R. Krishna. *Journal of Physical Chemistry C* **113**, 19756-19781 (2009).

53 R. Krishna and J. M. van Baten. *Microporous and Mesoporous Materials* **109**, 91-108 (2008).

54 A. I. Skoulidas and D. S. Sholl. *Journal of Physical Chemistry B* **106**, 5058-5067 (2002).

55 D. Selassie, D. Davis, J. Dahlin, E. Feise, G. Haman, D. S. Sholl and D. Kohen. *Journal of Physical Chemistry C* **112**, 16521-16531 (2008).

56 M. Sant, J. M. Leyssale, G. K. Papadopoulos and D. N. Theodorou. *Journal of Physical Chemistry B* **113**, 13761-13767 (2009).

57 A. F. Combariza, G. Sastre and A. Corma. *Journal of Physical Chemistry C* **115**, 875-884 (2011).

58 D. Dubbeldam, E. Beerdsen, T. J. H. Vlugt and B. Smit. *Journal of Chemical Physics* **122**, 224712 (2005).

59 R. Krishna and J. M. van Baten. *Microporous and Mesoporous Materials* **125**, 126-134 (2009).

60 A. I. Skoulidas and D. S. Sholl. *Journal of Physical Chemistry A* **107**, 10132-10141 (2003).

61 D. A. Reed and G. Ehrlich. *Surface Science* **102**, 588-609 (1981).

62 J. van den Bergh, S. A. Ban, T. J. H. Vlugt and F. Kapteijn. *Journal of Physical Chemistry C* **113**, 17840-17850 (2009).

63 J. van den Bergh, S. A. Ban, T. J. H. Vlugt and F. Kapteijn. *Journal of Physical Chemistry C* **113**, 21856-21865 (2009).

64 T. J. H. Vlugt, J. van den Bergh, D. Dubbeldam and F. Kapteijn. *Chemical Physics Letters* **495**, 77-79 (2010).

65 E. García-Pérez, J. B. Parra, C. O. Ania, J. M. van Baten, R. Krishna and S. Calero. *Applied Surface Science* (2006).

66 A. Wender, A. Barreau, C. Lefebvre, A. Di Lella, A. Boutin, P. Ungerer and A. H. Fuchs. *Adsorption-Journal of the International Adsorption Society* **13**, 439-451 (2007).

67 M. A. Granato, T. J. H. Vlugt and A. E. Rodrigues. *Industrial & Engineering Chemistry Research* **46**, 321-328 (2007).

68 R. Krishna, J. M. van Baten, E. Garcia-Perez and S. Calero. *Industrial & Engineering Chemistry Research* **46**, 2974-2986 (2007).

69 C. Baerlocher, W. M. Meier and D. H. Olson. *Atlas of Zeolite Structure Types*. Fifth edn, (Elsevier, 2001).

70 A. Corma, U. Diaz, B. Ferrer, V. Fornes, M. S. Galletero and H. Garcia. *Chemistry of Materials* **16**, 1170-1176 (2004).

71 A. García-Sánchez, D. Dubbeldam and S. Calero. *Journal of Physical Chemistry C* **114**, 15068-15074 (2010).

72 R. Krishna and J. M. van Baten. *Langmuir* **26**, 2975-2978 (2010).

73 J. G. Harris and K. H. Yung. *Journal of Physical Chemistry* **99(31)**, 12021-12024 (1995).

74 D. Frenkel and B. Smit. *Understanding Molecular Simulations: From Algorithms to Applications*. Second edn, (Academic Press, 2002).

75 D. Dubbeldam and R. Q. Snurr. *Molecular Simulation* **33**, 305-325 (2007).

76 R. Krishna and D. Paschek. *Chemical Engineering Journal* **85**, 7-15 (2002).

77 D. Dubbeldam, D. C. Ford, D. E. Ellis and R. Q. Snurr. *Molecular Simulation* **35**, 1084-1097 (2009).

78 E. Beerdsen, D. Dubbeldam and B. Smit. *Physical Review Letters* **95**, 164505 (2005).

79 H. Ahn, J. H. Moon, S. H. Hyun and C. H. Lee. *Adsorption-Journal of the International Adsorption Society* **10**, 111-128 (2004).

80 D. Dubbeldam, E. Beerdsen, S. Calero and B. Smit. *Journal of Physical Chemistry B* **110**, 3164-3172 (2006).

Chapter 6

Predictive Model for Optimizing Guest-Host Interactions in Zeolites*

* This chapter is based on: A. García-Sánchez, E. Eggink, E.S. McGarrity, S. Calero and T.J.H. Vlugt: "Predictive Model for Optimizing Guest-Host Interactions in Zeolites" *Journal of Physical Chemistry C* **115**, 10187-10195 (2011)

.

ABSTRACT: A computationally efficient method to fit force field parameters for guest-host interactions in zeolites is proposed. In this method, each zeolite is modelled as an annulus with oxygen atoms distributed uniformly on the inner radius of the pore. This model has four parameters, the inner and outer radii, the density of the oxygen atoms and a potential offset. These parameters are first fitted against simulation results for the heat of adsorption and the Henry coefficient. Once the parameters are estimated, the model can be used in place of the simulations in order to optimize the Lennard-Jones parameters for the guest-host interactions. Since the model requires more than an order of magnitude less computational time than the simulation, the force field parameters can be estimated more rapidly than in the standard way. The strategy also allows for a quantitative prediction of the Henry coefficient and heat of adsorption for a system as a function of the guest-host force field parameters. The model is validated against adsorption isotherms obtained from molecular simulations for methane, against experiments and a fluids density functional theory. The model is also validated for adsorption properties of ethane against molecular simulations. We found that this model accurately describes the adsorption characteristics of these systems. Finally, the model can be used to determine the guest-host force field parameters for a system using experimentally determined heats of adsorption and Henry coefficients if they are known.

6.1 Introduction

Zeolites are aluminosilicate crystals based on robust frameworks of SiO_4 and AlO_4 tetrahedra linked to each other by the sharing of oxygen atoms[1]. This linkage results in a nonporous material which has a network of cavities interconnected by channels. Due to this structure, these materials are of great importance in many technological fields and environmental applications[2-5]. The widespread use of zeolites is due to their unique shape- and interaction-selective adsorption, diffusion, and catalysis properties[6,7]. Recently, there has been tremendous activity to synthesize new nonporous materials[3] which have specific functional properties[8] according to their specific use.

For the practical application of zeolites, it is of crucial importance to understand their ad sorption properties. The selection or design of a zeolite for a particular use requires knowledge of the interaction between the zeolite and the adsorbate. This interaction can be determined from experiments, however, an experiment must be performed for each zeolite and substance and these experiments can be time-consuming[9]. Alternatively, given a sufficiently accurate force field, molecular simulation techniques can be used to quantitatively predict the adsorption and diffusion behaviour of a substance in a zeolite. In addition they can be used to predict the properties of potential new materials before they are synthesized. Several research groups have developed force fields to reproduce and predict experimental adsorption measurements[10-13].

Due to these efforts, molecular simulation methods are becoming a powerful tool to predict equilibrium and transport properties of guest molecules adsorbed in zeolites[14-20]. Because accurate force fields are vital to obtaining accurate simulation results, their determination remains an active field of research[21-24].

Constructing a transferable force field for describing the adsorption of small molecules in zeolites is a complex task that requires the simultaneous fitting of all force field parameters to a set of experimental data[9]. There are two main challenges in fitting a force field to data. The first challenge lies in choosing an appropriate experimental data set because experimental measurements performed

by different research groups often provide different results at the same conditions[9,13,15]. To avoid over fitting of a force field to a particular set of experimental data, it is important to have a set of control experiments that are not used during the fitting procedure. This set can be used to verify the obtained force field. The second challenge in fitting a force field is in the application of the parameter fitting method, since all force field parameters have to be fitted simultaneously[9] and the number of parameters can be quite large. For example, for CO_2 adsorption in aluminosilicates with sodium non-framework cations, one must fit nine force field parameters at the same time. Several methods have been proposed for the fitting procedure[25-28], all of them requiring a large number of time-consuming simulations. Previously, we showed that constructing a force field for CO_2 adsorption in zeolites with sodium non-framework cations using the simplex algorithm[25] required a total of 264 molecular simulations, each requiring typically 90 hours on a modern workstation, resulting in almost 3 years of CPU time. Since the rate-limiting step lies in the molecular simulations, it would be valuable to develop a procedure that would reduce their number.

In this chapter, we present a model for estimating the parameters of a transferable force field for the simulation of adsorption in zeolites. We demonstrate the application of this model to adsorption of short alkanes in several zeolites. Further, we show that the model itself can be used to calculate the Henry coefficients and heats of adsorption for these systems. In addition, we present the adsorption isotherms for methane in a TON-type zeolite generated by the model. These isotherms are compared with grand-canonical Monte Carlo (GCMC) simulations, fluids density functional theory (FDFT)[29-31] and experiments[32].

The rest of this chapter is built up as follows: in Section 6.2 the methods used for simulation and modelling are explained. In Section 6.3 results of fitting the model equations to molecular simulations of adsorption of methane and ethane in different zeolite types are given. Heats of adsorption and Henry coefficients calculated with the model equations are compared to simulation results and experimental data. In addition, a comparison of the simplified model with a FDFT calculation is shown for the methane adsorption in TON-type zeolite. The findings are discussed and summarized in Section 6.4.

6.2 Methodology

6.2.1 Zeolite Model

Herein, the adsorption of methane and ethane are studied in AFI, LTL, TON, ITQ-29 and MTT type zeolite structures. These zeolites consist of SiO_4 units connected by oxygens in different ways resulting in different pore topologies. The crystallographic positions of the atoms from each of these can be found in the IZA database of zeolite structures[33]. A cross-sectional slice of each is shown in Fig. 6.1. As can be seen in the figure, the channels of these zeolites differ in pore size and geometry. All of the zeolites shown in this figure have channels in one direction except ITQ-29, which has a 3D network of channels and cages.

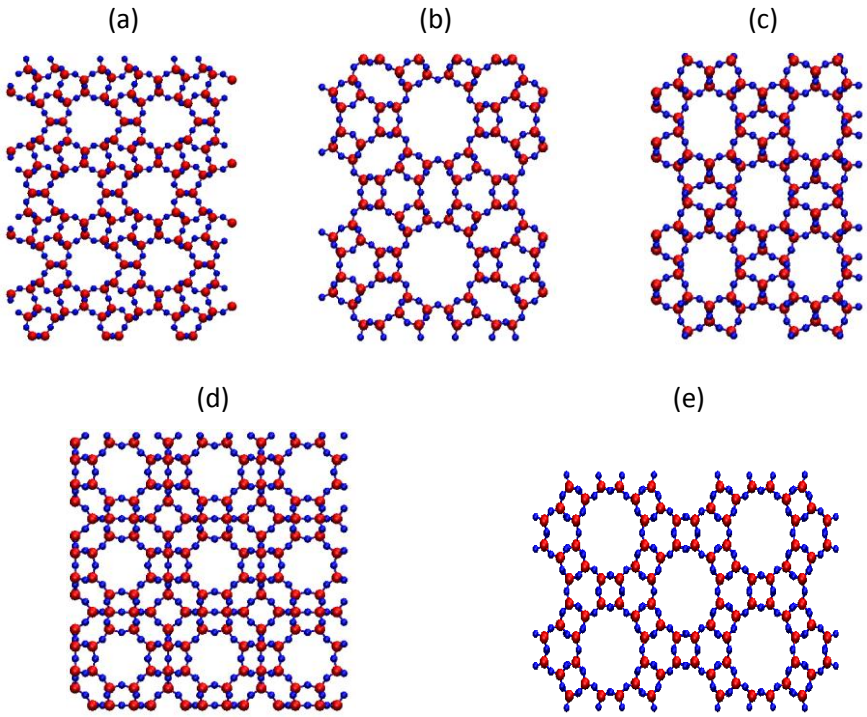

Figure 6.1: Channels of different zeolites: (a) MTT, (b) LTL, (c) TON, (d) ITQ-29, and (e) AFI.

The dimension of the unit cell, density and pore volume for each of these zeolites is listed in Table 6.1. The pore volumes reported here were calculated using test particle insertions of helium[34]. Since each zeolite has a distribution of pores with different sizes, we used the average pore volume in our calculations.

The average pore radius is then calculated from the pore volume assuming a cylindrical pore. In this study we considered zeolites where the channels are very straight, such as AFI-type zeolite, as well as those with corrugated channels, *e.g.*, LTL-type zeolite.

Zeolite	x/[Å]	y/[Å]	z/[Å]	ρ/ [kg m^{-3}]	Vpore/ [Å/u.c.]	Rpore/[Å]
AFI	2.774	13.726	8.484	1730	776.0	5.3960
LTL	31.984	18.466	7.476	1627	1211.0	7.1806
TON	13.859	17.420	5.038	1969	218.5	3.7155
ITQ-29	11.867	11.867	11.867	1433	684.6	4.2818
MTT	5.010	21.520	11.130	1995	175.5	3.3392

Table 6.1: Dimensions of one unit cell of the zeolites, zeolite density, pore volume per unit cell and pore radius. (All listed zeolites have an orthorhombic structure).

To create a statistical mechanic model for the prediction of the thermodynamic properties of a substance in a zeolite it is necessary to specify the interactions between the molecules constituents. In this work, the zeolites are treated as rigid structures so their self-interactions are not present as previous studies provide that framework flexibility is not so important for adsorption[35]. The alkane-alkane (or guest-guest) and alkane-zeolite (or guest-host) interactions are dispersive and thus are treated with a Lennard-Jones (LJ) potential[36]. The LJ potential uses two parameters for each interaction, which specify the guest-host diameter σ and energy ε. The alkanes are modelled with a united atom approach: methane as a single unit and ethane as two interactions sites connected by a rigid, freely jointed link with 1.54 Å of length[37]. The ethane molecule is growing bead by bead using a CBMC technique[38]. The growth process is biased to generate energetically favourable configurations. For all of the calculations in this work

the range of the LJ potential is truncated to 12 Å and shifted to zero at that point[38].

A simple model for a zeolite pore is constructed by assuming that the geometry of the pore is an annulus with inner radius R_1 and outer radius R_2. Fig. 6.2 depicts a top view of the model geometry. The oxygen atoms of the zeolite are smeared uniformly over the surface of the inner cylinder of the annulus.

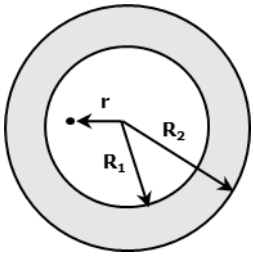

Figure 6.2: Schematic representation of our model for a zeolite pore. The model consists of an annulus with inner radius R_1 and outer radius R_2. The inaccessible part of the zeolite lies in the volume between R_1 and R_2. The oxygen atoms are smeared uniformly over the surface of the cylinder with radius R_1.

By integrating the LJ potential over this surface, we arrive at the following expression for the potential as a function of the distance from the pore centre r[39-41]:

$$U_{pore}(r) = \lambda\varepsilon\sigma^2\left(\frac{63}{32}\right)\left(\frac{R_1 - r}{\sigma}\right)^{-10}\left(2 - \left(\frac{R_1 - r}{R_1}\right)\right)^{-10} \times F\left[-9/2, -9/2, 1; \left(1 - \left(\frac{R_1 - r}{R_1}\right)\right)^2\right] - 3\left(\frac{R_1 - r}{\sigma}\right)^{-4}\left(2 - \left(\frac{R_1 - r}{R_1}\right)\right)^{-4} F\left[-3/2, -3/2, 1; \left(1 - \left(\frac{R_1 - r}{R_1}\right)\right)^2\right] \quad (6.1)$$

where λ is a fitting parameter, and σ and ε are the size and energy for the guest-host interactions. The hypergeometric function $F\ [\alpha, \beta, \gamma; \zeta]$ is needed to calculate values in Eq. (6.1).

To calculate the Henry coefficient, the ratio of accessible to inaccessible volumes in the zeolite must be known. The inaccessible part of the zeolite is modelled by adjusting R_2 and setting the potential between R_1 and R_2 to infinity.

This can be expressed formally as

$$U(r) = \begin{cases} \mathrm{U}_{\mathrm{pore}}(r) - \mathrm{U}_{\mathrm{min}} & 0 < r < R_1, \\ \infty & R_1 < r < R_2 \end{cases} \qquad (6.2)$$

where $\mathrm{U}_{\mathrm{min}}$ is a potential offset that simplifies the calculation. The expression in Eq. (6.1) is analytic, therefore Eqs. (6.1) and (6.2) provide a very efficient way for calculating guest-host interactions, compared to using the atomistic zeolite structure in which calculations over all atoms must be made.

6.2.2 Simulation Techniques

Two types of Monte Carlo simulations were performed in this work: canonical (*NVT*) and grand-canonical (μVT) ensembles. The former was used to compute the Henry coefficients and heats of adsorption and the latter was used for isotherm calculations. In all of this work the zeolites were treated as rigid frameworks[35]. The simulation box was generated by repeating unit cells of the zeolites in all three directions until it was at least 24 Å long on each side. Pores with connecting channels whose diameters were too small for the guest molecules to penetrate ($d_{chan} \leq 2.5$ Å) were artificially blocked[42]. This prevented molecules from being inserted or moved into inaccessible regions during the simulations.

For the simulations in the *NVT* ensemble[43], one single guest molecule was placed in the simulation box. This molecule was translated, rotated and, in the case of ethane, re-grown using the configurational-bias MC technique[44]. In the μVT simulations[38] the chemical potential μ was fixed and the number of particles in the domain was allowed to vary. This was achieved by inserting and removing particles into the zeolite from and to a bulk reservoir at chemical potential μ.

Molecules were translated, rotated, swapped and re-grown in the case of ethane. The acceptance ratio was adjusted to 50% for all the simulations.

From the simulations, the heat of adsorption and Henry coefficient of the adsorption of alkanes in different types of zeolites were calculated. The heat of adsorption Q at temperature T was calculated using

$$Q = \langle U_{zeo} \rangle - \langle U_{gas} \rangle - k_B T \tag{6.3}$$

where U_{zeo} and U_{gas} are the zeolite and gas phase internal energies and k_B is Boltzmann's constant. The quantities in brackets indicate the ensemble average. The Henry coefficient for each system was obtained using the average Rosenbluth factor $\langle W \rangle$ [45]. It is given by

$$K_H = \frac{1}{\rho_{u.c.} k_B T} \langle W \rangle \tag{6.4}$$

where the unit cell density $\rho_{u.c.}$ is the amount of unit cells per cubic meter. For the model, KH and Q can easily be calculated by integration of U(r)[38]. For methane it results in a 1D integral.

To construct a transferable force field for a given zeolite it is first necessary to estimate its parameters, R_1, R_2, λ, and U_{min}. These model parameters are adsorbate-specific, which means that for different adsorbates, different model parameters will be obtained. A schematic of this estimation procedure is shown in Fig. 6.3. The fitting begins with known values of the Henry coefficient and heat of adsorption (K_H*, Q*) from an experiment (or simulation). A set of n trial guest-host force field parameters is generated, along with their corresponding Henry coefficients and heats of adsorption, denoted by $\left\{ \left(\sigma^i, \varepsilon^i, K_H^i, Q^i \right);\ i = 1 \ldots n \right\}$ where these values are in the neighbourhood of K_H* and Q*. From this initial set, the model parameters, R_1, R_2, λ, and U_{min}, are fitted starting with randomly generated initial values. The target for the fit is the squares of relative errors of Henry coefficients and heats of adsorption. As the calculations of Henry coefficients and heats of adsorption of using Eqs. (6.2),

(6.3) and (6.4), is extremely fast, the number of iterations in this fitting procedure is less important.

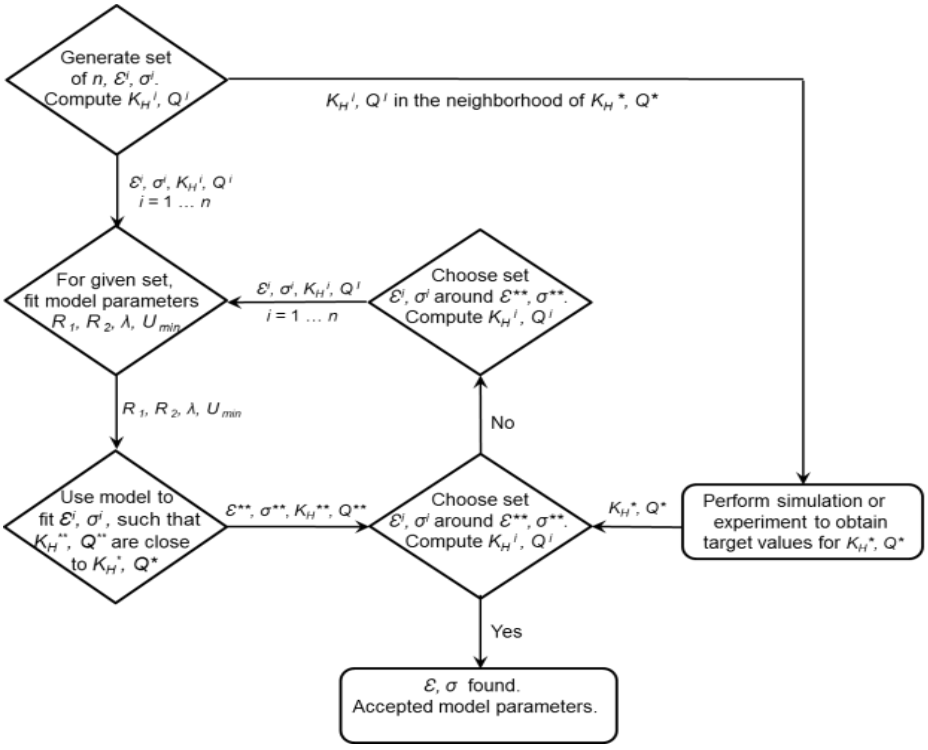

Figure 6.3: Schematic of the parameter fitting procedure described in section 6.2.2.

Therefore, the fitting of R_1, R_2, λ, and U_{min}, can be performed using the simplex algorithm. In the next step, the model is used to fit the guest-host interaction parameters σ^* and ε^* to $K_H{}^*$ and Q^*. In this step, the predictive model is used to compute theses quantities. If the fit is acceptable, then the model can be used, otherwise the fitting procedure is repeated with a new set values nearby the best tuple (σ^{**}, ε^{**}, $K_H{}^{**}$, Q^{**}). This tuple is then used to generate new values for the model parameters, R_1, R_2, λ, and U_{min}, and so on until an acceptable solution is found. The procedure in Fig. 6.3 is insensitive to the initial guess, which makes it applicable even when the magnitude of the guest-host interaction parameters, σ^* and ε^* are unknown. A huge advantage of using this method compared to

conventional force field fitting methods is that only a small amount of molecular simulations is needed to generate K_H^i and Q^i.

An alternative theoretical approach for examining the adsorption of Lennard-Jones fluids in a pore is classical fluids density functional theory[29-31,46]. This approach has been shown to give accurate results compared with GCMC simulations[38] at a fraction of the computational cost[47,48]. However, care must be taken with small pore diameters and high pressures to account for freezing[48-51], pore roughness[52-54], pore size distributions[55], and quantum effects [56]. Corrections for each of these difficulties remain open areas of research. We focused on the simplest system in this work, the methane adsorption in a TON-type zeolite, to assess whether further investigations are warranted for these systems. The details we used in our calculations are given in the Appendix B and the references therein.

6.3 Results and Discussion

For both adsorption of methane and ethane in different zeolites the model, R_1, R_2, λ, and U_{min}, were found by fitting Eqs. (6.1) and (6.2) to data obtained from Monte Carlo molecular simulations via Eq. (6.3) and Eq. (6.4). Using the model with these fitted parameters, we calculated the adsorption properties for the previously mentioned systems. In addition, we present adsorption isotherms obtained from the model and compare these with simulations, FDFT and experiments for methane in a TON-type zeolite, and with simulations for methane in LTL-type zeolite.

6.3.1 Henry Coefficient and Heat of Adsorption

A comparison of the model and simulations for methane adsorption in zeolites AFI-, LTL- and TON-type can be seen in Fig. 6.4 to 6.6. The comparison for ITQ-29 and MTT-type zeolites can be seen in Fig. B.4 and B.5 of the Appendix B. The figures depict the Henry coefficient and the heat of adsorption for

methane in each of the zeolites as a function of the guest-host size parameter σ for different guest-host interaction strengths ε. Values calculated by the model are depicted with open symbols and those from simulation are plotted with closed symbols. In all cases, the temperature was taken to be 300 K. These figures show that the model parameter space for the Henry coefficient and heat of adsorption is in excellent agreement with those from the simulation. This means that the model can give accurate values for these quantities. Therefore, it can be used in place of the simulations during the guest-host force-field parameter optimization step. This leads to a drastic reduction in computational time.

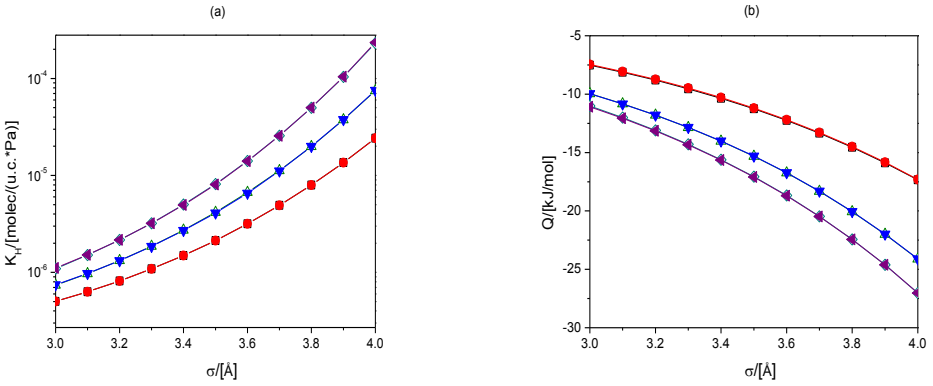

Figure 6.4: Henry coefficient (a) and heat of adsorption (b) of methane in AFI-type zeolite at 300 K as a function of the Lennard-Jones parameters describing the guest-host interactions. Data from MC simulations and model equations after fitting simulation data. White square, ε/k_B = 100 K, model; red circle, ε/k_B = 100 K, MC; white triangle, ε/k_B = 115 K, model; blue triangle, ε/k_B = 115 K, MC; white diamond, ε/k_B = 130 K, model; purple triangle, ε/k_B = 130 K, MC.

The Henry coefficient and heat of adsorption for methane in AFI-type zeolite is shown in Fig. 6.4. From this figure, it can be seen that the simulation and the model produce nearly identical Henry coefficient and heat of adsorption for given values of the force field parameters. In the case of the Henry coefficient, the agreement spans orders of magnitude. This result is expected since the pores of AFI-type zeolite are smooth and rather cylindrical.

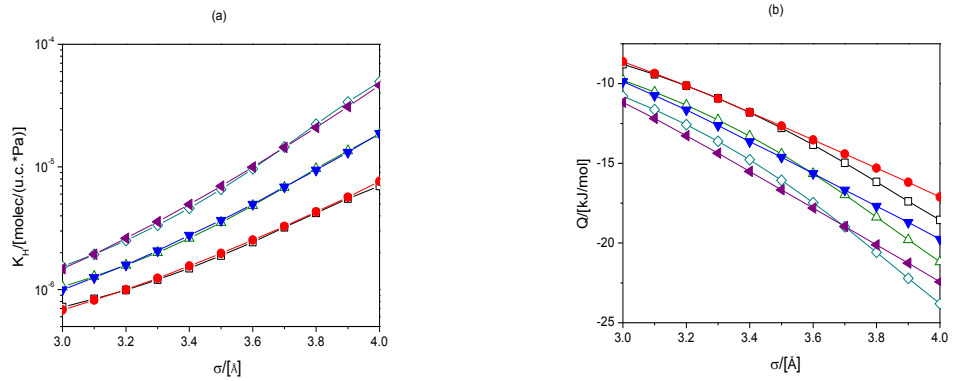

Figure 6.5: Henry coefficient (a) and heat of adsorption (b) of methane in LTL-type zeolite at 300 K as a function of the parameters describing the guest-host interactions. Data from MC simulations and model equations after fitting simulation data. White square, ε/k_B = 100 K, model; red circle, ε/k_B = 100 K, MC; white triangle, ε/k_B = 115 K, model; blue triangle, ε/k_B = 115 K, MC; white diamond, ε/k_B = 130 K, model; purple triangle, ε/k_B = 130 K, MC.

The effect of pore roughness can be seen in Fig. 6.5. In this figure, the Henry coefficient and heat of adsorption are shown for methane in LTL-type zeolite. While the agreement is not perfect, the curves follow each other indicating the annular model describes them well even though the actual zeolite pores are not completely smooth.

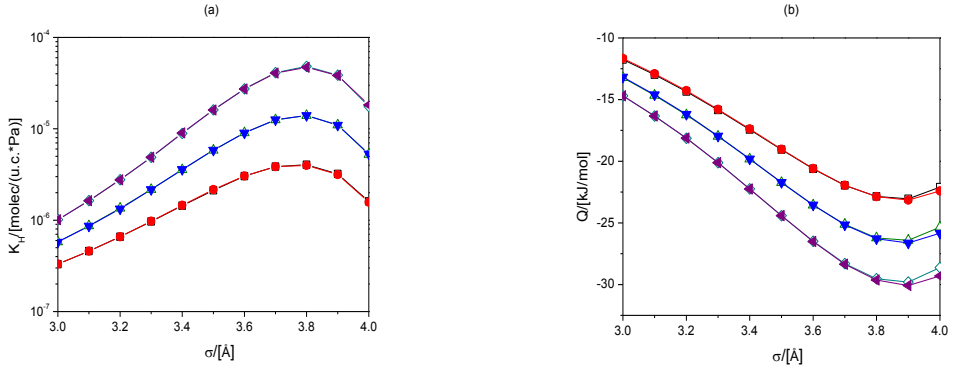

Figure 6.6: Henry coefficient (a) and heat of adsorption (b) of methane in TON-type zeolite at 300 K as a function of the parameters describing the guest-host interactions. Data from MC simulations and model equations after fitting simulation data. White square, ε/k_B = 100 K, model; red circle, ε/k_B = 100 K, MC; white triangle, ε/k_B = 115 K, model; blue triangle, ε/k_B = 115 K, MC; white diamond, ε/k_B = 130 K, model; purple triangle, ε/k_B = 130 K, MC.

The effect of pore size can be seen in Fig. 6.6. In this figure, the results of the model for methane in TON-type zeolite are shown. The maximum and minimum in the Henry coefficient and heat of adsorption respectively occur due to the fact that the pore size is only slightly larger than the methane molecules. If the value of σ for methane is chosen to be too large then it will fit tightly in the pore which causes a decrease in the amount of adsorption.

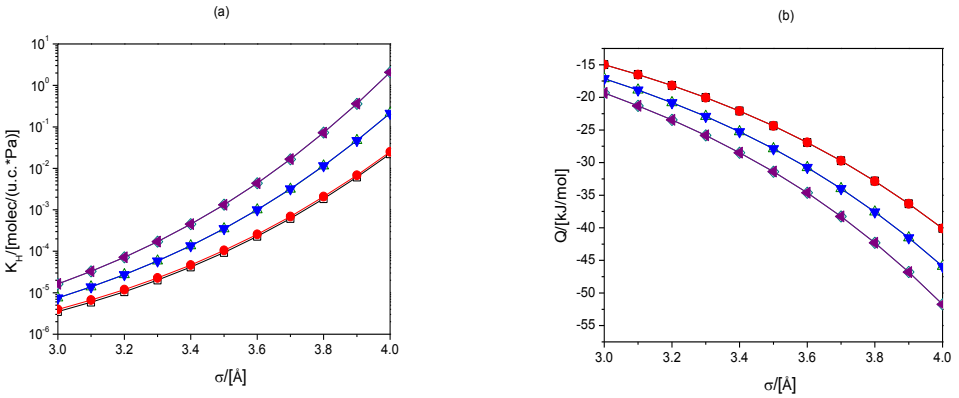

Figure 6.7: Henry coefficient (a) and heat of adsorption (b) of ethane in AFI-type zeolite at 300 K as a function of the parameters describing the guest-host interactions. Data from MC simulations and model equations after fitting simulation data. White square, ε/k_B = 100 K, model; red circle ε/k_B = 100 K, MC; white triangle ε/k_B = 115 K, model; blue triangle, ε/k_B = 115 K, MC; white diamond, ε/k_B = 130 K, model; purple triangle, ε/k_B = 130 K, MC.

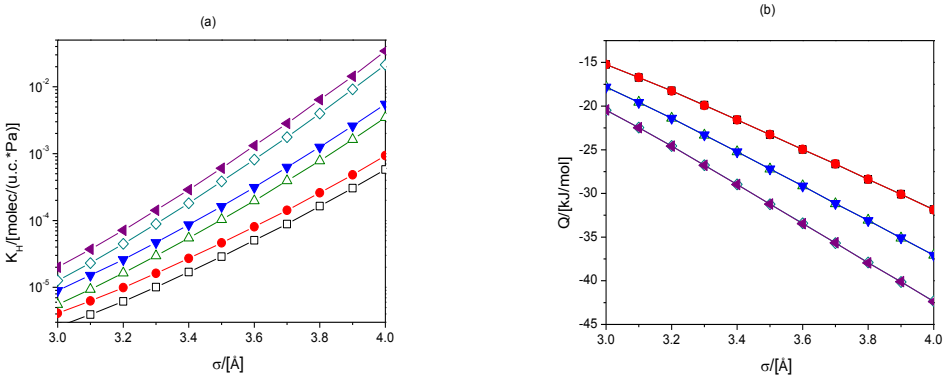

Figure 6.8: Henry coefficient (a) and heat of adsorption (b) of ethane in LTL-type zeolite at 300 K as a function of the parameters describing the guest-host interactions. Data from MC simulations and model equations after fitting simulation data. White square, ε/k_B = 100 K, model; red circle ε/k_B = 100 K, MC; white triangle ε/k_B = 115 K, model; blue triangle, ε/k_B = 115 K, MC; white diamond, ε/k_B = 130 K, model; purple triangle, ε/k_B = 130 K, MC.

The performance of the model for ethane adsorbed in AFI-type zeolite and LTL-type zeolite is shown in Fig. 6.7 and 6.8. Again, it can be seen that the Henry coefficients from the model agree with the simulations. The heats of adsorption for the model, however, are slightly lower, which indicates that the molecules are in better contact with the pore, that is, they have access to more oxygen interactions than in the real zeolite. For the LTL-type zeolite, the effects of the corrugations are evident, especially in the heat of adsorption. In this case, it is clear that the geometries of both the pore and molecule play roles in the adsorption process.

An important parameter for the model is the pore radius R_1. The fitted value can be compared to the real value of the average pore radius in a particular zeolite to validate the model. For the zeolites in this study, the average pore size can be found in Table 6.1, together with the dimensions of a unit cell and their density. The fitted values of R_1 from the model zeolites are presented in Table 6.2.

	Model parameters			
Zeolite	R_1/[Å]	R_2/[Å]	λ	$U_{min}k_B^{-1}$/[K]
AFI	5.1477	10.255	1.4918	0.33747
LTL	4.9196	10.975	1.0451	2.9283
TON	4.0420	8.1378	1.4223	0.48647
ITQ-29	5.3815	9.2728	1.3664	1.2072
MTT	3.9261	7.9745	1.5245	-1.9371

Table 6.2: Model parameters for the adsorption of methane in the various zeolites.

Differences between the pore radii in the model and the zeolite can be understood by taking into consideration that the zeolites have a distribution of pore radii, as shown in Fig. 6.1. The pore radius in Table 6.1 is the average of all these pores, while the ones obtained from the fitting of the model only consider those pores in which a methane molecule can adsorb. Considering this, the pore diameters found by fitting the model should be larger than those in Table 6.1. For LTL-type

zeolite this is, however, not the case since its pores are highly corrugated. As explained above, not all spaces in the zeolite pore are taken into account. The pore that is modelled is thus biased toward smaller values.

The other important quantity when calculating the adsorption properties is the outer pore radius R_2. This parameter represents the excluded volume of the zeolite in the model. The ratios of the accessible volume to total volume for the zeolite and the model are plotted against each other in Fig. 6.9. Examining this plot we can see that the values are well correlated. The model ratio is given by R_1^2/R_2^2 and the zeolite ratio is that of the pore volume to the unit cell volume.

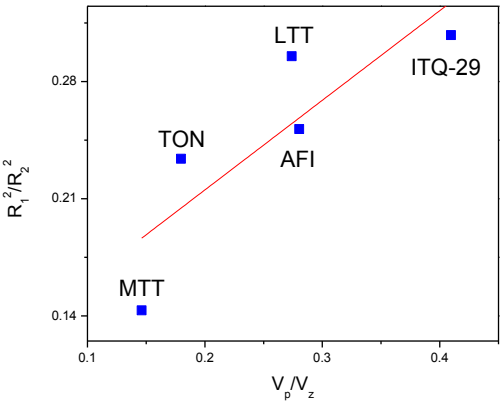

Figure 6.9: Correlation of pore volume fractions for the zeolite versus the model values. Here, R_1 and R_2 are the inner and outer cylinder diameters of the model pore and V_p and V_z are the pore volume and unit cell volume of the zeolite.

6.3.2 Predictions of Lennard-Jones Force Field Parameters Using the Model

Once the model parameters R_1, R_2, λ, and U_{min} are fixed for a particular zeolite and guest species (cf., Table 6.2), the LJ guest-host parameters ε and σ for different guests can be predicted by the model. For each different guest, new values of these parameters can be found using known values for the Henry coefficient and the heat of adsorption. These values can be from either

simulations or experiments. In this work, the guest-host parameters for methane and ethane in all the previously mentioned zeolites were computed following the scheme shown in Fig. 6.3.

To perform these calculations, we generated the target data values with molecular simulations using the accepted values from the literature (ε/k_B = 115 K and σ = 3.47 Å)[13]. The results for methane can be seen in Table 6.3. The entries in this table indicate the values of the guest-host interaction parameters after one, two and three iterations of the scheme. For the AFI-, LTL-, and TON-type zeolites convergence was achieved in two iterations and for ITQ-29 and MTT a third iteration was needed. The same procedure was used on ethane in the 5 zeolites discussed here. The results from these calculations are shown in Table B.2 of the Appendix B.

	Target Values		Predicted ε and σ	
Zeolite	K_H/[molec./u.c./Pa]	Q/[kJ/mol]	$\varepsilon\ k_B^{-1}$/[K]	σ/[Å]
		First Iteration		
AFI	$3.62 \cdot 10^{-6}$	-14.91	114.00	3.4781
LTL	$3.37 \cdot 10^{-6}$	-14.33	113.22	3.5110
TON	$5.09 \cdot 10^{-6}$	-21.14	115.71	3.4626
ITQ-29	$3.38 \cdot 10^{-6}$	-20.98	110.15	3.5273
MTT	$2.26 \cdot 10^{-6}$	-13.94	112.91	3.5009
		Second Iteration		
AFI	$3.62 \cdot 10^{-6}$	-14.91	115.04	3.4698
LTL	$3.37 \cdot 10^{-6}$	-14.33	114.78	3.4730
TON	$5.09 \cdot 10^{-6}$	-21.14	115.35	3.4660
ITQ-29	$3.38 \cdot 10^{-6}$	-20.98	114.23	3.4799
MTT	$2.26 \cdot 10^{-6}$	-13.94	113.68	3.4844
		Third Iteration		
ITQ-29	$3.38 \cdot 10^{-6}$	-20.98	114.55	3.4753
MTT	$2.26 \cdot 10^{-6}$	-13.94	114.29	3.4760

Table 6.3: The guest-host parameters ε/k_B and σ for adsorption of methane predicted with the pore model using the algorithm described in section 6.2.2 and depicted in Fig. 6.3. (All values in this table were predicted starting with random initial values within the ranges 80 K $\leq \varepsilon/k_B \leq$ 130 K and 3.0 Å $\leq \sigma \leq$ 4.0 Å).

The time for calculating the force field parameters with the analytic potential is at least an order of magnitude less than that required by the respective simulations. As an example, in ethane the new estimation procedure requires 1/20th of the amount of time that would be needed if simulations were used instead of the model at each step in the simplex method. Because the computation time for fitting the force field parameters increases quadratically with the number of pair interactions, (*e.g.*, from extra framework cations in the zeolite, or a dipole moment in the adsorbed gas) any degree of savings is crucial.

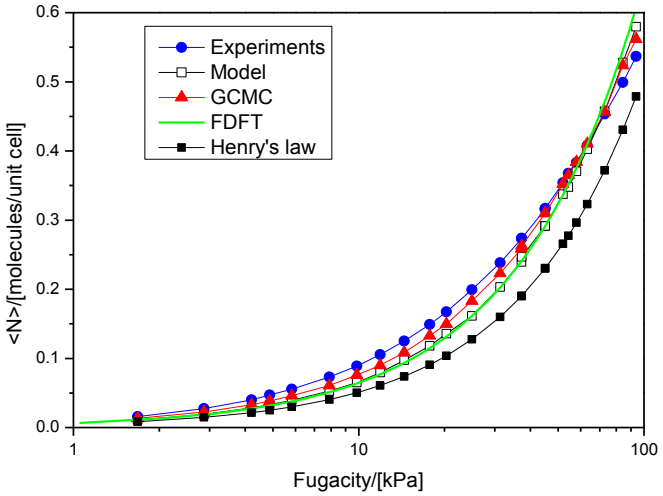

Figure 6.10: Adsorption isotherms of methane in TON-type zeolite at 309.5 K from experiments[32], model equations, MC simulation and fluids density functional theory. Values of ε/k_B = 115 K and σ = 3.47 Å are used for the guest-host interactions in both the simulations and the model equations. The model parameters for these calculations can be found in Table 6.2. Predictions using Henry's law are shown for comparison.

With the fitted model and force field parameters, an adsorption isotherm can be calculated using the model equations. The results of the calculation have been compared to grand-canonical MC simulation results and in the case of TON-type zeolite to experimental data[32] and FDFT. The methane isotherm of TON-type zeolite can be seen in Fig. 6.10, where the loading of methane in molec./u.c. is plotted against the fugacity. From this figure, it is clear that the model, theories, and simulations perform similarly to each other. All are in good agreement with

the experimental data for the range which was available. As can be seen from the plot, care must be taken when extrapolating outside this region as they all overestimate the adsorption. This effect is probably due to the assumption that the pore is smooth[54].

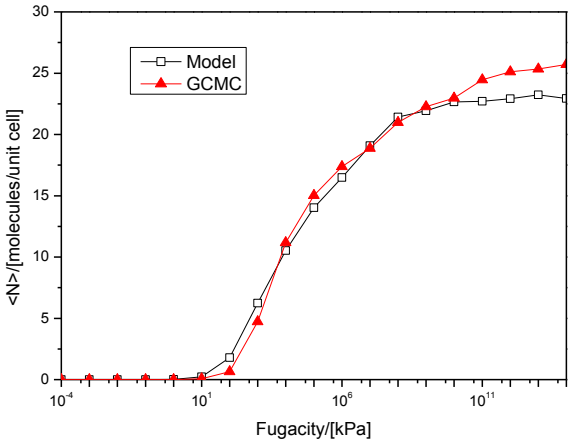

Figure 6.11: Adsorption isotherm of methane in LTL-type zeolite at 300 K from both model equations and MC simulation. Values of ε/k_B = 115 K and σ = 3.47 Å are used. The calculations using the model are performed with the model parameters listed in Table 6.2.

6.4 Conclusions

We proposed a model to describe adsorption of alkanes in zeolites for which the interactions are described using the Lennard-Jones force field. This model represents the zeolite channel as an annular pore, where oxygen atoms are uniformly distributed over the inside of the annulus. The force field inside the annulus can be calculated analytically by integrating the LJ potential over the entire inner pore surface. The solid part of the annulus represents the excluded volume of the zeolite, which is important for recovering the correct Henry coefficients. The parameters of the model can be fitted using Henry coefficient and heat of adsorption values from either experiments or a small number of Monte Carlo simulations. Also, this model can be used to reduce the number of molecular simulations needed to optimize the force field parameters. The main

advantage of the model is that calculations of the Henry coefficient and heat of adsorption are orders of magnitude faster than MC simulations using the atomistic zeolite structure. In addition, the model accurately produces these quantities as a function of the force field parameters, (σ, ε) once a set of model parameters (R_1, R_2, U_{min}, λ) is determined. Therefore, optimization of the force field parameters can be performed using the model instead of the MC simulations.

The model was used to predict force field parameters for adsorption of methane and ethane in various zeolites. Accurate results for the force field parameters for these two simple alkanes were obtained in one or two optimization steps. Also, the model was shown to accurately reproduce GCMC simulation results for the adsorption isotherms of methane in the LTL- and TON-type zeolites. This is true even if the channel topology of the zeolite adsorption surface is not smooth and cylindrical, as is the case in ITQ-29. The results from the model equations were shown to correspond with molecular simulation and FDFT results, as well as with experimental data[32].

In the future, the model could be applied for adsorption of longer alkanes, when interactions between different methane beads like bending and torsion energies are included. In addition, the technique could be applied to other potentials in a similar way so that different guest-host interactions could be accounted for.
One may also fit the Lennard-Jones part of the guest-host interactions, whereas other guest-host interactions (*e.g.*, dipolar or quadrupolar interactions) are also present. The latter then serve as a constant background potential. This model could also be transferable to different zeolite structures and extended to other porous adsorbents such as aluminophosphates, metal-organic frameworks (MOFs), zeolite-like metal-organic frameworks (ZMOFs), zeolitic imidazolate frameworks (ZIFs), and other novel hosts. Therefore, we feel that our approach may significantly contribute to a faster development of newly synthesized nanoporous materials.

6.5 Bibliography

1 C. Baerlocher, W. M. Meier and D. H. Olson. *Atlas of Zeolite Structure Types*. Fifth edn, (Elsevier, 2001).

2 B. Smit and T. L. M. Maesen. *Nature* **451**, 671-678 (2008).

3 J. Caro and M. Noack. *Microporous and Mesoporous Materials* **115**, 215-233 (2008).

4 M. Guisnet and J.-P. Gilson. *Zeolites for cleaner technologies*. Vol. 3 (Imperial College Press, 2002).

5 A. Corma. *Chemical Reviews* **97**, 2373-2419 (1997).

6 A. Petushkov, S. Yoon and S. C. Larsen. *Microporous and Mesoporous Materials* **137**, 92-100 (2011).

7 J. Caro, M. Noack and P. Kolsch. *Adsorption-Journal of the International Adsorption Society* **11**, 215-227 (2005).

8 S. S. Y. Chui, S. M. F. Lo, J. P. H. Charmant, A. G. Orpen and I. D. Williams. *Science* **283**, 1148-1150 (1999).

9 A. García-Sánchez, C. O. Ania, J. B. Parra, D. Dubbeldam, T. J. H. Vlugt, R. Krishna and S. Calero. *Journal of Physical Chemistry C* **113**, 8814-8820 (2009).

10 J. B. Nicholas, A. J. Hopfinger, F. R. Trouw and L. E. Iton. *Journal of the American Chemical Society* **113**, 4792-4800 (1991).

11 J. R. Hill and J. Sauer. *Journal of Physical Chemistry* **98**, 1238-1244 (1994).

12 E. Jaramillo and S. M. Auerbach. *Journal of Physical Chemistry B* **103**, 9589-9594 (1999).

13 D. Dubbeldam, S. Calero, T. J. H. Vlugt, R. Krishna, T. L. M. Maesen and B. Smit. *Journal of Physical Chemistry B* **108**, 12301-12313 (2004).

14 A. H. Fuchs and A. K. Cheetham. *Journal of Physical Chemistry B* **105**, 7375-7383 (2001).

15 T. J. H. Vlugt, R. Krishna and B. Smit. *Journal of Physical Chemistry B* **103**, 1102-1118 (1999).

16 T. J. H. Vlugt, W. Zhu, F. Kapteijn, J. A. Moulijn, B. Smit and R. Krishna. *Journal of the American Chemical Society* **120**, 5599-5600 (1998).

17 D. Dubbeldam, S. Calero, T. J. H. Vlugt, R. Krishna, T. L. M. Maesen, E. Beerdsen and B. Smit. *Physical Review Letters* **93**, 088302 (2004).

18 D. Dubbeldam, S. Calero, T. L. M. Maesen and B. Smit. *Physical Review Letters* **90**, 245901 (2003).

19 E. Beerdsen, D. Dubbeldam and B. Smit. *Physical Review Letters* **95**, 164505 (2005).

20 E. Beerdsen, D. Dubbeldam and B. Smit. *Physical Review Letters* **96**, 44501 (2006).

21 C. M. Nguyen, M. F. Reyniers and G. B. Marin. *Physical Chemistry Chemical Physics* **12**, 9481-9493 (2010).

22 A. García-Sánchez, D. Dubbeldam and S. Calero. *Journal of Physical Chemistry C* **114**, 15068-15074 (2010).

23 E. García-Pérez, D. Dubbeldam, T. L. M. Maesen and S. Calero. *Journal of Physical Chemistry B* **110**, 23968-23976 (2006).

24 S. Calero, D. Dubbeldam, R. Krishna, B. Smit, T. J. H. Vlugt, J. F. M. Denayer, J. A. Martens and T. L. M. Maesen. *Journal of the American Chemical Society* **126**, 11377-11386 (2004).

25 W. H. Press, Teukolsky, S. A., Vetterling, W. T., Flannery, B. P. *Numerical recipes in Fortran 77 : the art of scientific computing*. (Cambridge University Press, 2001).

26 M. Hulsmann, T. Koddermann, J. Vrabec and D. Reith. *Computer Physics Communications* **181**, 499-513 (2010).

27 P. Ungerer, C. Beauvais, J. Delhommelle, A. Boutin, B. Rousseau and A. H. Fuchs. *Journal of Chemical Physics* **112**, 5499-5510 (2000).

28 E. Bourasseau, M. Haboudou, A. Boutin, A. H. Fuchs and P. Ungerer. *Journal of Chemical Physics* **118**, 3020-3034 (2003).

29 R. Evans. *Advances in Physics* **28**, 143-200 (1979).

30 L. J. D. Frink and A. G. Salinger. *Journal of Computational Physics* **159**, 407-424 (2000).

31 J. Wu. *AIChE Journal* **52**, 1169-1193 (2006).

32 S. Savitz, F. Siperstein, R. J. Gorte and A. L. Myers. *Journal of Physical Chemistry B* **102**, 6865-6872 (1998).

33 C. Baerlocher and L. B. McCusker. *Database of Zeolite Structures: www.iza-structure.org/databases* (April 2011).

34 L. D. Gelb and K. E. Gubbins. *Langmuir* **15**, 305-308 (1999).

35 T. J. H. Vlugt and M. Schenk. *Journal of Physical Chemistry B* **106**, 12757-12763 (2002).

36 A. V. Kiselev, A. A. Lopatkin and A. A. Shulga. *Zeolites* **5**, 261-267 (1985).

37 J. P. Ryckaert and A. Bellemans. *Faraday Discussions*, 95-106 (1978).

38 D. Frenkel and B. Smit. *Understanding Molecular Simulations: From Algorithms to Applications*. Second edn, (Academic Press, 2002).

39 T. Yamazaki, S. Ozawa and Y. Ogino. *Molecular Physics* **69**, 369-378 (1990).

40 G. J. Tjatjopoulos, D. L. Feke and J. A. Mann. *Journal of Physical Chemistry* **92**, 4006-4007 (1988).

41 F. Cruz and J. P. B. Mota. *Physical review B* **79** (2009).

42 R. Krishna and J. M. van Baten. *Langmuir* **26**, 2975-2978 (2010).

43 T. J. H. Vlugt, E. Garcia-Perez, D. Dubbeldam, S. Ban and S. Calero. *Journal of Chemical Theory and Computation* **4**, 1107-1118 (2008).

44 J. I. Siepmann and D. Frenkel. *Molecular Physics* **75**, 59-70 (1992).

45 M. N. Rosenbluth and A. W. Rosenbluth. *Journal of Chemical Physics* **23**, 356-359 (1955).

46 *https://software.sandia.gov/DFTfluids*.

47 P. I. Ravikovitch, A. Vishnyakov and A. V. Neimark. *Physical Review E* **6401** (2001).

48 A. V. Neimark, P. I. Ravikovitch and A. Vishnyakov. *Journal of Physics-Condensed Matter* **15**, 347-365 (2003).

49 A. Gonzalez, J. A. White, F. L. Roman, S. Velasco and R. Evans. *Physical Review Letters* **79**, 2466-2469 (1997).

50 R. Roth, R. Evans, A. Lang and G. Kahl. *Journal of Physics-Condensed Matter* **14**, 12063-12078 (2002).

51 P. Tarazona and Y. Rosenfeld. *Physical Review E* **55**, R4873-R4876 (1997).

52 P. I. Ravikovitch and A. V. Neimark. *Langmuir* **22**, 11171-11179 (2006).

53 P. I. Ravikovitch and A. V. Neimark. *Langmuir* **22**, 10864-10868 (2006).

54 A. V. Neimark, Y. Z. Lin, P. I. Ravikovitch and M. Thommes. *Carbon* **47**, 1617-1628 (2009).

55 P. I. Ravikovitch, G. L. Haller and A. V. Neimark. *Advances in Colloid and Interface Science* **76**, 203-226 (1998).

56 S. Patchkovskii and T. Heine. *Physical Review E* **80** (2009).

Chapter 7

Conclusions

This chapter summarizes the main conclusions from the research work undertaken in this thesis.

Regarding the effect of cations on the adsorption and diffusion of apolar gases in LTA-type zeolites, we showed that the number of molecules of an apolar gas adsorbed in the zeolite strongly depends on the amount of sodium and calcium cations present in the structure. In particular, for methane, we found that cations control its diffusion by blocking or allowing the adsorbate in the windows of the zeolite framework. Also, the cations occupy free volume in the framework and modify, thereby, its thermodynamic properties, especially at high loadings.

Related to the effect of the type of zeolite framework, *i.e.* rigid or flexible, we studied the adsorption and diffusion of methane in LTA-type zeolites. In LTA-4A and LTA-5A, the adsorption and diffusion of methane is strongly determined by the cations. The effect of cations is as follow: (1) they create additional adsorption sites at low pressures, (2) they occupy free volume, modifying the adsorption and diffusion properties, especially at high methane loading, and (3) they control diffusion by blocking or allowing the access of methane to the windows.

We found that the framework flexibility affects differently adsorption and diffusion of methane. The effect that the flexibility exerts on adsorption is quite small. However, the influence on diffusion appears to be much larger and strongly dependent on three factors: (1) the density and type of the non-framework cations located in the LTA zeolite, (2) the loading of methane in the structure, and, most importantly, (3) the force field parameters used to model the framework.

We developed a new transferable force field applicable to CO_2 adsorption in zeolites with and without Na^+ cations. Simulations using this force field provide adsorption data in very good agreement with experimental values. The novelty of this force field is that it is fully transferable between zeolites. In addition, it can be applied to all possible Si/Al ratios (with sodium as non-framework cation).

With this force field we are able to provide a reliable screening tool of topology-specific and chemical composition-specific adsorption properties.

Concerning diffusion processes of CO_2 in zeolites, we showed that both self- and transport diffusion strongly depend on the force field of choice. To describe the dependence of the loading on the diffusion in such zeolites we applied the Relevant Site Model (RSM). The analysis of the positions of the adsorbed CO_2 molecules shows a clear dependence of the CO_2 position on the diffusion coefficients in LTA-type zeolites. We conclude that the RSM accurately describes the transport diffusion of CO_2 in LTA-type zeolites. However, it seems that it does not provide a physical explanation for the different shapes of the loading dependence of diffusion coefficients. The reason for this is that the number of molecules present at the relevant sites significantly differs from the fitted value obtained from the RSM.

We successfully developed a method to fit force field parameters for describing adsorption in zeolites in a computationally easier and less time consuming way. The zeolite is modeled as a cylindrical pore with oxygen atoms distributed uniformly on its inner surface. This model has four parameters (the inner and outer radii, the density of the oxygen atoms, and a potential offset) that can be fitted using Henry coefficients and heats of adsorption from either experiments or simulations. Our model accurately predicts force field parameters for adsorption of methane and ethane using experimental data for several all-silica zeolites: AFI, LTL, ITQ-29, MTT and TON. Therefore, it can be used to optimize guest-host Lennard-Jones interactions in orders of magnitude faster than molecular simulation methods. Moreover, the model accurately reproduces adsorption properties in all-silica zeolites for methane and ethane, such as adsorption isotherms, Henry coefficient and heat of adsorption by using less computational time than the simulation.

Appendix A

Supporting Information for Chapter 3

A.1 Force Field Parameters for Flexible Frameworks

The energy potentials and force field parameters used in this work are shown below. All the values are based on the force fields reported by Nicholas *et al.*[1] and by Hill and Sauer[2,3].

A.1.1 Force Field Reported by Nicholas *et al.*[1]

i) Bond Stretch:

$$U^{bond}(r) = \frac{k_r}{2}\left(r - r_{eq}\right)^2$$

Si-O_{zeo} Bond Stretch (Harmonic Bond)	
K_r/k_B = 300724.7766358210 (K/Å^2)	r_0= 1.61 Å
Al-O_a Bond Stretch (Harmonic Bond)	
K_r/k_B = 300724.7766358210 (K/Å^2)	r_0= 1.61 Å

ii) Bond Angle Bend: (O_{zeo}-Si-O_{zeo})

$$U^{bend}_{O-Si-O}(\theta) = \frac{k_\theta}{2}\left(\theta - \theta_0\right)^2$$

O_{zeo}-Si-O_{zeo} Bond Angle Bend (Harmonic Bend)	
K_θ/k_B = 69537.44416550520 (K/rad^2)	r_θ = 109.5 rad
O_a-Al-O_a Bond Angle Bend (Harmonic Bend)	
K_θ/k_B = 69537.44416550520 (K/rad^2)	r_θ = 109.5 rad

iii) Bond Angle Bend: (Si-O_{zeo}-Si)

$$U^{bend}_{Si-O-Si}(\theta) = \frac{k_{\theta_1}}{2}\left(\theta - \theta_0\right)^2 - \frac{k_{\theta_2}}{2}\left(\theta - \theta_0\right)^3 + \frac{k_{\theta_3}}{2}\left(\theta - \theta_0\right)^4$$

Si-O_{zeo}-Si Bond Angle Bend (Quartic Bend)			
$K_{\theta 1}/k_B$= 5462.506 (K/rad^2)	$K_{\theta 2}/k_B$= -17157.805 (K/rad^2)	$K_{\theta 3}/k_B$= 13351.673 (K/rad^2)	θ_0=149.5^0
Al-Oa-Si Bond Angle Bend (Quartic Bend)			
$K_{\theta 1}/k_B$= 5462.506 (K/rad^2)	$K_{\theta 2}/k_B$= -17157.805 (K/rad^2)	$K_{\theta 3}/k_B$= 13351.673 (K/rad^2)	θ_0=149.5^0

iv) Bond Angle Coupling:

$$U^{U-B}(r) = \frac{k_r}{2}\left(r_{Si-Si} - r_0\right)^2$$

Si-O_{zeo}-Si Urey-Bradley Term (Harmonic Urey-Bradley)	
K_r/k_B = 27488.73770226310 (K/Å^2)	r_0= 3.1261 Å
Al-Oa-Si Urey-Bradley Term (Harmonic Urey-Bradley)	
K_r/k_B = 27488.73770226310 (K/Å^2)	r_0= 3.1261 Å

v) Dihedral Angle:

$$U^{tors}(\theta,\phi,\theta') = S(\theta)\left[\frac{k_\phi}{2}(1+\cos(3\phi))\right]S(\theta')$$

Si-Ozeo-Si-Ozeo Torsion (Smoothed three cosine dihedral)
k_ϕ/k_B = -352.419714131579 (K)

vi) Nonbonded Potential Parameters (Lennard-Jones Potential)

Atom	ε/k_B (K)	σ (Å)	q (e$^-$)
Si	81.76308187	3.962387454	1.1
Al	81.76308187	3.962387454	0.8
O_{Si}	29.4338257	3.062219744	-0.55
O_{Al}	29.4338257	3.062219744	-0.6091
Na	--	--	0.5366
Ca	--	--	1.0732

The O_{zeo} oxygen atom has two types: (a) O_{Si} connected to two silicon atoms, and (b) O_{Al} connected to aluminium.

The smoothing function S(θ) is defined as:

$$S(\theta) = \begin{cases} 1 & \theta < \theta_{on} \\ \left(\theta_{off} - \theta\right)^2 \dfrac{\theta_{off} + 2\theta - 3\theta_{on}}{\theta_{off} - \theta_{on}} & \theta \geq \theta_{on} \end{cases}$$

with $\theta_{on} = 170^0$ and $\theta_{off} = 180^0$.

A.1.2 Force Field Reported by Hill and Sauer[2,3]

i) Bond Stretch:

$$U^{bond}(r) = k_2(r - r_0)^2 + k_3(r - r_0)^3 + k_4(r - r_0)^4$$

Si-O-O Bond Stretch (CFF Quartic Bond)			
k_2/k_B= 231017.255 (K/Å^2)	k_3/k_B= -338387.114 (K/Å^2)	k_3/k_B= 223109.917 (K/Å^2)	r_0= 1.6104 Å
Si-O_a Bond Stretch (CFF Quartic Bond)			
k_2/k_B= 248642.816 (K/Å^2)	k_3/k_B= -18468.957 (K/Å^2)	k_3/k_B= 1082265.698 (K/Å^2)	r_0= 1.6157 Å
Al-O_a Bond Stretch (CFF Quartic Bond)			
k_2/k_B= 165400.667 (K/Å^2)	k_3/k_B= -171605.009 (K/Å^2)	k_3/k_B= 1101564.816 (K/Å^2)	r_0= 1.7193 Å

ii) Bond Angle Bend:

$$U^{angle}(\theta) = k_2(\theta - \theta_0)^2 + k_3(\theta - \theta_0)^3 + k_4(\theta - \theta_0)^4$$

O-Si-O Bond Bending (Bond Angle Bend) (CFF Quartic Bend)			
k_2/k_B= 41248.441 (K/rad^2)	k_3/k_B= -18408.470 (K/rad^2)	k_4/k_B= 58854.427 (K/rad^2)	θ_0= 112.0200º
O_a-Si-O Bond Bending (Bond Angle Bend) (CFF Quartic Bend)			
k_2/k_B= 44318.985 (K/rad^2)	k_3/k_B= -28705.144 (K/rad^2)	k_4/k_B= 46537.881 (K/rad^2)	θ_0= 112.4279º
O_a-Al-O_a Bond Bending (Bond Angle Bend) (CFF Quartic Bend)			
k_2/k_B= 150991.986 (K/rad^2)	k_3/k_B= -16387.793 (K/rad^2)	k_4/k_B= 33846.084 (K/rad^2)	θ_0= 113.4000º
O_a-Si-O_a Bond Bending (Bond Angle Bend) (CFF Quartic Bend)			
k_2/k_B= 77589.386 (K/rad^2)	k_3/k_B= -34550.792 (K/rad^2)	k_4/k_B= 11890.672 (K/rad^2)	θ_0= 110.612º
Si-O-Si Bond Bending (Bond Angle Bend) (CFF Quartic Bend)			
k_2/k_B= 150991.986 (K/rad^2)	k_3/k_B= -16387.793 (K/rad^2)	k_4/k_B= 33846.084 (K/rad^2)	θ_0= 113.4000º
O_a-Si-O_a Bond Angle Bend (Harmonic Bend)			
k_2/k_B= 77589.386 (K/rad^2)	k_3/k_B= -34550.792 (K/rad^2)	k_4/k_B= 11890.672 (K/rad^2)	θ_0= 110.6120º

Si-O-Si Bond Angle Bend (Harmonic Bend)			
k_2/k_B= 10417.396 (K/rad^2)	k_3/k_B= 13863.996 (K/rad^2)	k_4/k_B= 5531.891 (K/rad^2)	θ_0= 173.7651º
Al-O_a-Si Bond Angle Bend (Harmonic Bend)			
k_2/k_B= 5206.006 (K/rad^2)	k_3/k_B= 6358.982 (K/rad^2)	k_4/k_B= 4530.887 (K/rad^2)	θ_0= 162.4000º

iii) Bond-Bond: (Si-O_{zeo}-Si)

$$U^{bond-bond}(rr') = k_{bb'}(r - r_0)(r' - r'_0)$$

Al-O_a-Si Bond-Bond (Bond Coupling) (CFF Bond Bond Cross)		
$k_{bb'}/k_B$= 41850.643 (K/Å^2)	r_0= 1.7193 Å	r'_0= 1.6157 Å
O_a-Si-O Bond-Bond (Bond Coupling) (CFF Bond Bond Cross)		
$k_{bb'}/k_B$= 23023.294 (K/Å^2)	r_0= 1.6157 Å	r'_0= 1.6104 Å
Si-O-Si Bond-Bond (Bond Coupling) (CFF Bond Bond Cross)		
$k_{bb'}/k_B$ = 76426.043 (K/Å^2)	r_0= 1.6104 Å	r'_0= 1.6104 Å
Oa-Al-Oa Bond-Bond (Bond Coupling) (CFF Bond Bond Cross))		
$k_{bb'}/k_B$= -28434.412 (K/Å^2)	r_0= 1.7193 Å	r'_0= 1.6157 Å
Oa-Si-Oa Bond-Bond (Bond Coupling) (CFF Bond Bond Cross)		
$k_{bb'}/k_B$ = 76426.043 (K/Å^2)	r_0= 1.6157 Å	r'_0= 1.6157 Å
Si-O-Si Bond-Bond (Bond Coupling) (CFF Bond Bond Cross)		
$k_{bb'}/k_B$ = 76426.043 (K/Å^2)	r_0= 1.6157 Å	r'_0= 1.6104 Å

iv) Bond Angle:

$$U^{bond-angle}(r, \theta, r') = (\theta - \theta_0)[k_r(r - r_0) + k_{r'}(r' - r'_0)]$$

Al-O_a-Si Bond-Bend (Bond-Bend Coupling) (CFF Bond Bend Cross)				
k_r/k_B= 4612.610 (Å/K/rad^2)	$k_{r'}/k_B$= 6918.160 (Å/K/rad^2)	θ_0=162.4000º	r_0= 1.7193 Å	r'_0= 1.6157 Å
O_a-Si-O Bond-Bend (Bond-Bend Coupling) (CFF Bond Bend Cross)				
k_r/k_B= 10125.881 (Å/K/rad^2)	$k_{r'}/k_B$= 39231.890 (Å/K/rad^2)	θ_0=112.4279º	r_0= 1.6157 Å	r'_0= 1.6104 Å
O-Si-O Bond-Bend (Bond-Bend Coupling) (CFF Bond Bend Cross)				
k_r/k_B= 39313.462 (Å/K/rad^2)	$k_{r'}/k_B$= 39313.462 (Å/K/rad^2)	θ_0=112.0200º	r_0= 1.6104 Å	r'_0=1.6104 Å

Si-O-Si Bond-Bend (Bond-Bend Coupling) (CFF Bond Bend Cross)				
k_r/k_B= 4649.244 (Å/K/rad^2)	$k_{r'}/k_B$= 4649.244 (Å/K/rad^2)	θ_0=173.7651º	r_0= 1.6104 Å	r'_0= 1.6104 Å
O_a-Al-O_a Bond-Bend (Bond-Bend Coupling) (CFF Bond Bend Cross)				
k_r/k_B= 55430.774 (Å/K/rad^2)	$k_{r'}/k_B$= 55430.774 (Å/K/rad^2)	θ_0=113.4000º	r_0= 1.7193 Å	r'_0= 1.7193 Å
O_a-Si-O_a i Bond-Bend (Bond-Bend Coupling) (CFF Bond Bend Cross)				
k_r/k_B= 117789.368 (Å/K/rad^2)	$k_{r'}/k_B$= 117789.368 (Å/K/rad^2)	θ_0=110.612º	r_0= 1.6157 Å	r'_0= 1.6157 Å

v) Angle-Angle:

$$U^{angle-angle}(\theta,\theta') = k_{\theta\theta'}(\theta-\theta_0)(\theta'-\theta'_0)$$

O-Si-O-O Bond-Bend (Bond-Bend Coupling) (CFF Bond Bend Cross)		
$k_{\theta\theta'}$ = -3171.792 (K/Å^2)	θ_0= 112.0200º	θ'_0= 112.0200º
O-Si-O-O Bond-Bend (Bond-Bend Coupling) (CFF Bond Bend Cross)		
$k_{\theta\theta'}$ = 9680.532 (K/Å^2)	θ_0= 112.4279º	θ'_0= 112.4279º

vi) Torsion:

$$U^{tors}(\theta,\phi,\theta') = S(\theta)[k_1(1-\cos\phi)k_1(1-\cos 2\phi)k_1(1-\cos 2\phi)]S(\theta')$$

Al-O_a-Si-O Bond-Bend (Bond-Bend Coupling) (CFF Bond Bend Cross)		
k_1/k_B= 1106.529126 (K)	k_1/k_B=378.82356 (K)	k_1/k_B= -248.38909 (K)
Si-O-Si-O_a Bond-Bend (Bond-Bend Coupling) (CFF Bond Bend Cross)		
k_1/k_B=19.9778 (K)	k_1/k_B= 6.69282 (K)	k_1/k_B=-123.43972 (K)
Si-O-Si-O Bond-Bend (Bond-Bend Coupling) (CFF Bond Bend Cross)		
k_1/k_B=15.39851 (K)	k_1/k_B=-5.28380 (K)	k_1/k_B=40.45884 (K)
Si-O_a-Al-O_a Bond-Bend (Bond-Bend Coupling) (CFF Bond Bend Cross)		
k_1/k_B=3061.48615 (K)	k_1/k_B= -286.935698 (K)	k_1/k_B=-745.6705 (K)
Al-O_a-Si-O_a Bond-Bend (Bond-Bend Coupling) (CFF Bond Bend Cross)		
k_1/k_B=935.837107 (K)	k_1/k_B= -11.62437 (K)	k_1/k_B=-218.64883 (K)

i) Angle Angle Torsion:

$$U^{angle-angle-torsion}(\theta,\phi,\theta') = k_{\theta\theta'}\cos\phi(\theta-\theta_0)(\theta'-\theta'_0)$$

O-Si-O-O Bond-Bend (Bond-Bend Coupling) (CFF Bond Bend Cross)		
$k_{\theta\theta'}$ = 4260.004 (K/Å^2)	θ_0= 112.4279º	θ'_0= 162.4000º
O-Si-O-O Bond-Bend (Bond-Bend Coupling) (CFF Bond Bend Cross)		
$k_{\theta\theta'}$ = -5243.093 (K/Å^2)	θ_0= 112.4279º	θ'_0= 173.7651º
O-Si-O-O Bond-Bend (Bond-Bend Coupling) (CFF Bond Bend Cross)		
$k_{\theta\theta'}$ = -2272.036 (K/Å^2)	θ_0= 112.0200º	θ'_0= 112.0200º
O-Si-O-O Bond-Bend (Bond-Bend Coupling) (CFF Bond Bend Cross)		
$k_{\theta\theta'}$ = -9067.208 (K/Å^2)	θ_0== 113.4000º	θ'_0= 162.4000º
O-Si-O-O Bond-Bend (Bond-Bend Coupling) (CFF Bond Bend Cross)		
$k_{\theta\theta'}$ = -5499.131 (K/Å^2)	θ_0= 110.6120º	θ'_0= 162.4000º

ii) Nonbonded Potential Parameters (CFF 9-6 Potential):

$$U(r) = \frac{p_1}{r^9} - \frac{p_2}{r^6}$$

Atom	P_1/k_B (K Å^9)	P_1/k_B (K Å^6)	q (e$^-$)
Si	94057219.175	0.0	2.05
Al	10316687.74	0.0	1.75
O_{Si}	40076506.50	0.0	-1.025
O_{Al}	28891069.825	0.0	-1.2
Na	--	--	1.0
Ca	--	--	2.0

A.2 Bibliography

1 J. B. Nicholas, A. J. Hopfinger, F. R. Trouw and L. E. Iton. *Journal of the American Chemical Society* **113**, 4792-4800 (1991).

2 J. R. Hill and J. Sauer. *Journal of Physical Chemistry* **98**, 1238-1244 (1994).

3 J. R. Hill and J. Sauer. *Journal of Physical Chemistry* **99**, 9536-9550 (1995).

Appendix B

Supporting Information for Chapter 6

B.1 Fluids Density Functional Theory

We employed the Tramonto FDFT code[1] to model the methane-TON system as a cylindrical pore at equilibrium with a bulk fluid at fixed chemical potential μ. Inside the pore we have a fluid with spatially varying density ρ(r). The governing principle for FDFT is that there exists a unique density distribution which minimizes the grand free energy of the system Ω at equilibrium[2]. With the Tramonto code Ω is computed using the definition:

$$\Omega\left[\rho(r)\right] = F^{id}\left[\rho(r)\right] + F^{hs}\left[\rho(r)\right] + F^{at}\left[\rho(r)\right] + \int dr'\rho(r')\left[\phi^{ext}(r') - \mu\right] \tag{B.1}$$

where F^{id} is the ideal Helmholtz free energy, and F^{hs} and F^{at} are the excess free energies arising from the hard-sphere and attractive interactions between the particles, respectively and ϕ^{ext} is the external potential coming from the pore. This interaction is computed by numerically integrating the guest-host potential:

$$u_{gh}(r) = 4\varepsilon_{gh}\left[\left(\frac{\sigma_{gh}}{r}\right)^{12} - \left(\frac{\sigma_{gh}}{r}\right)^{6}\right] \tag{B.2}$$

where ε_{gh} and σ_{gh} are the guest-host force field parameters, over the material volume of the pore. The minimum of this function with respect the spatially inhomogeneous density ρ(r) corresponds to the grand potential of an open (μVT) system. The minimization procedure produces a set of of Euler-Lagrange (EL) equations which must be solved for all points on the grid in the domain. The EL equations are calculated at constant chemical potential μ, volume V, and temperature T, i.e., $\left(\delta\Omega\left[\tilde{\rho}\right]/\delta\tilde{\rho}\right)_{\mu,\mathrm{V,T}} = 0$. These non-linear, integro-differential equations are solved with a bound-constrained quasi-Newton method[3-5].

The ideal gas function is exact and is given by

$$F^{id}\left[\rho(r)\right] = k_B T \int dr' \rho(r')\left[\ln \Lambda^3 \rho(r') - 1\right] \tag{B.3}$$

where k_B is the Boltzmann constant, T is the temperature and Λ is the thermal wavelength of the methane.

To compute the hard sphere term we use the White Bear functional[6] which is based on the fundamental measure theory (FMT) of Rosenfeld[7]. It is

$$F^{hs}\left[\rho(r)\right] = k_B T \int dr' \Phi^{hs}\left[\left\{n_\alpha(r')\right\}\right] \tag{B.4}$$

where the energy density for the hard sphere system, Φ^{hs}, is a functional of a set of inhomogeneous weighted densities of the system, n_α. These weighted densities are

$$n_\alpha(r) = \int dr' \rho(r') \omega^{(\alpha)}(r - r'), \tag{B.5}$$

where $\omega^{(\alpha)}$ are the four scalar, two vector and one tensor weighting functions, $\alpha \in \{0, 1, 2, 3, V_1, V_2, m2\}$. Essentially, these weighting functions are based on the fundamental geometric properties of a sphere, *i.e.*, radius $R_i = \sigma_i/2$, surface area, and volume. The scalar and vector functions are:

$$\begin{aligned}
&\omega^{(0)}(\mathbf{r}) = \frac{\omega^{(2)}(\mathbf{r})}{4\pi R^2}, && \omega^{(1)}(\mathbf{r}) = \frac{\omega^{(2)}(\mathbf{r})}{4\pi R}, \\
&\omega^{(2)}(\mathbf{r}) = \delta(R - |\mathbf{r}|), && \omega^{(3)}(\mathbf{r}) = \theta(R - |\mathbf{r}|), \\
&\omega_i^{(V_2)}(\mathbf{r}) = \frac{\mathbf{r}}{r}\delta(R - |\mathbf{r}|), && \omega_i^{(V_1)}(\mathbf{r}) = \frac{\omega^{(V_2)}(\mathbf{r})}{4\pi R},
\end{aligned} \tag{B.6}$$

where δ(r) and θ(r) denote the Dirac delta function and Heaviside step function, respectively. The tensor function is

$$\omega^{(m_2)}(\mathbf{r}) = \omega^{(2)}(\mathbf{r})\left(\mathbf{rr}/r^2 - \mathbf{I}/3\right) \tag{B.7}$$

where I is the identity matrix.

With the weighting functions above, the free energy of the hard-sphere system can be written as[6]

$$\Phi^{hs} = -n_0 \ln(1-n_3) + \frac{n_1 n_2 - n_{V_1} \cdot n_{V_2}}{1-n_3} + \\ + \frac{n_3 + (1-n_3)^2 \ln(1-n_3)}{36\pi n_2^3 (1-n_3)^2} \left(n_2^3 - 3 n_2 n_{V_2} \cdot n_{V_2} + 9 \left(n_{V_2} n_{m_2} n_{V_2} - Tr(n_{m_2}^3)/2 \right) \right) \tag{B.8}$$

This functional corresponds to the MCSL equation of state[8] has been shown to perform well against GCMC simulations across all densities.

The free energy due to the attractions between the methane molecules was calculated using

$$F^{at}\left[\rho(r)\right] = \iint d\mathbf{r}' d\mathbf{r}'' \frac{1}{2} \rho(\mathbf{r}') \rho(\mathbf{r}'') u_{ij}\left(|r' - r''|\right) \tag{B.9}$$

where u(r) represents the van der Waals attraction is computed by the standard WCA method[9,10]

$$u_{ij}(r) = \begin{cases} -\varepsilon_{ij} & r \le 2^{1/6}\sigma_{ij} \\ 4\varepsilon_{ij}\left[\left(\sigma_{ij}/r\right)^{12} - \left(\sigma_{ij}/r\right)^{6} \right] & r > 2^{1/6}\sigma_{ij} \end{cases} \tag{B.10}$$

where $\varepsilon_{i\,j}$ and $\sigma_{i\,j}$ are taken to be the same as those from the guest-guest interactions in the simulations.

B.2 Henry Coefficient and Heat of Adsorption

A comparison of the model and simulations for methane and ethane adsorption in the various zeolites can be seen in Fig. B.1 to B.4. The figures depict the Henry coefficient and the heat of adsorption for methane and ethane in each of the zeolites as a function of the guest-host size parameter σ for different guest-host interaction strengths ε. Values calculated by the model are depicted with open symbols and those from GCMC simulation are plotted with closed symbols. In

all cases, the temperature was taken to be 300 K. These figures show that the model parameter space for the Henry coefficient and heat of adsorption is in excellent agreement with that of the simulation in the neighbourhood of the optimal parameter values for the guest-host interactions. The actual values for ε/k_B and σ in methane are 115 K and 3.47 Å, respectively. The force field parameters values for ethane are ε/k_B = 93 K and σ = 3.48 Å. The carbon-carbon bond length was set to 1.54 Å in all of our simulations of ethane.

Fig. B.1(a), B.2(a), B.1(d) and B.2(d) show that for the AFI and ITQ-29 hosts the model agrees nearly perfectly with the simulation for the Henry coefficient and heat of adsorption for the entire parameter space explored. This indicates that the annular model describes them well even though the actual pores are not completely smooth.
If we compare Fig. B.1(a) and Fig. B.3(a), we see that for adsorption of methane in AFI the Henry coefficient is 1-3 orders of magnitude lower than for ethane. Also, Fig. B.2(a) and Fig. B.4(a) show that for adsorption of ethane the magnitude of the heat of adsorption is larger.

Fig. B.1(b), B.2(b), B.3(b) and B.4(b) show that there is good agreement between the model and simulation for the LTL-type zeolite. This result is somewhat surprising since the LTL-type zeolite has highly corrugated pores and the pore surface is not cylindrical. In Fig. B.1(e), B.2(e), B.3(e), and B.4(e) the same comparison is shown for the MTT-type zeolite. The agreement here is not as good as the other cases since the pore size is only slightly larger than the guest molecule. This causes the potential in the model to be dominated by repulsions, thereby reducing the magnitude of the heat of adsorption.

The model parameters for the adsorption of methane and ethane for each zeolite are shown in table B.1 and table B.2 respectively.

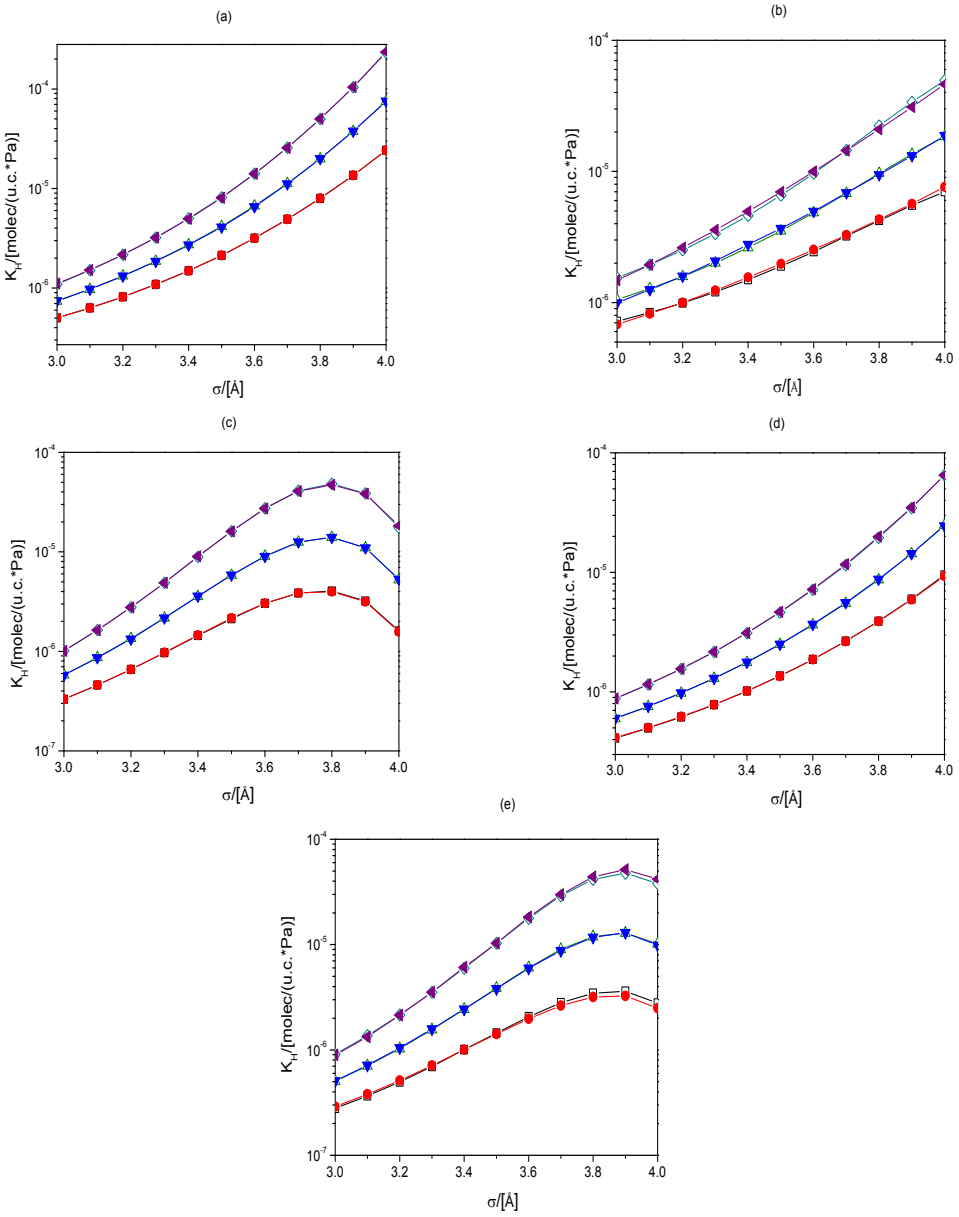

Figure B.1: Henry coefficient of methane in (a) AFI-, (b) LTL-, (c) TON-, (d) ITQ-29 and (e) MTT-type zeolite at 300 K as a function of the parameters describing the guest-host interactions. Data from MC simulations and model equations after fitting simulation data. White square, ε/k_B = 100 K, model; red circle, ε/k_B = 100 K, MC; white triangle, ε/k_B = 115 K, model; blue triangle, ε/k_B = 115 K, MC; white diamond, ε/k_B = 130 K, model; purple triangle, ε/k_B = 130 K, MC.

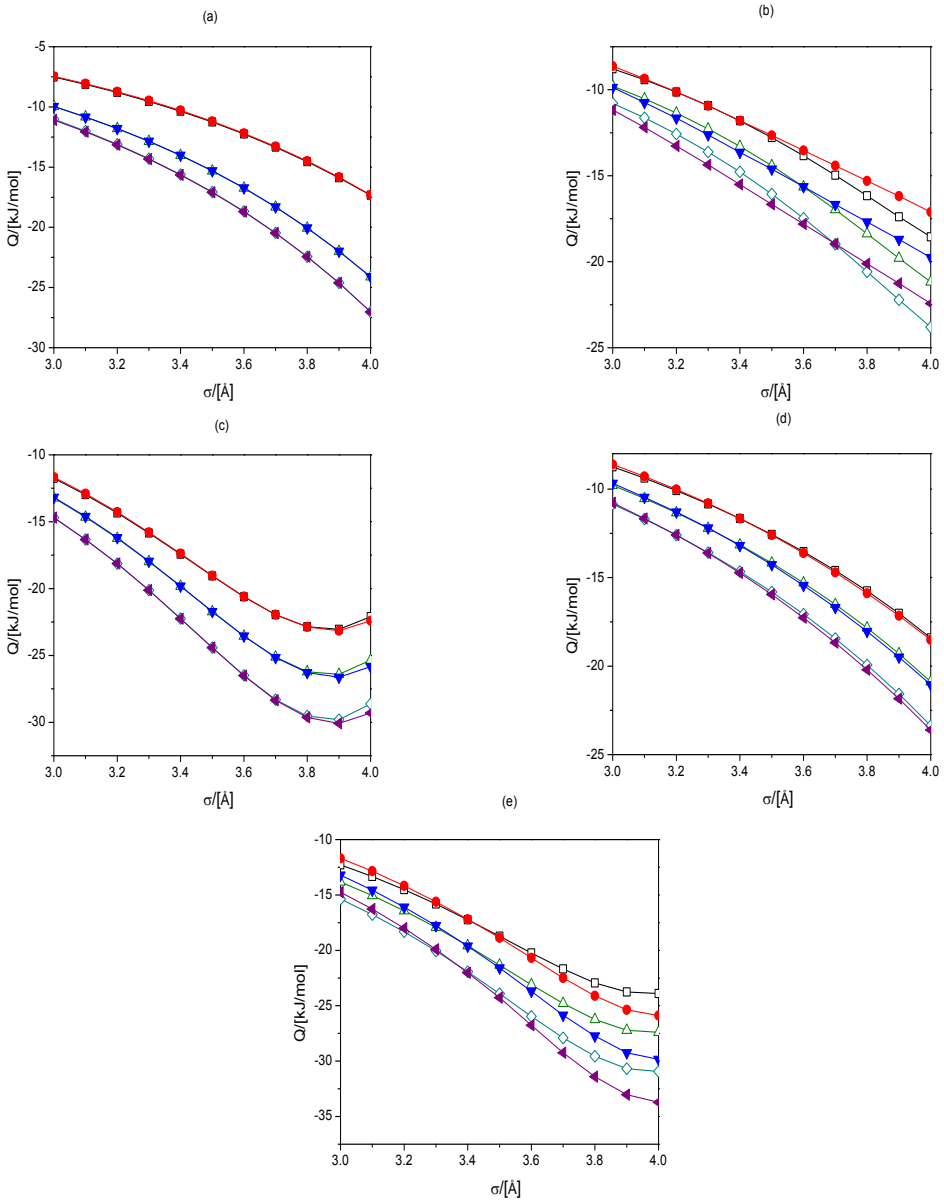

Figure B.2: Heat of adsorption of methane in (a) AFI-, (b) LTL-, (c) TON-, (d) ITQ-29 and (e) MTT-type zeolite at 300 K as a function of the parameters describing the guest-host interactions. Data from MC simulations and model equations after fitting simulation data. White square, ε/k_B = 100 K, model; red circle, ε/k_B = 100 K, MC; white triangle, ε/k_B = 115 K, model; blue triangle, ε/k_B = 115 K, MC; white diamond, ε/k_B = 130 K, model; purple triangle, ε/k_B = 130 K, MC.

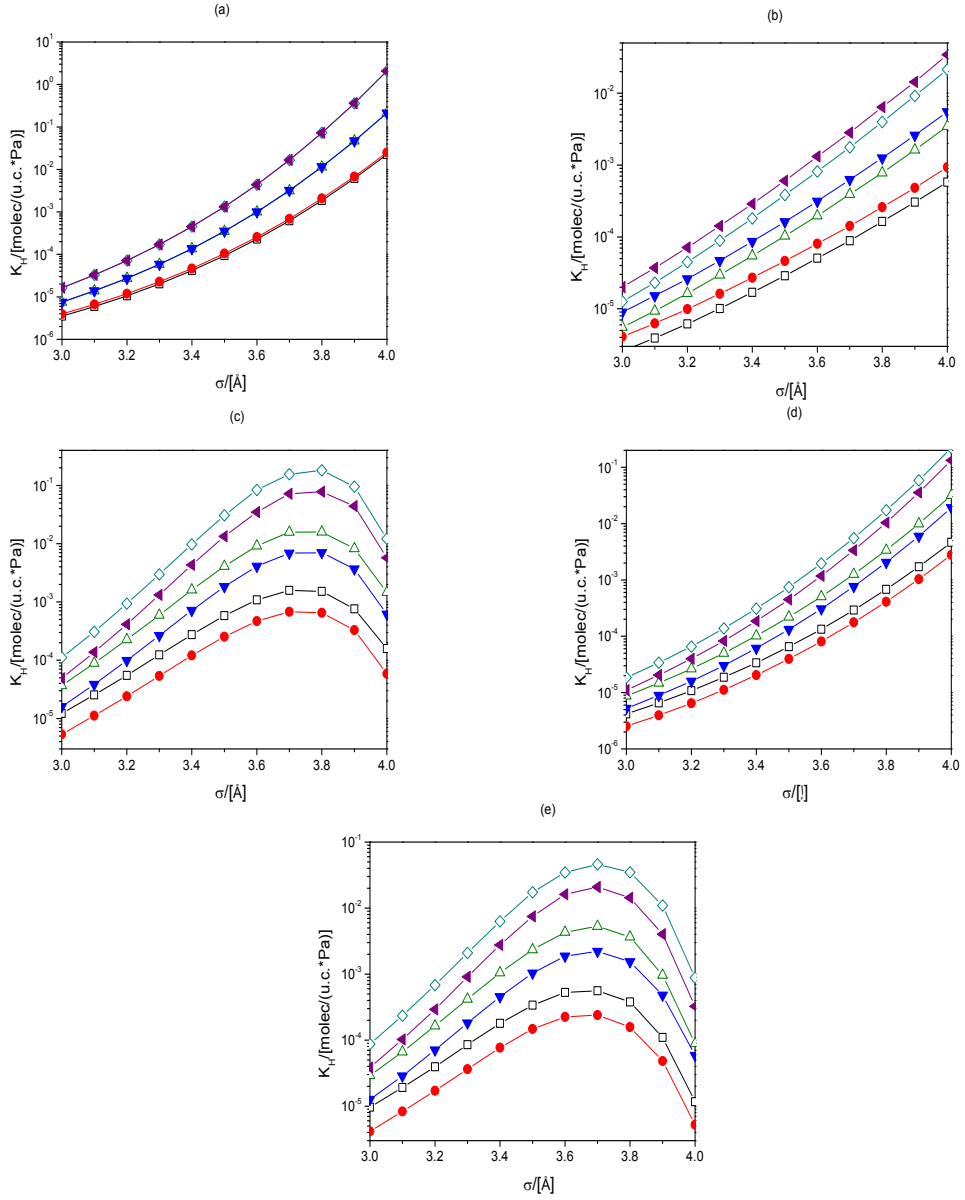

Figure B.3: Henry coefficient of ethane in (a) AFI-, (b) LTL-, (c) TON-, (d) ITQ-29 and (e) MTT-type zeolite at 300 K as a function of the parameters describing the guest-host interactions. Data from MC simulations and model equations after fitting simulation data. White square, ε/k_B = 100 K, model; red circle, ε/k_B = 100 K, MC; white triangle, ε/k_B = 115 K, model; blue triangle, ε/k_B = 115 K, MC; white diamond, ε/k_B = 130 K, model; purple triangle, ε/k_B = 130 K, MC.

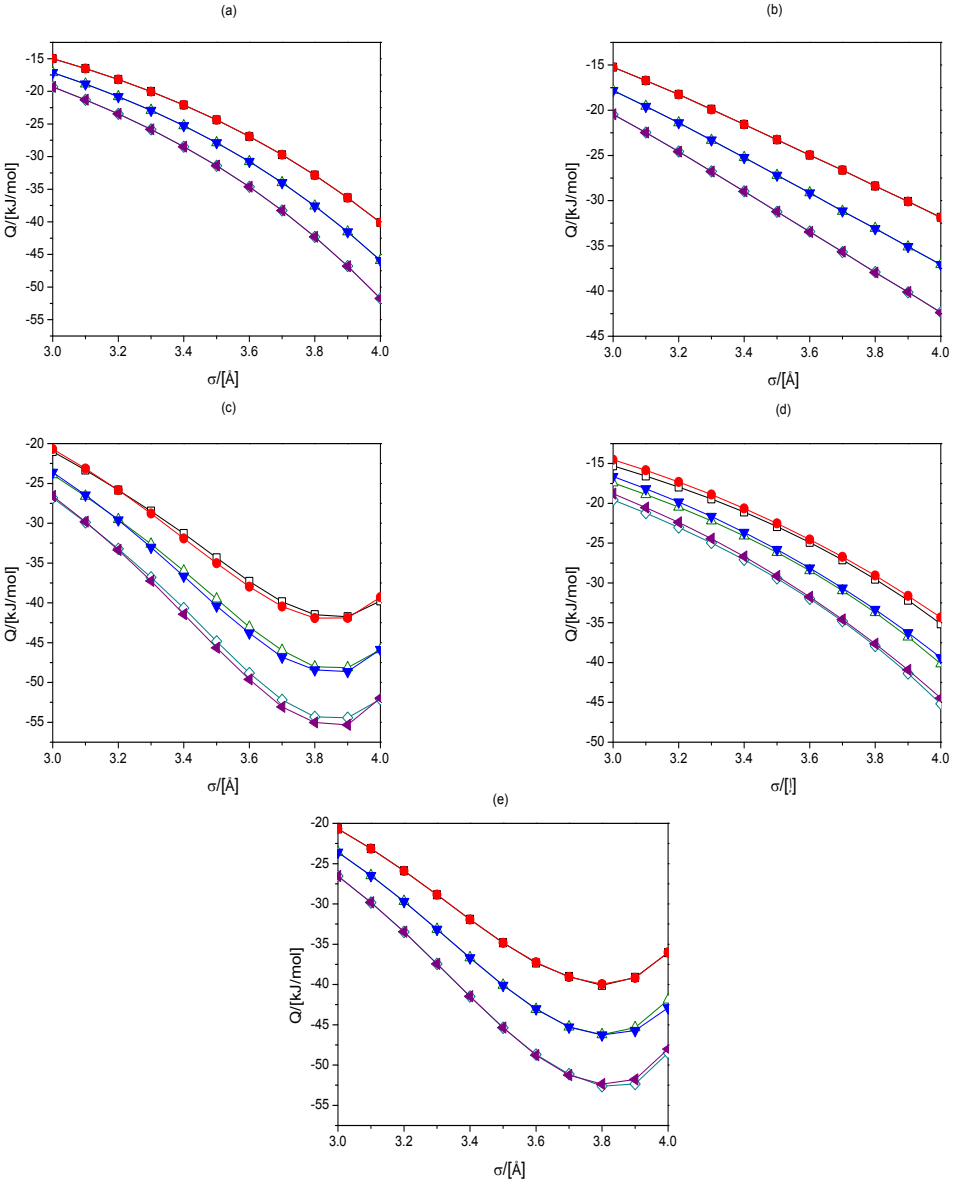

Figure B.4: Heat of adsorption of ethane in (a) AFI-, (b) LTL-, (c) TON-, (d) ITQ-29 and (e) MTT-type zeolite at 300 K as a function of the parameters describing the guest-host interactions. Data from MC simulations and model equations after fitting simulation data. White square, ε/k_B = 100 K, model; red circle, ε/k_B = 100 K, MC; white triangle, ε/k_B = 115 K, model; blue triangle, ε/k_B = 115 K, MC; white diamond, ε/k_B = 130 K, model; purple triangle, ε/k_B = 130 K, MC.

Zeolite	Model Parameters for Methane			
	R1/[Å]	R2/[Å]	λ	$U_{min}k_B^{-1}$/[K]
AFI	5.1477	10.255	1.4918	0.33747
LTL	4.9196	10.975	1.0451	2.9283
TON	4.0420	8.1378	1.4223	0.48647
ITQ-29	5.3815	9.2728	1.3664	1.2072
MTT	3.9261	7.9745	1.5245	-1.9371

Table B.1: Model parameters for the adsorption of methane in the various zeolites.

Zeolite	Model Parameters for Ethane			
	R_1/[Å]	R_2/[Å]	λ	$U_{min}k_B^{-1}$/[K]
AFI	5.8917	9.7009	1.9367	-0.47840
LTL	4.6671	7.8873	0.97362	1.3430
TON	4.0485	7.9992	1.3666	2.0229
ITQ-29	5.4878	5.7262	1.3934	0.39721
MTT	4.0323	13.123	1.2397	2.7993

Table B.2: Model parameters for the adsorption of ethane in the various zeolites.

B.3 Bibliography

1 L. J. D. Frink and A. G. Salinger. *Journal of Computational Physics* **159**, 407-424 (2000).

2 R. Evans. *Advances in Physics* **28**, 143-200 (1979).

3 G. H. Golub and C. F. V. Loan. *Matrix computations*. 3rd edn, (The Johns Hopkins University Press, 1996).

4 S. Bellavia, M. Macconi and B. Morini. *Applied Numerical Mathematics* **44**, 257-280 (2003).

5 M. A. Heroux, A. G. Salinger and L. J. D. Frink. *Siam Journal on Scientific Computing* **29**, 2059-2077 (2007).

6 R. Roth, R. Evans, A. Lang and G. Kahl. *Journal of Physics-Condensed Matter* **14**, 12063-12078 (2002).

7 Y. Rosenfeld. *Physical Review Letters* **63**, 980-983 (1989).

8 G. A. Mansoori, N. F. Carnahan, K. E. Starling and T. W. Leland. *Journal of Chemical Physics* **54**, 1523-& (1971).

9 H. C. Andersen, J. D. Weeks and D. Chandler. *Physical Review A* **4**, 1597-+ (1971).

10 J. D. Weeks, D. Chandler and H. C. Andersen. *Journal of Chemical Physics* **54**, 5237-5247 (1971).

List of Publications

Chapter 2

A. García-Sánchez, E. García-Pérez, D. Dubbeldam, R. Krishna, and S. Calero: "A Simulation Study of Alkanes in Linde Type A Zeolites" *Adsorption Science & Technology*, **25**, 417-427 (2007)

Chapter 3

A. García-Sánchez, D. Dubbeldam, and S. Calero: "Modeling Adsorption and Self-Diffusion of Methane in LTA Zeolites: The Influence of Framework Flexibility". *Journal of Physical Chemistry C* **114**, 15068-15074 (2010)

Chapter 4

A. García-Sánchez, C.O. Ania, J.B. Parra, D. Dubbeldam, T.J.H. Vlugt, R. Krishna, and S. Calero: "Transferable Force field for Carbon Dioxide Adsorption in Zeolites" *Journal of Physical Chemistry C* **113**, 8814-8820 (2009)

Chapter 5

A. García-Sánchez, J. van den Bergh, J.M. Castillo, S. Calero, F. Kapteijn and T.J.H. Vlugt: "Influence of Force Field Parameters on Computed Diffusion Coefficients of CO_2 LTA-type Zeolites". *In preparation*

Chapter 6

García-Sánchez, E. Eggink, E.S. McGarrity, S. Calero and T.J.H. Vlugt: "Predictive Model for Optimizing Guest-Host Interactions in Zeolites" *Journal of Physical Chemistry C* **115**, 10187-10195 (2011)

Not included in this thesis

A. Martín-Calvo, E. García-Pérez, A. García-Sánchez, R. Bueno-Pérez, S. Hamad, and S. Calero: "Effect of Air Humidity on the Removal of Carbon Tetrachloride from Air Using Cu-BTC Metal Organic Framework" *Physical Chemistry Chemical Physics*, **13**, 11165-11174 (2011)

E. García-Pérez, J. B. Parra, C. O. Ania, A. García-J. M. van Baten, R. Krishna, , D. Dubbeldam and S. Calero: "A Computational Study of CO_2, N_2, and CH_4 Adsorption in Zeolites" *Adsorption*, **13**, 469-476 (2007)